Universiteit Gent
Faculteit Ingenieurswetenschappen
Vakgroep Elektrische Energie, Systemen en Automatisering

Impact of voltage distortion on energy efficiency of induction machines and line start permanent magnet machines

Impact van spanningsvervorming op de energie-efficiëntie van inductiemachines en lijnstartpermanentmagneetmachines

Colin Debruyne

Proefschrift tot het bekomen van de graad van
Doctor in de Ingenieurswetenschappen:
Werktuigkunde-Elektrotechniek
Academiejaar 2013-2014

Universiteit Gent
Faculteit Ingenieurswetenschappen en Architectuur
Vakgroep Elektrische Energie, Systemen en Automatisering
Vakgroep Industrieel Systeem- en Productontwerp

Promotoren:
Prof. dr. ir. Lieven Vandevelde (Universiteit Gent- EA08)
Prof. dr. ir. Jan J. Desmet (Universiteit Gent- EA19)

Lees- en examencommissie:
Prof. dr. ir. Luc Taerwe (Universiteit Gent- chairman)
Prof. dr. ir. Elena Lomonova (T.U. Eindhoven- Nederland)
Prof. dr. ir. Peter Sergeant (Universiteit Gent- EA20)
Prof. dr. ir. Jos Knockaert (Universiteit Gent- EA19)
dr. ir. Kurt Schipman (A.B.B. Jumet- België)
Prof. dr. ir. Fernando J.T.E. Ferreira (University of Coimbra- Portugal)

Universiteit Gent
Faculteit Ingenieurswetenschappen en Architectuur

Vakgroep Elektrische Energie, Systemen en Automatisering
Sint-Pietersnieuwstraat 41, B-9000 Gent, België
Tel.: +32-9-264.34.18
Fax.: +32-9-264.35.82

Vakgroep Industrieel Systeem- en Productontwerp
Graaf Karel deGoedelaan 8, B-8500 Gent, België
Tel.: +32-56-24.12.35
Fax.: +32-56-24.12.34

Proefschrift tot het behalen van de graad van
Doctor in de Ingenieurswetenschappen:
Werktuigkunde-Elektrotechniek
Academiejaar 2013-2014

Dankwoord

Hier ligt het dan... Na een onderzoeksperiode van ruim 9 jaar en een doctoraatsperiode van iets meer dan 4 jaar kan ik uiteindelijk de laatste pagina van mijn studeerperiode omslaan. Misschien start ik het best op basis van een persoonlijke noot. Alhoewel het vaak goed bedoeld werd, leidde de opmerking *Het zal wel gaan!* vaak tot grote ergernis en fustratie. Deze woorden worden vaak geuit in een blijk van vertrouwen en steun, maar dezelfde woorden leggen de lat soms -te- hoog, en bijgevolg probeer ik eraan te houden deze woorden van steun in de toekomst weinig in de mond te nemen. Dit dankwoord mag echter geen manifest van zelfbeklag worden en bijgevolg wens ik dit dankwoord naar iedereen te richten die mij gedurende deze periode heeft bijgestaan. Er rest me bijgevolg nog één essentiële taak en dit is het uitschrijven van een dankwoord. Alhoewel dit het minst wetenschappelijke stuk vormt, zal dit waarschijnlijk het meest gelezen hoofdstuk worden uit mijn volledig doctoraat. Hoe begin je aan dergelijk gevoelig huzarenstukje, zonder iemand over te slaan?

Vooreerst moet ik mijn promotoren erkennen in hun blijk van vertrouwen en inzicht, toen zich eind 2009 een langharige - en in dialect volhardende- West-Vlaming zich spontaan kwam opdringen als doctoraatstudent. Het onuitputtelijk rotsvast vertrouwen van Prof. Dr. ir. Lieven Vandevelde als van Prof. Dr. ir. Jan Desmet zijn een continue houvast geweest gedurende deze periode. Natuurlijk dienen de leden van de lees- en examencommissie expliciet bedankt te worden voor de kritische blik met betrekking tot mijn werk. Graag citeer ik in dit kader Francis Crick [mede-ontdekker van de moleculaire DNAstructuur]: A good scientist values criticism almost higher than friendship. No, in science criticism is the height and measure of friendship.

During my research i had the fortune and opportunity to establish several national and international relations. I would like to recognize M. Polikarpova and J. Pyrhonen of the LUT in Finland and F.J.T.E Ferreira of the University of Coimbra in Portugal. Specific aknowledgement and words of gratitude are also given towards Briam Cavalca Bork and all the people of WEG-Brasil. Prof. Dr. ir. Peter Sergeant verdient zeker een prominente plaats in dit dankwoord. Ontegensprekelijk is het dankzij zijn bijdrage dat ik dit werk nu kan neerleggen.

Koffie is de diesel van de onderzoeker en menig onverbloemde verzuchting

werd opgeworpen tijdens de broodnodige koffiepauzes. Ik dank dan ook uit de grond van mijn hart alle collega's van de opleiding, maar met meer dan 40 collega's is een opsomming onbegonnen werk. Maar dit poog ik zoals gewoonlijk te compenseren met het nodige gerstenat. Toch wens ik mijn lotgenoten Stijn Derammelaere en Bram Vervish expliciet te bedanken. Heel in het bijzonder wens ik Steve Dereyne en alle collega's van LEA bedanken voor de input, ondersteuning en de cachaça's in Rio.

Alhoewel dit werk uiteindelijk mijn naam draagt, zou het van een te groot opportunisme getuigen mocht ik de collega-lemckonauten niet expliciet vermelden. Woorden van dankbaarheid schieten te kort voor alle (ex-)medewerkers, maar heel in het bijzonder aan Lien, Fleur, Bart, Dimitry, Cis en Bram C. Graag vermeld ik Dries Putman, die me destijds dermate ondersteund heeft dat ik daar tot op vandaag nog de vruchten van pluk. Karakter en doorzettingsvermogen is essentieel in de verschillende aspecten van het leven, en ik kan gerust toegeven dat zowel de familie Callewier-Verhaeghe als elkeen van de vrienden uit KSA, Chiro en WKS mij getekend hebben tot de persoon die ik nu ben. De (kerst)poker, rietputheemfeestjes en de sport hebben de taak als emotioneel overdrukventiel mooi vervuld.

Graag zou ik u, de lezer, willen aanspreken. Gezien het feit dat u dit stuk naleest toont ofwel een professionele ofwel een persoonlijke interesse in mij of in het voorgelegde onderzoek. Graag sta ik jullie te woord voor eventuele vragen. Indien ik, waarschijnlijk onterecht, heb nagelaten u persoonlijk te bedanken bied ik bij deze alvast mijn oprechte excuses aan. Ik ben altijd bereid dit recht te zetten bij een natje en een droogje.

De laatste paragraaf van dit dankwoord draag ik heel speciaal op aan mijn (schoon)familie, ouders, broer en gezin. De steun, oprecht medeleven en empathie van mijn ouders vormen een voorbeeld omtrent de opvoeding en omgang naar mijn gezin. Delphine, we hebben al heel wat stormen doorzwommen. Ik hoop van uit de grond van mijn hart dat we nu eindelijk op rustigere wateren verder kunnen varen. Zonder jou stond ik hier nooit vooraan.[1] Als laatste kom ik tot de essentie, mijn Marie. Papa zal je niet iets toewensen wat je later toch niet begeert. Maar weet dat wij ons uiterste best zullen doen om voor jou alle kansen te creëren, het grijpen ligt bij jou. Dikke kussen van papa en mama.

Kortrijk, april 2014
Debruyne Colin

[1] Maar die vette Harley Davidson, die we stelselmatig nastaarden in Roeselare, die zal waarschijnlijk toch ooit wel eens blinken in onze garage.

Contents

List of Figures

List of Tables

List of Acronyms

A

AC	Alternating Current

C

CEMEP	European Committee of Manufacturers of Electrical Machines and Power Electronics
CHP	Combined Heat Power
CT	Current Transformer

D

DCR	Die-cast Copper Rotor
DC	Direct Current
DF	Derating Factor
DOL	Direct On Line

E

EMF	ElectroMotive Force

F

FEM	Finite Element Method

H

HVF	Harmonic Voltage Factor

I

IEC	International Electrotechnical Commission
IG	Induction Generator
IGBT	Insulated Gate Bipolar Transistor
IM	Induction Motor

L

LCC	Life Cycle Cost
LBD	Loss Based Derating
LSPMM	Line Start Permanent Magnet Motor

M

MMF	MagnetoMotive Force

N

NdFeB	Neodymium Iron Boron

P

POC	Point Of Connection
PE	Power Electronics
PF	Power Factor
PM	Permanent Magnet
PWM	Pulse Width Modulation

PQ	Power Quality
pu	per unit

R

RMS	Root Mean Square

S

SCIM	Squirrel Cage Induction Motor
SHAF	Shunt Harmonic Active Filter
SLL	Stray Load Losses
SRM	Switched Reluctance Motor
SWT	Small Wind Turbine
SynRM	Synchronous Reluctance Machine

T

TBD	Thermal Based Derating
TEFC	Totally Enclosed Fan Cooled

V

VSD	Variable Speed Drive

List of Symbols

α	instantaneous electrical angle [rad]
$a(x,t)$	instantaneous current layer at position x and at time t [A]
$\hat{B}$	peak induction [T]
$b_u(x,t)$	instantaneous induction of phase u at position x and at time t [T]
δ	penetration depth due to the skin effect [m]
$e(t)$	electromotive force t [V]
E_{avg}	average electromotive force over half cycle [V]
f	frequency [Hz]
$f(x,t)$	force at position x and at time t [N]
h	harmonic order of the time harmonic, referenced to the grid
I_{RMS}	RMS value of the current [A]
$I_{\mathrm{RMS\_h}}$	RMS value of the harmonic current of order h [A]
$I_{\mathrm{h\_RMS}}$	total RMS value of the current including all harmonics [A]
i_r	instantaneous rotor current [A]
$I_{\mathrm{RMS\_k}}$	RMS value of the harmonic rotor current k [A]
K_r	skin effect coefficient for the resistance
K_x	skin effect coefficient for the inductance
k	harmonic order of the time harmonic, referenced to the rotor
L	inductance [H]
μ	relative permeability
μ_0	absolute permeability[H/m]
η	efficiency
η_c	efficiency after derating
ν	spatial harmonic order
P_{el}	electrical power [W]
P_{mech}	mechanical power [W]
P_{w}	windage and friction losses [W]
P_{iron}	iron losses [W]
P_{ed}	iron losses related to eddy currents [W]
P_{hy}	iron losses related to hysteresis [W]
P_{an}	anomalous iron losses [W]

P_{s}	stator joule losses [W]
P_{r}	rotor joule losses [W]
P_{SLL}	stray load losses [W]
P_{loss}	total power losses, covering all the losses [W]
$P_{\mathrm{h\_loss}}$	total amount of additional losses due to supply voltage distortion [W]
$P_{\mathrm{loss\_h}}$	additional losses due to supply voltage harmonic h [W]
$P_{\mathrm{h\_el}}$	additional harmonic electrical power [W]
$\mathbf{P}$	power loss matrix [W]
φ_h	harmonic phase angle of the voltage [degrees]
$\Phi(t)$	total Flux linkage [Volt-seconds]
R_s	stator electrical resistance [Ω]
R_r	rotor electrical resistance [Ω]
R_{cond}	thermal resistance due to conductivity [K/W]
R_{conv}	thermal resistance due to convection [K/W]
R_{th}	thermal resistance [K/W]
$\mathbf{R}$	thermal resistance matrix [K/W]
S	surface area [meters squared]
S_{sc}	short circuit power [VA]
s	slip value
T	average mechanical torque [Nm]
$T(x,t)$	instantaneous torque at position x and at time t [Nm]
Θ	absolute temperature [°C]
$\Delta\Theta$	temperature variations [K]
$\mathbf{\Delta\Theta}$	temperature distribution matrix [K]
τ_{temp}	thermal time constant [s^{-1}]
$u(t)$	instantaneous value of the voltage at time t [V]
$u_{\mathrm{h}}(t)$	instantaneous value of the voltage of order h at time t [V]
U_{RMS}	RMS value of the voltage [V]
$U_{\mathrm{RMS_h}}$	RMS value of the voltage of harmonic order h [V]
$U_{\mathrm{RMS_1}}$	RMS value of the fundamental voltage [V]
$U_{\mathrm{h\_RMS}}$	RMS voltage covering all higher order harmonic voltages [V]
U_{avg}	total averaged voltage [V]
$U_{\mathrm{h\_avg}}$	averaged value of the voltage including harmonics [V]
$u_{\mathrm{f\_x}}(t)$	instantaneous phase voltage of phase x [V]
$U_{\mathrm{L\_12}}$	RMS line to line voltage [V]
ω_{mech}	mechanical angular speed [rad/s]
ω	electrical pulsation [rad/s]
$\Omega_{\mathrm{s\_h}}$	Synchronous electrical rotational/angular speed of harmonic h [rpm]
Ω_{m}	Mechanical rotational/angular speed of the rotor [rpm]

X	electrical reactance, determined by both inductance and frequency [Ω]
X_{σ_h}	total leakage reactance at harmonic frequency [Ω]
X_m	total mutual reactance [Ω]
ξ	reduced height
γ	electrical conductivity [S]
Y	Similar to φ_h, the relative phase shift of 2 harmonics [degrees]
Z	complex impedance [Ω]

Nederlandse samenvatting

In de komende decennia wordt een globale stijging van de energiebehoefte voorspeld. Bijgevolg stimuleren economische en ecologische drijfveren het efficiënt gebruik van energie. Indien het huidig elektriciteitsverbruik in detail wordt geanalyseerd, kan opgemerkt worden dat globaal ongeveer 50% van de elektriciteit geleverd wordt voor elektromechanische energieconversie. Omwille van zijn lage productiekost, relatief hoge efficiëntie en zijn robuust karakter neemt de standaard kooianker inductiemachine het leeuwendeel van de elektromechanische energieconversie voor zijn rekening. De aankoopprijs van inductiemachines vormt slechts 1,5% tot 4% de totale Life Cycle Cost, de rest van de kosten bestaan voornamelijk uit energiekosten ($\pm$ 98%) en onderhoudskosten ($\pm$ 1%).[2] Hieruit volgt dat de efficiëntie van inductiemachines een belangrijke investeringsparameter vormt. Daardoor wordt er zowel op academisch als industrieel niveau massaal onderzoek verricht naar de optimalisatie van de energie-efficiëntie van dergelijke inductiemachines. Het omzetten van energie resulteert altijd in een bepaald verlies. De efficiëntie η van eender welk systeem kan bepaald worden op basis van de benodigde input voor een bepaalde gewenste output. In het specifieke geval van een inductiemotor is de input de hoeveelheid elektrische energie P_{el}, de gewenste output een bepaald mechanisch vermogen P_{mech} en de efficiëntie is de verhouding:

$$\eta = \frac{P_{\mathrm{mech}}}{P_{\mathrm{el}}} \tag{1}$$

Desondanks de vele voordelen van een inductiemachine, ligt het toerental van een kooiankermachine inherent vast door de constructie en de voedingsfrequentie. Gezien pomp-, ventilatie- of positioneersystemen vaak een mechanisch variabel toerental vereisen wordt dit euvel meestal opgelost door het gebruik van vermogenelektronische omvormers. Daarnaast worden massaal vermogenelektronische omvormers gebruikt voor bijvoorbeeld algemene automatisering, aansturing van verlichting, speciale elektromotoren, IT toestellen of voor de productie van DC spanning in elektrolyse of vlamboogovens. Het gebruik van vermogenelektronische omvormers zorgt vaak voor een vervorming of vervuiling van de aanwezige netspanning. Deze spanningsvervorming zorgt op zijn beurt voor extra verliezen en dus een daling van het rendement in machines

[2] CET Motoren Seminarie: *"Zin en onzin van hoog rendement bij aandrijvingen"*,7/10/2010, Howest-Kortrijk

die rechtstreeks gekoppeld zijn op het elektriciteitsnet. De extra verliezen zorgen niet alleen voor een stijgende energiekost, maar vanuit technisch oogpunt zorgen deze verliezen ook voor een extra opwarming van de machine. Aangezien te hoge temperaturen in de machine kunnen leiden tot een vervroegd statorfalen dient men in geval van extreme spanningsvervorming machines te overdimensioneren (ook wel derating genoemd).

De aangehaalde problemen van efficiëntiedaling en bijhorende opwarming van inductiemotoren ten gevolge van een vervormde spanning werden reeds uitvoerig besproken in wetenschappelijke literatuur. Echter vormt de inductiemachine in specifieke toepassingen ook een ideale machine om mechanische energie om te zetten naar elektrische energie. Inductiegeneratoren worden ingezet in zowel warmtekrachtkoppelingen, kleine windturbines of (nood)stroomaggregaten. Daar waar inductiegeneratoren rechtstreeks op het net gekoppeld worden, dient de invloed van netspanningsvervorming op inductiegeneratoren geëvalueerd te worden. Op basis van een nauwgezette analyse van de huidige literatuur kan gesteld worden dat dergelijke problematiek tot op heden nog niet fundamenteel werd aangehaald binnen wetenschappelijke studies.

De stijgende vraag naar efficiënte energieomzetting heeft geresulteerd in een aangepast design van standaard inductiemachines. Zo kan men permanente magneten integreren in de rotor van de machine. Op deze manier dient de magnetiseringsenergie voor de rotor niet meer door het net geleverd te worden en stijgt de totale energie-efficiëntie van de machine. Speciale aanpassingen aan de rotor zorgen ervoor dat de machine kan aanlopen op de netfrequentie (Line Start) en éénmaal op toeren neemt het magnetisch veld van de Permanente Magneten (PM) over. Deze machine wordt dan ook aangeduid als een Line Start Permanent Magneet Machine of LSPMM. Indien deze machine binnen afzienbare termijn de standaard inductiemotor zou vervangen, is het essentieel om ook de invloed van de aanwezige spanningsvervorming op zijn verliezen te analyseren. Dit blijkt tevens een hiaat binnen de huidige wetenschappelijke literatuur.

Hoofdstuk 1 start met het schetsen van de rode draad doorheen het doctoraat. De huidige innovaties en trends om de energie-efficiëntie van elektrische machines te verhogen worden kort aangehaald. Gezien de grote industriële relevantie van de standaard kooianker inductiemachine heeft dit geleid tot een uniformisering en standaardisering omtrent de bepaling van zijn efficiëntie. Daarnaast worden binnen Hoofdstuk 1 eveneens kort de meest courante Power Quality parameters aangehaald, evenals de technische implicaties van verscheidene Power Quality fenomenen op de correcte werking van inductiemotoren. Echter, om de effecten van spanningsvervorming op machines correct te kunnen verklaren is een meer gefundeerde analyse nodig van de verliezen die optreden in standaard inductiemachines.

Hoofdstuk 2 beschrijft de verschillende verliesmechanismen in een inductiemachine in sinusregime, evenals de technische evoluties ten einde

deze verliezen te reduceren. De invloed van de spanningsvervorming op inductiemachines is niet enkel functie van de machine, maar logischerwijs is de aanwezige mate van vervorming essentieel in een verliesanalyse. Hoofdstuk 3 bespreekt in detail de verschillende mechanismen die resulteren in een vervorming van de spanning aan de klemmen van de eindverbruiker. In Hoofdstuk 3 wordt gepoogd een limiet voorop te stellen van de maximale spanningsvervorming. De resulterende spanningsvervorming kan ten dele geëlimineerd worden door het plaatsen van filtersystemen, bijgevolg wordt in Hoofdstuk 3 de invloed van filtersystemen op de resulterende spanningskwaliteit geanalyseerd voor drie industriële sites.

Hoofdstuk 4 van dit werk vormt een eerste essentieel hoofdstuk met een relevante onderzoeksbijdrage omtrent de invloed van de aanwezige netvervorming op de energie-efficiëntie van inductiemotoren. De bestaande wiskundige motormodellen die deze extra verliezen proberen te voorspellen worden in Hoofdstuk 4 gevalideerd met metingen. Daarnaast wordt via thermisch modeleren de extra temperatuurstijging ten gevolge van deze spanningsvervorming in kaart gebracht voor de verschillende machineonderdelen. Aangezien de inductiegenerator constructief dezelfde machine is als de inductiemotor, lijkt het plausibel om de harmonische motormodellen te extrapoleren naar inductiegeneratoren. Hoofdstuk 5 toont aan dat, omwille van verzadiging, de bestaande motormodellen niet rechtstreeks extrapoleerbaar zijn voor inductiegeneratoren. Daarnaast zorgt generatorwerking voor bijkomende moeilijkheden om het extra verlies uniform en nauwkeurig te bepalen.

Hoofdstuk 6 bespreekt de LSPMM, dit zowel naar constructie, efficiëntie bij sinusvormig regime, als de extra verliezen ten gevolge van de spanningsvervorming. Aangezien de LSPMM constructief nauw verbonden is met de standaard inductiemachine, lijkt het opportuun om de harmonische motormodellen te projecteren op de LSPMM. Naast de mogelijke verzadiging van dergelijke machines, zorgt de synchronisatie tussen het magnetisch draaiveld in de stator en de mechanische snelheid van de rotor voor bijkomende problemen.

In Hoofdstuk 7 worden de belangrijkste conclusies nogmaals aangehaald en worden deze in een breder perspectief geplaatst. Alhoewel het voorgelegde werk een afgerond geheel poogt te presenteren zal blijken dat het onderzoek omtrent de interactie tussen spanningsvervorming en inductiemachines heel wat nieuwe en bijkomende onderzoeksmogelijheden biedt. Zeker gezien de stijgende relevantie van decentrale energieproductie, verdient de invloed van spanningsvervorming op inductiegeneratoren extra aandacht.

English summary

Due to both economic and ecological incentives, has energy become a scarce product. According to the International Energy Agency [IEA], approximately 50% of all generated electrical power is consumed by Induction Machines (IM) for electromechanical energy conversion. Squirrel Cage IM (SCIM) have several advantages in respect to other electric motors such as the low production cost, the abcense of brushes, line start capability and the general robustness. The initial purchase cost of an IM only accounts for approximately 1,5% to 4% of its total Life Cycle Cost (LCC). Maintance costs only are a fraction of the LCC (1%) and the energy costs accounts up to 98% of the LCC. Consequently the efficiency of the machine represents an important investment parameter. A lot of research has been executed in both industrial and academic institutions in order to increase the efficiency of these machines. Converting energy always results in additional losses. The efficiency η of any system can be evaluated by the amount of input for a certain desired output. In case of an IM the input is the amount of electrical input power P_{el}, the desired output is the mechanical power P_{mech} and the efficiency is the ratio of output to input power:

$$\eta = \frac{P_{\mathrm{mech}}}{P_{\mathrm{el}}} \tag{2}$$

SCIM have one major disadvantage: the mechanical speed of the machine is directly coupled to the frequency of the supply voltage. This limits its flexibility when supplied directly from the grid. Advances in Power Electronic (PE) energy conversion have resulted in Variable Speed Drives (VSD) for IM. Although the usage of VSD can adjust the supply frequency, only 25% of the currently installed machines are supplied from a VSD. PE can result in a general optimization of electrical equipment, other practical examples of power electronic controlled energy conversion are dimmable halogen lighting, low and high pressurized discharge lights etc. Additional to the advantages of PE in terms of energy optimization, a lot of PE is also used as rectifiers in for example IT equipment, DC arc furnaces or electrolysis.

AC/DC converters are generally built with passive components. Inherently to the operation of diodes the discretization of current results in a discontinuous current wave shape. This wave shape differs from an ideal sinusoidal wave shape and results in additional losses in the power grid. As this current flows in the feeder, this also results in a nonsinusoidal voltage drop over the present grid impedance. Consequently the massive integration of PE distorts the supply voltage

at end-user. Subsequently does the distortion of the supply voltage inversely affect the efficiency of Direct On-Line (DOL) IM and the increased losses directly imply an increased operating temperature. Excessive operating temperatures should be avoided as excessive temperatures generally reduce the life expectancy of stator winding insulation. The effect of supply voltage distortion on the overall losses is already well discussed in scientific literature.

Both consumption and electrical generation should also be performed with the highest possible efficiency and overall yield. The rise of decentralized production such as small wind, hydro or combined heat power resulted in an increased interest towards Induction Generators (IG). Anomalies in the supply voltage will probably also affect the operation and efficiency of IG systems, however a detailed literature review indicated a large research gap within this specific domain.

The efficiency of the standard IM is practically limited. This is due to the fact that the magnetization of the rotor has to be delivered through the stator. The integration of Permanent Magnets (PM) is one way to tackle the problem. However, if the motor would consist of only PM, the motor would be unable to start up at line frequency. The combination of PM and a standard SCIM rotor cage results in a machine which is able to start up as a standard IM and once near synchronism, the PM can synchronize with the magnetic field in the stator. This machine is commonly referred to as a Line Start Permanent Magnet Motor (LSPMM). If LSPMM are to become an actual substitute for standard IM, the influence of voltage anomalies on their overall energy efficiency should be evaluated. To the author's knowledge no studies have been executed concerning the influence of supply voltage distortion on LSPMM efficiency.

Chapter 1 presents a global introduction to this dissertation. A lot of effort is currently done to increase the efficiency of IM and the state-of-the-art innovations and trends are elucidated in Chapter 1. Due to the large interest of industrial costumers towards SCIM, some industrial normative references specifically related to IM are listed. Chapter 1 also presents a general overview of the most significant Power Quality parameters and the effects of these Power Quality parameters on the operation of IM. However, in order to be able to accurately explain the measured effects, a more detailed assessment concerning the loss mechanisms and the resulting energy efficiency in case of non distorted supply voltage of IM is needed.

Chapter 2 presents the fundamental loss segregation of a standard IM, as does it hint towards the possibilities to reduce the losses. However, the effect of supply voltage distortion is not only function of the geometry of the machine, but it is obvious that the effect is also related to the magnitude of the distortion. Chapter 3 elucidates on the complex mechanisms resulting in voltage distortion at end-user, and consequently concludes by proposing the extreme limits concerning the amount of distortion. As harmonic filtering can positively affect the voltage quality at end-user, this has also been validated at three individual industrial sites.

Chapter 4 presents one of the essential chapters of this research as it illustrates the effect of supply voltage distortion on the energy efficiency of IM. The existing mathematical harmonic motor models, which enable estimations of the additional losses, are validated by measurements throughout Chapter 4. Knowledge of these losses can then be combined with a thermal motor model in order to estimate the maximal temperature rise of the different motor parts. Although IM and IG are physically the same machine, the saturation will not enable the straightforward implementation of harmonic motor models. The results given in Chapter 5 will illustrate that the adaptation of harmonic motor models are insufficient to estimate the effect of harmonic distortion on the energy efficiency of IG.

Chapter 6 starts with the fundamental loss segregation of these LSPMM. However, if the LSPMM has to become the next evolutionary step of IM, the influence of supply voltage distortion on LSPMM should be evaluated. LSPMM closely relate to IM, they share identical stator winding layout, apart for the PM a fairly similar rotor construction is noticed and both machines are built accordingly. Consequently, at first sight, straightforward adaptation of the harmonic loss mechanisms for IM to LSPMM seems to be appropriate. In Chapter 6 it will be elucidated that both the possible saturation as the perfect synchronous operation of the magnetic field in the stator and the mechanical speed of the rotor does highly increase the evaluation of the influence of supply voltage distortion in relation to LSPMM efficiency.

Chapter 7 not only rounds up the general conclusions of this research, it also tries to present them within the wider scope of energy efficiency and energy savings. Although the presented research should be a coherent study, the research will unveil a significant potential towards future research. Specifically the rise of decentralized energy production triggers a large amount of questions towards the effect of supply voltage distortion on the energy efficiency of IG.

1 Introduction

1.1 The induction machine

The presented research will evaluate the influence of distortion of the supply voltage on the energy efficiency of Induction Machines (IM). Before a detailed analysis can be presented some essential background knowledge concerning both IM and power quality phenomena are presented in respectively §1.1 and §1.3. The concept of copper wound IM has been introduced by G. Ferraris and N. Tesla between 1885-1888. SCIM have been introduced by M. Dolivo-Dobrovolsky in 1889. Because alternating current (AC) was easily transformed in voltage level by the use of a static transformer, AC was already generally adopted for power transportation. IM have several advantages to other motor types. It has inherent line start capability combined with reasonable high starting torques. Secondly, the absence of collector and brushes in standard SCIM increases the robustness of the machine. These advantages combined with the presence of AC supply voltage has led to the wide spread use of IM as means of electromechanical conversion. Currently, almost 50% of the global electrical energy and 70% of the industry related electrical power consumption is allocated for electromechanical energy conversion. About 90% of this power is converted by SCIM [1–3].

However, to this day the initial design methods of an IM have not been changed radically. When designing an IM two important criteria should be met, starting with the mechanical design, or the desired output such as mechanical speed or torque. Because up to 50% of motor failures are caused by bearing faillure [4], specific attention during the design process is placed in both

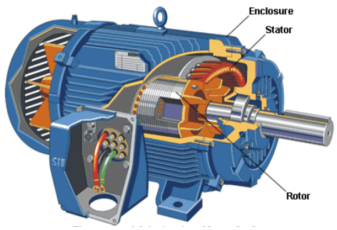

Figure 1.1: Induction machine (courtesy of Siemens)

correct implementation of bearings and possible predictive bearing maintenance. Secondly, the thermal design has to be taken into account. This is highly intertwined with the electrical design and the energy efficiency of the machine. Correct thermal design prohibits excessive temperature rise in motor components. Motor temperatures above the design limits result in an acceleration of the oxidation process in insulation materials, which eventually leads to loss of dielectrical properties. As stator winding failure is the second main cause of motor failure, accounting for 16% of all IM failure, excessive losses should be avoided [4].

The initial purchase cost of an IM only accounts for approximately 1,5% to 4% of its total Life Cycle Cost (LCC). Maintance costs only are a fraction of the LCC (1%) and the energy costs accounts up to 98% of the LCC. Due to the high volumes of IM sold, and the huge power consumption linked to IM, the industry aims for ever increasing efficiency of IM. Although Chapter 2 does present a more detailed, theoretical and segregated loss analysis of the SCIM, the major trends in terms of innovative motor design are addressed in §1.1.1 to §1.1.3. An energy efficient machine dissipates less power, which does not only reduce the power consumption and its operating cost, but also implies a direct decrease of the operating temperature in the different areas of the motor [5].

Due to its industrial relevance, there is a high level of standardization related to IM. This does not only result in a uniform product which enables low production cost, the standardization should also result in a high level of interchangeability. This is of the utmost importance for industrial costumers for whom a downtime is generally linked to high costs in terms of maintenance costs and production loss. Paragraph 1.2 addresses the IEC norms linked to IM which are of specific interest within the presented research.

1.1.1 Copper rotor technology

If the energy efficiency of the IM is to be increased, a wide variety of adjustments is possible. In order to maintain an economic benefit, it is obvious that the

largest savings can be allocated with the largest loss components. As more than 50% of the loss is generally generated as Joule losses in both rotor and stator, it seems logical that improvements within this area have a significant impact on the overall energy efficiency. In Figure 1.2 the relative influence of design adjustments towards IM efficiency are listed.

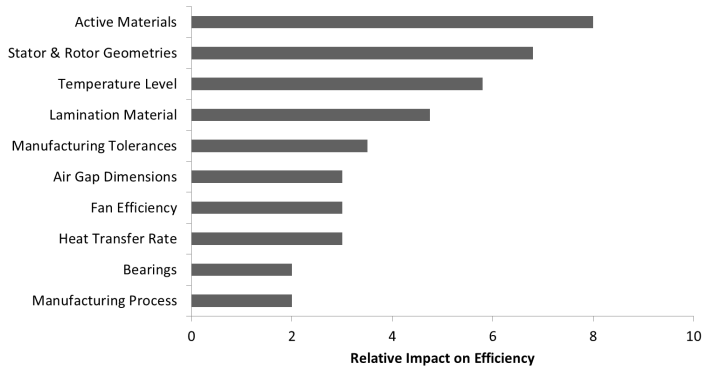

Figure 1.2: Impact of the possible areas for improving the motor performance [6]

In order to reduce stator Joule losses both stator RMS current and the stator resistance can be reduced. Reducing the total RMS current is an effective way to reduce the total stator Joule losses as these losses are proportional to the square of the current. Reducing the stator current can be achieved by reducing either rotor or magnetizing current. Another option is to reduce the stator windings resistance for example by cooling them more effectively, as is obtained in cryogenic cooled motors. However, these machines are specifically designed motors and are not considered within this research.

Rotors are generally constructed by high pressurized die casted aluminum bars, because of the reduced price. In order to further reduce the Joule losses, copper can be used as rotor bar material [6, 7]. Studies suggest that implementation of copper rotor technology can reduce the overall losses by approximately 20% to 25%. If copper rotor bars are to be inserted on the rotor, two construction methods are generally used. The first method is using a prefabricated rotor bar construction, forcing the bars into the lamination stack of the rotor and finally welding the end rings. The other fabrication method is using die cast methods similar to the fabrication of aluminum rotors.

In case of a prefabricated copper rotor, the difficult welding of copper is the major setback. Additionally, the prefabricated rotor bars should be accurately fitted in the rotor slots. The mechanical fitting can result in minor air inclusions which largely increase local thermal resistance from rotor bar to rotor back iron.

(a) *(b)*

Figure 1.3: Fabrication of copper rotors:(a)-welding,(b)-die casting

If the die cast manufacturing process is evaluated, the high die cast temperature of copper $1093°\mathrm{C}$, in comparison with $648°\mathrm{C}$ for aluminum, results in technical and economic limitations. The high temperature can cause thermal stress and fatigue in the rotor lamination steel. The higher initial temperature also results in a faster thermal gradient in case of copper and this limits the die cast time. The technical constraints increase production difficulty and a compromise should be made between the lower losses versus the higher initial cost. When the economical validity of copper rotor technology is evaluated, the additional cost is only recovered if the motor has sufficient operation hours. In terms of iron losses, focus is placed on material design to achieve low loss lamination iron. New technologies also suggest the use of amorph iron to significantly reduce iron losses. However, production of amorph iron and integration in the frame is still expensive compared to standard lamination steel.

1.1.2 Line start permanent magnet machines

The main drawback of the SCIM is that the excitation for the whole magnetic circuit needs to be externally delivered by the power supply, thus leading to inevitable additional losses. The use of Permanent Magnets (PM) in the rotor is the most commonly used way to tackle the problem. However, simple PM motors are unable to start at line frequency and additional startup methods are required [8]. The use of VSD is one way to achieve sufficient startup torque. However, if line start capability is essential, rotor bars can be inserted. This allows the motor to startup as an IM and once near synchronism the flux created by the rotor PMs can synchronize with the stator flux. In this way, the machine combines the advantages of both induction and PM machines. This machine is commonly known as a Line Start Permanent Magnet Machine (LSPMM) [5].

In the last decade LSPMMs have evolved from fractional horsepower, single-phase motors [9] into mature commercial three-phase machines in a power range up to 7.5 kW. [10–13]. The fundamental losses of an LSPMM are fully elaborated in Chapter 6.

(a) Rotor configuration of a LSPMM *(b) Rotor Mounted PM*

Figure 1.4: Design aspects of LSPMM (courtesy of WEG)

1.1.3 Synchronous reluctance machines

Next to the LSPMM one of the promising designs is the Synchronous Reluctance Machine (SynRM), introduced by ABB. In both machines there is a significant difference between the direct inductance L_d and the quadrature inductance L_q. This saliency enables both machines to operate at synchronous speed. However, the large difference between L_d and L_q prohibits DOL startup. In case of SynRM the use of a VSD is mandatory, while for LSPMM one of the design criteria was to enable DOL start. Consequently a squirrel cage was added to enable the startup as a SCIM.

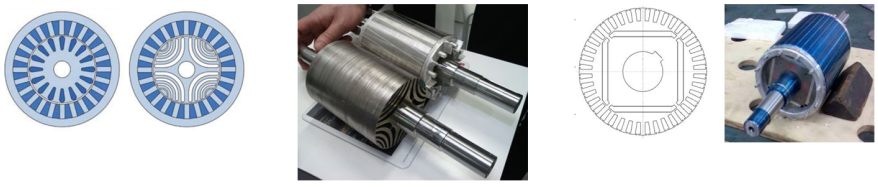

[A] [B] [C] [D] [E]

Figure 1.5: Rotor Geometry for an IM[A], synRM[B][C] and LSPMM[D][E]

1.2 Standards related to Induction Machines

Due to the large amount of units sold, industry requested a high level of standardization in relation to IM. The International Electrotechnical Commission [IEC] strives towards a high level of standardization in the general field of electrotechnical engineering. Specifically for industrial drive applications is the IEC 60034 of interest. Within the IEC 60034 there are a lot of subcategories and the most relevant IEC standards related to this dissertation are briefly addressed in the subsequent paragraphs. IEC standards are generally valid, however, depending on the location national institutions can impose more specific standards. Europe generally follows the IEC recommendations, transforming the IEC references to

EN references. North America uses a different set of standards. The National Electrical Manufactures Association published the industrial reference NEMA MG1, which also specifically relates to IM. From a more academic perspective the IEEE standards are often cited (IEEE-112 series).

1.2.1 IEC60034-7: Frame sizes

The demand for ever increasingly efficient electromechanical energy conversion has resulted in multiple innovative designs of electrical machines. As these machines are to become a substitute for standard SCIM, a lot of effort is also done to build these machines still complying to the standard frame sizes as defined in IEC60034-7 [14]. This research will specifically address Totally Enclosed Fan Cooled Squirrel Cage Induction Motors (TEFC SCIM), as these are generally used in Europe. In North America open drip proof motors are often implemented, but these types of machines are not taken into consideration.

(a) Front Frame dimensions *(b) Side Frame Dimension*

Figure 1.6: Frame Dimensions according to IEC60034-7

	Main dimensions													
Type	A	AB	B	BB	C	x	AA	K	HA	H	AC	HD	LB	LB1[1]
FLS 80 L	125	157	100	130	50	20	32	9	11	80	170	231	216	178
FLS 90 S	140	170	100	162	37	27	26	9	10	90	185	251	251	225
FLS 90 L	140	170	125	162	52	27	26	9	10	90	185	251	251	225
FLS 100 L	160	196	140	185	63	29	40	12	12	100	204	258	300	253
FLS 100 LK	160	200	140	174	63	22	42	12	12	100	226	288	323	276
FLS 112 M	190	230	140	185	70	32	48	12	12	112	231	294	309	265
FLS 132 S	216	255	140	240	89	50	63	12	16	132	264	347	385	330
FLS 132 M	216	255	178	240	89	50	63	12	16	132	264	347	385	330
FLS 132 MU	216	255	178	240	89	50	63	12	16	132	264	347	412	351
FLS 160 M	254	294	210	294	108	20	65	14	20	160	310	440	495	435
FLS 160 L	254	294	254	294	108	20	65	14	20	160	310	440	495	435
FLS 180 MR	279	324	241	295	121	25	80	14	25	180	310	460	515	450
FLS 180 L	279	330	279	335	121	28	70	14	28	180	350	481	555	480
FLS 200 L	318	374	305	361	133	28	80	18	44	200	394	530	681	595

Figure 1.7: Frame dimensions according to the IEC60034-7

1.2.2 IEC60034-2-1: Measuring efficiency

When evaluating the efficiency of machines several standards have been established in order to be able to compare machine efficiencies. In North-America

the IEEE 112 [15] is favored, while in Europe the IEC 60034-2-1 is used [16]. Although two different standards, the content is nearly similar.

When obtaining the efficiency of IM, two different techniques are used, each with its own advantages and drawbacks. The first technique is the basic input-output technique, also referred to as the raw efficiency measurement or the direct measurement as elaborated in §1.2.2.1. The second technique is indirect efficiency measurement by loss segregation, which is presented in §1.2.2.2. The individual losses are measured, some additional losses are taken into account and the overall efficiency is determined based on the calculated full-load losses.

1.2.2.1 Direct measurement technique

The direct measurement technique implies basic measurement of input and output power. In case of motor operation the input power is supplied by the utility grid and can be obtained by:

$$P_{\mathrm{el}} = 3.I_{\mathrm{RMS}}.U_{\mathrm{RMS}}.\mathrm{PF} \tag{1.1}$$

with I_{RMS} is the RMS value of the phase current, U_{RMS} the RMS value of the phase voltage and PF is the power factor. Subsequently, the output power can be obtained using:

$$P_{\mathrm{mech}} = \omega_{\mathrm{mech}}.T \tag{1.2}$$

where ω_{mech} represents the mechanical speed [rad/s] and T is the averaged output torque [Nm]. The resulting efficiency is the ratio of output over input power. The accuracy of the obtained efficiency is determined by the accuracy of the measurement of the individual quantities. The IEC 60034-2-1 clearly states both the measurement procedure and the required measurement accuracy of the different quantities. These accuracy levels are presented in Table 1.1.

Table 1.1: Minimum measurement accuracy according to IEC 60034-2-1

Quantity	Accuracy	
Electrical	0.2%	IEC 60051
Transformers	0.5%	IEC 60044-1
Torque	0.2% FS	IEC 60051
Speed	0.1% or 1 rpm	

1.2.2.2 Indirect measurement technique

If the indirect method is used, the windage and friction losses (P_{w}) and magnetizing/iron losses (P_{iron}) are measured during a no-load test under reduced supply voltage conditions. The stator Joule losses (P_{s}) are calculated by measuring both the nominal load current and the stator resistance at nominal operating

temperature. The rotor losses P_{r} are estimated based on the rotor resistance and are measured under reduced supply voltage and with short circuited rotor (locked rotor with slip equal to 1). The Stray Load Losses P_{SLL} are estimated in function of the output power, which can be approximated at 0.5% of the nominal input power. Detailled analysis of the individual losses is presented in Chapter 2. Summation of all these losses results in the total loss P_{loss}, and in combination with the measured electrical input power P_{el} the efficiency can be determined according to:

$$\eta = \frac{P_{\mathrm{mech}}}{P_{\mathrm{el}}} \tag{1.3}$$

$$= \frac{P_{\mathrm{el}} - P_{\mathrm{loss}}}{P_{\mathrm{el}}} \tag{1.4}$$

The advantage of this method is that all the losses are measured individually, resulting in correct estimation of the losses. The practical test setup only needs an accurate electrical measurement device and a variable sine wave supply voltage. The need for an expensive torque measurement is eliminated.

1.2.2.3 Comparison of the direct and the indirect measurement method

There are plenty of standards and studies available which focus on the actual measurement procedures [2, 17–20]. However, within the presented dissertation it is important to accurately measure the efficiency of the machines, in both pure sine wave condition and supplied from a distorted power supply. Therefore a comparison between both measurement techniques should be performed. The discussions of the above question date as far back as 1912. Reference [21] provides a comparison of input-output (direct method) and the loss segregation method using a number of test results. Historically the main drawback of the direct measurement method was the absence of accurate torque sensing equipment combined with the high complexity of controlling the generator/load. In contrast to the direct measurement does the indirect measurement estimate the additional losses. The estimation guidelines to obtain the actual additional losses, has proven to be its main drawback. In [22] a comparison between the indirect and the direct measurement is presented based on a statistical analysis of approximately 1000 IM, in a power range from 750W to 250kW. In this study, the indirect measurement is used as the reference and the findings of the analysis are that the direct method efficiency may be up to 1.26% higher or up to 1.86% points lower than the values obtained by the indirect method. Some of the other conclusions from this research are:

- the spread of the efficiency is unacceptable if the results are to be used for economical calculations
- in order to uniformly address the efficiency for nameplate efficiency reporting, the indirect method presents the most accurate results for comparison studies.

- with increasing efficiency the discrepancies between the two methods reduce. For higher power ratings of machines (above 200 hp or 150kW), the increased accuracy of both the torque measurement in the direct method as the estimation of the additional losses in the indirect method result in a reduced deviation between the two methods.

The previous indicates that the indirect method is most suitable to evaluate the efficiency of IM in the evaluated power range. However, the indirect measurement technique adds some difficulties if this is used to evaluate the additional losses in IM caused by supply voltage distortion as within the indirect measurement method a sine wave supply voltage is mandatory. IEC 60034-2-3 presents a method based only on electrical quantities to evaluate the additional losses generated inside the IM by a VSD. In Chapter 4 minor modifications to this test procedure will be presented which allow to evaluate the additional losses caused by supply voltage with high accuracy. Consequently, these additional losses can be integrated into the indirect measurement method according to IEC 60034-2-1.

Although the proposed method in Chapter 4 will enable accurate evaluation of the additional losses in case of motor operation, it will be illustrated in Chapter 6 that this method is prohibited for LSPMM. When evaluating the losses in an LSPMM the indirect measurement method is prohibited due to technical aspects. The reduced voltage tests are not applicable because the flux of PM will result in excessive stator currents. Synchronous operation prohibits the use of the short circuit test. A detailed analysis of the limitations of the indirect measurement method according to the IEC 60034-2-1 with respect to LSPMM is presented in [5].

Although §1.2.2.4 will suggest other measurement techniques, practical constraints such as time and accuracy of the results will result in discarding these methodologies. Consequently, to uniformly test both IM, IG as LSPMM in both sine wave and distorted supply voltage conditions, the direct measurement technique has been used as a reference in this research.

1.2.2.4 Additional measurement techniques

Additional direct measurement techniques are the back-to-back measurement setup or the caloric method. In back-to-back measurements two identical machines are coupled mechanically. One machine operates as a motor and the second machine is operating as a generator. Only electrical quantities are measured, and the efficiency is measured by calculating the total efficiency of the setup and dividing the losses by two in order to obtain the efficiency of one machine. Although this techniques is very interesting due to its simplicity and high measurement accuracy, it is not applicable in this research, because the

efficiency of the IM and the IG is not identical. Additionally, as will be addressed in Chapter 5, the influence of voltage distortion on IM and IG is totally different.

In the caloric measurement technique, the losses are measured while cooling the machine with fluid, generally air or water. Identical conditions are maintained until the fluid reaches a steady state temperature. The total temperature rise indicates the additional losses. Although this technique is a highly accurate technique -accuracies less than 1W can be achieved- due to the large time frame for one measurement, this technique is not applicable within this research. Results presented in [23] indicate that, without preheated systems the measurement period is approximately 16 hours for 37kW IM. If a preheater is used, the time frame per measurement point can be reduced to approximately 5h. Measurements were performed on the efficiency of a 11kW 1500 rpm SRM motor, with water jacket cooling. Additionally this measurement indicated that, if caloric measurements are to be executed at thermal steady state, a time frame per measurement point of more than 7 hours is required. These time frames well exceed the limit of practicality, as a large number of data is to be presented.

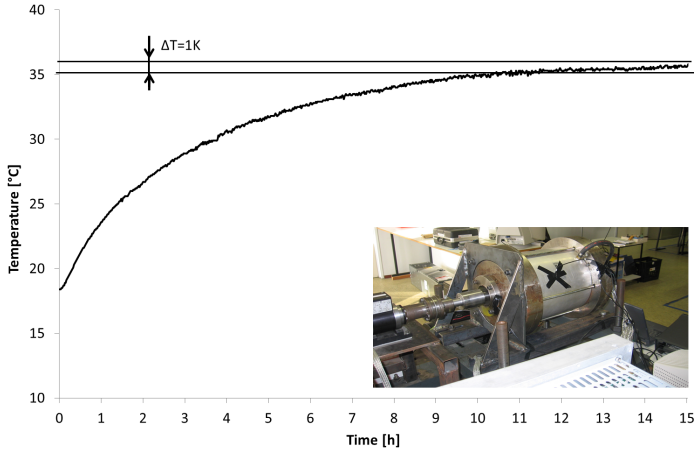

Figure 1.8: Thermal steady state time frame of a water cooled 11kW SRM at 1500 rpm

1.2.2.5 Used measurement procedure and equipment

In this paragraph the used test setup will be briefly addressed. Two specific test setups have been built which are used to validate the theoretical assumptions proposed during the research. The first test setup enables testing of small scale machines up to 22kW. A second test setup enables testing of machines up to 132kW (@1500 rpm).

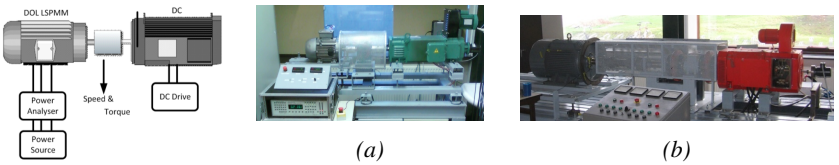

(a) *(b)*

Figure 1.9: Test setup for 4kW [a] and 55kW [b] machines

1.2.2.6 Power source

The focus of this research is to evaluate the energy efficiency of IM, both operated as motor and as generator, and LSPMM in relation to voltage distortion. Consequently, the supply voltage should be programmable. Two power sources are available:

- for 4kW and 11kW motors, the voltage is controlled is by a programmable power source with a rated power of 15kVA. This power source has a PWM IGBT output fitted with an low-pass filter. This source is unable to simultaneously control the output voltage and dissipate the power in case of generator operation.
- For 55kW machines and generator testing, the supply is delivered by a 240kVA programmable power source. Generator operation implies that the power supply has to be able to simultaneously control the voltage and dissipate the generated power. The used programmable power source consists of three single phase class A amplifiers of 80kVA per phase. The DC link consists of a DC capacitor link, with a 30 % dissipation possibility. The dissipation is done by dissipation resistors and this enables testing of generator systems to 80kW in a continuous regime. In transient regime higher power ratios can be dissipated within very limited timeframes.

1.2.2.7 Efficiency measurements

The efficiency is measured according to IEC 60034-2-1 using the direct method [16]. For the measurement of the electrical input power P_{el}, a calibrated PM3000A-Voltech power analyzer is used. In case of both 4kW and 11kW machines, current is directly measured over the internal shunt with a current range of $30A_{\mathrm{peak}}$. For the 55kW machines external Current Transformers (CT) were used. These CT have a reduced accuracy of 0.5% full scale. Both the minimal limits as stated in [16] as the accuracy levels of the used equipment in the actual test setup are listed in Table 1.2. Several additional aspects such as linearity, the influence of torque ripple or operating temperature have a significant influence on the torque measurement output. Subsequently, the use of additional CT and Analog to Digital Converters also affect the accuracy of the measurement. A detailed accuracy analysis of both test setups is presented in Appendix 1.

Table 1.2: Measurement accuracy

Quantity	IEC 60034-2-1	Test setup 4kW/11kW	Test setup 55kW
Electrical	0.2%	0.1%	0.1%
Transformers	0.5%	-	0.5%
Torque	0.2% Full Scale	0.1 % Full Scale	0.14 % Full Scale
Speed	0.1% or 1 rpm	1 rpm	1 rpm
Temperature	1 K	0.14 K	-

1.2.3 IEC60034-30: Efficiency classification

If the total cost of ownership of an IM is evaluated, the initial cost to buy the machine only accounts for approximately 2% of the total cost. The remaining cost is mainly determined by the electrical power consumption. Consequently, in addition to technical incentives economical incentives also push to increase the energy efficieny of the IM. Because the large amount of units installed yearly, several standards categorize IM into energy efficiency classifications. In order to uniform the efficiency of IM, the IEC has introduced a classification system (IEC 60034-30) which categorizes the efficiency of IM from IE1 up to IE4 [Table.1.3]. Motors with an efficiency lower than IE1 are categorized as IE0 and, although not yet approved by the IEC, there are already suggestions to propose the IE5 class.

Table 1.3: Rated efficiency levels for commercial 50-Hz, 4-pole IM up to 7,5 kW from IE1- to IE4-class limits defined in IEC60034-30/31

Frame size	80	L90S	90L	100L	100L	112M	132S	132M
P_{mech}[kW]	0.75	1.1	1.5	2.2	3	4	5.5	7.5
IEC IE4	85.6	87.4	88.1	89.7	90.3	90.9	92.1	92.6
IEC IE3	84.0	85.3	86.3	87.5	88.4	89.2	90	90.8
IEC IE2	81.1	82.7	83.9	85.3	86.3	87.3	88.2	89.1
IEC IE1	72.1	75	77.2	79.7	81.5	83.1	84.7	86.0
IEC IE0								

The nameplate of the motors used within this dissertation still make reference to the old CEMEP classification in which the EFF2 motor roughly corresponds to an IE1 efficiency and the EFF1 class relates to an IE2 motor. Consequently, the motors are still referred to the original nameplate efficiency and thus the CEMEP classification. Although the latter of this research often refers to both older CEMEP as these new IEC efficiency levels, a large amount of studies and publications can be cited which relate specifically to this subject.

1.3 Power quality

1.3.1 Supply voltage anomalies

The supply voltage delivered throughout the public grid is assumed to be 50Hz, uninterrupted, three phase and equally balanced, sine wave supply voltage of constant magnitude. Every deviation of these conditions can be categorized under the main term ”supply voltage anomalies”. For a large amount of industrial costumers the continuous presence of supply voltage is essential for the continuous operation of their production processes. A long term of absence of supply voltage is addressed as a blackout, and long term of highly reduced supply voltage (less than 10% of the nominal voltage) is referred to as a brownout. However, even very small but severe voltage drops can inversly affect the correct operation of electrical equipment. These events, in which the supply voltage reduces between 10% and 90% of the nominal voltage in a timeframe from 10ms up to 1 minute, are addressed as voltage dips. If the voltage deviation is very fast, order of microseconds but always lower than 10ms, these effects are referred to as transients. The previously stated voltage variations generally result in accute problems as these effects can imply an instant abruption of normal operation or in severe cases even equipement failure. Although this subject is highly interesting from an industrial/economical perspective, this dissertation will not futher elaborate on these topics.

A second major topic of interest is what often is regarded as a more dormant problem. If the supply voltage is not equally balanced over the three phases, this results in supply voltage unbalance. IMs are very susceptible to voltage unbalance, as this generally results in excessive losses and consequently high temperatures in the machine. If the supply voltage is no longer pure sinusoidal this can be addressed as flicker (with oscillation periods longer than the fundamental frequency) and harmonic voltage distortion (oscillation periods smaller than the fundamental frequency). The previous effects generally do not result in an instantaneous malfunction of electrical equipment, but cause excessive losses and consequently a reduced life expectancy and an increased operational cost. Although the effect of supply voltage unbalance on IM has been researched extensively, there is still a vast amount of research opportunities in relation to the harmonic supply voltage distortion. This will be illustrated in §1.5.3.

Quantification of these effects will be discussed in the subsequent paragraphs, however, it is also important to address the origin of these deviations. Loads draw a certain amount of current from the distribution grid. Because the grid consists of a network of cables and transformers, the grid has a certain impedance and consequently the voltage at end-user is affected by the voltage drop over this impedance. If the loads are unequally balanced in the grid, this will result in

an unbalanced voltage drop and consequently the voltage at end-user will also be unbalanced. AC/DC converters, often referred to as rectifiers, are generally built with power electronic components. Inherently to the operation of PE the discontinuity of current results in a discontinuous current wave shape. This wave shape differs from an ideal sinusoidal wave shape and results in additional losses in the power grid. As this current flows in the feeder, this results in a non-sinusoidal voltage drop over the present grid impedance. Consequently, the massive integration of PE distorts the supply voltage at end-user. In Figure 1.10 the actual waveforms of voltage and current are plotted for a PE load in an industrial plant. The distortion in both current and voltage are clearly observed.

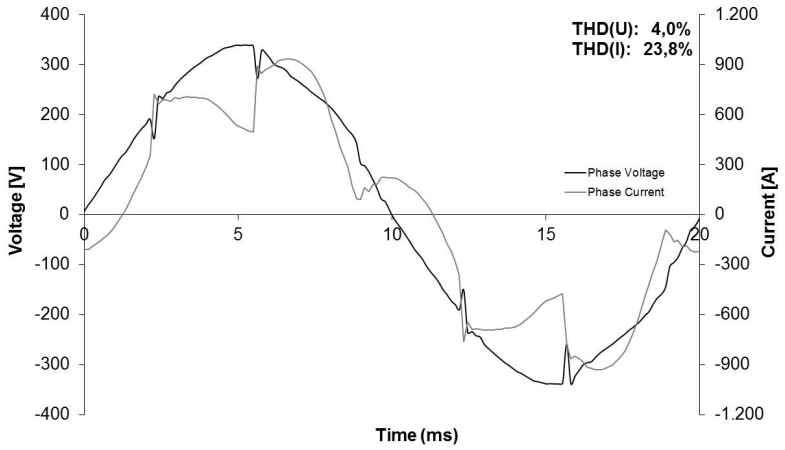

Figure 1.10: Current and voltage distortion at end-user inside an industrial site

1.3.2 Harmonic distortion

As noticeable in Figure 1.10 the current is no longer sinusoidal. If calculations are required, one should actually evaluate the relation between instantaneous current and voltage by implementing discrete solvers for analytical calculations. However, from an electro-technical perspective it is often desired to refer to sine wave calculations as engineers are very familiar with this concept. A vast amount of parameters have been introduced in order to simplify calculations while still accurately addressing the specific waveform. A Fourier Transform splits the actual waveform into a DC component and a sum of sine wave components with increasing frequency. The waveforms of voltage and current presented in Figure 1.10 have been decomposed into the individual harmonic components. The values of current and voltage are listed for each discrete frequency and are presented in a per unit scale of the 50Hz component.

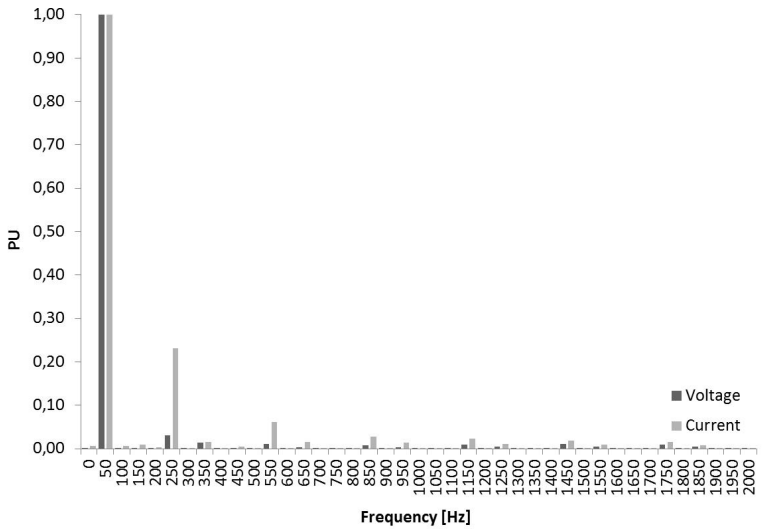

Figure 1.11: Fast Fourier Transformation (FFT) of the waveforms of Figure 1.10

Each individual frequency component, generally referred to as harmonic, is a sine wave which again allows standard electro-technical equations and calculations, taking into account the increased frequency. However, to accurately describe any periodic signal, both the magnitude as the phase angle is outputted by an FFT analysis. The RMS value of any periodic voltage waveform can be calculated according to:

$$u(t) = \sum_{h=0}^{\infty} \sqrt{2} U_{\mathrm{RMS_h}} . \sin\left(h\omega t + \varphi_h\right) \tag{1.5}$$

$$U_{\mathrm{RMS}} = \sqrt{\frac{1}{T}\int_0^T u^2(t)dt} \tag{1.6}$$

with $u(t)$ the instantaneous voltage, h the harmonic order and ω is the pulsation of the fundamental component, equal to $(2\pi/T_1)$. φ_h is the harmonic phase angle of the voltage, however, if the RMS value of the voltage is calculated based on (1.6) the φ_h has no influence. In electro-technical engineering most of the losses are generally related to the RMS value. Additionally, if the total RMS value $U_{\mathrm{h\_RMS}}$ is to be calculated based on the individual RMS values of each harmonic obtained by the FFT $U_{\mathrm{RMS_h}}$, this can be done according to:

$$U_{\mathrm{h\_RMS}} = \sqrt{\sum_{h=2}^{\infty} U_{\mathrm{RMS_h}}^2} \tag{1.7}$$

Similar equations of (1.5), (1.6) and (1.7) can be formulated for the RMS current. Although most of the losses are related to the RMS current or voltage, some losses such as the iron losses inside a machine are related to the averaged voltage. The average value of a voltage over half of a period including harmonic content $U_{\mathrm{h\_avg}}$ can be calculated by:

$$\begin{aligned} U_{\mathrm{h\_avg}} &= \frac{2}{T_1}\int_0^{T_1/2}\sum_{h=1}^{\infty}\sqrt{2}U_{\mathrm{RMS_h}}\sin(h\omega t+\varphi_h)dt \\ &= \frac{4\sqrt{2}}{T_1\omega}\sum_{h=1}^{\infty}\frac{U_{\mathrm{RMS_h}}}{h}\cos\varphi_h \end{aligned} \tag{1.8}$$

Contradictory to the RMS values where no weighting factors are introduced, low order harmonics will have a more significant influence on the average voltage. Additionally, the introduction of $\cos\varphi_h$ implies that the phase of the harmonic voltage influences the averaged voltage. If a waveform is to be addressed accurately, one should state for each individual harmonic the magnitude and phase angle. In order to address the amount of distortion present in a certain signal the concept of Total Harmonic Distortion (THD) has been introduced. The THD is one of the most commonly used parameters to evaluate the quality of voltage or current. The mathematical expression of the THD of the voltage ($\mathrm{THD_U}$) is given by:

$$\mathrm{THD_U} = \sqrt{\sum_{h=2}^{40}\left(\frac{U_{\mathrm{RMS_h}}}{U_{\mathrm{RMS_1}}}\right)^2} \tag{1.9}$$

where $U_{\mathrm{RMS_1}}$ is the value of the fundamental RMS voltage, $U_{\mathrm{RMS_h}}$ the RMS value of the voltage of harmonic order h [24]. The analogue expression can be made for the THD of the current ($\mathrm{THD_I}$).

1.4 Standards related to Power Quality

In order to define the quality of the supplied power, one often refers to the reliability, continuity and quality of the supply voltage. It is the responsibility of the (distribution) network operator to supply sufficient quality of voltage at the point of connection in order for the installation downstream to operate correctly. The limits to which the quality of the supply voltage should comply are presented in the EN50160 and is fully discussed in §1.4.1. However, as a significant amount of voltage anomalies are caused by the consumers itself, it is often impossible to discard the current quality of the load.

1.4.1 EN50160: Supply voltage quality

The EN50160 states the "*Voltage characteristics of electricity supplied by public electricity networks*". Because a perfect supply voltage is impossible due to technical limitations, this reference states for nearly all of the voltage quality related parameters upper limits. As this research specifically relates to supply voltage distortion, the limits concerning voltage distortion are listed in Table 1.4. In addition to individual harmonics the THD_U must be below the 8% upper limit. If the THD_U exceeds the 8% threshold, this can be interpreted as the grid impedance being too high. In order to reduce the distortion ratio the grid has to be "strengthened" or the impedance should drop. This is the responsibility of the Distribution Network Operator.

Table 1.4: Threshold limits according to the EN50160

Odd Harmonics				Even Harmonics	
Non Triple-N		Triple-N			
Order h	Voltage [pu]	Order h	Voltage [pu]	Order h	Voltage [pu]
5	6%	3	5%	2	2%
7	5 %	9	1.5%	4	1%
11	3.5%	15	0.5%	6-24	0.5%
13	3%	21	0.5%		
17	2%				
19	1.5%				
23	1.5%				
25	1.5%				

1.4.2 IEC61000-3-XX: Current quality

Passive rectifiers consist of four to six diodes in a Graetz configuration for a single phase or three phase configuration. The DC side is often equipped with a DC-capacitor link. Due to the specific nature of diodes, the discretization of current leads to a non-sinusoidal current demand [25]. In order to maintain sufficient quality of voltage, several standards have been established in order to limit the amount of current distortion. The IEC61000-3 series specifically addresses all the limits of current quality by loads. This covers a wide range of phenomena such as harmonic distortion, unbalance, distortion due to decentralized production etc. Specifically the IEC61000-3-2, IEC61000-3-4 and IEC61000-3-12 are of interest in the presented research as they state limits for harmonic current emissions:

- IEC61000-3-2: Limits for harmonic current emissions (equipment input current less than 16 A per phase) [26]

- IEC61000-3-4: Limits of emission of harmonic currents in low-voltage power supply systems for equipment with rated current greater than 16 A [27]
- IEC61000-3-12: Limits for harmonic currents produced by equipment connected to public low-voltage systems with input current higher than 16 A and less than 75 A per phase [28]

1.5 The effect of voltage anomalies on Induction Machines

1.5.1 Introduction

The rise of PE Variable Speed Drives (VSD) has enhanced both speed and torque control of IM and a large number of studies present the effect of PWM voltages on the operation of IM [29, 30]. However, according to [3] only 25% of the newly installed IMs are fitted with such a VSD. Consequently, the presented research relates to Direct On Line (DOL) operation and the distortion present in the grid voltage. Every deviation from a stable, balanced, 50Hz, sine wave supply voltage can result in undesirable behavior of DOL electrical machines:

- The dominating aspect in the behavior of DOL IM in relation to voltage dips is the torque. Although voltage dips can result in abrupt torque variations, these transient torques are generally limited to the startup torque [31]. In practice, dips with more than 30% voltage drop result in torques smaller than the load torque, causing a speed decrease that may be unacceptable [32].
- Voltage unbalance results in large inverse currents inside the machine. Sufficient unbalance will imply additional heating and a rapid decrease of the electrical insulation life expectancy [33, 34].
- Fast transients, with high dV/dt ratio but limited to a time frame less than 10ms, normally do not affect correct operation of the IM. However, if these fast transients are repetitive and severe, as is the case for VSD IM combinations, this can cause partial discharge at the coil head and consequent breakdown of the stator coil insulation. Additionally, if higher frequencies are evaluated, generally exceeding 4kHz, the focus is shifted towards vibration, noise or common mode currents in bearings [35].
- Voltage waveform deviation, or voltage harmonics, result in additional currents similar to supply voltage unbalance [36].

The presented research will focus on the effects of supply voltage distortion on the energy efficiency of IM. The evaluated distortion is limited to 2kHz or the 40^{th}

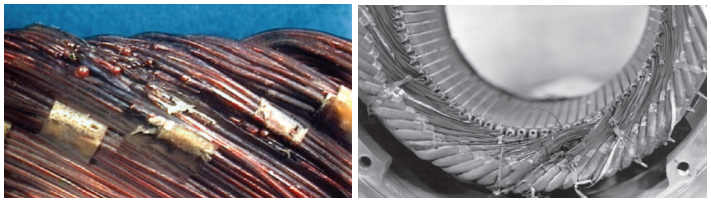

(a) *(b)*

Figure 1.12: (a) typical turn-to-turn short caused by voltage spikes from an inverter,(b) typical phase-to-phase fault caused by excessive winding temperature [4]

harmonic, referring to the frequency limit in [37]. Although the actual voltage at end-user may additionally be unbalanced, the presented research assumes balanced conditions of both fundamental as harmonic magnitudes. A small comment towards additional unbalance is given in the conclusions of Chapter 4.

In 1929 Doggett and Queer published *" Induction Motor operation with non sinusoidal impressed voltages."* paving the path by presenting preliminary investigations of IM operation with non-sinusoidal impressed voltages [38]. They suggested that for a known pattern of non-sinusoidal supply, the voltage profile can be analyzed into a fundamental component and a series of time harmonics. In 1968 Klingshirn published *" Polyphase Induction Motor Performance and Losses on Non sinusoidal Voltage Sources"* which specifically addressed IM operation in case of cyclo-converter fed operation [39]. Due to the low frequency range and the high distortion ratio of cyclo-converters the discussed effects were all below the grid frequency. Harmonics in the supply voltage result in additional losses and Linders described in 1979 the additional cost linked to supply voltage distortion [39]. Cummings was the first in 1986 to suggest simplified lumped harmonic models to estimate the harmonic losses and to link these losses to additional temperature rise [40]. Shortly after, Landa [41] was the first author to suggest derating factors of IM when supplied with distorted voltages back in 1990. Within the last two decades, the rise of low-cost VSD has redirected most of the related research specifically to inverter fed motor operation. Only a handful of researches currently focusses on the energy efficiency of DOL IM when supplied with non-sinusoidal wave shapes [de Abreu J.P.G. [42],Agamloh E.B. [43], Quispe E.C. and Ferreira F.J.T.E. [44, 45] a.o.].

1.5.2 NEMA MG1: Derating of IM in case of voltage distortion

Both NEMA MG1 and IEC 60034-17 present derating methods in case of supply voltage unbalance. Additionally, due to both the increase in distortion of the supply voltage and the increase of IM supplied from VSDs, there was a demand for a relatively easy method of derating in case of supply voltage distortion.

Consequently the NEMA MG1 presents a normative derating method in case of supply voltage distortion. As will be illustrated in Chapter 4, the losses are proportional to the applied voltage distortion, and inversely proportional to the harmonic order. As a result it makes more sense to introduce a weighted voltage distortion ratio, rather than using the linear parameter Total Harmonic Distortion $\mathrm{THD_U}$. The Harmonic Voltage Factor (HVF) is calculated as:

$$\mathrm{HVF} = \sqrt{\sum_{h>1} \frac{(U_h)^2}{h}} \tag{1.10}$$

with U_h the per unit value of the magnitude of the voltage of harmonic order h in reference to the magnitude of the fundamental voltage. Notice that in (1.10) no phase reference of the distinctive harmonics is needed. Triple-N harmonics are not considered within the NEMA MG1. Similar to the derating in case of supply unbalance, the derating curve for harmonic distortion is based on many tests of a variety of motors. This curve suggests the derating as function of the maximum thermal limits:

$$1 + \frac{\%\mathrm{IncreaseWindingTemperature}}{100} = \frac{\%\mathrm{load}}{100}^{-1.7} \tag{1.11}$$

In order to avoid additional thermal stress, the nameplate efficiency and mechanical power should be derated using the HVF, and the Derating Factor (DF) according to Figure 1.13.

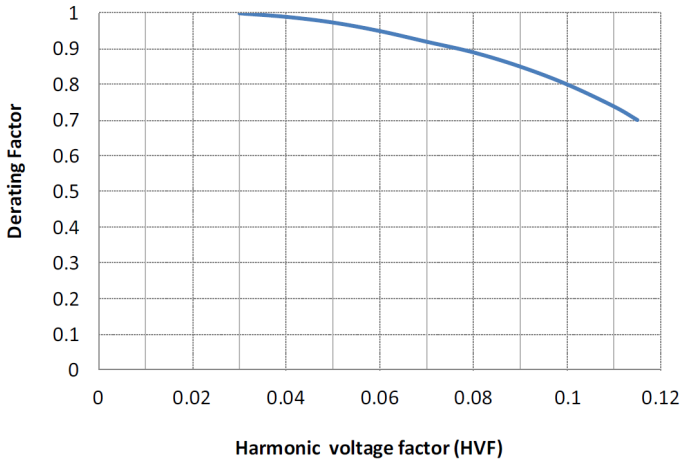

Figure 1.13: Derating Factor (DF) as a function of HVF [43, 46]

Accordingly, for a given efficiency at sine wave conditions, the derated efficiency of the DOL IM supplied with distorted voltage can be estimated using the results obtained in (1.10), Figure 1.13 and solving:

$$\eta_c = \frac{\mathrm{DF}^2}{\eta^{-1} + \mathrm{DF}^2 - 1} \tag{1.12}$$

with η_c the derated efficiency for a certain DF, DF the derating factor as function of the HVF and η the reference efficiency, which is the efficiency at sine wave conditions. By means of example the η_c for 10% fifth harmonic distortion is obtained by calculating a HVF of 0.044, the corresponding Derating Factor is 0.975 and with a nameplate efficiency of 87.5% the calculated reduced efficiency is 86.9%.

1.5.3 Research goals

The goal of this short introduction was to roughly hint the specific mechanisms which result in both the reduction of the supply voltage quality, as the specific interaction of supply voltage distortion in relation to IM efficiency. However, a more rigorous analysis of the individual losses in both distorted and non distorted supply conditions is needed in order to accurately explain the additional losses caused by supply voltage distortion in IM. In Chapter 2 the losses at sine wave supply voltage are segregated in the individual loss components. As they can be designated to specific areas of the machine, thermal modeling will enable relatively accurate estimations of motor temperatures. Before the effect of supply voltage distortion is to be addressed, limits should also be stated towards the maximum amount of supply voltage distortion. This has not been presented in previous literature and efforts were done to obtain certain limits in Chapter 3.

Although a validation of the additional losses caused by supply voltage distortion is highly important, up till now obtaining the total loss linked to harmonic supply voltage distortion is difficult. As harmonic power theoretically results in both averaged mechanical power and additional electrical losses inside the machine, studies generally prefer to address the decrease of efficiency rather than stating the actual additional losses caused by supply voltage distortion. However, evaluating the direct efficiency has two significant drawbacks. First of all, when evaluating the efficiency, both electrical P_{el} and mechanical power P_{mech} should be evaluated. Although electrical quantities can be measured with high accuracy, the measurement of mechanical power is still difficult due to the need of a torque measurement device. Secondly, as efficiency is a ratio, minor variations in consumed active power are hardly noticed and consequently detailed information is lost.

In Chapter 4 a new method of evaluating the additional harmonic losses is proposed. This method is predominantly based on IEC 60034-2-3. Minor adjustments are suggested which result in only evaluating the electrical power linked to a certain harmonic. Although this method will eliminate some effects

which should be taken into account when evaluating the direct efficiency, the increased measurement accuracy results in more accurate estimations and evaluation of the supply voltage distortion. Once this parameter is throughly validated, this parameter will be used to compare the susceptibility of efficiency rating and power rating of machines in reference to harmonic voltages. As these losses can be accurately measured, these losses can also be designated into the different areas of the machine. In combination with the thermal modeling of Chapter 2, the temperature increase due to harmonic losses can be estimated.

The literature study of §1.5.1 indicates that a lot of attention has been given to the problem for the IM in motor operation. However, when this IM is used as a generator, similar effects will occur. Due to the difficult laboratory setup - when testing generators the power supply must be able to control the voltage distortion, and simultaneously dissipate active power - no results are known to date. Although IMs and Induction Generators (IGs) are physically the same machine, the saturation will prohibit the straightforward implementation of harmonic motor models. The measurement results presented in Chapter 5 will illustrate that the adaptation of harmonic motor models are insufficient to estimate the effect of harmonic distortion on the energy efficiency of IG.

If the innovative designs, such as LSPMM and synRM are to become an actual substitute for standard IM, the influence of voltage anomalies on their overall energy efficiency should be evaluated. In case of SynRM the use of a VSD is mandatory, for LSPMM one of the design criteria was to enable DOL start and consequently a squirrel cage was added to enable the startup as a SCIM. The use of a VSD inherently implies the rectification of the voltage. Harmonics are completely blocked at the DC bus and consequently synRM are taken out of consideration. LSPMM closely relate to IM, they share identical stator winding layout, apart for the PM a fairly similar rotor construction is noticed and both machines are built according to IEC60034-7. Consequently, at first sight, straightforward adaptation of the harmonic loss mechanisms for IM to LSPMM seems to be appropriate. In Chapter 6 it will be elucidated that both the possible saturation and the perfect synchronous operation of the magnetic field in the stator and the mechanical speed of the rotor does highly increase the complexity of the evaluation of the influence of supply voltage distortion in relation to LSPMM efficiency.

References

[1] P. Waide and C. Brunner. *Energy-Efficiency Policy Opportunities for Electric Motor-Driven Systems*, International Energy Agency, 2011.

[2] W. Deprez. *Energy efficiency of the induction machines: a critical assessment*. PhD thesis, KU Leuven, 2008.

[3] A. De Almeida, F. Ferreira, J. Fong, and P. Fonseca. *European Ecodesign Directive on Energy- Using Products (EUP's), Project LOT 11 Motors*.

[4] A. Bonnett. *Root Cause Methodology for Induction Motors: A Step-by-Step Guide to Examining Failure*. IEEE Industry Applications Magazine, 18(6):50–62, 2012.

[5] F. Ferreira and A. De Almeida. *Technical and Economical Considerations on Line-Start PM Motors including the Applicability of the IEC60034-2-1 Standard,*. In 7th Energy Efficiency in Motor Driven Systems (EEMODS'11), Alexandria, USA, 2011.

[6] S. Manoharan, N. Devarajan, M. Deivasahayam, and G. Ranganathan. *Review on efficiency improvement in squirrel cage induction motor by using DCR technology*. Journal of Electrical Engineering, 60(4):227–236, 2009.

[7] J. Goss, D. Staton, and M. Popescu. *Practical Aspects in the Design and Analysis of Electric Machinery for Power Traction Applications (IEMDC 2013 Tutorial Session)*, 2013.

[8] A. Aliabad, M. Mirsalim, and N. Ershad. *Line-Start Permanent-Magnet Motors: Significant Improvements in Starting Torque, Synchronization, and Steady-State Performance*. IEEE Trans. on Magnetics, 46(12):4066–4072, 2010.

[9] M. Rahman, A. Osheiba, K. Kurihara, M. Jabbar, H.i Ping, K. Wang, and H. Zubayer. *Advances on Single-Phase Line-Start High Efficiency Interior Permanent Magnet Motors*. IEEE Trans. on Ind. Electronics, 59(3):1333–1345, 2012.

[10] W. Fei, P. Luk, J. Ma, J.X. Shen, and G. Yang. *A High-Performance Line-Start Permanent Magnet Synchronous Motor Amended From a Small Industrial Three-Phase Induction Motor*. IEEE Trans. on Magnetics, 45(10):4724–4727, 2009.

[11] C. da Silva, J. Cardoso, and R. Carlson. *Analysis of a Three-Phase LSPMM by Numerical Method*. IEEE Trans. on Magnetics, 45(3):1792–1795, 2009.

[12] X. Feng, L. Liu, and Zhang Y. *Super Premium Efficient Line Start-up Permanent Magnet Synchronous Motor*. In 19th International Conference on Electrical Machines (ICEM), Rome, Italy, 2010.

[13] F.. Ferreira, G. Baoming, and A. De Almeida. *Stator winding connection mode management in line-start permanent magnet motors to improve their efficiency and power factor*. In 20th Int.Conf. on Electrical Machines (ICEM), pages 775–783, Marseille, France, 2012.

[14] *IEC 60034-7 ed2.1 Consol. with am1 : Rotating electrical machines - Part 7: Classification of types of construction, mounting arrangements and terminal box position (IM Code)*, 2001.

[15] IEEE112. *"Standard Test Procedure for Polyphase Induction Motors and Generators"*.

[16] *IEC 60034-2-1: 2007 (BS EN 60034-2-1) Rotating Electrical Machines-Part 2-1: Standard methods for determining losses and efficiency from tests (excluding machines for traction vehicles).* 2007.

[17] A. Boglietti, A. Cavagnino, M. Lazzari, and M. Pastorelli. *International standards for the induction motor efficiency evaluation: a critical analysis of the stray-load loss determination*. IEEE Trans. on Ind. App., 40(5):1294–1301, 2004.

[18] A. De Almeida, F. Ferreira, J. Busch, and P. Angers. *Comparative analysis of IEEE 112-B and IEC 34-2 efficiency testing standards using stray load losses in low-voltage three-phase, cage induction motors*. IEEE Trans. on Ind. App., 38(2):608–614, 2002.

[19] A. De Almeida, F. Ferreira, and J. Fong. *Standards for Efficiency of Electric Motors*. IEEE Ind. App. Magazine, 17(1):12–19, 2011.

[20] B. Renier, K. Hameyer, and R. Belmans. *Comparison of standards for determining efficiency of three phase induction motors*. IEEE Trans. on Energy Conv., 14(3):512–517, September 1999.

[21] E. Olin. *Determination of Power Efficiency of Rotating Electric Machines*. Trans. of the American Institute of Electrical Engineers, XXXI(2):1695–1718, 1912.

[22] E. Agamloh. *The Partial-Load Efficiency of Induction Motors*. IEEE Trans. on Ind. App., 45(1):332–340, 2009.

[23] L. Aarniovuori, A. Kosonen, M. Niemela, and J. Pyrhonen. *Calorimetric measurement of variable-speed induction motor*. In 20th International Conference on Electrical Machines (ICEM), pages 872–878, Marseille, France, 2012.

[24] *IEC 61000-4-30 ed2.0: Electromagnetic compatibility (EMC) - Part 4-30: Testing and measurement techniques - Power quality measurement methods*, 2008.

[25] N. Mohan, T. Undeland, and W. Robbins. *Power Electronics: Converters, Applications, and Design*. 2003.

[26] *IEC 61000-3-2 ed3.2 Consol. with am1&2: Electromagnetic compatibility (EMC) - Part 3-2: Limits - Limits for harmonic current emissions (equipment input current 16 A per phase)*, 2009.

[27] *IEC/TS 61000-3-4 ed1.0 Electromagnetic compatibility (EMC) - Part 3-4: Limits - Limitation of emission of harmonic currents in low-voltage power supply systems for equipment with rated current greater than 16 A*, 1998.

[28] *IEC 61000-3-12 ed2.0 : Electromagnetic compatibility (EMC) - Part 3-12: Limits - Limits for harmonic currents produced by equipment connected to public low-voltage systems with input current between 16 A and 75 A per phase*. 2011.

[29] A. Malfait, R. Reekmans, and R. Belmans. *Audible noise and losses in variable speed induction motor drives with IGBT inverters-influence of the squirrel cage design and the switching frequency*. In Conference Record of the 1994 IEEE Industry Applications Society Annual Meeting, pages 693–700 vol.1, 1994.

[30] S. Van Haute, A. Malfait, R. Reekmans, and R. Belmans. *Losses, audible noise and overvoltages in induction motor drives*. In 26th Annual IEEE Power Electronics Specialists Conference, 1995. PESC '95, pages 586–592, Atlanta, USA, 1995.

[31] J. Das. *Effects of momentary voltage dips on the operation of induction and synchronous motors*. IEEE Trans. on Ind. App., 26(4):711–718, 1990.

[32] M. Didden. *Techno-economic analysis of methods to reduce damage due to voltage dips*. PhD thesis, KU Leuven, 2003.

[33] P. Pillay and M. Manyage. *Loss of Life in Induction Machines Operating With Unbalanced Supplies*. IEEE Trans. on Energy Conv., 21(4):813–822, 2006.

[34] C. Lee, B. Chen, W. Lee, and Y. Hsu. *Effects of various unbalanced voltages on the operation performance of an induction motor under the same voltage unbalance factor condition*. Electric Power Systems Research, 47(3):153–163, 1998.

[35] A. Muetze and A. Binder. *Calculation of influence of insulated bearings and insulated inner bearing seats on circulating bearing currents in machines of inverter-based drive systems*. IEEE Trans. on Ind. App., 42(4):965–972, 2006.

[36] G. Singh. *A research survey of induction motor operation with non-sinusoidal supply wave forms*. Electric Power Systems Research, 75:200–213, 2005.

[37] *EN50160: Voltage Characteristics of electricity supplied by public electricity networks*, 2010.

[38] L. Doggett and E. Queer. *Induction Motor Operation With Non-Sinusoidal Impressed Voltages*. Transactions of the American Institute of Electrical Engineers, 48(4):1217–1220, 1929.

[39] E. Klingshirn and H. Jordan. *Polyphase Induction Motor Performance and Losses on Nonsinusoidal Voltage Sources*. IEEE Trans. on Power Apparatus and Systems, PAS-87(3):624–631, 1968.

[40] P. Cummings. *Estimating Effect of System Harmonics on Losses and Temperature Rise of Squirrel-Cage Motors*. IEEE Trans. on Ind. App., IA-22(6):1121–1126, 1986.

[41] P. Sen and H. Landa. *Derating of induction motors due to waveform distortion*. IEEE Trans. on Ind. App., 26(6):1102–1107, 1990.

[42] J. de Abreu and A. Emanuel. *Induction motor thermal aging caused by voltage distortion and imbalance: loss of useful life and its estimated cost*. IEEE Trans. on Ind. App., 38(1):12–20, 2002.

[43] E. Agamloh, S. Peele, and J. Grappe. *An experimental evaluation of the effect of voltage distortion on the performance of induction motors*. In Conference Record of 2012 Annual IEEE Pulp and Paper Industry Technical Conference (PPIC), pages 1–7, 2012.

[44] F. Ferreira, A. De Almeida, W. Deprez, R. Belmans, and G. Baoming. *Impact of steady-state voltage supply anomalies on three-phase squirrel-cage induction motors*. In International Aegean Conference on Electrical Machines and Power Electronics, 2007. ACEMP '07., pages 607–615, Bodrum, Turkey, 2007.

[45] F. Ferreira, Anibal T De Almeida, and G Baoming. *Three-Phase Induction Motor Simulation Model Based on a Multifrequency Per-Phase Equivalent Circuit Considering Stator Winding MMF Spatial Harmonics and Thermal Parameters*. In 17th International Conference on Electrical Machines (ICEM), Chania Greece, 2006.

[46] *NEMA Standards Publication MG 1-2006 Revision 1-2007 Motors and Generators*, 2007.

2

Fundamental loss segregation of IM

2.1 Losses inside IM

Converting energy always results in losses. High quality energy, such as electrical energy, needs to be converted into a desirable output such as mechanical power or light. The conversion of energy always results in additional heat generation. The efficiency η of any system can be evaluated by the amount of input for a certain desired output. In case of an IM the input is the amount of electrical input power P_{el}, the desired output is mechanical power P_{mech} and the efficiency is the ratio of output to input power:

$$\eta = \frac{P_{\mathrm{mech}}}{P_{\mathrm{el}}} \tag{2.1}$$

$$= \frac{P_{\mathrm{el}} - P_{\mathrm{loss}}}{P_{\mathrm{el}}} \tag{2.2}$$

According to (2.1) and (2.2) the efficiency of an IM can be evaluated based on 2 methods [1]. If the efficiency is obtained by using (2.1), this is referred to as the direct method, while evaluation of the losses and the corresponding efficiency according to (2.2) is generally referred to as the indirect method. Eq.(2.2) also indicates that the losses in case of motor operation are being supplied by the electrical supply. Simplified loss evaluation assumes perfect sinusoidal voltage and sinusoidal current distribution. When a loss evaluation at nominal load and at fundamental frequency of an IM is executed, the electrical losses generated in the machine are stator Joule losses P_{s}, rotor Joule losses P_{r} and iron losses P_{iron} in both stator and rotor. In order to obtain the overall efficiency, mechanical losses

caused by friction and windage P_{w} should be taken into account:

$$P_{\mathrm{loss}} = P_{\mathrm{s}} + P_{\mathrm{r}} + P_{\mathrm{iron}} + P_{\mathrm{w}} \tag{2.3}$$

Active power dissipation is generally modeled by a resistance and Figure 2.1 [A] represents a single phase equivalent scheme of a IM. The losses can be designated to specific areas in the machine and the losses of a 4-pole 4kW EFF2 IM are presented in the Sankey Diagram of Figure 2.1 [B] [2].

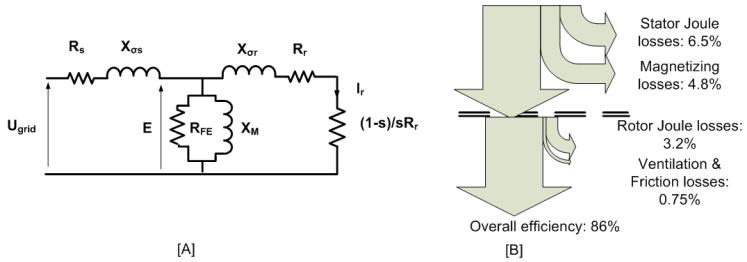

Figure 2.1: Equivalent Scheme of an IM [A] and a segregated loss analysis obtained by measurement for a 4kW TEFC EFF2 [B]

However, if only the fundamental losses of Figure 2.1 are taken into account, there is an underestimation of the total losses. Additional losses can be designated to the magnetic property limitations of electrical steel and industrial imperfections. Extra losses also occur due to the discrete winding lay out of the windings into slots (leakage flux and space harmonics). All these additional losses are generally lumped into the Stray Load Losses (SLL) [3–7]. Consequently (2.3) is expanded to:

$$P_{\mathrm{loss}} = P_{\mathrm{s}} + P_{\mathrm{r}} + P_{\mathrm{iron}} + P_{\mathrm{w}} + P_{\mathrm{SLL}} \tag{2.4}$$

For standard IM the estimation of SLL according to the indirect method is still a topic of discussion and is specifically addressed in § 2.1.5.

2.1.1 Stator Joule losses

The stator is generally constructed from coils consisting of copper windings and this copper has some inherent losses. The Joule losses in the windings are referred to as stator Joule losses and these losses are modeled by the resistance R_s. The stator Joule loss can be calculated by:

$$P_{\mathrm{s}} = 3.R_s(f, \Theta).I^2_{\mathrm{RMS}} \tag{2.5}$$

The value of the stator resistance R_s is function of both the supply frequency f and temperature Θ.

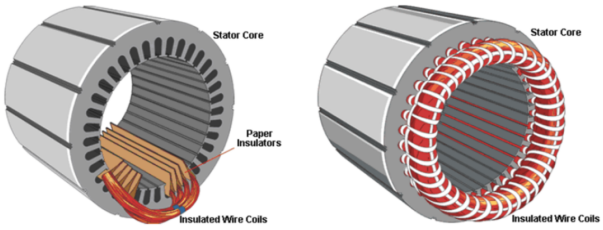

Figure 2.2: Construction of stator windings (Courtesy of Siemens)

The evaluated distortion of stator current in this dissertation is limited to the 40^{th} harmonic as stated in the EN50160. With a grid frequency of 50 Hz this relates to frequencies below the 2kHz limit. Because stator coils are generally copper wire wound, the section is small and the influence of the skin effect inside the stator coils is negligible for low frequency distortion [8].

2.1.2 Iron losses

In order to transfer energy from the fixed stator to the physically moving rotor, a rotating magnetic field is used. However, because the magnetic field changes, this generates losses in the lamination stack in both stator and rotor. For most of the rotating electrical machines, the use of ferromagnetic steel in rotor and stator has several advantages: the amount of magnetizing power can be reduced, leakage fields are reduced to a minimum and parasitic effects can be guided to stator teeth. Only in super conducting generator systems, which normally operate at 6 to 10 Tesla, is the steel regarded as a disadvantage because the material limit the induction to 2.2 Tesla. The steel also increases inertia, which is a drawback for very dynamic machines.

Losses originating due to magnetization are logically referred to as magnetization or iron losses. Bertotti [9] developed a low frequency domain model which divides the losses down into three components: eddy current losses P_{ed}, hysteresis losses P_{hy}, and anomalous/excess losses P_{an}. The total iron losses can be calculated according to:

$$P_{\text{iron}} = P_{\text{ed}} + P_{\text{hy}} + P_{\text{an}} \tag{2.6}$$

1. Eddy current losses are due to induced currents inside the lamination stack. The electrical conduction is mainly influenced by adding silicium to the steel. However, adding silicon also increases the frailty of the steel and is consequently limited. In order to reduce the eddy current losses, the magnetic material is generally laminated. Eddy current losses in [W/kg] are given by :

$$P_{\text{ed}} = K_e.f^2.\hat{B}^2 \tag{2.7}$$

2. Hysteresis losses are caused by irreversible dislocations of the surfaces of Weiss-areas, the more imperfections in the crystalline network, the higher the hysteresis losses (cfr. Barkhausen-effect). Hysteresis losses are independent of the lamination thickness. Hysteresis losses in [W/kg] can be obtained by:

$$P_{\mathrm{hy}} = K_h.f.\hat{B}^{\alpha} \tag{2.8}$$

3. The anomalous losses are surface dislocations which result in additional eddy current losses. Anomalous losses [W/kg] are calculated by :

$$P_{\mathrm{an}} = K_a.f^{1,5}.\hat{B}^{1,5} \tag{2.9}$$

As observed from the segregated iron losses, all the losses are function of the peak induction $\hat{B}$ the frequency f and K_h,K_a,K_e and α are constants depending on the type of material and the operating temperature. For practical use, the individual losses are often combined into the Steinmetz equation.

$$P_{\mathrm{iron}} = C_m.f^{\alpha}.\hat{B}^{\beta} \tag{2.10}$$

with P_{iron} the iron losses [W/kg], $\mathrm{C_m}$ the first Steinmetz coefficient, f the frequency [Hz], α the second Steinmetz coefficient, $\hat{B}$ representing the peak induction [T] and β the third Steinmetz coefficient. The coefficients in (2.10) are depending of the steel used. Two types of commercially used magnetic steel in electrical machines are M400-50A and M800-50A, listed in Table 2.1. The first number indicates the specific iron losses in W/kg at a peak induction of 1.5 T. For M400-50A the specific iron losses are 4W/kg. The second number indicates the thickness of the lamination, for M400-50A the thickness is 0.5mm [10].

Table 2.1: Steinmetz coefficients for commercial grade steel

	C_m	α	β
M400-50A	0.0035	1.516	2.05
M800-50A	0.0112	1.363	1.92

Note that for M400-50A the parameter β is higher than 2, which is contradictory to the averaged iron losses obtained by (2.6). However, the value of β in [10] has been obtained by curve fitting. The high value of β indicates that at pure sine wave voltage, the eddy current losses are dominant. The specific iron losses are only valid for the steel and does not represent a physical value of the actual iron losses inside a machine. First of all, when evaluating identical steel qualities a spread of more than 25% of the actual losses has been reported between product batches [10]. Secondly, machines are constructed by lamination resulting in practical imperfections due to mechanical operations such as cutting

and stamping, insulation and physical construction, adding more additional losses [11–13]. These parameters can be integrated in the so-called construction factor K.

Table 2.2: Construction Factor K [14]

Machine Type	Teeth	Yoke
Synchronous machine	2.0	1.5-1.7
Asynchronous machine	1.8	1.5-1.7
DC machine	2.5	1.6-2.0

In case of IM, the iron losses are generated in both the stator and the rotor iron. The rotor rotates slightly out of synchronism. The nominal slip is generally less than 4%, consequently due to the very low frequency, less than 2Hz, this is often neglected and all the iron losses are assumed to be located within the stator.

2.1.3 Rotor Joule losses

In order to generate torque the rotor consists of conductors and in case of SCIM the rotor bars are short circuited by an end ring. Because the rotor of an IM rotates out of synchronism with the stator, voltage and consequently currents are induced inside the rotor bars resulting in output torque. These rotor bars are generally die casted inside lamination steel and placed on a massive shaft.

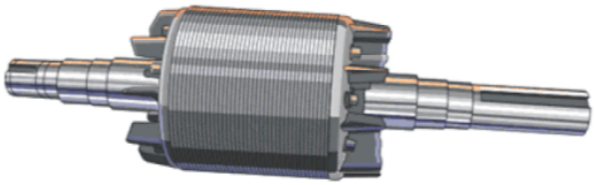

Figure 2.3: Rotor construction

Because current flows in these rotor bars additional losses are generated because of the rotor bar resistance. Similar to stator Joule losses, the rotor Joule losses are modeled by R_r:

$$P_{\mathrm{r}} = 3.R_r(f,\Theta).I_{RMS}^2 \tag{2.11}$$

In contrast to the stator resistance is the rotor resistance highly function of the applied frequency, mainly due to the relative large cross section of the rotor bars. As the frequency increases the current is forced to the top region of the bar and consequently the current density reduces to the center of the bottom of

the bar. The decrease of active surface is well known as the 'skin effect'. In the rotor the reduction of the active surface results in additional resistance, which is sometimes desirable to increase the start up torque as is the case for double cage IM. Consequently, the skin effect in IM is often specifically addressed as the 'deep bar' effect. Besides an increase of the overall resistance, it also results in a decrease of the leakage inductance in the rotor. As this research will present a detailed analysis of the influence of higher frequencies imposed on the supply voltage of DOL IM, the skin effect is of the utmost importance. Consequently, this effect will be discussed in detail in Chapter 4.

2.1.4 Friction and Windage losses

As mentioned in the introduction, excessive temperatures inside the IM should be avoided. Because machine stators are constructed from laminated steel, 70% of the generated heat is transferred in a radial direction via the stator housing. The lamination not only imposes a high electrical resistance in axial direction, it inherently has a high axial thermal resistance. In order to reduce thermal resistance from frame to ambient, the heat transfer in Totally Enclosed Fan Cooled machines (TEFC) is forced by a fan. By adding a fan, the convection conductance increases from natural convection [5-10 W/(m^2K)] to forced convection [10-300 W/(m^2K)].

In addition to the power dissipation of the fan, which is generally mounted at the end of the shaft, losses also occur due to the friction in the bearings. The mechanical losses consist of both friction and windage losses and both losses mainly depend on the mechanical speed of the machine. For IM these losses can be derived by testing the machine at synchronous speed or by using IEC 60034-2-1 [15].

2.1.5 Additional or Stray Load Losses (SLL)

In addition some losses are not taken into account in the lumped parameter model as presented in Figure (2.1). These losses are partially generated by harmonic distortion of the MMF by discretization of the windings into slots. Because this dissertation focuses on harmonic interaction these harmonics will be extensively elucidated in Chapter 4. Although measurements according to the Eh-Y method enable accurate measurement of SLL at sine wave conditions, according to [7] the Eh-Y method is still a rigorous and highly time consuming method. Consequently, the SLL are often estimated by using standards. Previous versions of the IEC 60034-2 [Ed.3] suggested simple and straightforward calculations of these SLL. The SLL were assumed fixed at 0.5% of its nominal input power. Currently, estimations of SLL are performed according to IEC 60034-2-1 by either:

1. P_{SLL} determined from residual loss (low uncertainty);

2. P_{SLL} from assigned value, Figure 2.4 (medium to high uncertainty);
3. P_{SLL} from removed rotor and reverse rotation test (high uncertainty);
4. P_{SLL} from Eh-Y test (medium uncertainty);

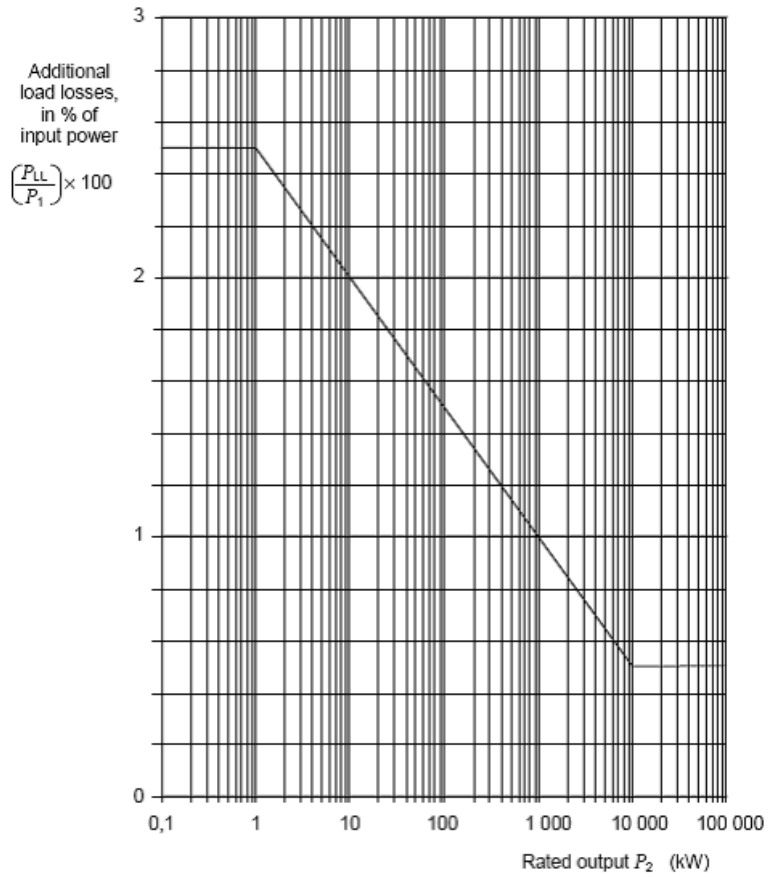

Figure 2.4: Stray load loss estimation according to IEC 61972 [6]

2.2 Loss segregation as function of motor load ratio, the nominal output power or the operating temperature

In the previous sections the different loss mechanisms are addressed. However, the actual losses and their relative ratio is function of several parameters such as the power ratio, the loading ratio, or the operating temperature of the machine.

2.2.1 Loss evaluation as function of power ratio

When evaluating IMs and their power ratio, according to Table 2.3 the machines are often divided in groups:

Table 2.3: EU-15 Low Voltage AC motor market information [16]

Power range [kW]	Market EU-15 in Mio. Units	Market share (Units)	Capacity (GW)	Market share (Capacity)
0.75-7.5	7.2	79.1%	22.5	28.2%
7.5-30	1.5	16.5%	30.0	37.6%
37-75	0.3	3.3%	15.6	19.6%
75-200	0.1	1.1%	11.6	14.6%
Total	9.1	100%	79.7	100%

- power ratio between 0.75kW [1hp] and 7.5kW [10hp]. These are the small IM. They have a low efficiency, generally lower than 90%. This section is the most relevant section as 79.1% of the installed machines are within this power ratio. Motors of 4kW are the median value and are therefore generally used as test objects.

- power ratio between 7.5kW [10hp] and 37kW [50hp]. Although the number of installed units is far less than the lower section, this section is the largest section in installed capacity.

- power ratio between 37kW [50hp] and 75kW[100hp]. The upper limit of 75kW relates the old CEMEP classification which used an upper limit of 90kW. Machines with a power limit to 90kW are generally series production. A lot of efforts have been made to optimize the machine in the design process. Once optimized, this is put into standard production. When machines up to this power ratio fail electrically, such as stator winding failure of rotor failure, it is often cheaper to buy a new motor rather than revising it.

- power ratio above 75kW.

Although this classification is still used, recent standards such as the IEC 60034 define limits and standards to IM in a 0.75kW to 375kW power range, which is equivalent to the 1hp to 500hp range. Large electric motors with more than 375kW output power are usually high voltage AC motors that are custom designed, built to order and assembled within an electromechanical system on site. They comprise just 0.03% of the electric motor stock in terms of numbers, but account for about 23% of all motor power consumption, making them very significant consumers of (about 10.4% of overall power consumption) [17]. However, if fed from a high

voltage network, this inherently implies a reduced voltage distortion. Due to both the absence of relevant distortion, and due to practical implications, this power ratio has been excluded from this research. In Figure 2.5 the distinctive losses are presented as function of the nominal power for an output power of 750W to 500kW.

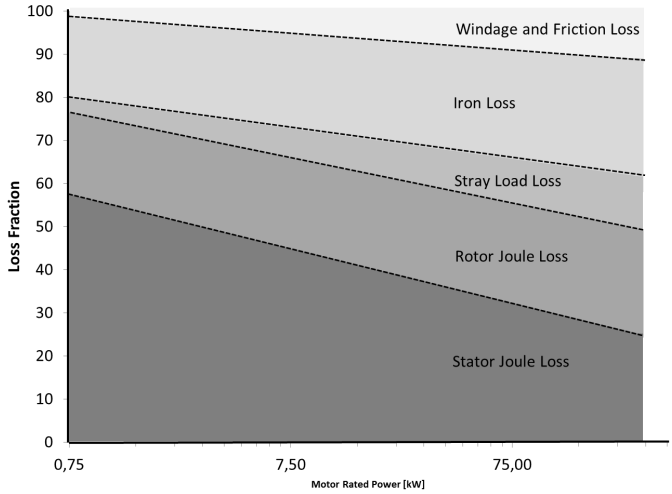

Figure 2.5: Typical loss fractions as function of the output power for 50-Hz, 4-pole IM [1-500hp] [18]

The losses of an IM are function of the power rating of the machines. As the amount of output power shifts, this also results in a shift of both the absolute value of the losses and the distribution. Small machines have a relatively large stator resistance, as the output power increases, the stator resistance decreases. This results in reduction of the p.u. stator losses.

2.2.2 Loss evaluation as function of the loading ratio

To this point the loss evaluation has presumed nominal loading. However, the loading ratio of the machine is of the utmost importance to analyze the losses and the loss distribution. The model presented in Figure (2.1) indicates that an increase of mechanical power implies an increase of current in the rotor. Subsequently, according to IEC 60034-2-1, the losses can be divided into constant losses, which do not significantly shift as the loading varies, and variable losses which are inherently coupled with the loading ratio [15]. For a constant supply voltage and frequency, the constant losses are iron, friction and stray load losses. Consequently, variable losses are the Joule losses in stator en rotor. The IEC 60034-2-1 specifically states the test procedure in order to obtain the individual losses from tests.

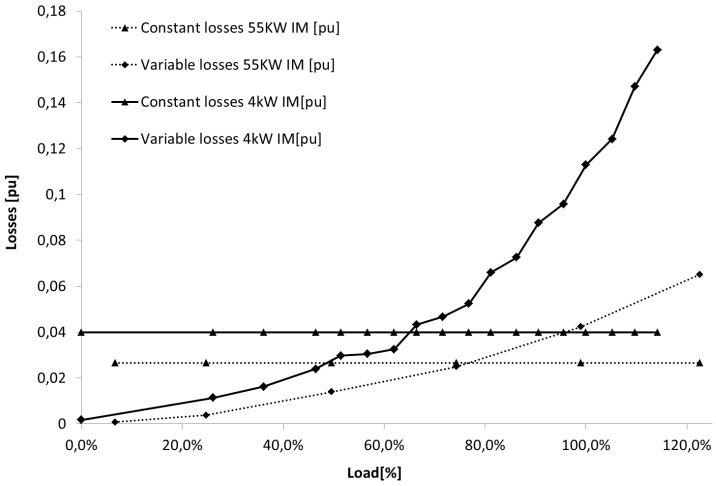

Figure 2.6: Variable and constant losses for a EFF 2 4-pole 4kW and a EFF2 2-pole 55kW IM as function of the loading ratio. Data obtained from tests.

At no load the constant losses are the dominating losses and with increasing loading the variable losses increase. At a certain loading ratio the constant losses equal the variable losses. This point is not only function of the loading ratio, but is also depending of the rated output power of the machine. However, it should be noted that the constant losses are not entirely constant over the loading range. As the loading ratio increases this generally results in a increased voltage drop over the stator impedance. If the supply voltage is assumed constant this implies a decrease of ElectroMotive Force (EMF) and the correlated peak induction and thus the resulting iron losses. In case of motor operation, loading generally results in a decrease of the iron losses and this effect is more pronounced for small IMs with a relatively high stator resistance. However, this effect is often neglected. Secondly, friction and windage losses are function of the physical speed of the machine. With increasing loading this results in a decrease of the physical speed and a reduction of these losses. Because these losses are marginal to the total losses (0,75% of input power), this shift of the losses is not important.

2.2.3 Loss evaluation as function of the operating temperature

For an IM, friction, windage and iron losses decrease as the temperature rise [19]. For the vast majority of IM, the sum of stator and rotor Joule losses are dominant, accounting for more than 50% of the total losses in the IM [20]. The stator and rotor Joule losses increase with a rising temperature. This is presented in the loss evaluation of an IM in Figure 2.7 in which the shift of losses is presented as the p.u. shift in reference to the losses at $40°\mathrm{C}$ ambient temperature.

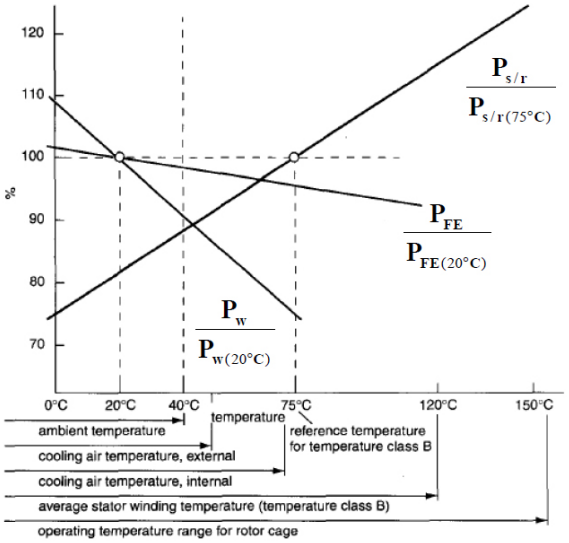

Figure 2.7: p.u. shift of windage(P_w), iron (P_{FE}) and stator or rotor winding losses ($P_{s/r}$) at $40°C$ ambient temperature [19]

For an IM up to a few kilowatt the losses increase approximately 8% between cold and hot stator windings, consequently the overall efficiency changes inversely proportional to the temperature. Measurements are presented in Figure 2.8 of a 4-pole 4kW EFF2 IM in order to evaluate the temperature effect. The machine was started in cold condition and due to the internal power consumption the machine achieved nominal temperature after approximately 2 hours. The test setup has already been extensively discussed in Chapter 1, however, it is important to address the load to the IM in order to explain the trend. The IM is loaded with a machine in constant torque control mode. Consequently, as the temperature increases, the mechanical speed of the machine will drop. Both the total power consumption as the energy efficiency of the machine reduces.

In order to illustrate this effect the torque-speed characteristic of the IM is plotted at cold and hot condition. The estimated temperatures of the rotor [130°C] and stator [100°C] resistance are obtained by Lumped Thermal Modeling [§ 2.3]. The fundamental torque-speed characteristic can be mathematically derived by using (2.12) [21]. Subsequently, both the hot and cold stator and rotor resistance $R_{\mathrm{s}}, R_{\mathrm{r}}$ are included in (2.12) in order to obtain Figure 2.9.

$$T_{\mathrm{T}} = \frac{3}{\omega} \frac{\frac{V_1^2}{(1+\sigma 1)^2}}{(\frac{R_{\mathrm{s}}}{(1+\sigma_1)^2} + \frac{R_{\mathrm{r}}}{s})^2 + (\sigma X2)^2} * \frac{R_{\mathrm{r}}}{s} \tag{2.12}$$

with $X2$ the sum of the mutual X_m and rotor leackage reactance X_{σ_r}, σ_1 the ratio of stator leackage reactance X_{σ_s} to mutual reactance and σ is:

$$\sigma = \frac{1 - X_m^2}{X_{\sigma\_r} X_{\sigma\_s}} \tag{2.13}$$

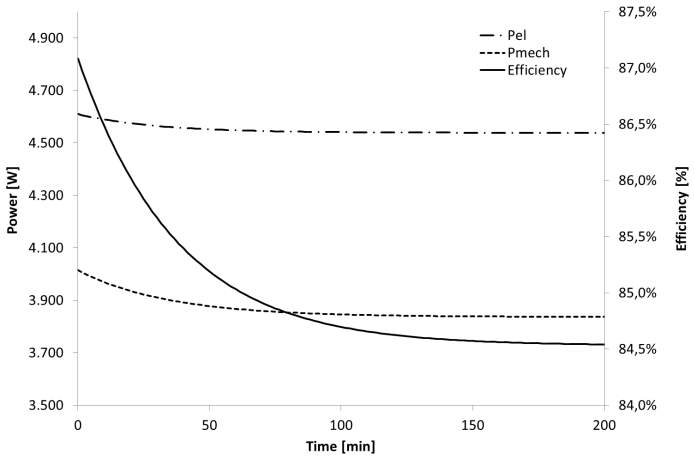

Figure 2.8: Variation of electrical input power P_{el}, mechanical output power P_{mech} and the overall efficiency in relation to the time from start up

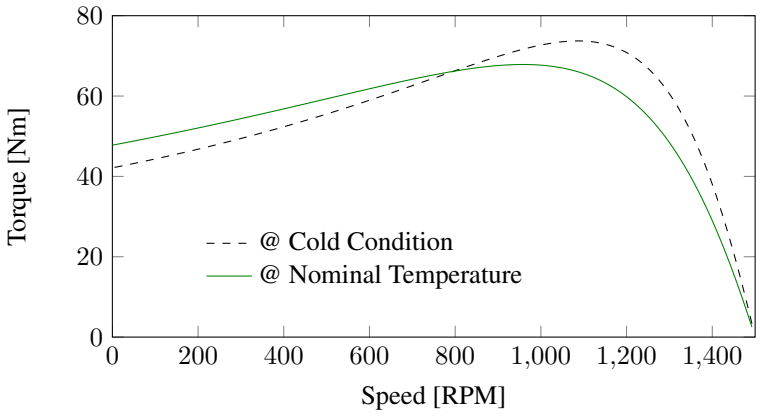

Figure 2.9: Torque/speed Characteristic of a 4kW IM as function of the operating temperature, ambient temperature is equal to 20°C

2.3 Lumped thermal modeling

2.3.1 Introduction

Up to this point the several loss mechanisms at fundamental frequency have been addressed. This will prove to be very valuable in order to explain the effects of supply voltage distortion and its related additional losses. Additional losses do not only imply an increased operational cost, additional losses also imply a direct increase of the operation temperature of the machine. As addressed in the introduction knowledge and control of the operating temperature of the IM is essential in maintaining its life expectancy. Consequently, IMs are generally designed towards certain thermal limits, as presented in Table 2.4.

Table 2.4: Thermal classes for insulation systems according to IEC 60085

Thermal class for insulation systems	A	E	B	F	H
Max. operating temperature (^{o}C)	105	120	130	155	180

Monitoring the averaged stator coil temperature is feasible and often implemented in motors using a built-in resistor. However, only monitoring the resistance is sometimes insufficient as this does not take into account adiabatic heat generation, it does not indicate certain hot spot temperatures and it does not evaluate the rotor temperature. If adiabatic heat generation is to be taken into account, generally for very steep duty ratios, thermal calculations are performed using the thermal proprieties of the stator coil. Calculations refer to $\mathrm{I^2t} \leq \mathrm{k^2S}$, which is fairly similar to calculations of short circuit behavior for electrical cables [22]. However, the heat dissipation is assumed not to be adiabatic. Consequently the heat dissipation is generally modeled by a first order thermal network, taking into account the thermal resistance and the thermal capacitance of the material and/or geometry.

Within the last decades, the rise of numerical computational software such as Finite Element Methods (FEM) and Computational Fluid Dynamics (CFD) introduced accurate modeling of temperature distribution inside machines. However, a lot of effort and computation time is still needed for FEM and CFD. Advanced Lumped Thermal Modeling (LTM) has been suggested as a worthy replacement [23–27]. LTM is very appealing to electrical engineers because the simple analogy between electrical networks and thermal networks. In LTM the power dissipation [W] is modeled as an electrical current source, the thermal resistance [W/K] is similar to the electrical resistance [Ω] and the resulting temperature variation [K] relates the voltage at a certain node. Up to a few decades, the heat transfer inside IM was modeled by simple convection/conduction models of a single cylinder, the basics of which are illustrated in Figure 2.10.

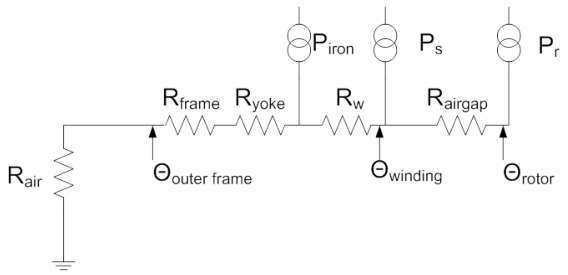

Figure 2.10: Basic radial LTM of a IM

If the additional losses are segregated to the different parts of the machine, the actual machine temperatures can be calculated using a lumped parameter model. In order to understand thermal models one needs to understand the basic heat transfer inside a machine. Because machine stators are constructed from laminated steel, 70% of the generated heat is transferred in a radial direction via the stator housing. The lamination not only imposes a high electrical resistance in axial direction, it inherently has a high axial thermal resistance. Especially in Totally Enclosed Fan Cooled (TEFC) IM the heat transfer from the stator housing is dominating for the resulting temperatures, with heat transfer coefficients of 20W/mK to 100W/mK. However, for flange mounted machines the heat transfer by conduction over the flanges may not be neglected as this can exceed to 30% of the total heat dissipation.

Consequently the basic model presented in Figure 2.10 only takes into account radial thermal resistances and still presents fairly accurate estimations of outer frame temperature $\Theta_{\mathrm{outerframe}}$, stator winding temperature $\Theta_{\mathrm{winding}}$ and rotor temperature Θ_{rotor}. Although the accuracy of the basic model is sufficient within this research, the accuracy of the LTM can be largely increased. Both radial and axial heat fluxes can be modeled and the number of nodes affect the accuracy. If sufficient nodes (over 100) are used, LTM can even result in estimations of hot spot temperatures over the entire machine with limited computation and time efforts [23, 24, 28].

In lumped models the heat transfer is modeled analytically using calculated conduction, convection and radiation thermal resistances. The thermal conduction matrix can be obtained by dividing the studied machine into several components, such as frame, stator yoke, stator tooth, stator coils, stator end-windings, air gap, rotor tooth, rotor winding, rotor end-winding, rotor yoke and shaft. All of them are represented by isothermal nodes and assumed thermally symmetrical in the radial directions [29] to reduce their number. Each node is coupled with the neighboring node by means of conduction and convection resistances. The convection and

conduction resistances of the components are defined by the following equations:

$$R_{\text{cond}} = \frac{l}{S}.k \tag{2.14}$$

$$R_{\text{conv}} = \frac{l}{S_c}.h \tag{2.15}$$

where l is the length of the body [m] in the heat flow direction, k the thermal conductivity [W/mK], S the cross-sectional area [m^2], S_c the surface area [m^2] and h the convection coefficient [W/mK]. Subsequently, the power losses can be segregated to the different areas in the machine and inserted into the loss matrix $\mathbf{P}$. The combination of the resistance matrix and the loss matrix results in actual temperature estimations for each node. The temperature rise $\mathbf{\Delta\Theta}$ for each node is calculated by solving:

$$\mathbf{\Delta\Theta} = \mathbf{R}.\mathbf{P} \tag{2.16}$$

Figure 2.11 is obtained from [14] which illustrates a more complicated equivalent network of thermal resistances for an IM and [14] subsequently uses this model to estimate temperatures of a 37kW IM. The ambient temperature was set to $40°C$.

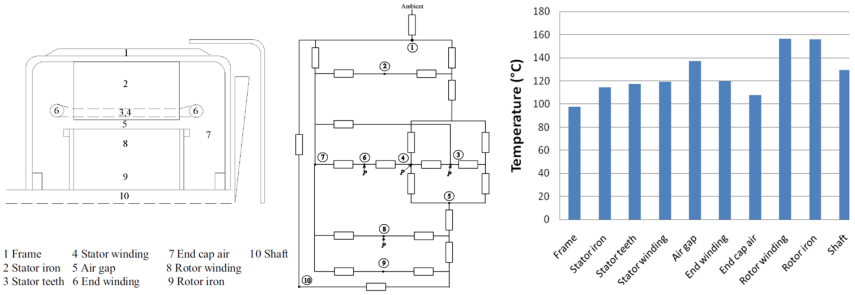

Figure 2.11: Lumped-parameter model according to [14]

2.3.2 Application of Lumped Thermal Modeling

This research suggests the use of LTM because the concept of LTM is very useful to analyze the thermal behavior of machines when the losses vary. If the loss variation can be designated to certain parts of the machine, the additional temperature rise can be estimated. If the thermal resistance is assumed independent of the temperature, this additionally results in a simple superposition of the individual temperature variations.

As will be illustrated in §2.3.3, the stator winding temperature is easily obtained from the cold and hot stator resistance. If additionally the outer frame

temperature and the total losses are known, an estimation of the radial thermal resistance from outer frame to winding can be recalculated. A similar method could be suggested to estimate the thermal resistance from rotor to frame, if only the cold and hot rotor resistance could be obtained from short circuit tests. Within this research this method has been evaluated, but this measurement procedure imposes practical difficulties. First of all, there is a significant amount of time needed to set up the short circuit test, and in this time frame the rotor cools down. In cold condition, the power injected at short circuit heats up the machine, prohibiting stable measurements. Finally, the stator resistance has to be segregated resulting in more complex calculations and an increased error. Mathematical derivation according to (2.14) seems to present more accurate estimations concerning the thermal resistance and convection between rotor iron and stator stack.

However, the main drawback of LTM is the estimation of the convection coefficient from frame to ambient. Although highly advanced - and also time consuming - modeling can present more accurate estimations of the convection resistance, within this research this problem has been bypassed by simply monitoring the outer frame temperature. As already stated several times, in [14] a lumped model was proposed and based on this paper a collaboration with Lappeenranta University of Technology (LUT) has been set up. The model developed at LUT has been used to validate the simple model of Figure 2.10, and has been additionally checked to a certain extend by measurements.

2.3.3 Validation of a 4kW Lumped Thermal Model

In this paragraph the 4kW LTM is validated. Measurements are executed on a 4kW IM and the corresponding motor construction parameters are specified in Table 2.5.

Table 2.5: Construction parameters of the 4kW IM

Rated speed	1460
Output power [kW]	4
Efficiency	88%
Frame size	112M
Insulation class	F
Stator windings	copper wound
Rotor bars	die cast aluminum

The value of the stator resistance is obtained in both cold (start up temperature) as at nominal condition. However, obtaining the stator winding temperature based on the stator resistance as function of its operating temperature has proven to be difficult. In order to determine the stator resistance, generally a small value of DC supply voltage is added to the stator winding at motor standstill. In cold

condition the winding heats up due to the DC power injected to measure the resistance. Once the value of the cold stator resistance was obtained, the motor has been mechanically loaded at nominal operating conditions until steady state operating temperature was achieved. However, to obtain the hot stator resistance, the machine has to be put to stop and DC power has to be applied. This action results in an instantaneous cool down of the windings. As the time span of the measurements increases, the windings cool down resulting in a lower stator resistance. This effect can be damped by applying sufficient DC power to partially compensate the cool down.

Table 2.6: Validation of hot and cold stator resistance for a EFF2 4kW 4-pole IM

	at 20^{o}C	at nominal condition
$R_s[\Omega]$	1.34	1.65

As noticed in Table 2.6, the increase of temperature will result in an increase of stator resistance. The stator windings are copper wound. As the thermal resistance coefficient for copper is known, knowledge of the hot and cold resistance can result in a fairly accurate estimation of the averaged stator winding temperature:

$$R_{\mathrm{sh}} = R_{\mathrm{sc}} \left(1 + 3.9110^{-3} * (\Theta_{\mathrm{s}} - 20)\right) \tag{2.17}$$

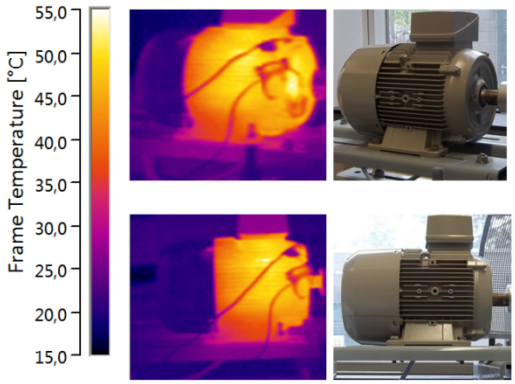

Figure 2.12: Frame Temperature of the 4kW IM

Based on the data obtained in Table 2.6 and (2.17), the nominal operating temperature of the windings can be estimated at 80.7^{o}C. In Figure 2.12 the frame temperature of 50.1^{o}C at nominal load is illustrated based on InfraRed (IR) Thermal Imaging. The temperature drop from frame to stator winding $\Delta\Theta$ can be calculated. The losses can be derived from Figure 2.7 and the power losses ΔP are known, the outer frame to winding temperature resistance R_{th} can be recalculated.

$$\begin{aligned} \Delta\Theta &= R_{\mathrm{th}} * \Delta P \\ 80.7^{o}C - 50.1^{o}C &= R_{\mathrm{th}} * 700W \\ R_{\mathrm{th}} &= 0.0437K/W \end{aligned} \tag{2.18}$$

2.4 Conclusion

The goal of this chapter was to present an introduction concerning the losses inside IM. Although there is much more basic information needed to understand the nuances concerning the operation of IM, such as fundamental mathematical modeling of IM, the representation in electrical equivalent schemes or the mathematical derivation of torque speed characteristics, this has been eliminated. The basics concerning IM operation are well addressed in [20, 21, 30]. Consequently this chapter started by presenting a general overview of the losses and the resulting energy efficiency of DOL SCIM at sine wave supply. This background knowledge will be essential in order to address the additional losses caused by supply voltage harmonics. Distortion in supply voltage will result in a variation of stator and rotor Joule losses, it will affect the magnetizing losses and can even affect the Stray Load Losses. Some key aspects will be extensively discussed in Chapter 4.

1. The additional losses will also result in an increase of operation temperature of the machine.

2. The effect of IE rating, partial loading, building size etc will affect the negative influence of distortion on to machines.

It is obvious that the effects of supply voltage distortion are function of both the magnitude and the harmonic order of the distortion present. Before evaluating the behavior of IM under distorted conditions in Chapter 4 it is imperative to obtain limits of reasonable voltage distortion at the clamps of the IM. To the authors knowledge no research has been presented to validate the limits of voltage distortion at end-user, subsequently no such limits are put into references. In Chapter 3 estimation guidelines concerning end-user voltage distortion are suggested.

References

[1] E. Agamloh. *Induction Motor Efficiency*. IEEE Industry Applications Magazine, 17(6):20–28, 2011.

[2] C. Debruyne, M. Polikarpova, S. Derammelaere, P. Sergeant, J. Pyrhonen, J. Desmet, and L. Vandevelde. *Evaluation of the efficiency of Line Start Permanent Magnet Machines as function of the operating temperature*. IEEE Trans. on Ind. Electr., PrePress:1, 2013.

[3] K. Yamazaki and Y. Haruishi. *Stray Load Loss Analysis of Induction MotorComparison of Measurement Due to IEEE Standard 112 and Direct Calculation by Finite-Element Method*. IEEE Trans. on Ind. App., 40(2):543–549, 2004.

[4] A. Jimoh, R. Findlay, and M. Poloujadoff. *Stray Losses in Induction Machines: Part II, Calculation and Reduction*. IEEE Trans. on Power Apparatus and Systems, PAS-104(6):1506–1512, 1985.

[5] A. Boglietti, A. Cavagnino, M. Lazzari, and M. Pastorelli. *International standards for the induction motor efficiency evaluation: a critical analysis of the stray-load loss determination*. IEEE Trans. on Ind. App., 40(5):1294–1301, 2004.

[6] A. De Almeida, F. Ferreira, J. Busch, and P. Angers. *Comparative analysis of IEEE 112-B and IEC 34-2 efficiency testing standards using stray load losses in low-voltage three-phase, cage induction motors*. IEEE Trans. on Ind. App., 38(2):608–614, 2002.

[7] W. Deprez. *Energy efficiency of the induction machines: a critical assessment*. PhD thesis, KU Leuven, 2008.

[8] G. Singh. *A research survey of induction motor operation with non-sinusoidal supply wave forms*. Electric Power Systems Research, 75(23):200–213, 2005.

[9] G. Bertotti. *General properties of power losses in soft ferromagnetic materials*. IEEE Trans. on Magnetics, 24(1):621–630, 1988.

[10] F. D'Hulster. *Optimisation platform for torque control of 8/6 SRM*. PhD thesis, KU Leuven, 2005.

[11] L. Dupré, R. Van Keer, and J. Melkebeek. *A study of the influence of laser cutting and punching on the electromagnetic behaviour of electrical steel sheets using a combined finite element - dynamic Preisach model*. In Proceedings 4th Intern. Workshop Electric and Magnetic Fields, Marseille, pages 195–200, 1998.

[12] A. Schoppa, J. Schneider, and J. Roth. *Influence of the cutting process on the magnetic properties of non-oriented electrical steels*. Journal of Magnetism and Magnetic Materials, 215-216(0):100–102, 2000.

[13] A. Schoppa, J. Schneider, and C. Wuppermann. *Influence of the manufacturing process on the magnetic properties of non-oriented electrical steels*. Journal of Magnetism and Magnetic Materials, 215-216(0):74–78, 2000.

[14] L. Popova, J. Nerg, and J. Pyrhonen. *Combined Electromagnetic and thermal design platform for totally enclosed induction machines*. In IEEE International Symposium on Diagnostics for Electric Machines, Power Electronics Drives (SDEMPED), pages 153–158, Bologna, Italy, 2011.

[15] *IEC 60034-2-1 ed1.0: Rotating electrical machines - Part 2-1:Standard methods for determining losses and efficiency from tests (excluding machines for traction vehicles)*, 2007.

[16] A. De Almeida, F. Ferreirra, J. Fong, and P. Fonseca. *European Ecodesign Directive on Energy- Using Products (EUP's), Project LOT 11 Motors*.

[17] P.l Waide and C. Brunner. *Energy-Efficiency Policy Opportunities for Electric Motor-Driven Systems*, 2011.

[18] A. De Almeida. *Beyond Induction Motors: LOT-30 New EU Ecodesign Study*. In Motor Summit 2012, Zurich, Switserland, 2012.

[19] H. Auinger. *Determination and designation of the efficiency of electrical machines*. Power Engineering Journal, 13(1):15–23, 1999.

[20] A. Emadi and JC Andreas. *Energy-efficient electric motors*. Marcel Dekker, New York, 2005.

[21] J. Melkebeek. *Electrische Aandrijftechniek: Course presented at the Ghent University, Faculty of Engineering and Architecture (in Dutch).*, 2010.

[22] V. Buyukdegirmenci and P. Krein. *Machine characterization for short-term or instantaneous torque capabilities: An approach based on transient thermal response*. In IEEE International Electric Machines Drives Conference (IEMDC), pages 801–808, Chicago, USA, 2013.

[23] A. Gerlando and I. Vistoli. *Improved thermal modeling of induction motors for design purposes*. IEEE Trans. on Energy Conv., 15(2):135–142, 2000.

[24] J. Nerg, M. Rilla, and J. Pyrhonen. *Thermal Analysis of Radial-Flux Electrical Machines With a High Power Density*. IEEE Trans. on Ind. Electr., 55(10):3543–3554, 2008.

[25] T. Jankowski, F. Prenger, D. Hill, S. O'Bryan, K. Sheth, E. Brookbank, D. Hunt, and Y. Orrego. *Development and Validation of a Thermal Model for Electric Induction Motors*. IEEE Trans on Ind. Electr., 57(12):4043–4054, 2010.

[26] L. Alberti and N. Bianchi. *A Coupled Thermal Electromagnetic Analysis for a Rapid and Accurate Prediction of IM Performance*. IEEE Trans. on Ind. Electr., 55(10):3575–3582, 2008.

[27] A. Boglietti, A. Cavagnino, D. Staton, M. Shanel, M. Mueller, and C. Mejuto. *Evolution and Modern Approaches for Thermal Analysis of Electrical Machines*. IEEE Trans. on Ind. Electr., 56(3):871–882, 2009.

[28] F. Incropera, D. Dewitt, T. Bergman, and A. Lavine. *Fundamentals of Heat and Mass Transfer*. John Wiley&Sons, 6 edition, 2007.

[29] G. Dajaku and D. Gerling. *An Improved Lumped Parameter Thermal Model for Electrical Machines*. In 19th International Conference on Electrical Machines (ICEM), Rome, Italy, 2010.

[30] R. Krishan. *Permanent Magnet Synchonous and Brushless DC Motor Drives*. CRC Press, 2010.

3 End-user voltage distortion

3.1 Introduction

Controlling electrical loads, such as lighting or electrical motors, by the aid of Power Electronic (PE) converters can drastically improve their overall efficiency. However, a vast majority of PE rectifiers draw a non-sinusoidal grid current, which is generally referred to as current distortion [1]. This current flows throughout the grid, resulting in a distortion of the voltage at every level from transport to distribution. Harmonic voltage distortion has been a continuous topic of interest, as a distorted voltage can cause reduction of efficiency, increase the aging and can even result in actual damage of electrical loads [2–4].

Distortion of the end-user voltage is function of the total current distortion (§3.2), the resulting impedance (§3.3) and the present background distortion (§3.4). In order to obtain sufficient quality of voltage, several standards have been established which limit the amount of current distortion drawn by individual loads [5–7]. Although some standards state the upper limit of the voltage distortion at the Point Of Connection (POC) [8], to investigate critical loads no standards are present concerning the actual possible voltage distortion at end-user. Consequently, in order to give some indication to the maximum distortion, often the maximum limits stated in EN50160 are used. Although this standard states maximum values of distortion at POC, it does not include internally generated distortion. The presented research will indicate that, additional to the background distortion present at POC, the distortion generated in the local low voltage power grid is often equally important.

In §3.2, the focus is to analyze the current behavior of PE loads. Specific attention is given to the superposition of current spectra of different loads. This section concludes by presenting a generalized current distortion. Analysis of the resulting grid impedance is equally important as not only the magnitude of the impedance but also the R/X ratio of the grid impedance is determining the resulting voltage distortion. Additional to the evaluation of the magnitude of the grid impedance in §3.3, the importance of the R/X is addressed with both simulated and measured results. Detailed simulations are presented in order to estimate the resulting end-user voltage quality combining internally generated and background distortion. Not only the magnitude of the end-user harmonic distortion is obtained, detailed evaluation of individual harmonic orders and their respective harmonic phase angles is presented in §3.6.

If the harmonic current could be mitigated, this would have a positive effect on both the additional harmonic Joule losses in the installation and the end-user voltage quality. Active harmonic filters are able to significantly reduce the current distortion injected into the grid. In §3.7 the positive influence of active filtering will be investigated by actual measurements performed in several industrial sites.

3.2 Harmonic currents

3.2.1 Introduction

The use of power electronic converters enables the voltage or current supplied to the load to be manipulated, resulting in a optimization of the behavior or efficiency of the load. Generally, the alternating voltage supplied by the grid is being rectified to DC. This DC voltage is then again manipulated by PE converters such as DC/DC Buck/Boost converters or DC/AC inverters [9]. As this research is focused on harmonic content injected by loads, abstraction of the actual load is done by simply modeling the active power demand as a constant demand of power at the DC side of the rectifier.

Passive rectifiers consist of four to six diodes in a Graetz configuration for a single phase or three phase configuration. The DC side is often equipped with a DC-capacitor link. Due to the specific nature of diodes, the discretization of current leads to a non-sinusoidal current demand [9]. In order to maintain sufficient quality of voltage, several standards have been set up in order to limit harmonic current emissions [5–7].

The voltage at the load is mainly determined by the current drawn by the load and the grid impedance. As the current is function of the applied voltage

and the resulting grid impedance, the voltage and current cannot be calculated in one single equation, but an iterative solver is needed. The voltage dependency of harmonic current components drawn by a non linear load is called the attenuation effect. For non linear loads the voltage distortion will usually result in a reduced current distortion. The attenuation is function of both the number of loads (§3.2.2) and the loading ratio (§3.2.3) of each load [10, 11].

3.2.2 Attenuation as function of the number of loads

When evaluating the current spectrum of multiple identical loads, efforts were made to estimate the total current distortion based on the current of a single load. Despite several studies indicate slightly different formulas of the Attenuation Factor (AF) [10, 12, 13], the AF for each individual harmonic h can be regarded as:

$$\mathrm{AF}_h = \frac{I_{\mathrm{RMS}_h N}}{N.I_{\mathrm{RMS}_h}} \tag{3.1}$$

with AF_h the attenuation factor of harmonic order h, $I_{\mathrm{RMS}_h N}$ the current of N identical loads, and I_{RMS_h} the current of an individual load. To illustrate this effect, measurements were executed on a large number of PC power supplies [14]. These results are purely illustrative and are plotted in Figure 3.1 in which the current has been rescaled to the maximum current value.

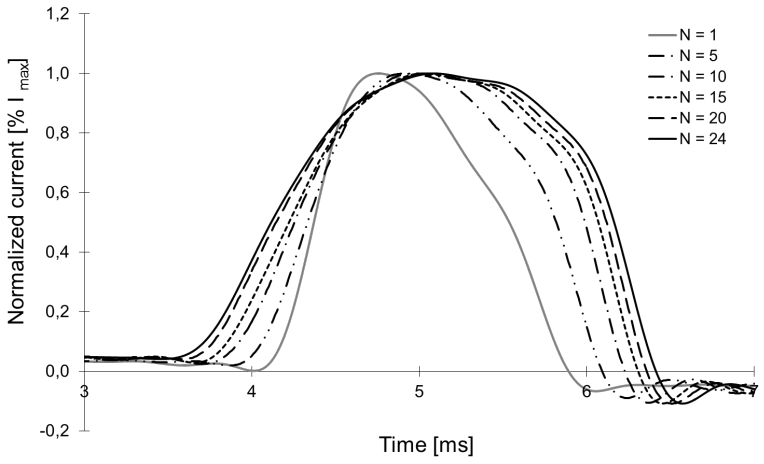

Figure 3.1: Attenuation effect for a 24 identical power supplies

From Figure 3.1 it is observed that with increasing number of loads, the current wave shape is less distorted. If the loads are not identical, the total current distortion is also function of the relative phase shift of the distinctive load currents.

This effect is called the diversity effect. If the resulting current of a number of mixed loads is to be calculated the following summation rule can be used:

$$I_{\mathrm{RMS}_h N} = \sqrt[\beta]{\sum_{i=1}^{N} (I_{\mathrm{RMS}_h i})^{\beta}} \tag{3.2}$$

with $I_{\mathrm{RMS}_h N}$ the total current at harmonic frequency, and $I_{\mathrm{RMS}_h i}$ the current of each individual load. The factor β is referred to as the summation coefficient, values of which can be found in IEC 610003-6, see Table 3.1 [15].

Table 3.1: Diversity factors

Harmonic order h	β
h <5	1
5< h ≤10	1.4
h >10	2

3.2.3 Attenuation as function of the loading ratio

In §3.2.2 the current distortion is evaluated as function of the number of loads. In this section the current distortion is evaluated as function of the loading ratio of a single rectifier. Simulations are performed for both single and three phase topologies. In order to be able to compare the topologies, the total amount of active power consumed by the three single phase inverters, equally balanced over the three phases, is equal to the active power consumed by the three phase rectifier. The resistance of the neutral conductor is assumed identical to the phase resistance. Simulations were executed in Matlab Simulink, by using the Power System Toolbox. Simulations were performed for a power demand of 10kW, a DC capacitor of 117,5μF/kW is used [14]. The supply voltage delivered by the grid is a pure sine wave and the voltage drop was 4% at nominal load, which is a realistic average value of voltage drop, as will be explained in §3.3.3. In a first simulation the spectrum of the current is evaluated as a function of the per unit load of the inverter. In Figure 3.2 the effect of attenuation is shown for a three phase rectifier for different loading ratios. The current is presented in p.u. value with the RMS value of the current as a reference. Harmonics of order $h = 3k$ are generally indicated as triple-N harmonics and in ideal and balanced conditions these harmonics form a zero sequenced system. Due to their specific nature, the triple-N harmonics are often excluded for analysis of three phase rectifiers. In Figure 3.3 a similar analysis is presented for three single phase rectifiers balanced over the three phases. In the analysis of single phase rectifiers, triple-N harmonics may not be excluded [14].

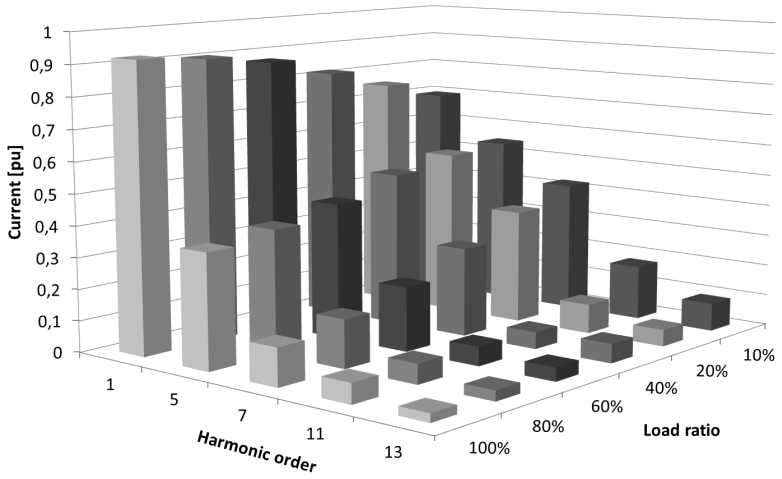

Figure 3.2: Attenuation effect for a three phase rectifiers for different loading ratios

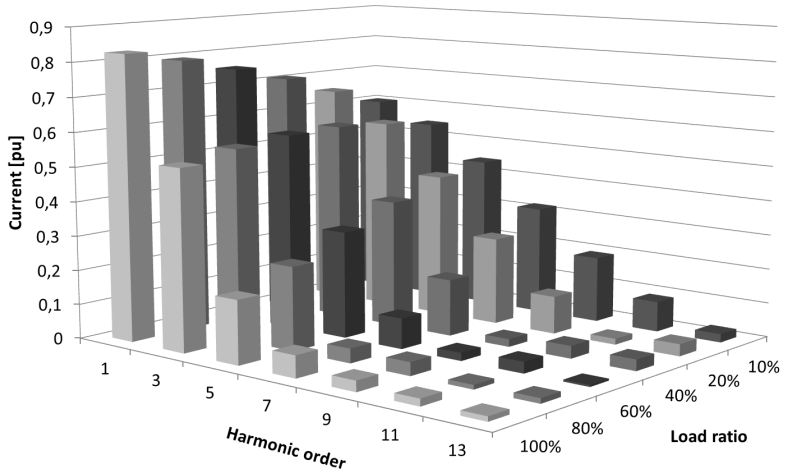

Figure 3.3: Attenuation effect for a single phase rectifier for different loading ratios

3.2.4 Evaluation of current distortion

The attenuation due to the increase in power demand leads to a reduction of the harmonic content in reference to the total current demand. These results will be used in the subsequent analysis although it needs to be addressed that this analysis is a worst-case scenario. The attenuation and diversity effect will result in almost all cases to additional damping. In the diversity effect damping originates from a phase shift in individual load current at identical harmonic frequency [10].

Individual harmonic currents interact when they are superimposed and summation rules have been suggested in literature. However, these factors are only usable when estimating the overall current distortion. Similar calculation methods have not yet been standardized for voltage distortion. In this chapter the end-user voltage quality is estimated by combining background distortion and internally generated distortion. These two distortions are also superimposed, and it is evaluated if similar summation rules can be suggested in relation to voltage distortion.

3.3 Interaction of the total impedance to harmonic voltage distortion

The resulting voltage distortion is originating from a certain current distortion and the overall impedance. Both the total complex impedance and the R/X ratio of the impedance are influencing the resulting voltage distortion. However, the resulting voltage distortion will be different if the impedance is mainly inductive (§3.3.1) or mainly resistive (§3.3.2).

3.3.1 Influence of the line reactance

If the total grid impedance is mainly inductive, the higher frequency components will induce a voltage drop increasing with the frequency as pointed out in:

$$\begin{aligned} u_{\mathrm{h}}(t) = \frac{dLi_{\mathrm{h}}(t)}{dt} &= L\frac{d\sqrt{2}I_{\mathrm{RMS_h}}\sin(h\omega t)}{dt} \\ &= \sqrt{2}I_{\mathrm{RMS_h}}Lh\omega\cos(h\omega t) \end{aligned} \tag{3.3}$$

with $u_{\mathrm{h}}(t)$ the resulting instantaneous voltage drop over the inductance L caused by the current $i_{\mathrm{h}}(t)$ of harmonic order h. The induction L of low voltage cables can be set constant. If the RMS value of the voltage drop $\Delta U_{\mathrm{h\_RMS}}$ is to be evaluated, the phase of the harmonic can be neglected:

$$\begin{aligned} \Delta U_{\mathrm{h\_RMS}} &= \sqrt{\frac{1}{T_1}\int_0^T u_{\mathrm{h}}^2(t)dt} \\ &= Lh\omega I_{\mathrm{h\_RMS}} \end{aligned} \tag{3.4}$$

As a result from (3.4) it is deduced that in case of an inductive grid impedance, the resulting voltage distortion is related to both the magnitude of the current distortion and the order of the harmonic. This leads to the conclusion that the inductance can amplify the resulting voltage distortion. Both simulations [Figure 3.4] as measurements [Figure 3.5] confirm this conclusion. The simulations presented in Figure 3.4 are simulations performed on a single

phase 350W rectifier, for which the grid inductance is increased from 0.2mH up to 1mH. A small, but negligible, grid resistance was insert in the model in order to eliminate numerical instabilities in the simulations.

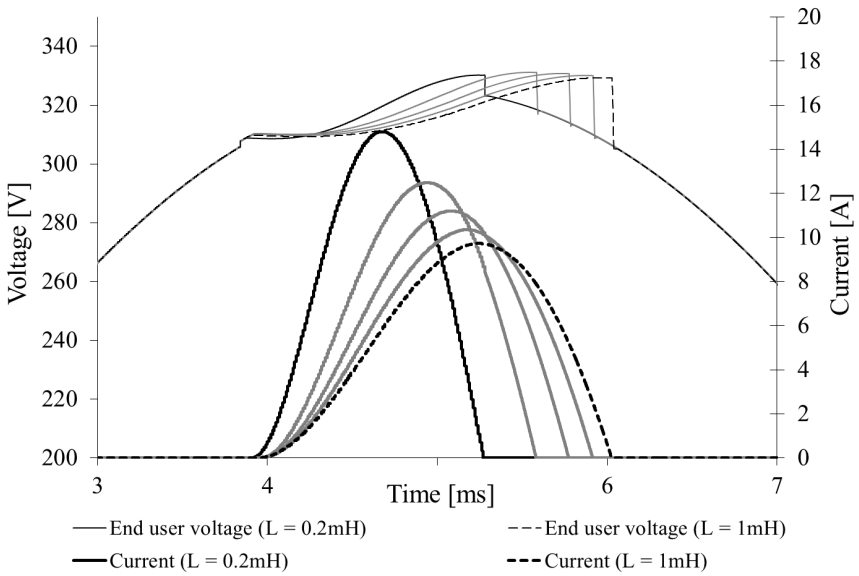

Figure 3.4: Simulation of the influence of inductance on the resulting current distortion

As an FFT analysis results in a broad spectrum [0 to 2kHz], in most cases the distortion ratio is calculated by using the Total Harmonic Distortion (THD). According to IEC 61000-4-30, this can be calculated as:

$$\mathrm{THD_I} = \sqrt{\sum_{h=2}^{40} \left(\frac{I_{\mathrm{RMS}_h}}{I_{\mathrm{RMS}_1}} \right)^2} \tag{3.5}$$

In Table 3.2 the values of the $\mathrm{THD_U}$ and $\mathrm{THD_I}$ obtained from the simulations presented in Figure 3.4 at end-user are listed.

Table 3.2: $\mathrm{THD_U}$ and $\mathrm{THD_I}$ with increasing grid induction

L [mH]	$\mathrm{THD_U}$	$\mathrm{THD_I}$
0.2	0.98	198.29
0.4	1.32	178.21
0.6	1.62	166.16
0.8	1.89	157.78
1	2.14	151.43

The effect of a dominantly inductive impedance has also been measured for

illustration. Measurements are presented in Figure 3.5 on a actual rectifier for which the grid impedance was set at 1mH.

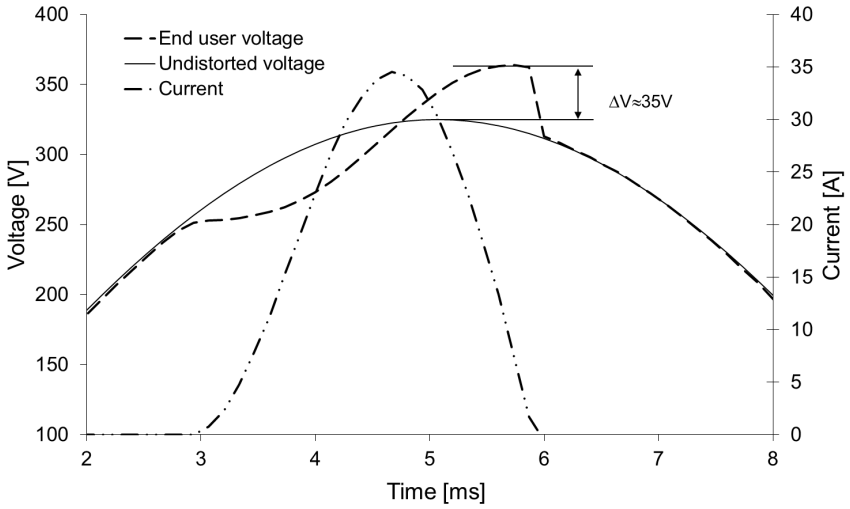

Figure 3.5: Measurement of the influence of inductance on the resulting current distortion

3.3.2 Influence of the line resistance

In the previous section the influence of the grid induction was elucidated. In this section the grid resistance is increased. As a purely resistive impedance is assumed, the resulting voltage drop is linear with the current distortion. However, the voltage drop over the grid resistance will result in an attenuation of the harmonic current distortion. To clearly demonstrate this effect similar simulations were performed with a 350W rectifier load and a grid resistance increasing from zero to 0.314Ω. A resistance of 0.314Ω gives rise to the same fundamental impedance related to an inductance of 1mH. Similarly to Table 3.2 the results of the simulations are listed in Table 3.3.

Table 3.3: THD_U and THD_I with increasing grid resistance

R [Ω]	THD_U	THD_I
0.01	0.55	199.95
0.086	0.57	198.66
0.162	0.62	195.99
0.238	0.70	192.40
0.314	0.67	187.96

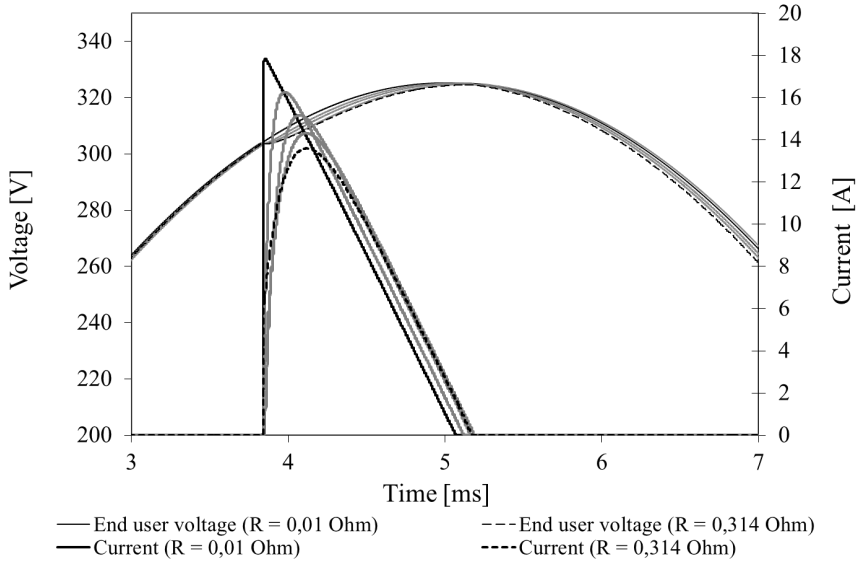

Figure 3.6: Simulation of the influence of resistance on the resulting current distortion

If the influence of the grid inductance (Table 3.2) is compared to the same fundamental impedance of the resistance (Table 3.3) it can be concluded that:

- the THD_I drops much faster for the same fundamental impedance in case of a inductive grid impedance. This is due to a larger voltage drop resulting in an increase of attenuation.
- although the THD_I drops, a large increase of THD_U is noticeable for a inductive grid impedance. Current harmonics are amplified by the inductance.

3.3.3 Resulting voltage drop

When estimating the resulting voltage distortion, both the absolute value of the impedance and the R/X ratio is essential. In this section a generalized grid impedance is calculated as function of the maximum allowed voltage drop. From the maximum allowed grid impedance the resulting end-user voltage can be simulated by using the models previously defined. Medium and high voltage networks are predominantly inductive. Therefore a pure inductive short circuit impedance is assumed. Short circuit impedances Z_{sc} can be recalculated from the short circuit power S_{sc} at POC, which normally shifts between 500MVA for "strong" grids and 180MVA for "weaker" grids. Medium voltage to low voltage transformers also influence the grid impedance. The impedance is mainly

inductive and transformer sizes vary from 250kVA, which holds the highest series impedance, to 630kVA and higher. As the power rating of the transformers increases, the series inductance at low voltage side will decrease [16]. Low voltage cables are predominantly resistive and the inductance is relatively fixed at 0.2mH/km, independent of cable diameter. The resistance is function of cross section, used material (aluminum or copper) and the length of the conductor. When rectifiers are used, the input of these rectifiers is often equipped with an RFI filter. The RFI filters' common mode inductance varies between 1.5mH and 4mH. [14]

Table 3.4: Network elements and their inductance

Network Element	Inductance	Remarks
Z_{sc} at LV	2.83 10^{-4}mH	S_{sc} 180MVA
MV/LV	0.032mH-0.041mH	Size: 250kVA to 630 kVA
LV Cable	0.2mH/km	Constant for LV cables
RFI filters	1.5mH-4mH	In common mode

From Table 3.4 it can be noticed that the largest inductance in a low voltage grid is the RFI filter. However, in differential mode the RFI inductance is highly reduced and consequently detailed analysis of the grid impedance indicates that the impedance is largely resistive.

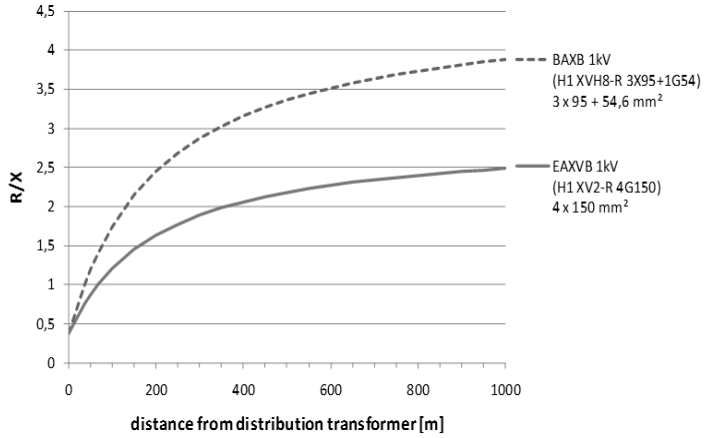

Figure 3.7: R/X ratio as function of the distance to the distribution transformer

In Figure 3.7, the RFI filter is eliminated and the R/X ratio is presented for 2 types of cable and it is noticed that only for very short physical cable lengths the inductance is predominant. This is caused by the dominating transformer inductance for short cable lengths. Cross sections of 150mm^2 are the largest sections placed in industry in order to maintain practicality, as the cross section reduces the R/X ratio will increase even more steep.

The voltage drops due to the impedance of the power grid and the impedance of the internal grid (a local industrial power grid inside a single plant). The voltage drop due to the impedance of the power grid is limited to 10% of the nominal value as stated in EN50160. When designing an industrial power grid, certain design rules have to be taken into account to assure a safe and reliable grid. European designers often use the French NFC15-100, which states for different appliances the maximum magnitude of the voltage drop [17].

Table 3.5: Maximum voltage drop according to the NFC15-100

	Lighting	Other
Type A: Installations direct fed from the public low voltage distribution grid	3 %	5%
Type B: Installations fed by a generator or distribution transformer from the high voltage grid	6 %	8%

If the cable length exceeds 100m, the voltage drop may be increased by 0.005% per meter of cable after 100m, without exceeding an additional 0.5% voltage drop.

For IM the voltage drop may not exceed 8%. An additional voltage drop of 0.5% is allowed for very long distances. If the total voltage drop at end-user is evaluated, this is up to 18.5% of the nominal supply voltage. When the load is regarded as a black box impedance Z_{load}, and the impedance of the grid is modeled as Z_{grid}, the ratio of Z_{load} and Z_{grid} can be calculated by:

$$\Delta U = \frac{I_{\mathrm{RMS}}.Z_{\mathrm{grid}}}{I_{\mathrm{RMS}}.Z_{\mathrm{total}}} = \frac{I_{\mathrm{RMS}}.Z_{\mathrm{grid}}}{I_{\mathrm{RMS}}.(Z_{\mathrm{grid}} + Z_{\mathrm{load}})} \leq 18.5\% \tag{3.6}$$

$$\frac{Z_{\mathrm{load}}}{Z_{\mathrm{grid}}} \geq 4.4 \tag{3.7}$$

If both active and reactive power are known, the RMS current I_{RMS} is known and Z_{load} can be calculated. In the subsequent paragraphs the parameter $\mathrm{THD_U}$ is evaluated in relation to the grid impedance. However, in the case of a single line feeding a single load, the impedance ratio is directly related to supply voltage drop ΔU as is illustrated in 3.6 and 3.7.

3.3.4 Evaluation of internally generated distortion

The following assumptions are made for Z_{grid} during simulations: the inductance for the calculation of Z_{grid} is assumed to be constant, the resistance can increase until the maximum voltage drop is obtained. The overall impedance is mainly resistive and is almost solely determined by the cable resistance. The models for single and three phase rectifiers from §3.2.3 are supplied from an ideal power

supply. The $\mathrm{THD_I}$ and $\mathrm{THD_U}$ as function of the RMS voltage drop for single phase and three phase loads are plotted in Figure 3.8.

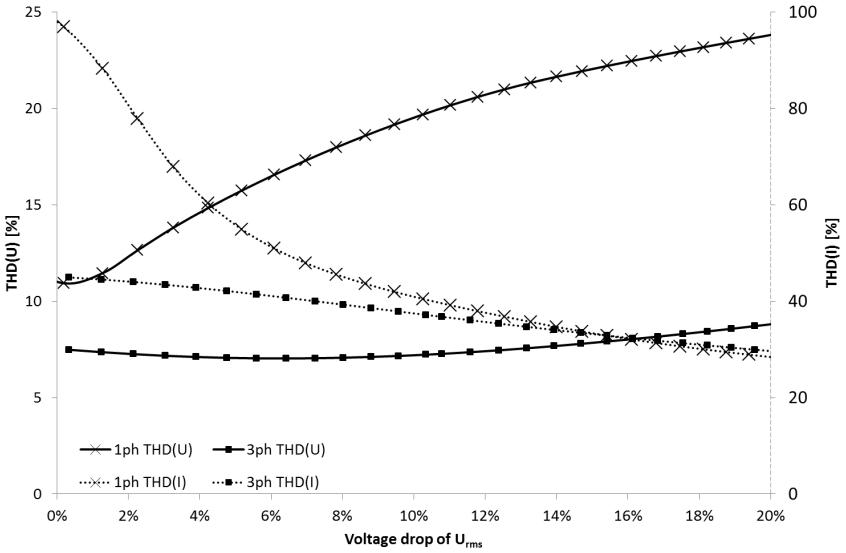

Figure 3.8: THD_I and THD_U for single phase and three phase loads as function of the RMS voltage drop

As the grid impedance increases, this results for both single and three phase rectifiers in a reduction of the current distortion. The reduction of the current distortion however does not correspond to a reduction of the voltage distortion. For single phase rectifiers the resulting voltage distortion is almost linear with increasing resistance. For three phase rectifiers it is noticed that there is indeed an optimal R/X ratio and magnitude of impedance which results in a minimum $\mathrm{THD_U}$.

The simulations were extrapolated to a total voltage drop of 20%. Although a worst case voltage drop of 18.5% still complies to all the standards, from a pragmatical point of view these excessive voltage drops will not occur frequently. Should these distortions actually occur, the resulting wave shape and the RMS value of the voltage will probably prohibit correct operation of electrical loads. When designing an actual power grid, usually a steady-state voltage drop of $\pm 4\%$ is the rule of thumb. In case of start up currents the resulting voltage will still be sufficient for starting torques of IMs.

3.4 Evaluation of background distortion

Residential grids mainly consist of single phase appliances and the majority of the power dissipation loads in industrial sites are assumed to be three phase loads. Based on the results in Figure 3.2 and Figure 3.3 this should lead to a difference in the background distortion ratio. As most of the transformers in a low voltage grid are built as Dy_0 transformers, balanced triple-N harmonic currents are closed at low voltage side and therefore are not injected upstream. Consequently, almost no triple-N harmonic content is to be found in the supply voltage. In order to have a generalized idea of background distortion, 42 measurements according to EN50160 have been performed and analyzed for both large power industrial sites (35) and sites situated in urban areas (7), see Figure 3.9. When a statistical analysis is performed the median of the measurements for industrial sites indicates a value of THD_U equal to 2.63%. For residential sites a lower value of 1.9 % THD_U is obtained. These values are similar values as described in [18].

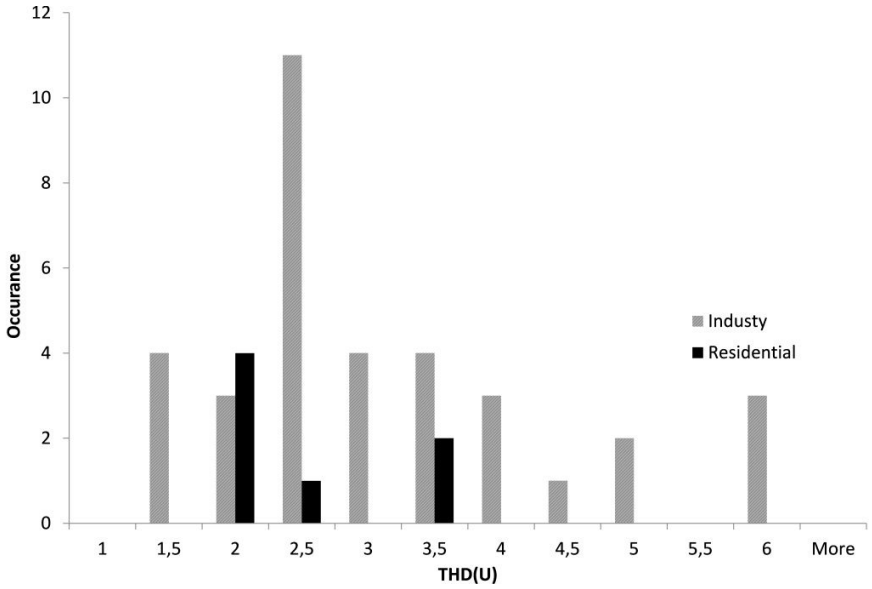

Figure 3.9: 95% occurance THD_U values obtained by EN50160 analysis for 42 sites

In an EN50160 analysis only the THD_U and the magnitude of the individual harmonics are evaluated. However, as already indicated, the phase angle of the harmonic is important if superposition of waveforms is to be evaluated. Consequently, the instantaneous voltage corresponding to the median value of the distortion is used. Using averaged or upper limits of the voltage distortion would prohibit correct evaluation of the distinctive harmonic phase angles.

3.5 Estimation of end-user voltage quality including background distortion

3.5.1 Introduction

The goal is to present an estimation of the voltage quality supplied at the end-user. Therefore the nature of the distortion has been addressed in §3.2 and the influence of the grid impedance on the resulting voltage distortion has been simulated in §3.3. In order to integrate the background distortion, a statistical analysis of the voltage at POC has been presented in §3.4. All parameters are now known and can be integrated in the simulation model for both single phase and three phase rectifiers. Whereas the previous simulation models (§3.2 and §3.3.4) used a perfectly balanced three phase voltage of $230V_{\mathrm{RMS}}$ an actual measured three phase voltage, including harmonic distortion and unbalance, has been integrated in the Matlab/Simulink model. The instantaneous values of the simulated grid voltage are those of the median value of the voltage analysis as presented in §3.4. The RMS value of the voltage is $233.3V_{\mathrm{RMS}}$ and it has a $\mathrm{THD_U}$ of 2.63%. The grid voltage is modeled as a constant voltage with the previous properties. The voltage is sampled as a discrete voltage with a sample frequency of 6.4kHz, leading to sufficient accuracy for an FFT analysis up to 2kHz.

3.5.2 Simulations

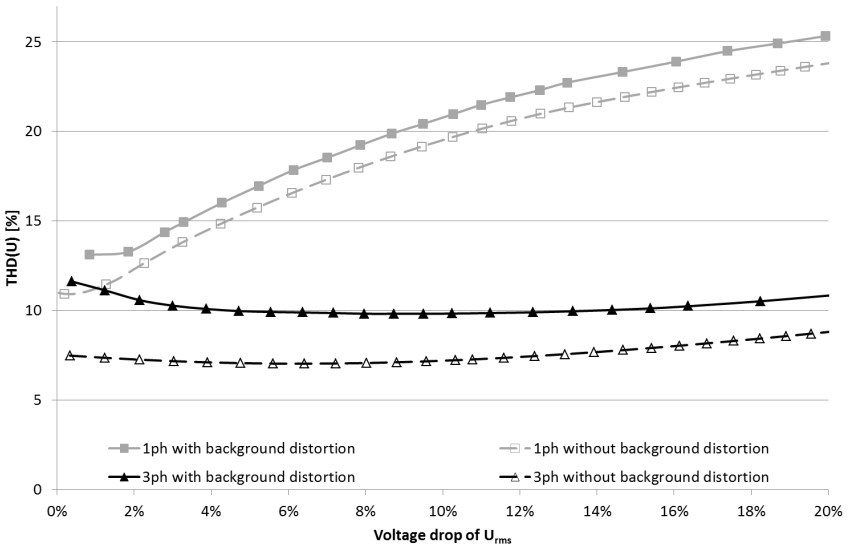

Figure 3.10: Harmonic analysis of the phase voltage as function of RMS voltage drop for three phase rectifiers including background distortion

Simulations presented in §3.3.4 have been repeated. In this simulation background distortion was integrated in the model and variation of the THD_U is plotted in Figure 3.10.

3.5.3 Evaluation

From these simulations is it is clear that the combination of both background distortion and internally generated distortion results in a general increase of the total voltage distortion at end-user. This is the case for both single phase and three phase rectifiers.

For three phase appliances the distortion for low resistance is relatively high. This is caused by a very low R/X ratio of the resulting grid impedance. The background distortion is amplified by the large inductive voltage drop, which has almost no damping. As the R/X ratio will rapidly increase the amplification is well damped by the resistance of the grid. Moreover, the large impedance will result in an attenuation effect. Nonetheless, the THD_U for single phase appliances is still well above the THD_U values for three phase appliances. Comparison between results obtained in §3.3.4 and §3.5 will be extensively described in §3.5.5.

3.5.4 Conclusions

From §3.3.1 and §3.3.2 it could be assumed that there is an optimal impedance and R/X ratio which leads to a minimum voltage distortion. These assumptions have proven to be correct as a minimum THD_U is noticeable for both single and three phase rectifiers, but the effect is more pronounced for three phase rectifiers. At a voltage drop of approximately 5% the resulting THD_U is at its minimum. This corresponds to R/X ratio at fundamental frequency of 2.85. For very small voltage drops, which is equivalent to short physical cable lengths, a small increase of THD_U is noticed. This is caused by a slight amplification of the background distortion due to the small R/X ratio.

The simulations were extrapolated to a total voltage drop of 20%. Although a worst-case voltage drop of 18.5% is still within normative limits, from a pragmatical point of view these excessive voltage drops will not occur frequently. Should these distortions actually occur, the resulting wave shape and the RMS value of the voltage will probably prohibit correct operation of electrical loads. When evaluating these excessive voltage drops, and the resulting voltage distortion, it is observed that due to the dominant resistive voltage drop, the THD_U increases linear with increasing resistance.

3.5.5 Harmonic summation rules applied to voltage distortion

In both situations the background distortion leads to an increase of the resulting $\mathrm{THD_U}$ at the end-user. Since the $\mathrm{THD_U}$ is a ratio calculation, straightforward summation of $\mathrm{THD_U}$ values is not allowed for two simple reasons. First reason is that the denominators are not equal, in this case the fundamental voltage at the POC and at end-user. Secondly, summation of the nominator would imply that the harmonic content is in phase, and as the nominator is made of the quadratic summation of the RMS voltages of the distinctive harmonic orders, which is not equal to the summation of the quadratic values. Straightforward summation of $\mathrm{THD_U}$ can be evaluated in Figure 3.11. Despite the mathematical incorrectness, according to Figure 3.11 the sum of both the internal and background distortion can result in a fairly good estimation of the resulting $\mathrm{THD_U}$.

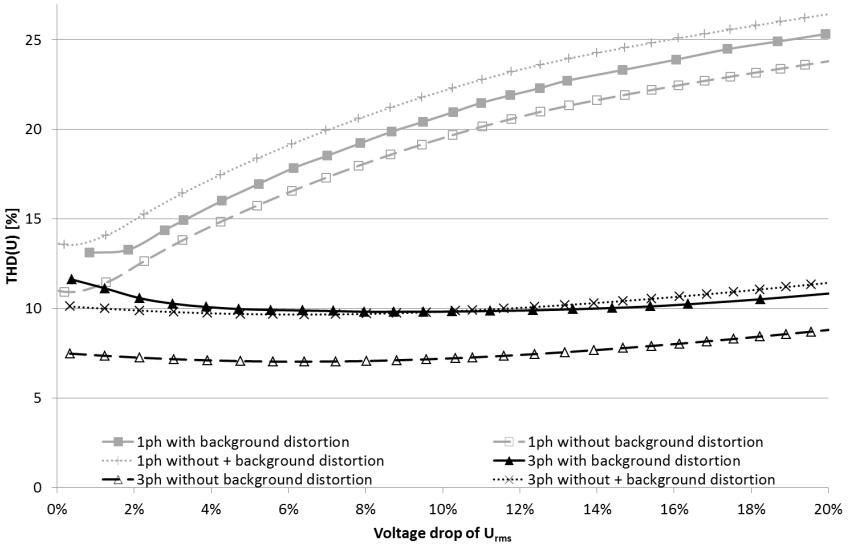

Figure 3.11: Summation of background distortion and internally generated distortion

As stated in §3.3, $\mathrm{THD_U}$ values do not show specific frequency content. In order to evaluate the summation of specific frequencies the third, fifth and seventh harmonic are evaluated for three single phase rectifiers, and the fifth and seventh harmonic are analyzed for a three phase rectifier. Both analyses are performed for a 8.5% allowed voltage drop, because summation of the $\mathrm{THD_U}$ values does fairly estimate the resulting voltage drop.

In Table 3.6 the RMS values of the harmonic end-user voltages are listed in case of sine wave supply voltage $U_{\mathrm{RMS\_int}}$, the RMS values of the harmonic background distortion $U_{\mathrm{RMS\_back}}$ and the simulated end-user voltage when

Table 3.6: Summation of harmonic magnitude for 8.5% voltage drop

	$U_{\mathrm{RMS\_int}}$	$U_{\mathrm{RMS\_back}}$	$U_{\mathrm{RMS\_end}}$
Three phase rectifier (5^{th})	6.13	1.73	7.46
Three phase rectifier (7^{th})	1.75	1.59	1.98
Single phase rectifier (3^{rd})	17.87	1.11	19.79
Single phase rectifier (5^{th})	2.4	1.73	4.46
Single phase rectifier (7^{th})	2.6	1.59	1.8

supplied with a distorted background voltage $U_{\mathrm{RMS\_end}}$. Values are presented in p.u. with the RMS voltage as a reference and for a voltage drop of 8.5%. Although straightforward summation is mathematically incorrect, according to the calculations presented in Table 3.7-middle colomn- this is a good estimation for low order voltage harmonics.

Table 3.7: Evaluation of harmonic Voltage Summation and Diversity Factors

	$U_{\mathrm{RMS\_int}}$+$U_{\mathrm{RMS\_back}}$	$Eq.\ 3.2$
Three phase rectifier (5^{th})	7.86	7.86
Three phase rectifier (7^{th})	3.34	3.34
Single phase rectifier (3^{rd})	18.98	18.98
Single phase rectifier (5^{th})	4.13	4.13
Single phase rectifier (7^{th})	3.47	4.19

It is commonly known that the sum of the squared values is not equal to the square of the sum of the values. Therefore summation of specific harmonic current always leads to errors. However, when the low frequency components, namely third and fifth harmonic, are evaluated, it is noticed that summation of harmonic content leads to fairly good estimation within a 6% error rate. If the rule of summation is to be generalized, it is noticed that the estimation by summation is relatively accurate for low frequent harmonics. If this is applied for higher frequencies, for example the seventh harmonic, this leads to an overestimation of harmonic content. However, as the lower harmonic content, third and fifth harmonic, are more dominant to higher order harmonics, the error due to higher harmonics is negligible in calculating the $\mathrm{THD_U}$ values.

It was also researched if the diversity factors, and the corresponding calculation, present a better estimation of the resulting voltage distortion. The estimated voltage harmonics according to Table 3.7-right colomn- are obtained using the calculations presented in §3.2.2, Table 3.1 and (3.2). As the diversity factors for harmonic orders $h < 5$ are equal to 1 this corresponds to straightforward summation. Higher order harmonics ($h > 5$), are estimated by using a value of $\beta = 1.4$. Although this results in a slightly better result, this still overestimates the corresponding harmonic magnitude. To conclude, calculation of the resulting

voltage distortion corresponds best to straightforward summation of the back ground distortion and the internally generated distortion in case of a reasonable voltage drop. A reasonable voltage drop implies a voltage drop less than 10% of the nominal voltage. The use of diversity factors for estimating the resulting current distortion does not increase the accuracy of estimation.

3.6 Evaluation of harmonic phase angles

3.6.1 Introduction to harmonic phase angles

In order to evaluate the influence of voltage distortion on the efficiency of DOL machines, limits should be stated to which the maximum voltage distortion can be related. The previous research indicated that a magnitude of 12% of fifth harmonic distortion at end-user can still comply to all the standards concerning voltage and current distortion. To accurately describe any periodic signal, both the magnitude as the phase angle is outputted by an FFT analysis. Because in electro-technical engineering the losses are generally related to the RMS value, the main focus is given towards the RMS values of the voltage harmonics. Although most of the losses are related to the RMS current or voltage, some losses such as the iron losses inside a machine are related to the averaged voltage. As already illustrated in Chapter 1, in order to calculated the RMS values no weighting factors are needed. However, low order harmonics have a more significant influence on the average voltage. Additionally, the introduction of $\cos(\varphi_h)$ implies that the phase of the harmonic voltage also influences the averaged voltage.

3.6.2 Cosine vs sine expansion

In Figure 3.12 a waveform is presented which consists of a fundamental 50 Hz component and both 10% fifth and seventh harmonic are superimposed onto the fundamental. As noticeable in Figure 3.12 the electrical angle $h\omega t + \varphi_h$ of the harmonic voltage h oscillates h times faster than the fundamental component. If the fifth harmonic is shifted over 90°, this relates to a shift of 1ms in the time domain for a 50Hz supply voltage, and thus with 18° in reference to the fundamental.

Consequently, the harmonic phase angle φ_h is function of the used reference. In electro-technical engineering it is common practice to evaluate the phase of the harmonic voltage at zero crossing of the signal (3.8). This is often referred to as the sine wave expansion. In scientific communities the cosine expansion is often used (3.9), this relates to a fundamental phase angle shift of 90° in reference to the sine wave expansion. Note that the used reference can have a distinctive influence of the reference of the harmonic.

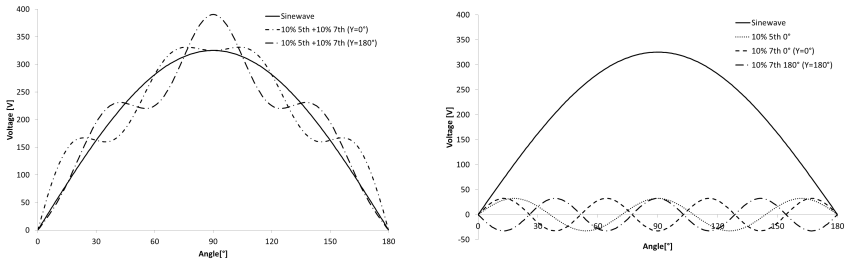

(a) Instantaneous voltage *(b) Harmonic wavefrom decomposition*

Figure 3.12: Superposition of waveforms of a fundamental and 10% fifth and seventh, with varying phase angle

$$u_{(t)} = \sqrt{2}.U_{\mathrm{RMS}_1}.\sin(\omega t) + \sum_{h=2}^{\infty} \sqrt{2}.U_{\mathrm{RMS}_\mathrm{h}}.\sin(h\omega t + \varphi_h) \tag{3.8}$$

$$u_{(t)} = \sqrt{2}.U_{\mathrm{RMS}_1}.\cos(\omega t) + \sum_{h=2}^{\infty} \sqrt{2}.U_{\mathrm{RMS}_\mathrm{h}}.\cos(h\omega t + \varphi_h) \tag{3.9}$$

3.6.3 Connection mode of three phase appliances

In (3.10) the phase voltage (voltage between the phase and the neutral conductor) is presented as the mathematical summation of all harmonic components. The second phase voltage is shifted over an electrical angle of 120 degrees or $\frac{2\pi}{3}$ radials. Both fundamental as harmonics are assumed balanced over the three phases, this implies that both the magnitude as the phase shifts are identical. The RMS value of the harmonic voltage of order h is represented as $U_{\mathrm{RMS}_\mathrm{h}}$.

$$u_{\mathrm{L1-N}}(t) = \sum_{h>0}^{\infty} \sqrt{2}.U_{\mathrm{RMS}_\mathrm{h}}.\cos(h\omega t + \varphi_h) \tag{3.10}$$

$$u_{\mathrm{L2-N}}(t) = \sum_{h>0}^{\infty} \sqrt{2}.U_{\mathrm{RMS}_\mathrm{h}}.\cos(h.(\omega t - \frac{2\pi}{3}) + \varphi_h) \tag{3.11}$$

Although generally single phase appliances are fed on phase voltages, three phase appliances can be fed in either Wye or Delta, consequently the voltage over one winding can either be the phase or the line voltage. The transition of phase to line voltage has some consequences on the harmonic phase angle as will be illustrated. The line voltage is equal to the difference between two phase voltages:

$$
\begin{aligned}
u_{\mathrm{L12}}(t) &= u_{\mathrm{L1-N}}(t) - u_{\mathrm{L2-N}}(t) && (3.12)\\
&= \sum_{h=1}^{\infty} \sqrt{2}.U_{\mathrm{RMS_h}}.\left(\cos(h\omega t + \varphi_h) - \cos(h.(\omega t - \frac{2\pi}{3}) + \varphi_h)\right)\\
&= \sum_{h=1}^{\infty} \sqrt{2}.U_{\mathrm{RMS_h}}.\left(-2\sin(h\omega t + \varphi_h - \frac{h\pi}{3}).\sin(\frac{h\pi}{3})\right) && (3.13)
\end{aligned}
$$

In terms of current and the resulting voltage distortion generally only odd harmonics are taken into account. Based on (3.13), the value of $\sin(\frac{h\pi}{3})$ becomes zero for triple-N harmonics. Consequently, these harmonics are eliminated in the line voltage in case of balanced conditions.

$$
\begin{aligned}
u_{\mathrm{L\_12}} &= \sum_{h=1,7,13\ldots}^{+\infty} \sqrt{3}.\sqrt{2}.U_{\mathrm{RMS_h}}.\cos(h\omega t + \varphi_h + \frac{\pi}{6})\\
&+ \sum_{h=5,11\ldots}^{+\infty} \sqrt{3}.\sqrt{2}.U_{\mathrm{RMS_h}}.\cos(h\omega t + \varphi_h - \frac{\pi}{6}) && (3.14)
\end{aligned}
$$

Note that in (3.14) the time reference is given for each individual harmonic. If the harmonics are to be linked in reference to the fundamental (3.14), the reference of the fundamental $\omega t + \frac{\pi}{6}$ is set equal to $\omega' t$ and this reference is substituted for the all higher harmonics. The fundamental phase shift φ_1 of $u_{\mathrm{f\_1}}$ is assumed zero at t zero.

$$
\begin{aligned}
U_{\mathrm{L\_12}} &= \sqrt{3}.\sqrt{2}.U_{\mathrm{RMS_1}}.\cos(\omega' t)\\
&+ \sum_{h=5,11\ldots}^{+\infty} \sqrt{3}.\sqrt{2}.U_{\mathrm{RMS_h}}.\cos(h\omega' t - \frac{h\pi}{6} + \varphi_h - \frac{\pi}{6})\\
&+ \sum_{h=7,13\ldots}^{+\infty} \sqrt{3}.\sqrt{2}.U_{\mathrm{RMS_h}}.\cos(h\omega' t - \frac{h\pi}{6} + \varphi_h + \frac{\pi}{6}) && (3.15)
\end{aligned}
$$

Although the influence of transition from line to phase voltage to harmonic phase angle shifts can be recalculated for any harmonic using (3.15), the specific phase angle shifts for the fundamental and harmonics 5 to 13 are listed in Table 3.8.

From Table 3.8 it is noticed that the fundamental phase shift from phase to line voltage is equal to $+\frac{\pi}{6}$ or 30 electrical degrees. If the harmonic phase angle shift is evaluated, it is noticed that there is an additional phase shift due to the transition from phase to line voltages. For the 5^{th} and 7^{th} harmonic there is a complete transition of phase angle from phase to anti-phase if the load is either supplied from

Table 3.8: Harmonic phase angle shift in case of transition phase to line voltage

h	φ_h at phase voltage	φ_h at line voltage
1	0	$+\frac{\pi}{6}$
5	φ_5	$-\pi$
7	φ_7	$+\pi$
11	φ_{11}	-2π
13	φ_{13}	$+2\pi$

phase or line voltages. For harmonics 11^{th} and 13^{th} there is no additional phase shift. The latter directly implies that, if loads are sensitive to averaged voltages, additional to the evaluation of the voltage distortion the electrical connection mode is to be evaluated. The practical implications of this transition of phase angle linked to IM will be elucidated in Chapter 4.

3.6.4 Evaluating the grid voltage distortion incl. the phase angle

In order to visually present both the harmonic magnitude and the corresponding phase angle polar plots are in the locus plots in Figures 3.13a and 3.13b.

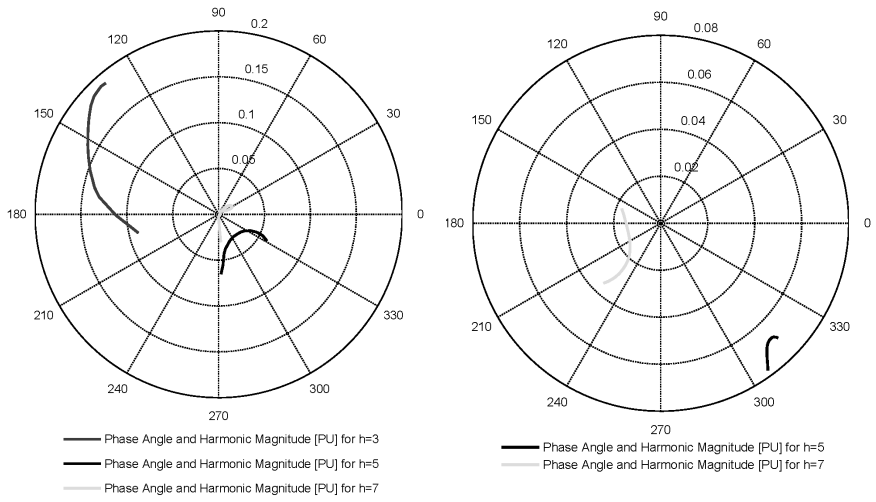

(a) Three single phase rectifiers *(b) Single three phase rectifier*

Figure 3.13: Variation of the phase angle in relation to the load condition

The length of the vector represents the magnitude of the harmonic, and the phase angle can be derived by evaluating the angle of the corresponding vector to the X-axis. Figure 3.13a relates to the voltage distortion in case of three single rectifiers and Figure 3.13b to a single three phase rectifier. The magnitude of the

distortion corresponds to the values in Table 3.6. As will be validated in Chapter 4, the phase angle of the individual harmonic components has no significant influence on the additional losses caused by supply voltage distortion inside IMs. However, for IG and LSPMM the additional losses are clearly linked to the harmonic phase angle. Consequently, this implies that evaluation of parameters such as THD_U or RMS voltage is insufficient for the intended evaluation.

3.7 Effect of harmonic current filtering on the supply voltage distortion

3.7.1 Introduction to harmonic filtering

Harmonic mitigation equipment, such as active filters, can significantly reduce the current distortion ratio. Consequently, this also suggests that active filters can have a positive effect on the resulting voltage distortion. The concept of harmonic filtering has been addressed in several studies. Several types of filters and filter strategies can be presented, but as industrial environments generally implement Shunt Harmonic Active Filtering (SHAF), this research will mainly focus on these active filters.

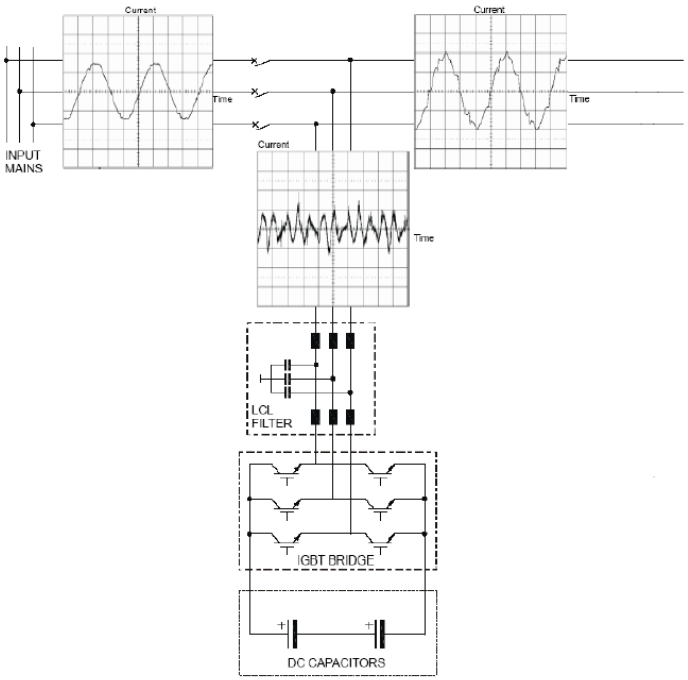

Figure 3.14: Working principle of a Shunt Harmonic Active Filter (SHAF)

SHAF has several practical advantages to other filter types:

- Parallel operation implies that this filter can be switched, maintenanced and replaced without the need to put the production process to stop.
- In case of failure the filter will be switched off by protective gear, while the production process can still be operational
- As this equipment is placed in parallel, this system cannot be overloaded by the production process. If the IGBTs reach their thermal limits, generally specified in I_{RMS}, the filter will maintain this limit without overloading.

Active filters are generally implemented in low voltage installations because harmonics results in physical effects, such as excitation of resonance phenomena or thermal overloading of transformers/conductors. Once the actual problem has been pin pointed, both the current rating as the physical implementation of the filter can be calculated. Besides the reduction of harmonic current, this filter is also capable of fundamental reactive power compensation. SHAF results in a decrease of the current distortion, however, filtering should also have a positive effect on the overall voltage distortion.

3.7.2 Effect of harmonic current filtering on the supply voltage distortion

Because this research focuses on the voltage distortion, the effect of SHAF to both the resulting current and voltage distortion has been monitored for 3 separate industrial installations. The results are listed in Table 3.9 and plotted in Figure 3.15 and 3.16.

Table 3.9: Effect of harmonic filtering on the end-user distortion

	THD_U			**THD_I**		
	L1	L2	L3	L1	L2	L3
Filter inactive (Site 1)	5.67	5.93	6.22	18.99	18.84	19.14
Filter active (Site 1)	1.99	2.00	2.06	2.42	2.91	2.34
	L1,L2,L3(AVG Value)			L1,L2,L3(AVG Value)		
Filter inactive (Site 2)	6.39			16.20		
Filter active (Site 2)	3.72			3.67		
	L1	L2	L3	L1	L2	L3
Filter inactive (Site 3)	6.70	6.85	7.10	25.9	24.8	26.7
Filter active (Site 3)	3.96	4.04	4.07	34.5	31.5	36.2

As noticeable in Figure 3.15 the SHAF positively affects the THD_U at end-user. Especially in site 1 the THD_U in case of filtering is within the same order of magnitude as the background distortion. Additionally the current distortion can also be evaluated in Figure 3.16.

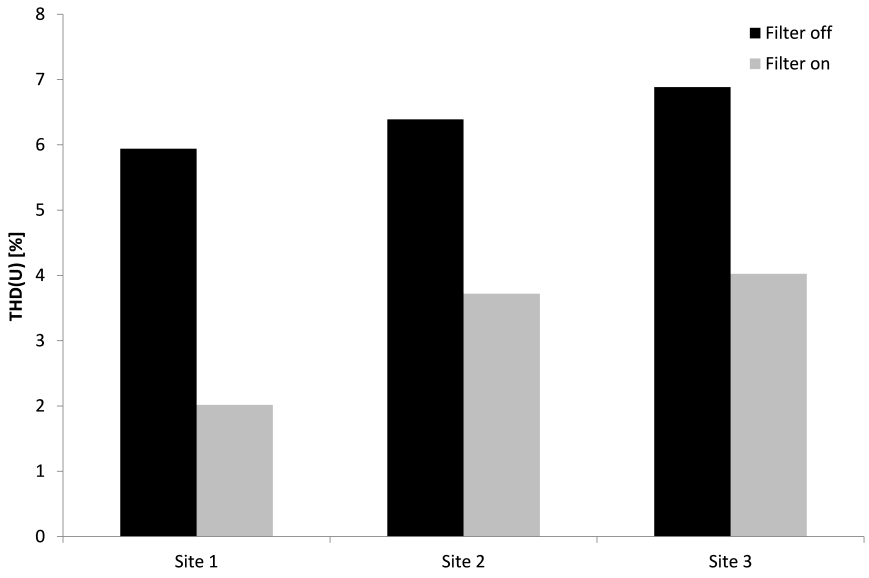

Figure 3.15: Active Filtering and its effect on the voltage distortion for 3 production sites

In site 1 and site 2 the SHAF results in a decrease of the THD_I. The monitored current in site 1 and 2 is the compensated current. It is noticed that the distortion in case of filtering is nearly reduced to zero. Only a small amount of current distortion is noticed. This can be allocated

- by a small amount of harmonic leakage current in the LCL filter caused by supply voltage distortion
- by the inability of the filter to reduce the total distortion to zero as CT have large errors at small loading
- the total bandwidth of the filtering system which is mainly determined by the CT

In site 3, it is noticed that the SHAF actually results in an increase of THD_I. The monitored current is in this case the uncompensated current to the load. Compensation of harmonics and fundamental reactive power results in an slight increase of supply voltage at end-user. Consequently, the attenuation effect results in an increase of the THD_I in relation to the load current.

3.8 Conclusions

The research presented in this section tries to estimate the supply voltage distortion at end-user. This upper limit can be used throughout the research

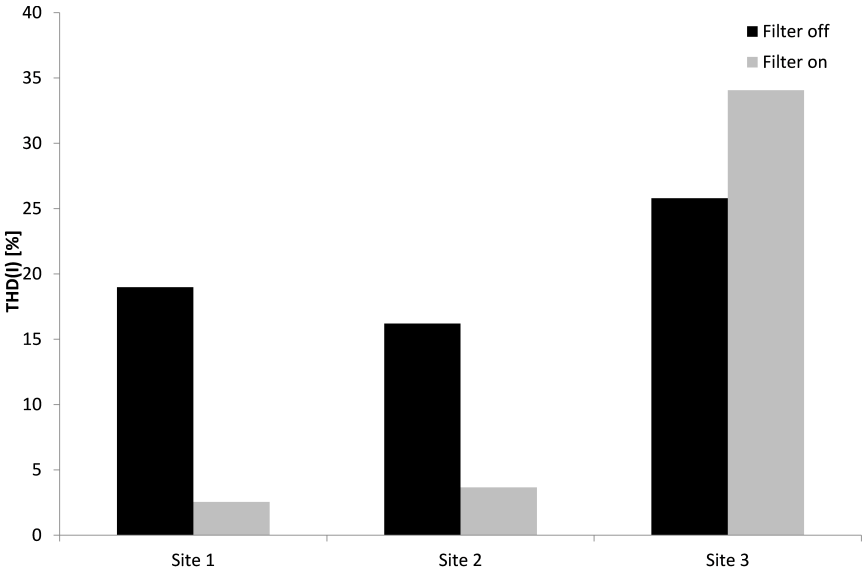

Figure 3.16: Active Filtering and its effect on the current distortion for 3 production sites

to evaluate IM operation under worst-case distortion. When regarding voltage quality, studies generally use EN50160 to give an estimation, or even maximum limit values, of the harmonic distortion at the end-user. This study indicates that the internally generated distortion is as dominant or even more pronounced in terms of end-user distortion. As a result, the limits of this distortion can exceed the limits stated by EN50160. By means of example, studies limit the fifth harmonic voltage distortion to 6%, because it is stated as a limit in EN50160. Internally generated distortion can lead to a fifth harmonic component of 6.13%. If the summation rule is used, the fifth harmonic could reach to 12.13%. The actual value will be smaller, due to the attenuation effect and some mathematical errors made by simply making a summation. This example however clearly indicates that the end-user voltage distortion can exceed the limits stated in EN50160. If the energy efficiency of appliances is to be evaluated, voltage distortion at end-user should be evaluated, and not the limits as stated in EN50160.

The phase angle of the supply voltage distortion is often neglected. Although Chapter 4 will validate that the harmonic phase angle has no significant influence in IM operations, the results in Chapters 5 and Chapter 6 will indicate that the harmonic phase angle is essential in evaluating the effect of supply voltage distortion on IG or LSPMM. Simplified Power Quality parameters such as the THD, HD, HVF, Form Factor or Crest Factor do not take the effect of both the order and phase angle into account. The presented research indicates that the harmonic phase angle of the supply voltage is related to the load current, but in

order to evaluate the averaged voltage over one winding the connection mode of the machine is also to be considered.

The positive influence of Shunt Harmonic Active Filters on the end-user voltage quality has been addressed. The values of Table 3.9 are measured values, however, it is delicate to generalize or even predict the effect of filtering harmonic currents in relation to the present distortion. The influence of the filtering to the present voltage distortion is function of the filter settings, the physical location on site and the power relation between the installed filter and injected current distortion. Table 3.9 does indicate the positive effect of reducing current harmonics and the relation to the present voltage distortion.

References

[1] M. Bollen. *Understanding power quality problems*. Power Engineering. Wiley-IEEE Press, 2000.

[2] J. de Abreu and A. Emanuel. *Induction motor thermal aging caused by voltage distortion and imbalance: loss of useful life and its estimated cost*. IEEE Trans. on Ind. App., 38(1):12–20, 2002.

[3] E. Fuchs and D. Roesler. *Agging of electrical appliences due to harmonics of the power systems voltage*. IEEE Trans. on Power Delivery, 2(3):301–307, 1986.

[4] G.. Jainy. *The Effect of Voltage Waveshape on the Performance of a 3-Phase Induction Motor*. IEEE Trans. on Power Apparatus and Systems, PAS-83(6):561–566, 1964.

[5] *IEC 61000-3-2 ed3.2 Consol. with am1&2: Electromagnetic compatibility (EMC) - Part 3-2: Limits - Limits for harmonic current emissions (equipment input current 16 A per phase)*, 2009.

[6] *IEC/TS 61000-3-4 ed1.0 Electromagnetic compatibility (EMC) - Part 3-4: Limits - Limitation of emission of harmonic currents in low-voltage power supply systems for equipment with rated current greater than 16 A*, 1998.

[7] *IEC 61000-3-12 ed2.0 : Electromagnetic compatibility (EMC) - Part 3-12: Limits - Limits for harmonic currents produced by equipment connected to public low-voltage systems with input current between 16 A and 75 A per phase*. 2011.

[8] *EN50160: Voltage Characteristics of electricity supplied by public electricity networks*, 2010.

[9] N. Mohan, T. Undeland, and W. Robbins. *Power Electronics: Converters, Applications, and Design*. John Wiley & Sons. Inc., 2003.

[10] E. Ahmed, W. Xu, and G. Zhang. *Analyzing Systems With Distributed Harmonic Sources Including the Attenuation and Diversity Effects*. IEEE Trans. on Power Delivery, 20(4):2602–2612, 2005.

[11] A. Nassif. *Modeling, Measurement and Mitigation of Power System Harmonics*. PhD thesis, University of Alberta, 2009.

[12] A. Mansoor, W. Grady, A. Chowdhury, and M. Samotyi. *An investigation of harmonics attenuation and diversity among distributed single-phase power electronic loads*. IEEE Trans. on Power Delivery, 10(1):467–473, 1995.

[13] N. Golovanov, M. Lazaroiu, G.and Roscia, and D. Zaninelli. *Harmonic summation in power systems with power electronic interfaced loads*. In 14th International Conference on Harmonics and Quality of Power (ICHQP), pages 1–5, Bergamo, Italy, 2010.

[14] J. Desmet. *Study and analysis of Losses in Low Voltage Cables under Harmonic Loading*. PhD thesis, KU Leuven, 2008.

[15] *IEC/TR 61000-3-6 ed2.0: Electromagnetic compatibility (EMC) - Part 3-6: Limits - Assessment of emission limits for the connection of distorting installations to MV, HV and EHV power systems*, 2008.

[16] *www.sgb-trafo.de*.

[17] *NF C15-100: Coordination des travaux sur les installations à basse tension*. 2002.

[18] S. Bhattacharyya. *Power Quality Requirements and Responsibilities at the Point of Connection*. PhD thesis, T.U. Eindhoven, 2011.

4

The effect of harmonic voltage distortion on Induction Motors

4.1 Introduction

Basic evaluation of the behavior of IMs is generally executed assuming a sine wave voltage, which presumably results in a sine wave MMF and a sine wave induction. However, discrete winding lay-out results in spatial harmonic MMF and the presence of rotor and stator slots results in additional slot harmonics. Even with a pure sinusoidal supply voltage is the resulting airgap MMF distorted [1]. These harmonics in the MMF are caused by the spatial lay-out and are accordingly addressed as spatial harmonics. This is basic motor knowledge, which is described in a lot of motor literature. Consequently this will be briefly discussed in §4.2.1. These harmonic components result in additional losses, the losses related to this distortion are lumped into the SLL and these losses can be effectively damped by constructive adjustments.

In chapter 3, it has also been deduced that the assumption of a sinusoidal supply voltage is no longer relevant to date. If higher frequencies are superimposed on the fundamental supply voltage, these harmonics will result in additional rotating MMF in the rotor [§4.2.2]. Although harmonics caused by supply voltage distortion will interact with harmonics caused by the spatial distribution, it will be elucidated in §4.2.4 that there is no significant averaged torque and resulting averaged power in the interaction of space and time harmonics [2]. As time and space harmonics can be regarded separately in terms of losses and efficiency, this

research will neglect space harmonics and solely focuses on harmonic voltage distortion.

This research continues by presenting some theoretical aspects concerning harmonics inside electrical machines. Supply voltage harmonics result in additional losses and a machine should be able to withstand these additional losses if the life expectancy of the machine has to be maintained. The losses in IM may not exceed certain limits, as excessive losses can result in excessive temperatures and consequently premature winding failure. In case of severe distortion the output power should be reduced, or derated, in order for the machine to cope with these additional losses [3]. Both the harmonic modeling as the different derating methods for IM when supplied with a distorted voltage are evaluated in §4.3.5.

The presented research concerning the influence of supply voltage distortion on IM tries to maintain industrial relevance. When evaluating the energy efficiency of IM under supply distortion, studies generally assume constant nominal loading. However, motors are often used under nominal loading due to the need of high starting torques, oversizing or standard series production.

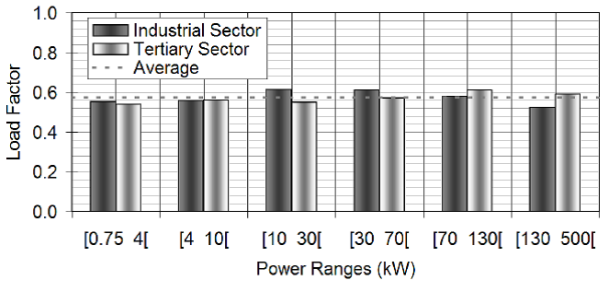

Figure 4.1: Average loading of IM [4]

According to [5, 6] and Figure 4.1 the general loading of IMs is less than 60% of their rated power. In case of partial loading the ratios of the distinctive losses shift, as explained in chapter 2. The effect of partial loading on the harmonic losses is elucidated in §4.6.2. Similarly to partial loading the loss ratio shifts in terms of output power ratio or efficiency class. The effect of the efficiency class and the power ratio is presented in §4.7.1 and §4.7.2 respectively. This chapter ends by presenting some generalized conclusions concerning the effect of supply voltage distortion on IMs.

4.2 Theoretical aspects concerning harmonics inside electrical machines

4.2.1 Spatial harmonics

Due to the mechanical positioning of windings into slots, harmonic MMFs are inherent to multi-slotted, poly-phase machines [1]. The resulting MMF distribution of a three phase IM with 3 slots per phase and pole over 2 pole pitches is plotted in Figure 4.2 for 90° electrical degrees and 0° electrical degrees. In Figure 4.2 the cosine expansion is used and consequently 0° electrical degrees correspond to maximum current in phase U, and 90° electrical degrees correspond to zero current in phase U. In Figure 4.2 the current distribution is concentrated in the center of the slot, according to the so-called Dirac idealization. This preliminary discretization discards the change of reluctance by passing a slot.

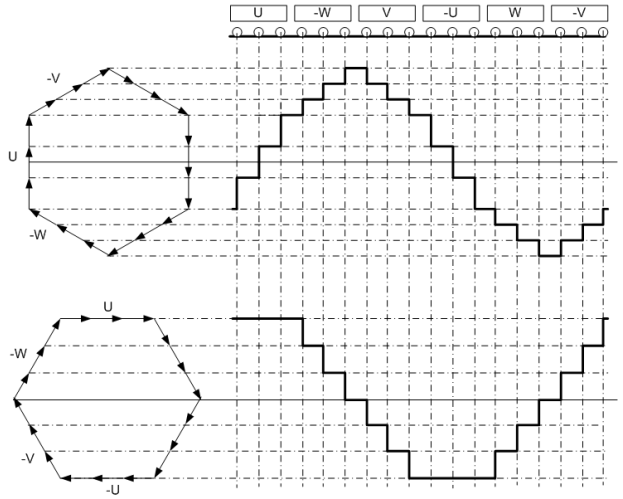

Figure 4.2: MMF spatial distribution at t=0 and at t=5ms (50Hz)

The instantaneous induction $b_u(t)$ of the reference winding U changes over time t and is linked to the location x inside the machine. According to (4.1), the induction can be decomposed into its harmonic components in which ν denotes the order of the space harmonic components and τ_p the pole pitch. Equation (4.1) assumes a non-saturated machine with diameter windings and a non distorted supply voltage.

$$b_u(x,t) = \left(\sum_{\nu=1}^{\infty} \hat{B}_{\nu,u} \cos\left(\nu . \frac{x.\pi}{\tau_p} \right) \right) \cos\left(\omega . t\right) \tag{4.1}$$

Assuming a balanced three phase supply current, the MMF of the second and third winding are shifted over an angle of 120^o both electrically and mechanically. The induction vector can be obtained according to the equation of Ferraris. The full derivation is elucidated in - §4.2.3,(4.8)- and specifically towards spatial harmonics (4.2) is obtained.

$$b(x,t) = \frac{3}{2}\sum_{\nu=1}^{\infty}\hat{B}_\nu \cos\left(\nu\frac{x.\pi}{\tau_p} \mp \omega.t\right) \tag{4.2}$$

Note that due to the symmetrical physical construction only odd MMF harmonics are generated inside the airgap of the machine. Harmonic fields can rotate counter wise or clockwise, this is indicated by the $\mp$ in (4.2). This will be addressed in §4.2.3. The speed of the induction wave in the airgap is a constant, consequently if the angular velocity of the harmonic ν is compared to the fundamental component it is noticed that:

$$\begin{aligned}(\nu\alpha \mp \omega.t) &= \mathrm{C^{te}} \\ \frac{d\,(\nu\alpha \mp \omega.t)}{dt} &= \nu\frac{d\,(\alpha)}{dt} \mp \omega\end{aligned} \tag{4.3}$$

Because the harmonic order ν is directly linked to the supply frequency ω, the rotational speed of ν order harmonic in reference to the fundamental can be calculated as:

$$\frac{d\alpha}{dt} = \mp\frac{\omega}{\nu} \tag{4.4}$$

and (4.4) can be physically translated as the harmonic order ν rotating at a frequency ω with ν number of pole pairs. Consequently, the synchronous speed of space harmonics is equal to the synchronous speed of the fundamental component divided by its harmonic order. For a fifth harmonic the synchronous speed for a single pole pair machine is equal to 3000rpm/5 or 600 rpm. In order to dampen these harmonics the number of slots per pole and phase can be increased (increasing q), or multi-layer windings can be placed inside the stator. Due to the increase of reluctance when passing a slot, additional harmonics are generated. Accordingly these harmonics are addressed as slot harmonics. Figure 4.3 is added merely to illustrate the presence of slot harmonics. The induction has been chosen low in order to avoid saturation effects and consequently is referenced in pu to its instantaneous peak induction. Multi-layering or increasing the number of slots per pole and phase q does affect the order of the slot harmonics, however, it does not affect the magnitude of these slot harmonics. Only skewing of the rotor bars results in an effective cancellation of the induced slot harmonics.

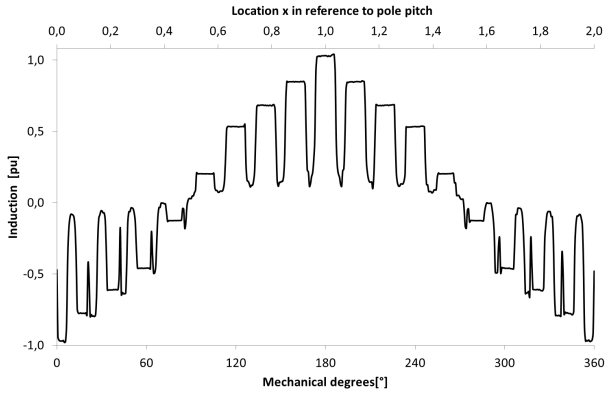

Figure 4.3: Induction spatial distribution obtained by FEM at t=0 including slot reluctance

Harmonics generated by the spatial distribution of harmonics into slots do generate additional losses. These additional losses are lumped into the Stray Load Load (SLL) losses. Several standards estimate these losses, however a general guideline is to estimate these SLL at 0.5% of the machine's input power [7]. This has been adressed in detail in chapter 2.

4.2.2 Time harmonics

The supply voltage results in magnetizing current. This current results in stator and rotor MMF. At first saturation is neglected, creating a linear link between supply voltage and induction. As will be illustrated in §4.3.1, this assumption will prove valid for IM used as a motor. In (4.5) only the fundamental component of the spatial distribution of the MMF is considered. Dual expressions can now be formulated as in §4.2.1, assuming a distorted supply voltage.

$$b_u(x,t) = \cos\left(\frac{x.\pi}{\tau_p}\right)\left(\sum_{h=1}^{\infty}\hat{B}_{h,u}\cos\left(h.\omega.t\right)\right) \tag{4.5}$$

In (4.5) h denotes the harmonic order of the distortion present in the supply voltage. The distortion is assumed equally and symmetrically balanced over the individual phases. Consequently the reference, or harmonic phase angle φ_h, is of no importance. The total induction including time harmonics can be obtained:

$$b_{(x,t)} = \frac{3}{2}\sum_{h=1}^{\infty}\hat{B}_h\cos\left(\frac{x.\pi}{\tau_p} \mp h.\omega.t\right) \tag{4.6}$$

If the angular velocity of the harmonic component is to be referred to the fundamental:

$$\frac{d\alpha}{dt} = \omega.h \tag{4.7}$$

This implies that the synchronous speed of voltage induced harmonics is equal to the fundamental velocity multiplied with its harmonic order h. For a fifth harmonic this implies for a 3000rpm machine that the speed of the fifth harmonic due to harmonic voltage distortion is equal to 15000 rpm. It is important to stress that constructive adjustments such as double layering the stator winding or skewing does not comply as an effective means of damping of the influence of supply voltage harmonics.

4.2.3 Direct and inverse rotation

Harmonics due to spacial distribution of the windings into slots are inherent to the construction of IM. Additionally the supply voltage can be distorted. Therefore, the instantaneous induction generated in phases u, v, w can be decomposed of both spatial and supply voltage harmonics. If the superposition rule is extrapolated, each harmonic voltage would again result in a set of harmonics linked to the spacial distribution. For example, considering the effect of the 5^{th} time harmonic on the 5^{th} spatial harmonic is the production of a rotating MMF with the same speed and direction of the fundamental MMF. Only one reference has been found which specifically addresses this phenomena. [2] suggests for each supply voltage harmonic a set of electrical equivalent models for each spacial harmonic, consequently they suggest superposition of all the harmonic models. It also states that the interaction of space and time harmonics result in air-gap torque pulsations and consequently vibration and acoustical noise, although the large damping implies that the overall contribution of spatial harmonics induced by supply voltage harmonics is small.

$$\begin{aligned}
b_u(x,t) &= \sum_{h,\nu=1}^{\infty} \hat{B}_{h,\nu,\text{u}}.\cos\left(\nu.\frac{x.\pi}{\tau_p}\right).\cos\left(h.\omega.t\right) \\
b_v(x,t) &= \sum_{h,\nu=1}^{\infty} \hat{B}_{h,\nu,\text{v}}.\cos\left(\nu.(\frac{x.\pi}{\tau_p}-\frac{2\pi}{3})\right).\cos\left(h.(\omega.t-\frac{2\pi}{3})\right) \\
b_w(x,t) &= \sum_{h,\nu=1}^{\infty} \hat{B}_{h,\nu,\text{w}}.\cos\left(\nu.(\frac{x.\pi}{\tau_p}-\frac{4\pi}{3})\right).\cos\left(h.(\omega.t-\frac{4\pi}{3})\right)
\end{aligned} \tag{4.8}$$

If the equation of Ferraris is used, the induction vector inside the machine can be evaluated.

$$b(\nu,h,x,t) = \frac{3}{2}\sum_{h,\nu=1}^{\infty} \hat{B}_{h,\nu}\cos\left(\frac{\nu.x.\pi}{\tau_p} - h.\omega.t\right) \tag{4.9}$$

with

$$\begin{aligned} h &= 1+6k \quad (4.10)\\ \nu &= 1+6i \quad (4.11)\\ -\infty < &\ k\ < +\infty\\ -\infty < &\ i\ < +\infty \end{aligned}$$

Up to (4.8), the index h simply denoted the harmonic order of the supply voltage distortion. However, in order to evaluate the influence of distortion on the operation of IM, it is common practice to denote harmonic orders in the form of $h = 1 + 6k$ or $\nu = 1 + 6i$. In this expression, k and i not only denote the harmonic order, they also indicate the sequence of the field. If k or i is equal to -1, h or ν equals -5. If k or i is 1, a h or ν of +7 is obtained and if k or i is equal to 0, the fundamental value of 1 is obtained. The previous indicates that a fifth harmonic generates an inverse field in reference to the fundamental component and a seventh harmonic generates a direct field in motor operation. By additionally assigning a $\pm$ index to the harmonics h and ν, this is automatically taken into account in (4.9). When evaluating non sinusoidal three phase systems, different transformations can be used to simplify calculation. Although the dq and $\alpha\beta$ transformation are very useful to evaluate the iron losses under distorted conditions or to accurately control speed and/or torque, generally a symmetrical component transformation (Fortescue transformation) is preferred in an harmonic evaluation.

4.2.4 Interaction of space and time harmonics

According to the basic laws of electromagnetism, the mechanical force $f(x,t)$ is the combination of a current distribution $a(x,t)$ at a certain point x at time t, and the magnetic field density $b(x,t)$ over the active length l.

$$f(x,t) = b(x,t).a(x,t).l \quad (4.12)$$

If the torque $T(x,t)$ of an IM has to be calculated, (4.12) can be expanded to (4.13):

$$T(x,t) = f(x,t).r \quad (4.13)$$

with $T(x,t)$ the torque induced by the force $f(x,t)$, and r the radius of the rotor. If the averaged force on the rotor is to be obtained, the force should be integrated over the entire pole pitch τ_p, the number of pole pairs N_p and over the fundamental period of the supply voltage T_1. As a result, the averaged torque can be calculated as:

$$T = C^{\text{te}} \int_0^{T_1} \int_0^{\tau_p} b(x,t).a(x,t)dxdt \quad (4.14)$$

with T_1 the period of the fundamental voltage component, τ_p the pole pitch, and

$$C^{\mathrm{te}} = 2.\frac{\tau_p.{N_p}^2}{\pi}.l \tag{4.15}$$

The theorem of Fubini states that the order of integration is of no importance.

$$\begin{aligned}\frac{1}{\tau_p}.\frac{1}{T}\int_0^{\tau_p}\int_0^{T} 2.N_p.r.f(x,t).l dxdt &= \frac{C^{\mathrm{te}}}{\tau_p.T}\int_0^{\tau_p}\int_0^{T} b(x,t).a(x,t)dxdt \\ &= \frac{C^{\mathrm{te}}}{\tau_p.T}\int_0^{T}\int_0^{\tau_p} b(x,t).a(x,t)dtdx \end{aligned} \tag{4.16}$$

In terms of spatial harmonics, a diameter winding distribution is assumed. Consequently, only odd spatial harmonics are generated (4.11). In terms of supply voltage distortion, according to chapter 3 only odd harmonics are generated. In both cases triple-N harmonics are excluded. Independent of the origin of the harmonic distortion, the instantaneous multiplication of harmonics of the same order result in a DC component, if different harmonic orders are combined this results in an additional torque ripple of order six. However, as the averaged torque is calculated the odd torque ripple is eliminated and only the DC component remains. Consequently, the theorem of Fubini directly implies that there is no average torque due to interaction of time and spacial harmonics. Although the phase of the harmonic might have an influence on instantaneous torque, the phase of the harmonic has no influence on the average torque. Shifting of the phase angle and its effect is illustrated in Figure 4.4, its goal is only additional clarification.

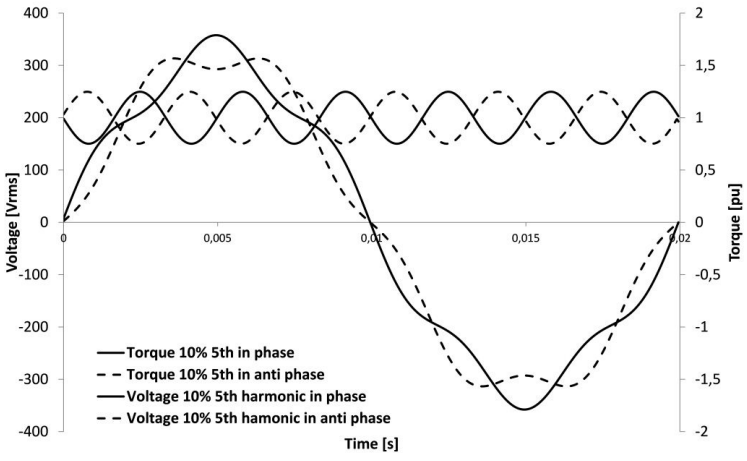

Figure 4.4: Variation of the harmonic phase angle and the effect on the instantaneous torque

4.3 Additional losses caused by supply voltage distortion

4.3.1 Linearization and additional iron losses

In the subsequent sections and chapters the effect of spatial harmonics is excluded and only supply voltage distortion is evaluated. If a linear induction is assumed, this largely simplifies harmonic analysis of machines as a direct link between voltage distortion, current distortion and distortion of the induction is established. Before this assumption is presumed this should be evaluated. As a reference for the magnetic saturation the sine wave condition is used. For machines of power rating above 4kW and at nominal supply frequency, the stator impedance is often neglected in calculation of the resulting induced voltage. Therefore the induced average voltage in one winding E_{avg} is nearly identical to the applied winding voltage U_{avg}.

$$u(t) \approx e(t) = \frac{dl(t)i(t)}{dt} = N\frac{d\Phi(t)}{dt} \tag{4.17}$$

with $u(t)$ the clamp voltage over one winding at time t, $e(t)$ the induced voltage in one winding at time t, $l(t)$ the inductance for a certain MMF level, $i(t)$ the current at time t, N the number of windings and $\Phi(t)$ flux at time t. The average value E_{avg} or thereby U_{avg} can be calculated as:

$$U_{\mathrm{avg}} = \frac{2}{T_1}\int_{t_0}^{t_0+T_1/2} u(t)dt \tag{4.18}$$

with:

$$u(t_0) = u(t_0 + \frac{T_1}{2}) = 0 \tag{4.19}$$

where T_1 is the period of the signal and therefore $1/T_1$ is the fundamental frequency f. The following common expression can be derived from (4.17) and (4.18):

$$E_{\mathrm{avg}} = \frac{2}{T_1}\int_{0}^{T_1/2} e(t)dt = \frac{2}{T_1}\int_{\Phi_{\max}}^{\Phi_{\min}} N\frac{d\Phi(t)}{dt} = 4fN\Phi_{\max} \tag{4.20}$$

where $\Phi_{\max}$ is the maximum or peak flux and for a stable situation $|\Phi_{\max}|$ equals $|\Phi_{\min}|$. Eq.(4.17) and (4.20) are generally valid, both for a perfect sine wave as for a distorted supply voltage. Eq.(4.20) illustrates that the average voltage is the main parameter for calculating the IM stator peak flux $|\Phi_{\max}|$. If the voltage is distorted, only the odd harmonics are taken into account. Even harmonics have no influence on the peak flux since the resulting integral over half a period equals zero. The average value of a voltage with harmonic content $U_{\mathrm{h\_avg}}$ can be calculated as:

$$
\begin{aligned}
U_{\mathrm{h\_avg}} &= \frac{2}{T_1}\int_0^{T_1/2}\sum_{h=1}^{\infty}\sqrt{2}U_{RMS\_h}\sin(h\omega t+\varphi_h)dt \\
&= \frac{2\sqrt{2}}{\pi}\sum_{h=1,3,5\ldots}^{\infty}\frac{U_{\mathrm{RMS\_h}}}{h}\cos(\varphi_h) \qquad (4.21)
\end{aligned}
$$

IMs are designed to work close to the saturation level conditions. In this way the magnetic material is used at its optimum weight/energy ratio. For commonly used magnetic steels an induction of 1,2T to 1,5T is targeted. In motor operation there is a voltage drop over the stator impedance generally reducing the total EMF. As a result it is generally assumed that IMs in motor operation operate below saturation levels. This implies a linear correlation between voltage and induction, thus facilitating calculations. In a first test the magnetizing current has been evaluated for seven different 4-pole TEFC 4kW IMs.

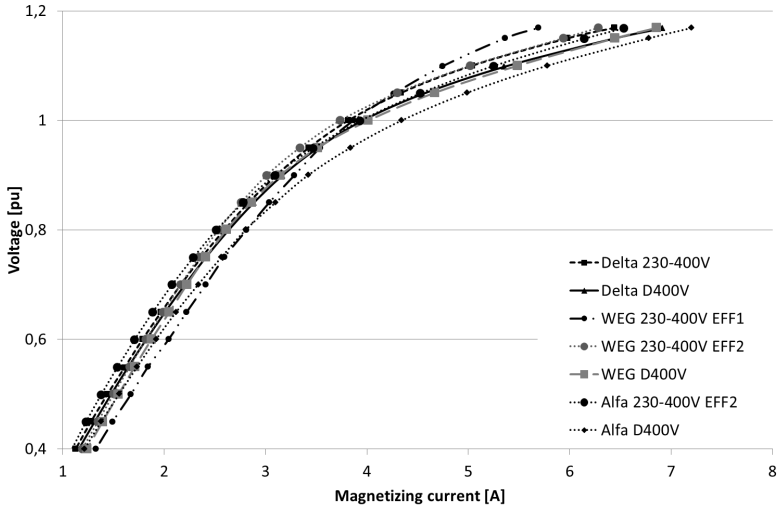

Figure 4.5: Magnetizing current for seven different 4kW IM

As noticeable from Figure 4.5 for a 4kW IM the magnetizing characteristic is within the same order of magnitude for different IMs of identical power. Only small deviations were observed comparing IE2-EFF1 and IE1-EFF 2 motors. If the maximum distortion of 15% fifth is shifted in phase angle this will result in a shift of 3% in averaged voltage according to (4.21). The shift in averaged voltage will result in a shift of resulting magnetizing current. The shift of the harmonic phase angle for 15% fifth is set out against an averaged magnetizing current of a 4kW IM in Figure 4.6.

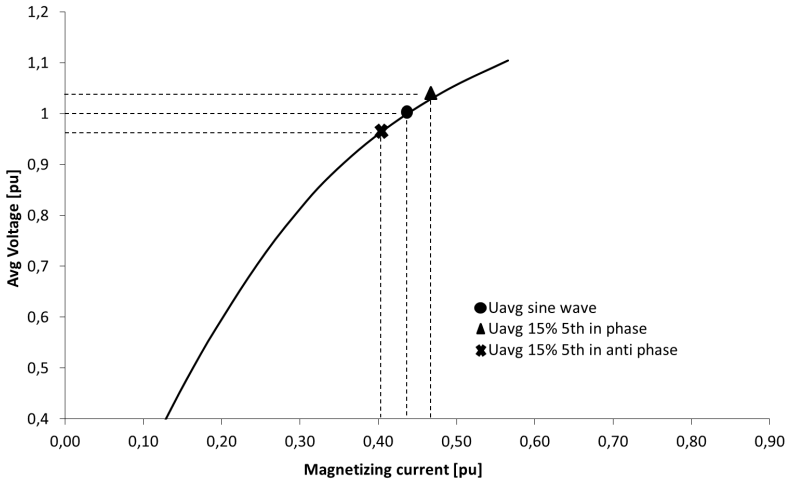

Figure 4.6: Shift of averaged voltage in reference to the magnetizing current for an averaged 4kW IM

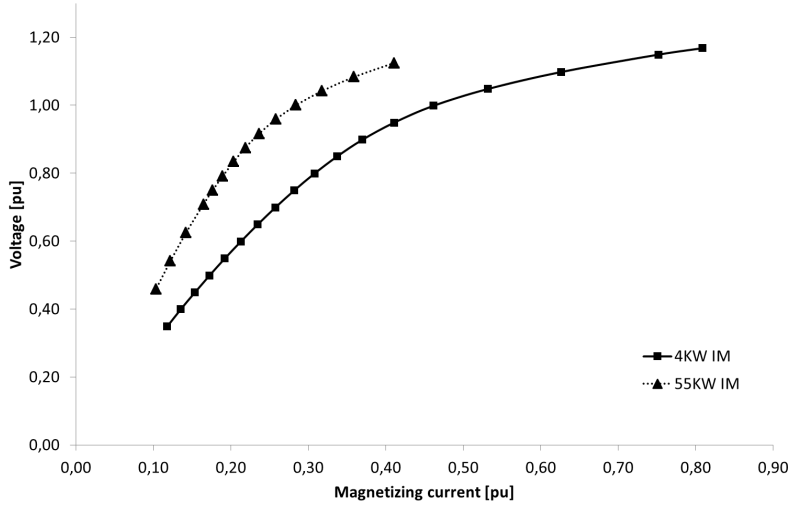

Figure 4.7: Magnetizing current for a 4-pole 4kW versus a 2-pole 55kW machine

The saturation is also evaluated in relation to the output power. A 4-pole 4kW and a 2-pole 55kW IM have been measured. With increasing power ratio, the stator resistance reduces. For the 55kW IM the stator resistance is very small $(\pm 0.05\Omega)$, for a 4kW IM the stator resistance is larger $(\pm 1.4\Omega)$. The increased number of pole pairs in the windings may result in a reduction of the amount of stator lamination steel. Consequently, it is plausible that the p.u. magnetizing current not only relates the power but also to the speed ratio of the machine.

Figure 4.7 confirms that with increased power and speed ratio the magnetizing current reduces. A more steep current/voltage characteristic is noticed, indicating an increased mutual induction. Although linearization of the induction is now roughly validated, the shifting of the harmonic phase angle results in a shift of the peak flux. Low order harmonics will have a more significant influence on the average voltage, and the resulting peak flux as shown in (4.21). Therefore the harmonic order with the largest influence is the fifth harmonic. In order to evaluate the increase or decrease of induced voltage, and in addition the flux, (4.21) can be set out to its reference value, being the induced voltage for sine wave condition.

$$\frac{U_{\mathrm{h\_avg}}}{U_{\mathrm{avg\_1}}} = \frac{\sum_h \frac{U_{\mathrm{RMS\_h}}}{h} \cos(\varphi_h)}{U_{\mathrm{RMS\_1}}} = \frac{\Phi_{\mathrm{h\_max}}}{\Phi_{\mathrm{max\_1}}} \tag{4.22}$$

Note that the phase angle of the harmonic distortion can have a significant influence on the magnetizing state of the machine. Chapter 2 already illustrated the variation of the harmonic phase angle of the voltage distortion as a function of either the loading ratio as the connection mode. If the transition from phase to line voltage is made, certain harmonics shift over 180° electrical degrees. This will affect the total averaged voltage and consequently the magnetizing of the machine. Eq. 4.22 presented in [8] is a simplification of (4.23), as the phase angle of each harmonic is assumed equal to 0:

$$\frac{\Phi_{h\_max}}{\Phi_{\mathrm{max\_1}}} = \frac{1 + \sum_{h \neq 1} \frac{U_{\mathrm{avg\_h}}}{hU_1}}{\sqrt{1 + (THD_U)^2}} \tag{4.23}$$

The magnetizing losses are linked to the flux density or induction (Φ/A) with A the surface area. In case of sinusoidal voltage, the magnetization losses can be derived from the classic Steinmetz equation presented in chapter 2. As the iron losses are coupled to the peak induction, and consequently the averaged supply voltage, the iron losses will increase in reference to sine wave conditions if the ratio in (4.22) is higher than 1. Although (4.22) presents the variation of the peak induction in case of supply voltage distortion, there are two main drawbacks to use the Steinmetz formula. The first problem is that the Steinmetz coefficients need to be derived by tests. Second drawback of the Steinmetz equation is that it is only valid for sinusoidal supply voltages. Consequently, the variation of the instantaneous induction level $(\frac{db_{(t)}}{dt})$ should evaluated and more detailed iron loss models are needed to accurately determine the iron losses in case of distorted supply conditions [9].

Although supply voltage distortion has a measurable influence on the iron losses, the measurements presented in §4.6.1 will indicate that the phase angle of the distortion is only of minor significance in terms of overall losses variation for small machines at partial load. Additionally the results will confirm that even for large scale machines linearization may be assumed if the voltage distortion is

less than 15% of fifth. Consequently, harmonic loss evaluation neglects the minor influence of supply voltage distortion on the overall losses. The linearization does inhibit the possibility to use superposition of harmonic models and the corresponding losses.

4.3.2 Skin effect in electrical conductors

Due to presence of higher frequencies in the rotor current not only the RMS value of the rotor current will increase. Because of the high frequency additional voltages will be induced inside the rotor bar forcing the current to flow in a reduced section. This effect is well known as the 'deep bar' effect or the 'skin effect'. The reduction of the active surface results in additional resistance, which is sometimes desirable to increase the start up torque as is the case for double cage IMs. However, at normal operation this additional resistance is undesirable because this results in additional losses. In addition the top of the rotor lamination may saturate and result in an increase in magnetic resistance or consequently a decrease in magnetic inductance. Both the increase of the resistance, as the decrease of rotor inductance are integrated in the correction coefficients K_r and K_x. For rectangular bars the values of K_r and K_x can be analytically obtained by (4.24) and (4.25).

$$K_r = \xi \frac{\sinh 2\xi + \sin 2\xi}{\cosh 2\xi - \cos 2\xi} = \frac{R_{\mathrm{ac}}}{R_{\mathrm{dc}}} \tag{4.24}$$

$$K_x = \frac{3}{2\xi} \frac{\sinh 2\xi - \sin 2\xi}{\cosh 2\xi - \cos 2\xi} \tag{4.25}$$

with

$$\xi = h\sqrt{\frac{\omega\mu\gamma}{2}} = \frac{h}{\delta} \tag{4.26}$$

h denotes the physical height of the rotor bar, ω is the angular velocity at a certain frequency, μ is the absolute permeablility and γ is the conductivity of the rotor bar material. The value of $\sqrt{\frac{2}{\omega\mu\gamma}}$ is often denoted as the penetration depth δ and consequently ξ is denoted as the reduced height. The skin effect becomes dominant if $\xi > 1$. The effect of an increase of each individual parameter towards the total resistance is presented in Table 4.1.

Table 4.1: Effect of parameter variation to skin effect

Parameter	δ	ξ	K_r
frequency [↗]	↘	↗	↗
conductivity [↗]	↘	↗	↗
conductor height [↗]	[-]	↗	↗

For wire wound coils the height of the conductor is very small to the penetration depth and this validates neglecting the skin effect in stator coils. For rotor bars supplied at very low frequencies the value of δ is high, and the value of ξ is small. Consequently for very low frequencies, the skin effect is less important. As the frequency increases, the penetration depth reduces, this implies that the ratio ξ, and consequently K_r, will also increase.

4.3.3 Additional stator Joule losses

If the supply voltage to the DOL machine is distorted, this will result in a distorted current. As stated in chapter 2, the stator Joule losses can be calculated according to Joule's law. In case of harmonics in the current, the losses in the stator coils can be calculated by (4.27). The RMS value of the harmonic current of order h is indicated by $I_{\mathrm{RMS_h}}$.

$$P_{\mathrm{s}} = 3.\sum_{h=0}^{\infty} R_{s\_h}.I^2_{\mathrm{RMS_h}} \tag{4.27}$$

Because stator coils are generally copper wire wound, the section is small and the influence of the skin effect inside the stator coils is negligible for low frequent distortion [10]. Consequently (4.27) can be recalculated to:

$$\begin{aligned} P_{\mathrm{s}} &= 3.R_s.\sum_{h=0}^{\infty}.I^2_{\mathrm{RMS_h}} \\ &= 3.R_s.I^2_{\mathrm{h\_RMS}} \end{aligned} \tag{4.28}$$

The RMS value of the current is larger in case of a distorted voltage in reference to a pure fundamental supply and for the same average torque this results in additional stator Joule losses.

4.3.4 Additional rotor Joule losses

In case of an IM the rotor rotates at a mechanical speed slightly differing from the synchronous speed of the magnetic field inside the machine. The parameter s, often referred to as slip value, is the difference between the mechanical rotation speed and the rotation speed of the fundamental magnetic field. The frequency of the induced currents in the rotor originate due to difference between the harmonic content of the induction and the actual mechanical speed of the rotor. The frequency of the induced harmonic currents in the rotor is coupled to the relative movement of the rotor Ω_{m} in reference to the speed of the harmonic current layer $\Omega_{\mathrm{s\_h}}$ (4.29).

$$\Omega_{\mathrm{s}\_h} - \Omega_{\mathrm{m}} = (1+6k)\frac{\omega_{\mathrm{s}}}{N_{\mathrm{p}}} - (1-s)\frac{\omega_{\mathrm{s}}}{N_{\mathrm{p}}} = (6k+s)\frac{\omega_{\mathrm{s}}}{N_{\mathrm{p}}} \tag{4.29}$$

Parameter $\Omega_{\mathrm{s\_}h}$ in (4.29) is the synchronous speed of the current layer induced by the stator harmonic current h. According to (4.29) the relative movement of stator harmonic current layers in reference to the rotor speed can be calculated for each individual stator harmonic. Up to this point all the harmonics were indicated by the index h, and subsequently the harmonics were referred to the supply voltage and consequently to the stator. However, according to (4.29) the transition to rotor reference results in a change in induced frequency. Consequently stator harmonics will be indicated using the index h, rotor harmonics are indexed by k. The instantaneous rotor current i_r is equal to (4.30):

$$i_r = \sum_{k=-\infty}^{+\infty} \hat{I}_{\mathrm{r\_k}} \sin\left(\left(6k+s\right)\omega_s t + \varphi_k\right) \tag{4.30}$$

with $k = 0$ referring to the fundamental component and $k \neq 0$ referring to harmonic components. $\hat{I}_{\mathrm{r\_k}}$ is the peak value of the rotor current linked to the stator harmonic $h = 1 + 6k$ and the value of phase angle φ_k is referenced to the rotor reference frame. Suppose two different stator harmonics result in rotor harmonic currents $i_{\mathrm{r\_k1}}$ and $i_{\mathrm{r\_k2}}$. Calculating the rotor current RMS value based on (4.30) results in:

$$\begin{aligned} I^2_{\mathrm{r\_RMS}} = I^2_{\mathrm{RMS\_k1}} + I^2_{\mathrm{RMS\_k2}} + 2.\tfrac{I_{\mathrm{RMS\_k1}}.I_{\mathrm{RMS\_k2}}}{T}. \\ \Big(\int_0^T \cos\left(6(k_1-k_2)\omega t + (\varphi_{k1}-\varphi_{k2})\right) dt \\ - \int_0^T \cos\left(\left(6(k_1+k_2)+2s\right)\omega t + (\varphi_{k1}+\varphi_{k2})\right) dt\Big) \end{aligned} \tag{4.31}$$

Some interesting conclusions from (4.31) can be observed:

- if $s \neq 0$, which is inherent to the operation of the IM, the integral from each cosine function becomes zero, independent of the relation k_1 to k_2.
- because $s \neq 0$, each stator harmonic h results in a specific rotor frequency

As a result in case of IM superposition of rotor harmonic losses is valid, as has been suggested in [11] and [8]. Consequently, if the harmonic rotor current is known, corresponding rotor losses can be calculated according to:

$$P_{\mathrm{r}} = \sum_{k=-\infty}^{+\infty} I^2_{\mathrm{RMS\_k}}.R_r.K_{\mathrm{r\_h}} \tag{4.32}$$

with $I_{\mathrm{RMS\_k}}$ the RMS value of the harmonic rotor current k, R_r the rotor resistance at fundamental frequency $h = 1$. Because of the high frequency of $6k + s$ for the rotor currents, additional voltages will be induced forcing the rotor current to flow near the top of the rotor bar. This effect is modeled for each individual harmonic by the parameter K_{rh}. Although superposition of the rotor losses is allowed a

simplification as presented in (4.28) for the stator Joule losses is prohibited due to the skin effect. The increase of rotor resistance is illustrated for a 4kW IM for fifth harmonic distortion. An rectangular aluminum rotor is presumed, the conductivity γ equals 28.10^6 S/m and the height of the rotor bar h of 17mm. The absolute permeability μ is $4.\pi.10^{-7}$ H/m. The frequency of the rotor current is $6 - s$ or approximately 300 Hz. The calculated losses of the equivalent scheme need to be multiplied with 3 in order to obtain the total three phase losses. A simplified derivation specifically for the 5^{th} harmonic is presented in (4.33). In this derivation the increased rotor resistance due to the high frequency is presented in relation to the rotor resistance obtained from the short circuit testing at fundamental frequency:

$$\frac{R_{\text{ac\_5}}}{R_{\text{ac\_1}}} = \frac{K_{r\_(6-s)}}{K_{r_1}} \approx \frac{\xi_6}{\xi_1} = \sqrt{6} = 2.45 \tag{4.33}$$

However, the approximation from (4.33) is no longer valid in case of higher harmonic frequencies. From constructional point of view, reducing the height of the rotor bar can easily dampen the skin effect. Although reducing the physical height seems like a valuable option, the skin effect is often used to increase starting torques. If the value of γ is altered this can also have an effect on the skin coefficients. Changing the rotor bar material from aluminum to copper should increase the skin effect, however, for an identical rotor surface area there is a 40% decrease of rotor resistance at fundamental frequency. This should result in an overall decrease of the additional harmonic losses. If the losses are to be estimated according to (4.32), it is not easy to estimate the influence of the skin effect, as this is function of the geometry of the rotor bars.

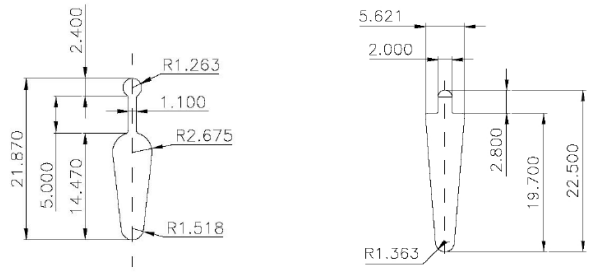

Figure 4.8: Design details of typical rotor slot shapes corresponding to a 2- (left) and a 4-pole (right) 7.5kW IM [12]

Equations (4.24) to (4.26) are only valid for rectangular bars. Because the skin effect in the rotor is highly dependent on the rotor geometry, using this straightforward calculation is not advised. A wide variety of rotor bar configurations can be presented. Sometimes, the skin effect is put to advantage to obtain sufficient start up capability, consequently these machines will be more

sensitive to supply voltage distortion [3]. Additionally surface slots can be open or closed. Consequently, the saturation effect and the influence on the overall leakage inductance will be more pronounced in case of closed rotor slots.

Analytical formulae are unable to present correct estimations of the value of K_r. In [11] it has been suggested that the increase of rotor Joule losses is equal to the order $h^{0.8}$. In [13] the authors from [8] suggest an empirical formula which estimates the increase in the total resistance as function of the supply distortion frequency:

$$K_r = \frac{4 + 7h}{11} \tag{4.34}$$

A comparison of between the analytical formula of (4.24) and the more empirical estimations of [11] and [13] is presented in Figure 4.9.

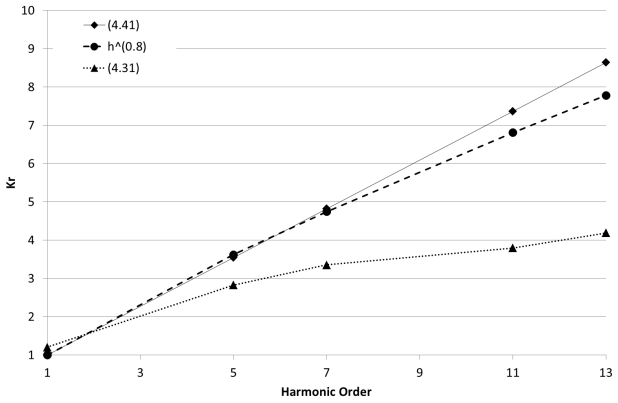

Figure 4.9: Calculated skin effect for the harmonic h on a 4kW IM

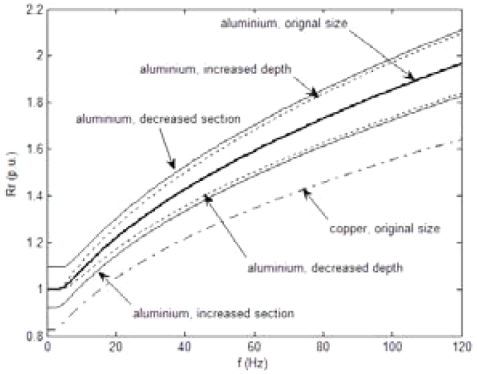

Figure 4.10: Rotor effective resistance as a function of frequency, for different rotor-bar types [3].

In Figure 4.10 the variation of K_{r} is presented as a function of conductor material (copper or aluminium) and for reduced size/depth. Note that the approximations suggested in [13] as in [8] closely relate to the values in Figure 4.10.

4.3.5 Harmonic modeling of Induction Motors

Studies generally assume a non saturated motor operation condition, consequently the non-linear behavior of the magnetizing inductance is neglected. Eq.(4.29) validates the assumption that for IM each harmonic voltage does result in separate rotor harmonic currents, superposition of the harmonic losses is allowed and a harmonic equivalent scheme can be suggested. A series harmonic model is obtained of stator resistance, total leakage inductance and a resistance which is a measure for rotor Joule losses (Fig. 4.11).

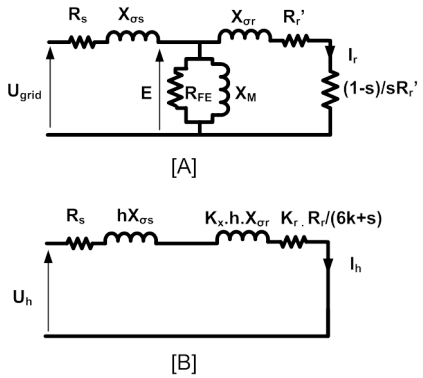

Figure 4.11: Fundamental equivalent scheme of an IM [A] and harmonic equivalent scheme of an IM [B] [11, 14]

According to (4.35), the harmonic current I_h due the harmonic voltage U_h is calculated by dividing the harmonic voltage by the total harmonic impedance:

$$I_{\mathrm{RMS\_}h} = \frac{U_{\mathrm{RMS\_h}}}{\sqrt{\left(\frac{R_r.K_r}{6k+s} + R_s\right)^2 + \left(X_{\sigma\_h}\right)^2}} \tag{4.35}$$

with R_r the rotor resistance at fundamental frequency, K_r the skin effect coefficient for the resistance at harmonic frequency h. X_{σ_h} is the total leakage reactance at harmonic frequency. Additional to an increase of rotor resistance, the skin effect also results in a decrease of the leakage inductance. Consequently, the skin effect has to be included in R_r and X_{σ_h}.

$$X_{\sigma\_h} = h.X_{\sigma s} + h.X_{\sigma r}.K_x \tag{4.36}$$

Sometimes rotor and stator leakage inductance is obtained by using the ratio of stator to rotor resistance. In order to simplify calculations when obtaining the leakage inductance from short circuit tests, the leakage inductance is often equally spread by dividing the total leakage inductance by 2 to separate rotor and stator leakage inductance:

$$X_{\sigma s} = X_{\sigma r} = \frac{X_{\sigma}}{2} \tag{4.37}$$

With X_{σ} the total reactance at fundamental frequency, and $\mathrm{X}_{\sigma \mathrm{s}}$ and $\mathrm{X}_{\sigma \mathrm{r}}$ the leakage inductance of stator and rotor. However, in order to correctly estimate the harmonic current, correct separation of stator and rotor inductance is imperative. Although the skin effect reduces the rotor leakage inductance, due to the higher supply frequency, the overall leakage reactance is very high in reference to the total resistance (4.38). This results in a approximated calculation of the current:

$$\left(\frac{R_r.K_r}{6k+s} + R_s\right)^2 << \left(X_{\sigma\_h}\right)^2 \tag{4.38}$$

$$I_h \approx \frac{U_{\mathrm{RMS\_h}}}{\sqrt{\left(X_{\sigma\_h}\right)^2}} = \frac{U_{\mathrm{RMS\_h}}}{|h.X_{\sigma s} + h.K_x.X_{\sigma r}|} \tag{4.39}$$

A higher stator inductance compared to the rotor will result in a decrease of current and consequently if leakage inductance in the rotor is higher, the skin effect will result in an increase of current. Because this effect is also function of geometry and frequency, it is hard to make a generalized sensitivity analysis. To conclude, the harmonic current is mainly determined by the total reactance. Although the total inductance can decrease with the skin effect in the rotor, the higher supply frequency results in an steep increase of total reactance. As a result the total impedance is mainly inductive and if the losses are to be evaluated, knowledge of both leakage inductance and resistance are of critical importance. For a 4-pole 4kW EFF1 IM with a aluminum rotor, shifting 10% inductance from stator to rotor results in a shift of current magnitude from $1.17\mathrm{A}_{\mathrm{RMS}}$ to $1.32\mathrm{A}_{\mathrm{RMS}}$ for 8% of fifth harmonic distortion. As the losses are equal to the current squared, the previous example illustrates that correct separation of rotor and stator leakage inductance is essential.

Once the harmonic current and the corresponding stator and rotor resistances are obtained, calculation of the additional stator and rotor losses can be calculated. The total amount of additional losses due to supply voltage distortion $P_{\mathrm{h\_loss}}$ can be calculated for each individual harmonic and superposition of all the losses for each individual harmonic $P_{\mathrm{loss\_h}}$ result in the total harmonic losses. In [11] the additional losses is modeled by:

$$P_{\text{loss\_}h} = \frac{E_h^2}{X_{h\sigma}^2}\left(R_{s\_h} + R_{\text{lln}} + R_{r\_h}\right) \tag{4.40}$$

$$P_{\text{h\_loss}} = \sum_{h=2}^{\infty} P_{\text{loss\_h}} \tag{4.41}$$

According to [8] the losses calculated are divided in additional rotor and stator losses.

$$\begin{aligned} P_{\text{h\_loss}} &= 3.R_s\left(K_{s\_1}I_u^2 + \sum_{h=2}^{\infty} K_{s\_h}I_{s\_h}^2\right) \\ &+ 3.R_r\left(K_{r\_1}I_u^2 + \sum_{h=2}^{\infty} K_{r\_h}I_{s\_h}^2\right) \end{aligned} \tag{4.42}$$

4.4 Derating of IM under distorted supply conditions

4.4.1 Loss based and thermal based derating

In order for an electrical equipment to cope with additional losses, and the resulting additional heat generation, the equipment has to be derated. For electrical transformers, this derating is been generally accepted [15], however, similar derating can also be presented for IM [3]. There are two types of derating. The first derating is referred to as Loss Based Derating (LBD). In LBD the additional harmonic losses are calculated by using the harmonic modeling. From the nameplate on the machine the nominal losses are derived, and the machine output is recalculated by using the losses as an upper limit. Thermal Based Derating (TBD) is based on technical limitations of an IM. The additional losses imply an increase of operating temperature, and if the temperature rise is sufficient, this could result in premature failure of stator insulation. In this type of derating the stator winding temperature is used as an upper limit, rather than the total losses inside the machine. Ref. [8] is often cited as reference concerning TBD.

A foot-mounted TEFC IM dissipates approximately 70% of its heat by convection on the stator surface and this effect can be modelled by a thermal resistance R_θ. Subsequently, knowledge of the losses as obtained by LBD, and combined knowledge of R_θ can result in actual motor temperatures. Ref.

[8] tries to avoid the complex calculations and consequently suggests that the ratio $R_s.R_\theta/X_\sigma$ is an indicator for the thermal sensitivity of IM to voltage distortion. If machines are underloaded [Figure 4.1], derating is often not necessary. Consequently, imprudent use of derating can overestimate the effects of supply voltage distortion.

4.4.2 Derating according to NEMA MG1

Both NEMA MG1 and IEC 60034-17 present derating methods in case of supply voltage unbalance. Additionally, due to both the increase in distortion of the supply voltage, and the increase of IM supplied from VSDs [16], there was a demand for a relatively easy method of derating in case of supply voltage distortion. Consequently, the NEMA MG1 presents a standardized method of derating [17] in case of supply voltage distortion. As will be illustrated is this derating method, with minor modifications, capable of estimating the additional losses linked to voltage distortion.

The total amount of additional losses due to supply voltage distortion $P_{\mathrm{h\_loss}}$ can be calculated for each individual harmonic and superposition of all the losses for each individual harmonic $P_{\mathrm{loss\_h}}$ result in the total harmonic losses:

$$P_{\mathrm{h\_loss}} = \sum_{h=2}^{\infty} P_{\mathrm{loss\_h}} = \sum_{h=2}^{\infty} \left(\frac{E_h}{h.X_\sigma} \right)^2 .R_h \tag{4.43}$$

The skin effect causes an increase of the total resistance R_h with increasing frequency, consequently the total losses can be estimated by simplifying (4.43) to:

$$P_{\mathrm{loss}\_h} = \left(\frac{E_h^2}{h} \right) .C_h \tag{4.44}$$

The value of C_h has to be calculated for each individual harmonic h. It is noticed that the losses are function of the applied voltage distortion squared, and inversely proportional to the harmonic order. As a result it makes more sense to introduce a weighted voltage distortion ratio, rather than using the linear parameter Total Harmonic Distortion $\mathrm{THD_U}$ [18]. The Harmonic Voltage Factor HVF is calculated as:

$$\mathrm{HVF} = \sqrt{\sum_{h>1} \frac{(U_h)^2}{h}} \tag{4.45}$$

with U_h the per unit value of the magnitude of the voltage of harmonic order h in reference to the magnitude of the fundamental voltage. Notice that in (4.45) no phase reference of the distinctive harmonics is needed. Triple-N harmonics are not considered within the NEMA MG1. Similar to the derating in case of supply unbalance, the derating curve for harmonic distortion is based on many tests of a

variety of motors. This curve suggests the derating as function of the maximum thermal limits:

$$1 + \frac{\%\mathrm{IncreaseWindingTemperature}}{100} = \frac{\%\mathrm{load}}{100}^{-1.7} \tag{4.46}$$

In order to avoid additional thermal stress, the nameplate efficiency and mechanical power should be derated by using the HVF, and the Derating Factor (DF) according to Figure 4.12.

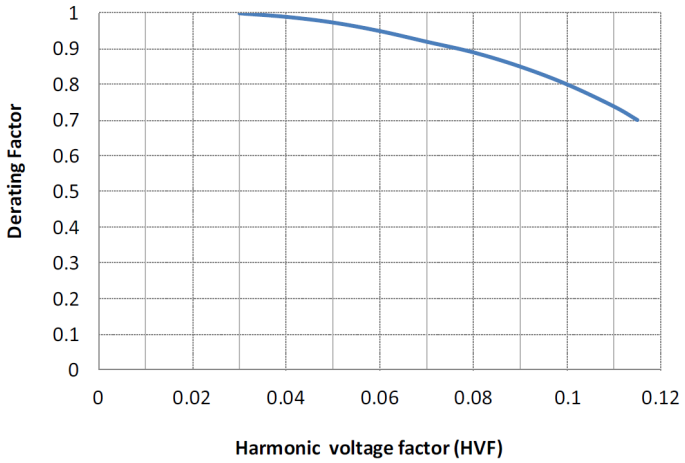

Figure 4.12: Derating Factor (DF) as a Function of HVF [19, 20]

Accordingly, for a given efficiency at sine wave conditions, the derated efficiency of the DOL IM supplied with distorted voltage can be estimated by using the results obtained in (4.45), Figure 4.12 and solving (4.47).

$$\eta_c = \frac{\mathrm{DF}^2}{\eta^{-1} + \mathrm{DF}^2 - 1} \tag{4.47}$$

with η_c the derated efficiency for a certain DF, DF the derating factor as function of the HVF and η the reference efficiency, which is the efficiency at sine wave conditions. By means of example the derated efficiency in case of 10% fifth harmonic distortion is obtained by calculating a HVF of 0.044, the corresponding Derating Factor is 0.975 and with the reference efficiency is 87.5% the calculated reduced efficiency is 86.9%. Derating by the NEMA MG1 is extensively described in [17] [19]. Although the derating curve according to the NEMA MG1 suggests a decrease of efficiency based on (4.47), the additional losses caused by harmonic distortion can be recalculated. If a constant mechanical output power is assumed, the additional losses caused by distortion $\mathrm{P_{h\_loss}}$ can be estimated by:

$$\frac{P_{\text{mech}}}{P_{\text{mech}} + P_{\text{loss}} + P_{\text{h\_loss}}} = \frac{\text{DF}^2}{\frac{P_{\text{mech}}+P_{\text{loss}}}{P_{\text{mech}}} + \text{DF}^2 - 1}$$
$$P_{\text{h\_loss}} = \frac{(1-\text{DF}^2)}{\text{DF}^2}.P_{\text{loss}} \quad (4.48)$$

4.5 Measuring harmonic losses

Up till now, obtaining the total losses linked to harmonic supply voltage distortion is difficult. Theoretically, harmonic power can result in both averaged mechanical power and additional electrical losses inside the machine. Consequently the decrease of efficiency is generally used to evaluate the negative effects caused by supply voltage distortion. However, evaluating the direct efficiency has two significant drawbacks. First of all, when evaluating the efficiency, both electrical and mechanical power should be evaluated. Although electrical quantities can be measured with high accuracy, the measurement of mechanical power is still difficult due to the need of a torque measurement device. Secondly, as efficiency is a ratio, minor variations in consumed active power are hardly noticed and consequently detailed information is lost. In this section a new method of evaluating the additional harmonic losses is proposed. This method is predominantly based on IEC 60034-2-3. However, minor adjustments are suggested which result in only evaluating the electrical power linked to a certain harmonic. Although this method will eliminate some effects which should be taken into account when evaluating the direct efficiency, the increased measurement accuracy results in more accurate estimations and evaluation of the losses reated to supply voltage distortion.

4.5.1 Loss measurement according to IEC60034-2-3

As hinted in the introduction, the rise of VSD has resulted in a shift of the evaluated frequencies towards the operation of IM. If an IM is converter fed, additional losses occur similar to the losses described previously in this chapter. The only difference is that the evaluated frequencies in this dissertation are well below 2kHz, in reference to the switching frequencies of VSD which are generally above 2kHz. However, the harmonics generated by a VSD also result in additional losses and this effect should be taken into consideration. Consequently, the IEC has introduced the standard IEC 60034-2-3 *Rotating electrical machines-Part 2-3: Specific test methods for determining losses and efficiency of converter-fed AC motors*. This standard clearly states that for motors below the 1MW range the most accurate method to determine these additional losses is the basic Input-Output method. However, as this standard assumes the harmonic losses inside machines independent of the applied load, the harmonic losses can also be measured by

connecting a unloaded motor to a sine wave supply and measure the no-load values of current, voltage and active power. Once the motor is connected to the inverter, the converter output voltage should be controlled in a way that the fundamental motor current equals the no-load current of the sinusoidal supply test. The harmonic losses for can be obtained by: [directly imported from IEC 60034-2-3]:

$$P_h = P_0 - P_{0,1} \tag{4.49}$$

where P_h is the load independent loss component in stator and rotor due to harmonics caused by converter operation, P_0 power absorbed at U_0 at converter supply and $P_{0,1}$ power absorbed at $U_{0,1}$ at sinusoidal supply.

4.5.2 Additional fundamental and harmonic power losses in IM

The additional harmonic electrical power consumption $P_{\mathrm{h\_el}}$ can be easily measured and calculated according to:

$$P_{\mathrm{h\_el}} = \sum_{h=3,5,7\ldots}^{\infty} U_{\mathrm{RMS\_h}}.I_{\mathrm{RMS\_h}} \cos(\varphi_h) \tag{4.50}$$

φ_h is the relative phase shift between the harmonic voltage and current. $P_{\mathrm{h\_el}}$ is also equal to the difference of the total RMS power $P_{\mathrm{h\_RMS}}$ and the fundamental power $P_{\mathrm{RMS\_1}}$.

$$P_{\mathrm{h\_el}} = P_{\mathrm{h\_RMS}} - P_{\mathrm{RMS\_1}} \tag{4.51}$$

Eq.(4.51) highly relates to (4.49) from the IEC 60034-2-3, although the values obtained from (4.51) can be derived from a single measurement and (4.49) still requires 2 consecutive measurements. If the total harmonic power losses could be calculated and measured according to (4.51) this would largely increase the measurement accuracy in the latter of the research. Consequently, the measurement error of the additional losses is only depending of the used electrical measurement equipment, which is generally high in relation to the measurement of mechanical power. Secondly, the additional losses caused by supply voltage distortion can be validated by a single measurement, instead of two consecutive measurements as suggested in IEC 60034-2-3. From the obtained additional losses the reduced efficiency could be calculated according to:

$$\eta = \frac{P_{\mathrm{mech}}}{P_{\mathrm{el}}} = \frac{P_{\mathrm{mech}}}{P_{\mathrm{mech}} + P_{\mathrm{loss}} + P_{\mathrm{h\_el}}} \tag{4.52}$$

with P_{loss} the losses at fundamental frequency. However, the suggested method directly implies that both P_{mech} and $P_{\mathrm{RMS\_1}}$ remain unaltered in reference to the sine wave condition. First of all, the combination of harmonic voltage and

harmonic current results in active power, this could also results in an average torque. This implies that this average torque caused by the harmonic power $P_{\mathrm{h\_el}}$ is superimposed on the fundamental torque generated by the fundamental voltage and current. Secondly, if the fundamental RMS current is altered both in I_{D} or I_{Q}, the fundamental stator Joule and iron losses may vary. In a worst case scenario this implies that in terms of the total losses caused by supply voltage distortion $P_{\mathrm{h\_loss}}$ can be higher than the additional active harmonic power $P_{\mathrm{h\_el}}$.

$$P_{\mathrm{h\_loss}} > P_{\mathrm{h\_el}} \tag{4.53}$$

$$\frac{P_{\mathrm{mech}}}{P_{\mathrm{mech}} + P_{\mathrm{loss}} + P_{\mathrm{h\_loss}}} < \frac{P_{\mathrm{mech}}}{P_{\mathrm{mech}} + P_{\mathrm{loss}} + P_{\mathrm{h\_el}}} \tag{4.54}$$

The use of the parameter "additional harmonic electrical power consumption $P_{\mathrm{h\_el}}$" is validated by measurements. $P_{\mathrm{h\_loss}}$ is the total harmonic losses based on the direct input-output efficiency of two consecutive measurements. $P_{\mathrm{h\_el}}$ is obtained from a single measurement and both parameters are plotted as function of the load for an 4kW motor. Additional measurements on a second 4kW 4-pole EFF1 IM validate the evaluation of $P_{\mathrm{h\_el}}$, which is representative for $P_{\mathrm{h\_loss}}$. The variation of both $P_{\mathrm{h\_el}}$ and $P_{\mathrm{h\_loss}}$ has also been tested for increased power ratio's for respectively 11kW and 55kW IM.

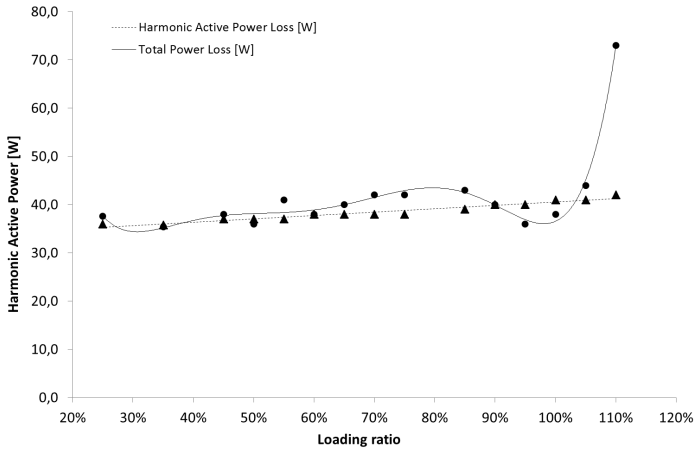

Figure 4.13: Harmonic Active Power $P_{\mathrm{h\_el}}$ and Total Additional Harmonic Losses $P_{\mathrm{h\_loss}}$ of a 4kW 4-pole EFF2 IM caused by 12% fifth voltage distortion

These measurements indicate that $P_{\mathrm{h\_loss}}$ is nearly equal to $P_{\mathrm{h\_el}}$ for relatively small IM at loads up to nominal load. The measurements presented in this section are for a 4kW EFF2 motor. However, at larger load and for larger power ratios of IM, $P_{\mathrm{h\_loss}} > P_{\mathrm{h\_el}}$ is validated. This indicates that $P_{\mathrm{RMS\_1}}$ varies

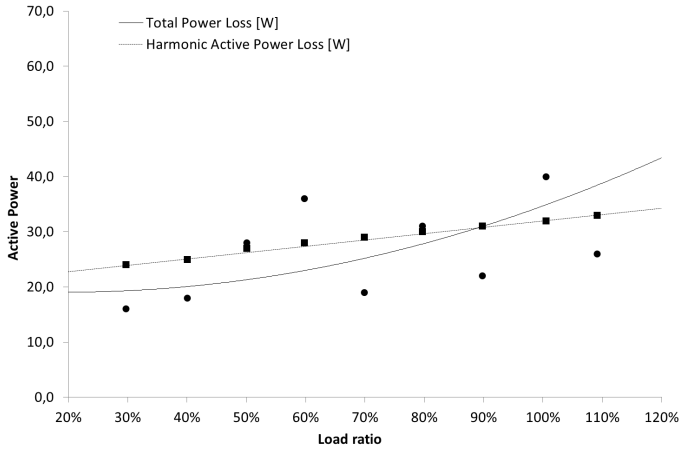

Figure 4.14: Harmonic Active Power $P_{\mathrm{h\_el}}$ and Total Additional Harmonic Losses $P_{\mathrm{h\_loss}}$ of a 4kW 4-pole EFF1 IM caused by 12% fifth voltage distortion

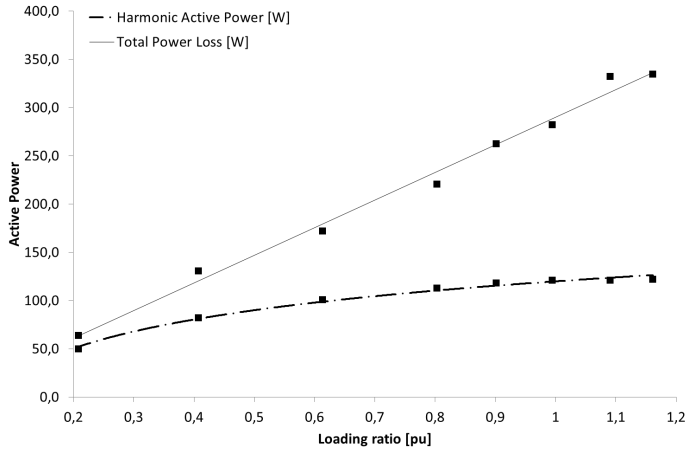

Figure 4.15: Harmonic Active Power $P_{\mathrm{h\_el}}$ and Total Additional Harmonic Losses $P_{\mathrm{h\_loss}}$ of a 11kW 4-pole EFF1 IM caused by 12% fifth voltage distortion

as the supply voltage is distorted. The latter also implies that the only correct harmonic loss estimation implies loss measurement and comparison at both sine wave and distorted supply condition. The deviation between $P_{\mathrm{h\_loss}}$ and $P_{\mathrm{h\_el}}$ at larger loads and power ratios is believed to be caused by additional fundamental stator Joule losses. In sine wave condition, measurements validate that the total RMS power P_{RMS} equals the fundamental power $P_{\mathrm{RMS\_1}}$. In distorted conditions $P_{\mathrm{h\_el}}$ is calculated as the difference between P_{RMS} and $P_{\mathrm{RMS\_1}}$ within one single measurement. Consequently, the total harmonic losses $P_{\mathrm{h\_loss}}$ are calculated as the difference between P_{RMS} in distorted conditions to the reference P_{RMS} in sine

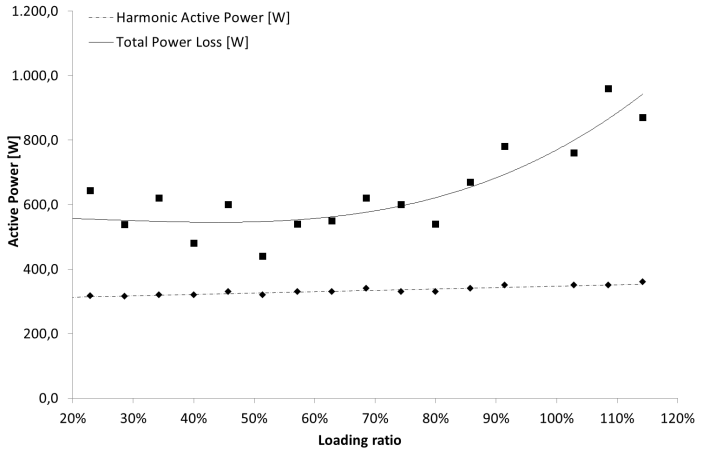

Figure 4.16: Harmonic Active Power $P_{\mathrm{h\_el}}$ and Total Additional Harmonic Losses $P_{\mathrm{h\_loss}}$ of a 55kW 2-pole EFF2 IM caused by 12% fifth voltage distortion

wave condition. As $P_{\mathrm{h\_el}}$ remains relatively constant, the measurements confirm an increase of $P_{\mathrm{RMS\_1}}$ if the voltage is distorted. As the fundamental voltage is unaltered, the increase of $P_{\mathrm{RMS\_1}}$ implies an increase of fundamental current and consequently an increase of fundamental stator Joule losses. The steep increase at high load ratios can be approximated by a quadratic curve, further strengthening the assumption of increased fundamental stator Joule losses in case of supply voltage distortion.

4.5.3 Harmonic mechanical power and torque ripple

The results of §4.5.2 imply that the use of the parameter $P_{\mathrm{h\_el}}$ is able to present highly accurate results for small machines. Subsequently, this parameter will be used to evaluate the susceptibility of small scale IM towards supply voltage distortion. However, as active power is delivered both from fundamental as higher order harmonics in the supply voltage, the higher order harmonics can also result in mechanical power. Studies generally neglect this mechanical power, consequently stating that all harmonic power can be considered as electrical losses. This assumption should be validated. Measurements have been executed at imposed and fixed mechanical torque. As additional harmonics are supplied, the only mechanical parameter which can differ is the mechanical speed of the machine. Although the mechanical power is measured with a reduced accuracy, the reduced accuracy is generally caused by the presence of the torque meter. Speed is often obtained with a very high accuracy of 1rpm and for a 4-pole machine this results in a measurement accuracy of $\pm 0.06\%$. Consequently the mechanical power introduced by supply voltage harmonics can be evaluated by the variation of the mechanical speed at fixed torque. In Figure 4.17 the mechanical speed is listed as

function of the load and for an excessive distortion of 15% fifth harmonic.

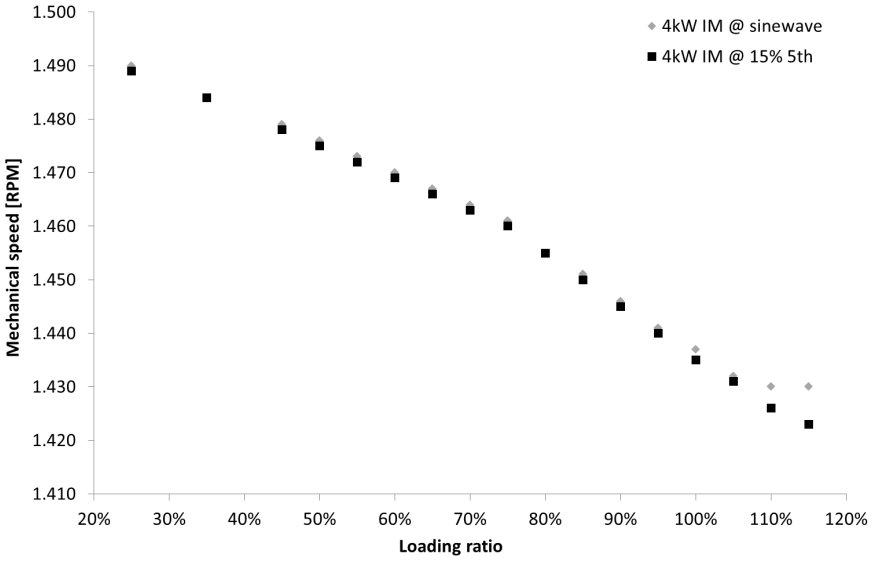

Figure 4.17: Mechanical speed as function of the total active output power as function for a 4-pole EFF2 4kW IM

In Figure 4.17 it is noticed that the mechanical speed at 100% load is still only deviating 1rpm or 0.06% by the interaction of supply voltage distortion. This is still within the measurement accuracy and accordingly it is validated that the mechanical power caused by additional harmonic distortion can be neglected up to nominal load. However, it is also noticed that for higher load ratios the mechanical power does differ when supply voltage distortion is added. At 120% of the load the mechanical power differs approximatly 7 rpm which can be linked to a mechanical power of 23W. This is no longer negligible. Consequently, if a generalized method should be suggested, the only valid option is to evaluate the overall energy efficiency in sine wave as in distorted conditions obtained by the direct measurement method.

$$\eta = \frac{P_{\mathrm{mech}}}{P_{\mathrm{el}}} = \frac{\omega_m.T}{3.U_{\mathrm{RMS}}.I_{\mathrm{RMS}}.PF} \tag{4.55}$$

The presence of supply voltage distortion induces mechanical torque ripples further adding difficulty to the evaluation of the mechanical output power. Measurements generally output instantaneous values of voltage, current, torque and speed. If the energy efficiency is evaluated, these instantaneous values are

post processed according to:

$$\eta = \frac{\frac{1}{T}\int_0^T \omega_m.T(t).dt}{\frac{3}{T}\int_0^T u(t).i(t)dt} \tag{4.56}$$

The averaged mechanical power is measured by multiplying the rotation speed ω_m and the output torque $T(t)$. For relatively small torque ripples, the mechanical inertia of the rotor/load effectively dampens the ripple and ω_m can be assumed constant.

$$\eta = \frac{\frac{\omega_m}{T}\int_0^T T_{(t)}.dt}{\frac{3}{T}\int_0^T u_{(t)}.i_{(t)}dt} \tag{4.57}$$

As already presented, the torque ripple caused by harmonic voltages is an odd harmonic ripple and according to (4.57) this torque ripple has no effect on the overall energy efficiency. However, if the efficiency in case of supply voltage distortion is obtained by evaluation of the instantaneous torque, this could result in a wrong estimation of the average efficiency as demonstrated in Figure 4.18.

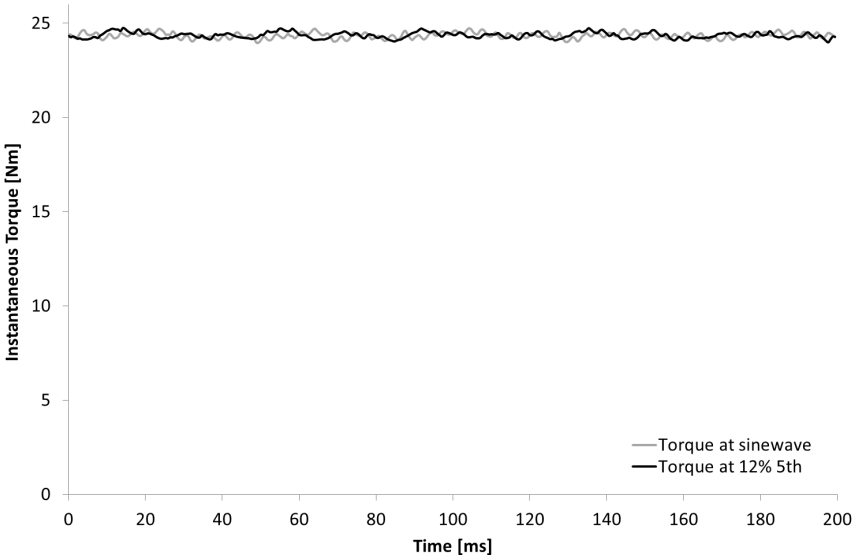

Figure 4.18: Instantaneous torque evaluation in case of torque ripple for a 4kW IM at 1440rpm

Figure 4.18 plots the instantaneous torque of a 4kW EFF1 1440 rpm IM measured by the torque sensor, both for sine wave and for distorted supply conditions. Evaluation of the measurements indicated averaged torques of 24.35Nm at sine wave condition and 24.34Nm in case of 12% fifth harmonic distortion. However a variation of 23.87 to 24.86 Nm is noticed in the measured values. A variation of 1Nm implies a loss variation equal to 150W. Consequently,

evaluating specific samples could result in both an over or under estimation of the efficiency of the machine. A correct sampling algorithm is needed to assure correct evaluation of the average output torque. From a construction point of view the coupling has been done with a high damping ratio to protect the shaft torque meter from high start torques. This implies a direct damping of higher frequencies. In order to assure the correct measurement of the output torque the bandwidth of the used torque meter is analytically calculated and measured using the impulse response. The calculated bandwidth of the torque transducer is 88.8Hz. The physical bandwidth of the torque transducer was measured by applying a dirac puls with an impact hamer tangential to the rotor shaft. The obtained bandwidth by measurement was 60Hz.

Contradictory, the lower the bandwidth of the torque transducer, the better the averaged torque is obtained by measurement. The low bandwidth combined with the higher frequency of the harmonic torque ripples, the first torque ripple originates at 300Hz, results in an accurate value of averaged torque. Although the low bandwidth of the torque meter prohibits correct evaluation of the torque ripple, the presented research does not focus on torque ripple. Additionally the output of the torque sensor has a 32 point sample averaging further damping any ripple.

4.5.4 Measurement procedure

It can be concluded that the use of the parameter $P_{\mathrm{h\_el}}$ is ideal to present highly accurate results for the effect of supply voltage distortion for small machines. As a result this parameter will be used to evaluate the additional losses in relation to supply voltage distortion (magnitude, order and phase angle) and the machine parameters (load ratio and efficiency rating). Because the overall efficiency is generally used to compare IM, and the fact that derating methods present an actual reduction of overall efficiency, the transition from losses to efficiency is presented. However, if the transition from actual power losses to efficiency is made, detailed information is lost. Efficiency is a ratio and as the amount of output power is increased, the effect of small loss variation is no longer visible. Consequently, for small machines (4kW), it is preferred to evaluate $P_{\mathrm{h\_el}}$ and subsequently present the link to the overall efficiency. However, for higher power ratings of machines, the only valid option is to evaluate the total reduction of efficiency.

Although a wide variety of tests has been performed, testing has been executed as uniformly as possible. The machine was loaded at nominal load until thermal equilibrium was reached. At this point testing started by decreasing the loading from approx.125% of nominal load to zero. At one torque setpoint, the input and output power were measured for sinewave conditions and the supply voltage was changed by adjusting the harmonic order, phase angle and/or magnitude. The magnitude of the harmonic was raised from zero over

8%-10%-12% to 15% of the fundamental and the phase angle was shifted from 0° (in phase) to 180°(antiphase). Subsequently, the torque setpoint was decreased and measurements were repeated. Specifically the fifth harmonic is addressed as this is the lowest harmonic linked to the highest losses. The case of 12% is studied in detail because according to the conclusions presented in chapter 3 this is the practical upper limit of the voltage distortion at end user.

4.6 Effect of varying supply voltage distortion conditions

4.6.1 Influence of the harmonic phase angle

The presented measurement evaluates the variation of the iron losses due to voltage distortion. Based on (4.22), the largest influence on the iron losses should be the lowest order of harmonic distortion with the highest magnitude, consequently test results are plotted for 15% fifth harmonic distortion with a altering phase angle of 0° and 180°. As these tests imply a constant RMS value of the voltage, according to the harmonic modeling concept the variable stator and rotor Joule losses can be set as a constant.

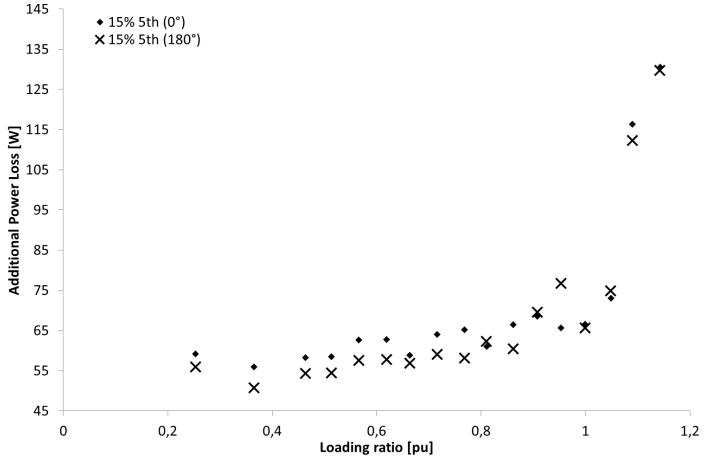

Figure 4.19: Influence of the harmonic phase angle of 15% fifth supply distortion on the overall additional harmonic losses of a 4-pole EFF2 4kW IM

For a 4-pole EFF2 4kW IM (Fig.4.19), the absolute losses are higher if the harmonic phase angle is set to zero. However, the difference between efficiency for phase and anti-phase harmonic injection disappears for loading close to the nominal working point. This is due to the fact that the magnetization losses are less

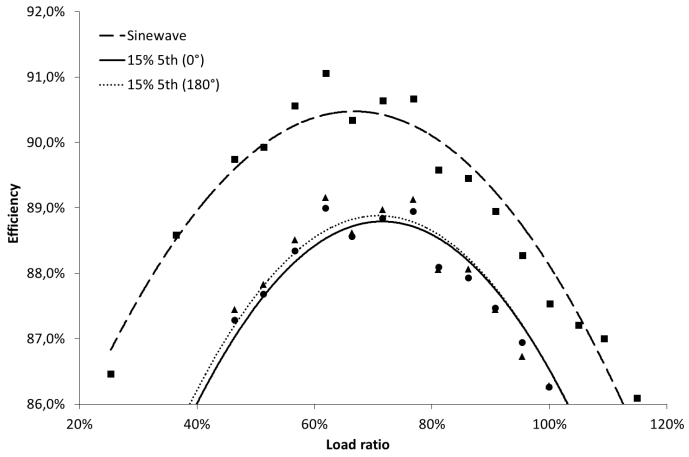

Figure 4.20: Influence of the harmonic phase angle of 15% fifth supply distortion on the overall energy efficiency of a 4-pole EFF2 4kW IM

dominant with respect to the variable losses (Fig.4.20). Therefore the influence of the phase of the harmonics is more important at partial loading rates. At 35% loading rate, the influence of the shift of phase angle from a 15% fifth results in a 7W shift in losses, however at nominal loading this effect is no longer measureable. For the 4kW machine, the variation of the losses is higher than the measurement accuracy. Because of the minor influence of the harmonic phase angle, within this chapter the influence of harmonic phase angles is neglected.

4.6.2 Influence of partial loading and harmonic magnitude

In §4.5.2 the correct setting to evaluate the behavior of IM towards supply voltage distortion has been deduced. In this paragraph measurements are presented in order to evaluate the behavior of the efficiency of IM in reference to supply voltage distortion. Both the actual supply voltage distortion (magnitude, order and phase angle) as the machine parameters (load ratio, power ratio and efficiency rating) will affect the overall susceptibility to supply voltage distortion.

In this first paragraph the influence of both the harmonic magnitude and partial loading on the losses, and the overall energy efficiency, is evaluated. As stated, the tested machine is a TEFC 4-pole EFF2 4kW IM. In Figure 4.21 $P_{\mathrm{h\_el}}$ is evaluated, which presents fairly good estimations when evaluating loading ratio's up to 110%, for larger load ratios this method however severely underestimates the additional losses. The results are presented in reference to the nominal output power (4kW) in order to present a unified reference. Consequently, Figure 4.22 presents the overall efficiency, as this takes into account all of the losses.

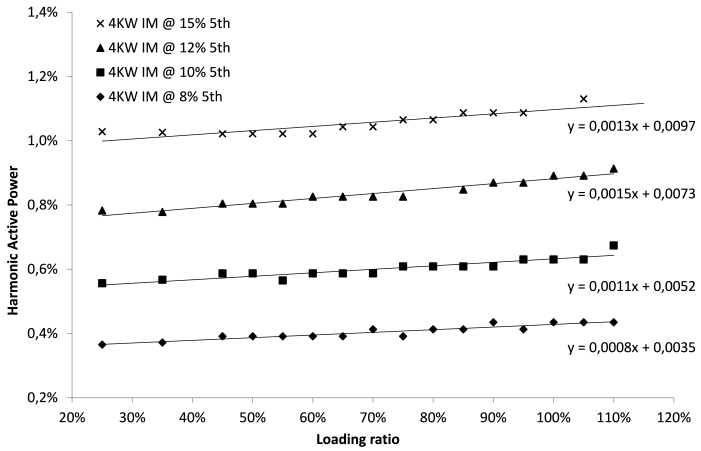

Figure 4.21: Variation of Harmonic Active Power $P_{\mathrm{h\_el}}$ as function of the loading ratio for a 4-pole EFF2 4kW IM

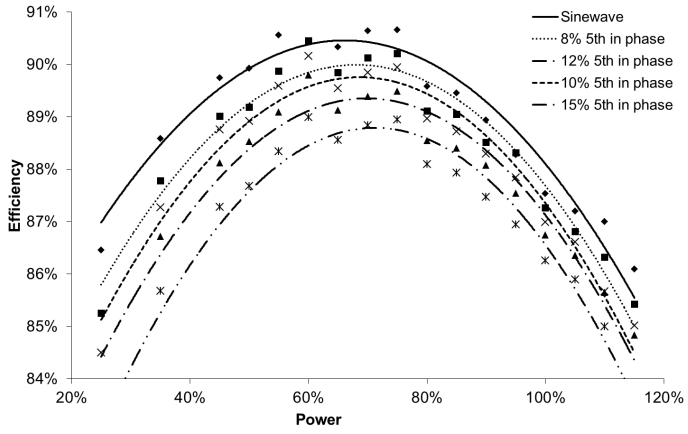

Figure 4.22: Efficiency for a 4-pole EFF2 4kW at 5th harmonic voltage distortion with a shift in harmonic magnitude

From Figure 4.21 the obvious conclusion can be made that with increasing harmonic magnitude, the corresponding harmonic losses increase. Up to a certain degree of distortion, less than 8%, the influence of supply voltage distortion is within the measurement accuracy. The effect of distortion ratio with a HVF less than 5% is generally neglected for IM [3]. For a fifth harmonic of 8% the HVF is equal to 3.5%. More interesting is to evaluate the loss variation in function of the load ratio. It is observed that with increasing slip the losses tend to increase, which is in contradiction to the harmonic modeling concept. On average the additional losses caused by harmonic voltage distortion shift about 15% between low and

high loading. Although the efficiency is a very important parameter, efficiency is a ratio of powers. The variation of harmonic losses is practically eliminated if the overall energy efficiency is evaluated.

4.6.3 Influence of harmonic order and superposition of losses

The previous measurements indicated an increase of harmonic losses with increasing harmonic magnitude. However, the actual voltage at end user has has multiple harmonics. Theoretical deduction already indicated that for identical magnitudes and increasing harmonic orders the total reactance increases and consequently the impact of higher harmonic orders is less noticeable. In order to validate these assumptions measurements were executed for a fifth, seventh, eleventh and thirteenth harmonic with an equal magnitude of 12% distortion on a 4-pole EFF1 4kW IM. Note that these harmonic magnitudes well exceed the acceptable limits of voltage distortion as presented in chapter 3.

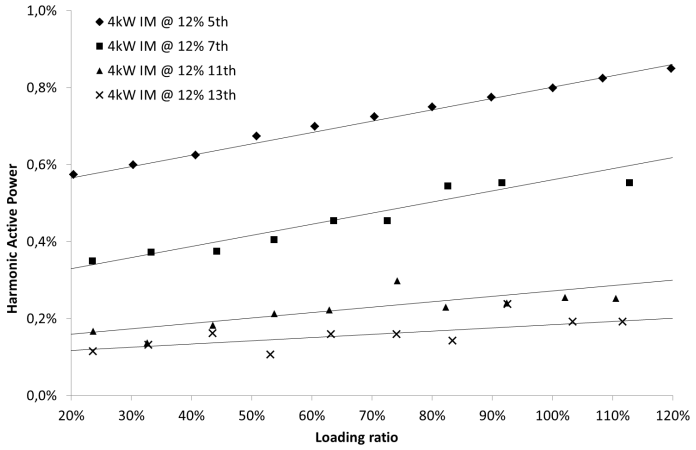

Figure 4.23: $P_{\mathrm{h\_el}}$ for a 4-pole EFF1 4kW IM supplied with 12% distortion of different order

From Figure 4.23 it is observed that with increasing order and equal magnitude, the losses reduce. This is caused by the more effective damping by the leakage reactance. In Figure 4.24 measurements are presented for individual superposition of 12% fifth and seventh, and the harmonic losses are also presented for the combination of 12% fifth and seventh. Harmonic modeling suggests that superposition of harmonic losses is permitted. Figure 4.24 strongly validates the superposition of harmonic losses, as only a small amount of deviation is noticed if superposition of losses is calculated.

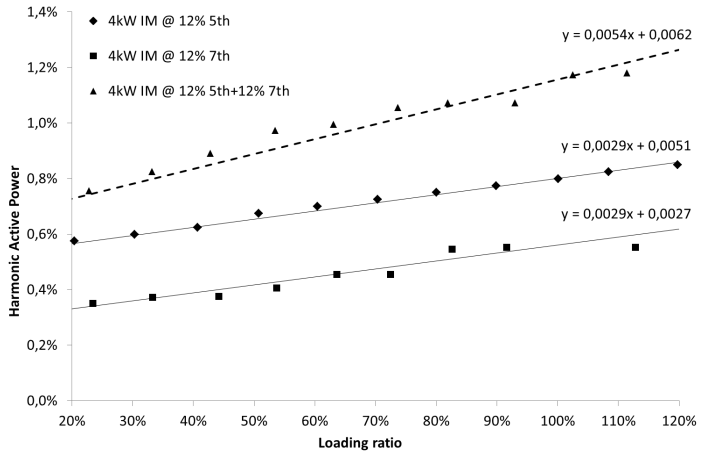

Figure 4.24: Evaluation of superposition of $P_{\mathrm{h\_el}}$ for a 4kW IM

4.7 Effect of varying IM conditions

4.7.1 Influence of the motor efficiency rating

As noticeable in Figure 4.14, evaluation of $P_{\mathrm{h\_el}}$ is a fairly good indication of the additional losses caused by supply voltage distortion for small machines $(\leq)$4kW. Consequently, the parameter $P_{\mathrm{h\_el}}$ is evaluated for an EFF2 and an EFF1 motor in order to present the susceptibility of the efficiency rating on the additional losses.

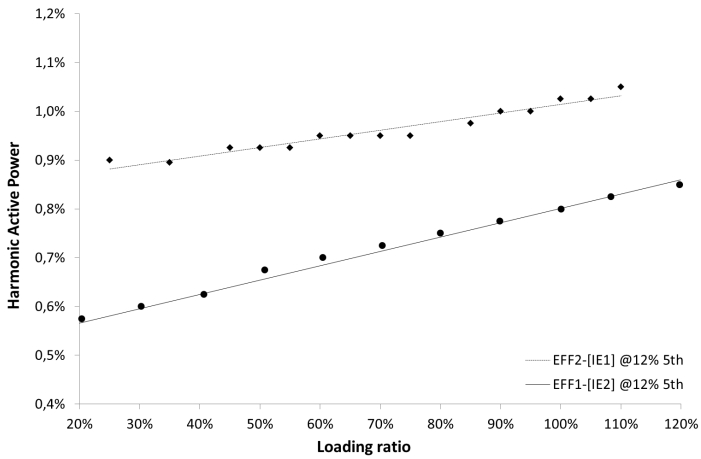

Figure 4.25: Harmonic losses for a EFF2 and EFF1 4kW IM at 12% 5th harmonic voltage distortion

In (4.47) can be deducted that for an identical HVF and consequently DF, an

IM with a higher efficiency is less susceptible to voltage distortion. Evaluation of Figure 4.25 confirms this conclusion.

4.7.2 Influence of the motor output power rating

Up to this point only measurements were validated for a 4kW IM. As has already been presented in Figure 4.13 to Figure 4.16 the total harmonic losses $P_{\mathrm{h\_loss}}$ increase as the machine power rating increases. For a 4kW IM $P_{\mathrm{h\_loss}}$ is approximately 40W at nominal load, for an 11kW IM the additional losses are 250W and for 55kW IM $P_{\mathrm{h\_loss}}$ is 675W. This validates that for higher power ratings of machines the harmonic losses increases. However, if the susceptibility of higher power ratings of machines is to be evaluated the relative ratio of the additional harmonic losses should be compared. In Figure 4.26 the parameter $P_{\mathrm{h\_el}}$ is evaluated in reference to the nominal output power for 4kW, 11kW and 55kW IMs at 12% fifth distortion.

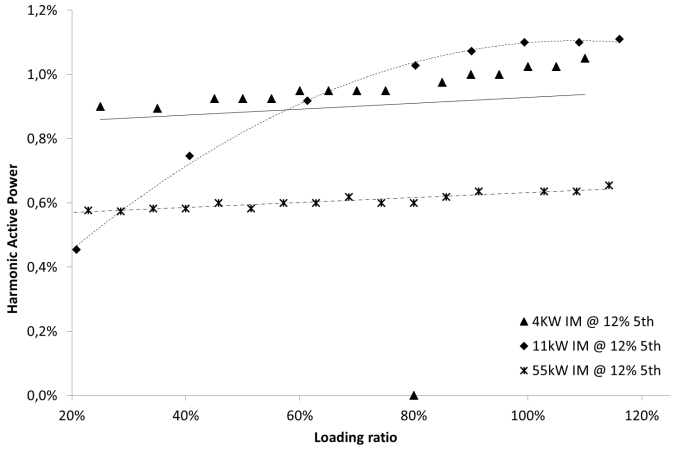

Figure 4.26: Variation of the parameter $P_{\mathrm{h\_el}}$ for a 4kW, 11kW and 55kW IM at 12% fifth harmonic distortion

As already stated in §4.5.2, evaluation of parameter $P_{\mathrm{h\_el}}$ is only allowed for small machines. In Figure 4.27 the total harmonic losses $P_{\mathrm{h\_loss}}$ is evaluated for the three machines. Evaluation of $P_{\mathrm{h\_el}}$ and Figure 4.27 does not result in clear conclusions concerning the relative additional harmonic losses in relation to the power ratio of the machine.

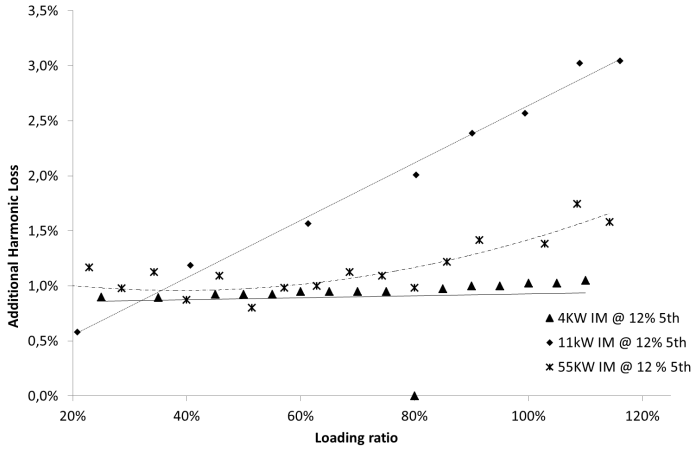

Figure 4.27: Variation of the parameter $P_{\mathrm{h\_loss}}$ for a 4kW, 11kW and 55kW IM at 12% fifth harmonic distortion

The absence of conclusions can be designated to several practical considerations:

1. the efficiency ratios at sine wave condition of the tested motors are very close. Measurements have to be performed with highest accuracy to obtain a shift in additional harmonic losses.
2. The measurement accuracy of the 55kW IM is insufficient to detect the minor shifts in losses.
3. When calculating the $P_{\mathrm{h\_loss}}$ the RMS power at sine wave is subtracted from the RMS power at distorted conditions. Minor changes in mechanical output power imply that this method introduces additional errors.
4. Rotor bar geometry can significantly differ between the tested motors. High power machines have larger inertias and an adjusted rotor bar design could result in increased start up capabilities. This will significantly affect the resulting skin effect and the corresponding harmonic losses.

Additionally the phase angle for 12% fifth harmonic has been altered from 0° to 180° for the 55kW IM. The difference of efficiency as a function of the harmonic phase angle could not be measured within measurement accuracy, consequently no conclusions are presented. Besides the reduced accuracy of measurements, at nominal loading the iron losses are less dominant in the total losses for a 55kW machine in respect to a 4kW machine. To conclude, for a 4kW IM the shift in magnetizing losses is noticeable for partial loading and at relatively high distortion, for a 55kW machine the variation of the magnetizing losses is almost unnoticeable in the total losses.

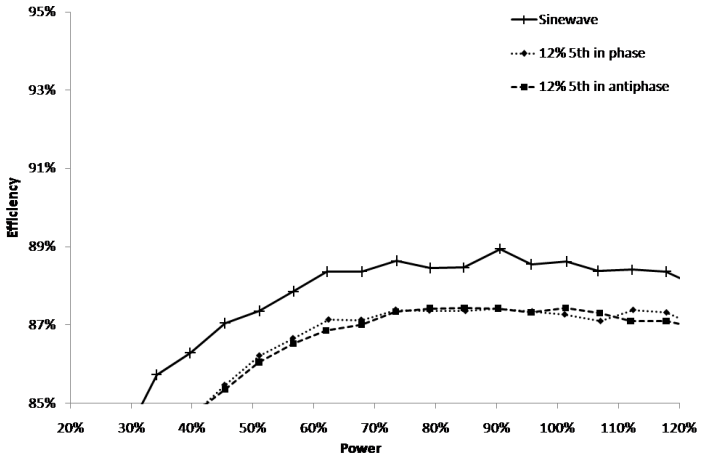

Figure 4.28: Influence of the harmonic phase angle of 12% fifth supply distortion on the overall additional harmonic losses of a 55kW IM

4.8 Thermal aspects linked to harmonic losses

In chapter 2, the thermal resistance of a 4-pole 4kW IM from frame to stator winding is deduced theoretically and obtained by measurement. In this section a detailed loss evaluation has been presented for a 4kW IM under distorted supply condition.

Knowledge of the additional losses caused by supply voltage harmonics, combined with LTM, results in an additional temperature rise of the different motor parts. Some assumptions are made, which have been validated in the previous sections. Phase angle shifts only have a minor influence at low loading ratios and the additional harmonic losses remain constant over the load ratio. These assumptions however only hold for small machines at power ratios up to nominal load. Subsequently Lumped Thermal Modeling assume fixed thermal resistances. The combination of ”fixed ” harmonic losses and ”fixed” thermal resistances imply that superposition of temperatures is allowed. The most interesting temperature rise is the winding temperature as this is one of the critical parameters related to failure of an IM.

In [21], the increase of temperatures inside a 4kW IM was monitored when supplied with an 8% distorted voltage and at different loading ratios (Table 4.2). Comparison from the results of [21] and the results from the LTM presented in Figure 4.29, indicates that there is an additional temperature increase of approximately 2K in a 4kW IM for 8% distortion.

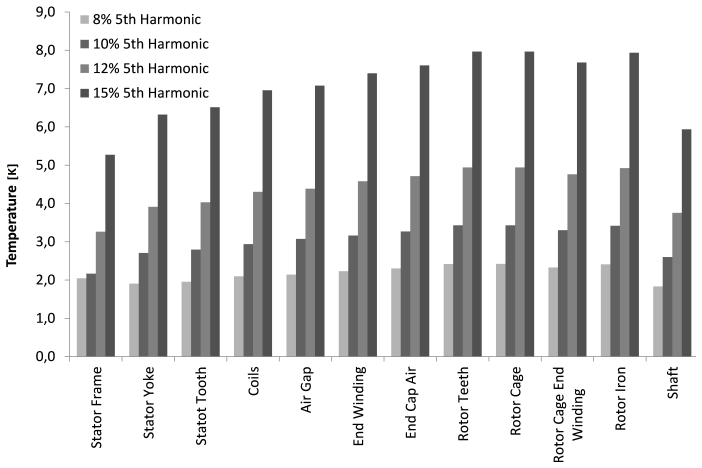

Figure 4.29: Estimation of temperature rise of 4kW EFF2 IM motor parts caused by different magnitudes of fifth distortion at full load

Table 4.2: Increase of motor part temperature[^{o}C] due to 8% fifth distortion for a 4kW IM [21]

Motor Part	0% load	50% load	100% load
Rotor	0.6	1.6	2.6
Stator winding	0.4	1.2	1.6

Low power ratings of machines (<4kW), have a reduced frame surface area in relation to the power ratio and have an increased slip at nominal load. The low speed in combination with relatively high winding to frame thermal resistances imply that small power ratings of machines are also more susceptible to thermal overload caused by supply distortion. However, both for partial loading as for higher power ratings, the heat is more easily dissipated which implies that the temperature rise will be smaller than 2K. LTM simulations confirm that at partial load the machine operates at lower stator housing temperatures. Consequently, at partial loading, reasonable harmonic distortion will not result in stator temperatures above the values cited in Table.4.3.

Table 4.3: Thermal Classes for insulation systems (IEC 60085)

Thermal class for insulation systems	A	E	B	F	H
Max. operating temperature (^{o}C)	105	120	130	155	180

In sine wave conditions the winding temperature decreases approximately 15K for an increased efficiency of EFF2 to EFF1 [22]. Additionally the higher efficiency classes also result in reduced harmonic losses for the same amount of harmonic voltage distortion. Consequently, in terms of thermal limits, if

the efficiency class increases, the machine is less susceptible towards harmonic heating and consequently thermal limits will only be reached at even more severe distortions.

It should also be noted that the additional increase in operation temperature can influence the stator resistance and the according stator Joule losses. A 2K temperature rise results in 0.7% increase of stator Joule losses. Consequently this effect is neglegible. Similar to the stator resistance the rotor resistance increases with approximatly 1% increase of rotor Joule losses. Consequently, the iterative process of resistance increase due to harmonic heat dissipation is neglected. Attempts have been made to validate this assumption by measurements, however, as the ambient temperature increased over the measurement interval, this affected the measurements disabling possible conclusions.

4.9 Evaluation of the derating methods

In this section the different derating procedures are evaluated for the 4kW EI 1 IM. The parameters used for the harmonic modeling, and the consequent Loss Based Derating, are obtained by the no-load and the short-circuit test. The values are listed in Chapter 2. The skin effect has been modeled according to [13] using $h^{0.8}$. The obtained harmonic losses is plotted against the losses obtained by measurement in Figure 4.30.

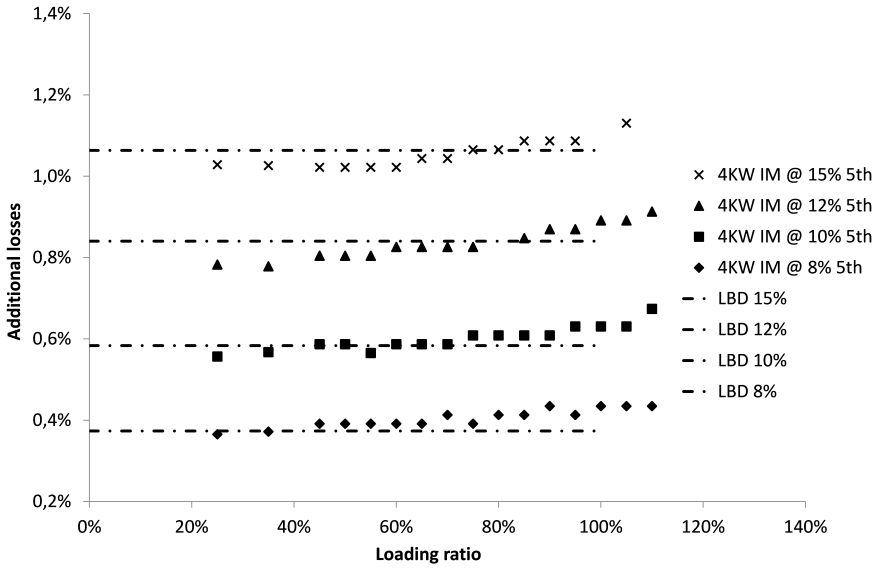

Figure 4.30: Comparison between LBD and measurements of a 4kW IM

Concerning the harmonic loss modeling, the loss calculations and

measurements correspond well at nominal loading as presented in Figure 4.30. When applying LBD, the losses are assumed constant over the loading range. However, the measurements indicate that there is a slight shift in power as the mechanical slip increases. This also indicates that LBD gives fairly good estimations of the derating of IM. The additional losses caused by supply voltage distortion can also be estimated according to NEMA MG1 (§ 4.4.2). If the example from §4.4.2 is used, for 10% fifth harmonic distortion the corresponding calculated losses by using (4.47) are 0.62%.

Table 4.4: Calculation of the additional losses for a 4kW IM according to Eq.4.47

THD_U	8%	10%	12%	15%
HVF	0.0358	0.0447	0.0537	0.0671
DF	0.982	0.975	0.965	0.945
$P_{h\_loss}[pu]$	0.44	0.62	0.89	1.43

However, some concerns are presented when using these derating methods. Although the power loss is calculated quite accurately, the derating of the machine is only useful if the machine is loaded at nominal load. As machines are only loaded on average at 60% load ratio, the additional derating of the IM can overstate the practical implications. Similar to LBD, TBD has identical drawbacks. LTM simulations confirm that at partial load the machine operates at lower stator housing temperatures. Consequently, at partial loading, reasonable harmonic distortion will not result in stator temperatures above the values cited in Table.4.3.

Straightforward derating, simply based on voltage quality parameters such as $\mathrm{THD_U}$ or the HVF, should be avoided. If the derating is executed in order to maintain the life expectancy of the IM, correct knowledge of the actual load ratio is essential. If the machine is underloaded, misuse of either LBD or TBD should be avoided. If an economical assessment is made of the additional harmonic losses, harmonic modeling gives reasonable accurate loss estimations.

4.10 Conclusions

This chapter started with a theoretical overview of the different types of harmonics present inside machines. Although one study refers to the interaction of spatial and time harmonics [3], literature review failed to find studies which accurately evaluate the interaction of these harmonics. Consequently, the theoretical deduction presented validates that in terms of efficiency these harmonics can be regarded independent of each other. The latter also indicates that supply voltage distortion has no influence on the fundamental SLL. As both the peak induction

varies, the temperature increases and the supply distortion additionally generates spatial harmonics, this assumption is not 100% accurate. However, due to the relative small ratio of both SLL and additional losses caused by supply distortion the interaction of voltage distortion on SLL is presumed negligible.

In a second paragraph this chapter presents the concepts of harmonic modeling. The harmonic modeling implies superposition of the individual losses, consequently linearization should be validated before superposition can be accepted. Measurements have been executed on different 4kW IMs and different power sizes which validate the linearization.

Measurements and comparison of efficiency to evaluate the influence of supply voltage distortion are hard because of the large measurement errors in reference to the relative small deviations caused by supply distortion. This research suggested the possibility to use the additional harmonic electrical power as a parameter to evaluate the total additional losses caused by harmonic distortion, this would largely increase accuracy and simplicity of measuring the related reduced efficiency. It has been presented that evaluation of the additional harmonic electrical power is only valid for small power rating of machines.

The effect of supply voltage distortion is function of both the distortion as the machine. Measurements have been presented which evaluate the influence of harmonic magnitude, order and phase of the distortion. Additionally the influence of partial loading, machine efficiency rating and machine power rating has been validated. A general conclusion is that in reference to the machine size, the losses in p.u. are within the same order of magnitude for different power ratios.

However, practical issues prohibit a generalized conclusion concerning machine size. With increasing size, the rotor cage is physically larger, resulting in an increase of the skin effect. Secondly, the additional losses have to be measured and the measurement accuracy significantly reduces as the power ratio increases. The presence of a torque meter and the necessary use of current clamps decreases measurement accuracy [23].

The different methodologies of derating a IM when supplied with a distorted voltage are compared and evaluated by measurements. If harmonic models are used, thermal based derating or loss based derating can be applied [3]. However, as IMs are usually over dimensioned, imprudent use of these derating methods could result in an over estimation of the actual losses and the corresponding stator winding temperature. Harmonic modeling presents fairly accurate loss calculations, and only with correct knowledge of the load ratio can result in correct derating. Derating according to the NEMA MG1 slightly overestimates

the losses at partial load, however, this presents fairly accurate estimations of the harmonic losses.

If the actual losses caused by supply voltage distortion are evaluated, it can be stated that for limited distortion ($\mathrm{THD_U} < 10\%$) the additional losses will generally not exceed the 1% point. However, excessive distortion should be avoided. If general supply anomalies are evaluated, machines are generally more influenced by voltage unbalance in reference to voltage distortion. This can be addressed to several factors. Fundamental unbalance results in low rotor frequencies ($\approx$ 100Hz) consequently fundamental unbalance is less dampened compared to supply voltage distortion. Additionally, the unbalance is mainly determined by the load, and although a voltage unbalance of 2% should be the upper limit, practical configurations can result in more severe unbalance and its negative impact.

References

[1] G. Wakileh. *Harmonics in rotating machines*. Electric power systems research, 66(1):31–37, July 2003.

[2] F. Ferreira, A. De Almeida, and G. Baoming. *Three-Phase Induction Motor Simulation Model Based on a Multifrequency Per-Phase Equivalent Circuit Considering Stator Winding MMF Spatial Harmonics and Thermal Parameters*. In 17th Inter. Conf. on Electric Machinery (ICEM06), Chania, Greece, 2006.

[3] F. Ferreira, A. de Almeida, W. Deprez, R. Belmans, and G. Baoming. *Impact of steady-state voltage supply anomalies on three-phase squirrel-cage induction motors*. In International Aegean Conference on Electrical Machines and Power Electronics, 2007. ACEMP '07., pages 607–615, Bodrum, Turkey, 2007.

[4] F.J.T.E. Ferreira and A.T. de Almeida. *Method for in-field evaluation of the stator winding connection of three-phase induction motors to maximize efficiency and power factor*. IEEE Trans. on En. Conv., 21(2):370–379, June 2006.

[5] D. Vanhooydonck, W. Symens, W. Deprez, J. Lemmens, K. Stockman, and S. Dereyne. *Calculating energy consumption of motor systems with varying load using iso efficiency contours*. In 19th International Conference on Electrical Machines (ICEM), pages 1–6, 2010.

[6] K. Stockman, S. Dereyne, D. Vanhooydonck, W. Symens, J. Lemmens, and W. Deprez. *Iso Efficiency Contour Measurement Results for Variable Speed Drives*. In 19th International Conference on Electrical Machines (ICEM), pages 1–6, 2010.

[7] A. De Almeida, F. Ferreira, J. Busch, and P. Angers. *Comparative analysis of IEEE 112-B and IEC 34-2 efficiency testing standards using stray load losses in low-voltage three-phase, cage induction motors*. IEEE Trans. on Ind. App., 38(2):608–614, 2002.

[8] J. de Abreu and A. Emanuel. *Induction motor thermal aging caused by voltage distortion and imbalance: loss of useful life and its estimated cost*. IEEE Trans. on Ind. App., 38(1):12–20, 2002.

[9] E. Barbisio, F. Fiorillo, and C. Ragusa. *Predicting loss in magnetic steels under arbitrary induction waveform and with minor hysteresis loops*. IEEE Trans. on Magnetics, 40(4):1810–1819, 2004.

[10] G. Singh. *A research survey of induction motor operation with non-sinusoidal supply wave forms*. Electric Power Systems Research, 75(2-3):200–213, 2005.

[11] P. Cummings. *Estimating Effect of System Harmonics on Losses and Temperature Rise of Squirrel-Cage Motors*. IEEE Trans. on Ind. App., IA-22(6):1121–1126, 1986.

[12] W Deprez. *Energy efficiency of the induction machines: a critical assessment*. PhD thesis, KU Leuven University, 2008.

[13] J. de Abreu, J. de Sa, and C. Prado. *Harmonic torques in three-phase induction motors supplied by nonsinusoidal voltages*. In 11th International Conference on Harmonics and Quality of Power, 2004, pages 652–657, 2004.

[14] P. Sen and H. Landa. *Derating of induction motors due to waveform distortion*. IEEE Trans. on Ind. App., 26(6):1102–1107, 1990.

[15] J. Desmet and G. Delaere. *Harmonics: Selection and Rating of Transformers*. Technical report, 2009.

[16] M. Melfi. *Quantifying the Energy Efficiency of Motors on Inverters*. IEEE Industry Applications Magazine, 17(6):37–43, 2011.

[17] E. Quispe, G. Gonzalez, and J. Aguado. *Influence of Unbalanced and Waveform Voltage on the Performance Characteristics of Three-phase Induction Motors*. pages 1–5.

[18] *IEC 61000-4-30 ed2.0: Electromagnetic compatibility (EMC) - Part 4-30: Testing and measurement techniques - Power quality measurement methods*, 2008.

[19] E. Agamloh, S. Peele, and J. Grappe. *An experimental evaluation of the effect of voltage distortion on the performance of induction motors*. In Conference Record of 2012 Annual IEEE Pulp and Paper Industry Technical Conference (PPIC), pages 1–7, 2012.

[20] *NEMA Standards Publication MG 1-2006 Revision 1-2007 Motors and Generators*, 2007.

[21] M. Anxo Prieto Alonso, X. Lopez Fernandez, and M. Perez Donsion. *Harmonic effects on temperature rise of a squirrel cage induction motor*. In Proceedings of the 14th International Conference on Electrical Machines (ICEM), pages 144–147, Espoo, 2000.

[22] A. De Almeida. *Beyond Induction Motors: LOT-30 New EU Ecodesign Study*, 2012.

[23] E. Agamloh. *Induction Motor Efficiency*. IEEE Industry Applications Magazine, 17(6):20–28, 2011.

5

The effect of harmonic voltage distortion on Induction Generators

5.1 Introduction

As global energy demand will continue to rise and man's negative impact on global warming is now known to be a fact, people are looking towards safe and green sources of power. Within a good energy mix the substantial input of decentralized renewable energy is undeniable. There are several possible topologies to connect distributed generation (DG) units to the distribution network. For different DG types different power converters are used. Some DG units generate direct current, for example photovoltaic panels or fuel cells, which should be converted to AC in order to deliver active power to the utility grid. For other technologies, such as high power wind turbines, efficiency and controllability are the main criteria. The use of controllable static converters is in these cases more appropriate [1].

Contrary, for combined heat power systems the most preferred choice of generation is the use of mechanical generator systems, since the speed of the prime mover is easily controlled [2]. If robustness and low cost are the main design criteria and efficiency is only of secondary interest, for example in Small Wind Turbines (SWT) for desolate regions, standard available electrical machines without VSD can be used as generator systems. Generator systems can be divided into Synchronous Generators and Induction Generators (IG). When reliability, robustness and low maintenance are the main design criteria, the preferred option is often an IG as brushes or fragile surface mounted permanent magnets are

eliminated. In [1] it is illustrated that for SWT in a power rating from 50kW to 100kW the most preferred generator system is IG.

5.2 Induction generator operation

5.2.1 Introduction to induction generator operation

When an induction machine is used as a motor, the machine is being supplied with electrical power P_{el} and the output is mechanical power P_{mech}. In generator mode, the machine consumes mechanical power, converting it to electrical output power. Due to the nature of the induction machine, the mechanical speed of the machine in motor operation reduces compared to the synchronous speed of the magnetic field inside the machine. This referred to as "sub-synchronous" operation. As a generator, the machine's mechanical speed is above the synchronous speed, the machine is now operated at "super-synchronous speed". As the operation of the machine is of importance, Induction Generators are addressed as IG, and Induction Motor operation is abbreviated as IM. When relating to the physical machine, independent of motor of generator operation the text refers to the "machine". The previous indicates that machines specifically built for motor operation can simply be used as a generator by increasing the mechanical speed over to super-synchronous speeds. However, some specific effects should be taken into account. If the machine is used as an IG, the active power flow changes direction. Consequently, the voltage drop over the stator impedance might reverse, resulting in an increase of the back-EMF.(Fig. 5.1)

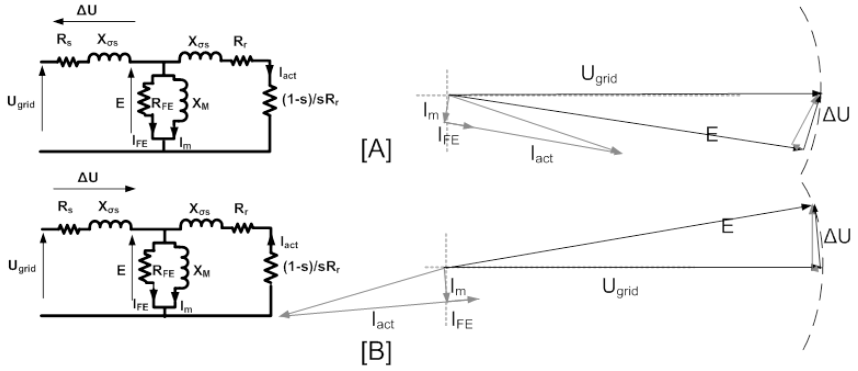

Figure 5.1: Stator voltage drop and decrease of back-EMF in case of IM [A], an increased back-EMF in case of IG [B] as illustrated by a simple vector diagram

Specifically designed IGs are intentionally built with low stator resistance and a high amount of lamination steel in the stator in order to cope with this reversed

stator voltage drop. In these cases linear induction can be assumed, however, if standard motors are used as IG, the higher stator resistance combined with the reduced amount of lamination steel can result in saturated operation, and thus possibly prohibiting linearization. In Figure 5.2 the magnetization characteristic is plotted for a 55kW Induction Motor and for a 55kW machine specifically built for generator operation.

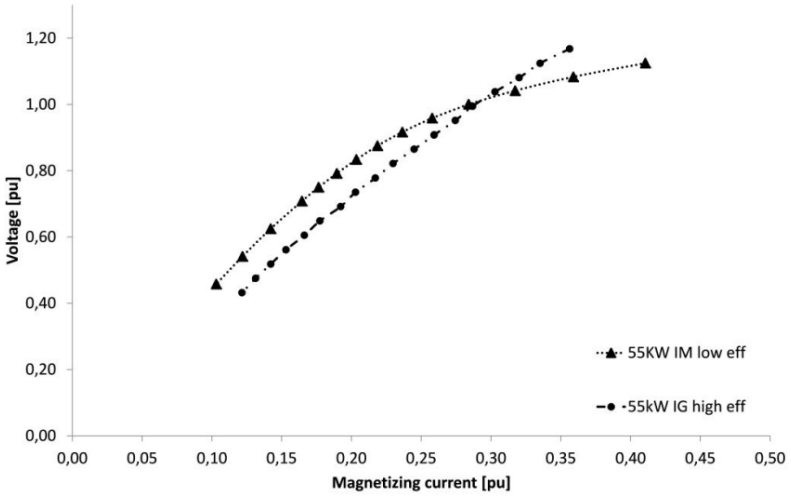

Figure 5.2: Magnetization characteristics for a 55kW IM and a 55kW IG

Measurement of the magnetization characteristic indicate that for an acceptable voltage rise the machine designed for generator operation does not work in saturated conditions. The machine designed for motor operation works in more saturated conditions when a higher voltage is applied. For lower voltages, the IM needs less magnetization current in p.u. compared to the IG. As also the stator Joule losses are reduced for the high efficient IG, the magnetization current p.u. will be higher.

5.2.2 Efficiency in generator operation

When evaluating the efficiency of motor and generator operation of machines, the input and output power are used to determine respectively motor efficiency,η_{motor} and generator efficiency $\eta_{\mathrm{generator}}$:

$$\eta_{\mathrm{motor}} = \frac{P_{\mathrm{out}}}{P_{\mathrm{in}}} = \frac{P_{\mathrm{mech}}}{P_{\mathrm{el}}} \tag{5.1}$$

$$\eta_{\mathrm{generator}} = \frac{P_{\mathrm{out}}}{P_{\mathrm{in}}} = \frac{P_{\mathrm{el}}}{P_{\mathrm{mech}}} \tag{5.2}$$

with P_{mech} the mechanical power and P_{el} the active electrical power. However, (5.1) and (5.2) can also be written in terms of desired output power and its losses:

$$\eta_{\mathrm{motor}} = \frac{P_{\mathrm{out}}}{P_{\mathrm{in}}} = \frac{P_{\mathrm{mech}}}{P_{\mathrm{mech}} + P_{\mathrm{loss}}} \tag{5.3}$$

$$\eta_{\mathrm{generator}} = \frac{P_{\mathrm{out}}}{P_{\mathrm{in}}} = \frac{P_{\mathrm{el}}}{P_{\mathrm{el}} + P_{\mathrm{loss}}} \tag{5.4}$$

Note that in case of motor operation the desired output is P_{mech}, and additional losses are supplied by the electric input power P_{el}. Subsequently, this also implies that in generator operation the the desired output is P_{el}, and additional losses are supplied by the mechanical input power P_{mech}.

5.2.3 Comparison of IM and IG efficiency

It is tempting to compare IM and IG operation, however the basis on which the comparison is made can largely influence the overall conclusions. If a machine is designed specifically for motor operation, but is used as a generator, what is the reference to which comparison should be made? Several possibilities can be presented to which the machines operation mode can be compared:

1. equal electrical power $P_{\mathrm{el\_IM}} = P_{\mathrm{el\_IG}}$
2. equal efficiency $\eta_{\mathrm{IM}} = \eta_{\mathrm{IG}}$
3. equal losses $P_{\mathrm{loss\_IM}} = P_{\mathrm{loss\_IG}}$
4. or equal output power $P_{\mathrm{mech\_IM}} = P_{\mathrm{el\_IG}}$

As will be illustrated in §5.5.1, based on the used reference, conclusions can alter. As the equal electrical power criteria is used, the load ratio is different for IG and IM. Subsequently, if the equal efficiency criteria is used, [2] indicates that for an identical electrical power the losses in generator mode can be $1/\eta_{\mathrm{IM}}$ higher than the losses in motor mode.

From a design point of view, machines are generally designed towards certain thermal limits. Although the increased fan speed results in a decrease of the frame to ambient thermal resistance, the equal loss criteria can be suggested. Besides the increased heat dissipation capability in generator mode, accurately determining the losses from tests imposes practical difficulties. For the vast majority of the machines, the stator and rotor Joule losses are dominant, accounting for more than 50% of the total losses in the machine. This implies that there is a possibility to relate to maximum allowed current. Within [2] it is already stated that this basis for comparison is not perfect because the reactive component of the power may shift, resulting in additional stator Joule losses.

Consequently, either the comparison based on active electrical power, equal losses or identical ampacity would result in an imperfect efficiency comparison. This is why in this chapter the efficiencies are related towards the nominal output power. For IM the p.u. output mechanical power P_{mech} is the reference, for IG the basis for p.u. the output power is the output electric power P_{el}. The previous pitfalls of efficiency comparison are increasingly important with increased per unit losses. This implies that the described problems occur for small sized or less efficient machines. With increasing efficiency, IE2 and IE3, the problems are less pronounced as for increasing power ratios.

In Figure 5.3 the efficiency is presented for both IM and IG operation for a 4-pole 4kW, 4-pole 11kW and a 2-pole 55kW machine, which were specifically designed for motor usage.

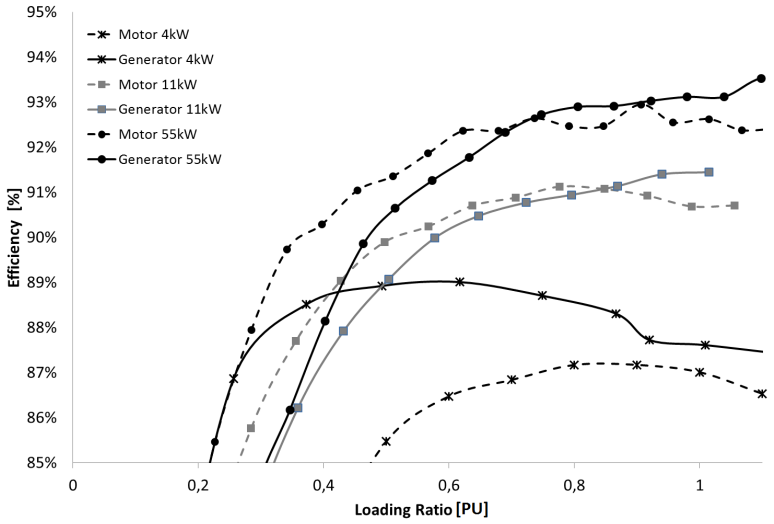

Figure 5.3: Efficiency characteristic in generator operation of the IM

For higher power ratings (11kW and 55kW) at partial load the iron losses becomes more dominant due to the significant reduction of stator resistance. This effect will even be more pronounced if generator operation is compared to motor operation due to the increase in back-EMF. This is validated in Figure 5.3, which illustrates that for higher power ratings (11kW and 55kW) at partial load the efficiency in generator operation is lower than the efficiency in motor operation. For small machines (4kW) the influence on the iron losses is less dominant as the losses at partial load are still dominated by the stator Joule losses. When machines reach nominal load, the rotor and stator Joule losses are more dominant. Because the slip value for generator mode is smaller than for motor operation and identical loading ratios, the total losses for an IG are lower compared to an IM.

5.3 Additional losses caused by supply voltage distortion

5.3.1 Introduction

Electrical machines are responsible for 50% of the total electric consumption worldwide. For the industry the electrical machines consume up to 70% of the total electrical energy. Almost 90% of the installed machines that convert electrical energy to mechanical energy are IM. This has led to the machines generally being optimized for motor operation [3, 4]. Subsequently this also resulted in studies which examine the influence of distorted voltages in motor operation. However, as both the use of PE and the integration of IG continues to rise, the effect of supply voltage distortion on IG should be considered. Chapter 4 indicates that a lot of attention has been given to the problem for the IM in motor operation. However, when this IM is used as a generator, similar effects will occur. To the author's knowledge no scientific research has been presented in this specific area.

The general goal of this chapter is to evaluate the harmonic losses generated inside an IG, test the validity of harmonic modeling in relation to IG, as to confirm some of these assumptions by practical measurements. However, due to difficult laboratory setup - when testing generators the power supply must be able to control the voltage distortion and simultaneously dissipate active power - it is hard to obtain measurements. Although it seems inevitable to link to the behavior of IM under distorted supply conditions, it will be addressed that straightforward adaptation of harmonic IM models, derating factors, efficiency comparison and measurement procedures will result in wrong conclusions.

5.3.2 Linearisation and additional iron losses

If distortion is added to the supply voltage this will affect the losses inside a machine. Chapter 4 specifically relates to the IM operation. If the influence of harmonic distortion on IG is to be evaluated, some aspects should be taken into account. In case of motor operation a linear induction is assumed. This assumption is strengthened if the additional stator voltage drop at nominal load is taken into account. However, as illustrated in §5.2.1, a linear induction is no longer generally valid for IG, even at pure sine wave supply. If a machine goes into saturated operating conditions this highly affects the harmonic loss mechanisms.

If the instantaneous induction reaches a saturated condition, the instantaneous mutual inductance drops. At fundamental operation this implies a larger magnetizing current and consequently larger stator Joule losses. As this inversely

affects the overall efficiency, designers choose not to operate in saturated conditions. However, in terms of harmonics the reduced mutual induction will result in a reduced parallel impedance of the combination mutual and rotor leakage reactance. Secondly, the linkage with the rotor would reduce due to the increased harmonic stator voltage drop. As the majority of the losses are generated in the rotor this could also imply a reduction of the rotor Joule losses. The previous has been illustrated in Figure 5.4.

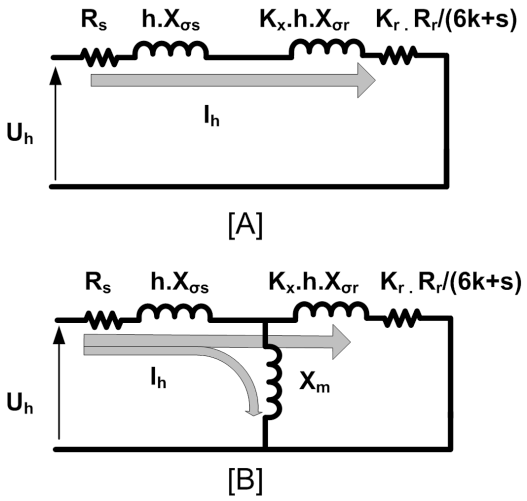

Figure 5.4: Harmonic Model of an IM [A], influence of mutual inductance on the harmonic current if saturation is taken into account [B]

Finally, as the machine operates in saturation this would also imply that at peak induction, the resulting MMF would change in wave shape. This would imply that there is no longer a one-to-one relation between the supply voltage harmonic and the resulting current distortion. Consequently this also implies that, if there is no longer a one-to-one relation of harmonic voltage to harmonic current, this could indicate saturated operation. In order to evaluate the previous statement, measurements are illustrated in Figure 5.5 on a 4kW machine in both motor and generator operation. The supply voltage was distorted with 12% 5^{th} and the harmonic phase angle was shifted. The results for motor operation are listed at nominal P_{mech}, no significant difference was measured between phase and anti-phase. In contrast to motor operation, a significant difference is noticed between phase and antiphase in case of generator operation. Both measurements of IG operation are executed at equal P_{el}.

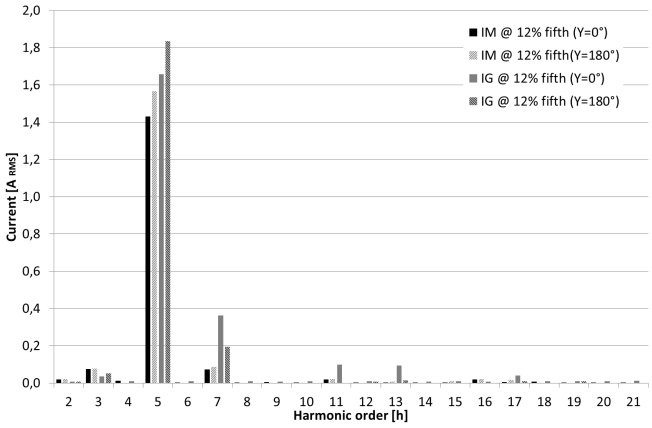

Figure 5.5: Evaluation of the harmonic currents [$I_{\mathrm{RMS\_h}}$]of a 4-pole 4kW EFF2 IM and IG at nominal load when supplied with 12% 5^{th} voltage distortion, the phase angle of the voltage distortion was shifted from 0° *to* 180°

As noticeable from Figure 5.5 there is a high correlation between the order of the harmonic voltage and the resulting current in case of motor operation. This was already confirmed in Chapter 4 as harmonic superposition of losses proved to be valid. However, for IG operation several effects are noticed. If the harmonic phase angle $\gamma = 0^\circ$, the machine operates in more saturated conditions as the averaged voltage increases compared to the sine wave condition. Additionally, harmonics of order h 7,11,13 and even 17 are generated. This indicates that straightforward linearization is no longer valid. If the harmonic phase angle is shifted to $\gamma = 180^\circ$, the averaged voltage reduces approximately with 50 V, reducing the peak induction significantly. Although the current of order 5 increases, the higher harmonics of 7 to 17 are effectively damped or even completely eliminated.

The previous already illustrated that the linearization is no longer valid for generator operation. Additionally the same harmonic magnitude, but with a different harmonic angle, the iron losses can shift due to the change in average voltage. As the iron losses are more dominant in generator operation in reference to motor operation, this effect should be more pronounced for IG.

5.3.3 Additional stator Joule losses

The additional stator Joule losses caused by supply voltage distortion has already been extensively addressed in Chapter 4. As these losses are linked to the stator RMS current, this is generally valid. The harmonic currents $I_{\mathrm{RMS\_h}}$ are mainly determined by the high leakage reactance, consequently the value of $I_{\mathrm{RMS\_h}}$ does not drastically change in relation to the harmonic phase angle.

5.3.4 Additional rotor Joule losses

As illustrated in Chapter 2, the frequency of the induced harmonic currents in the rotor is coupled to the relative movement of the rotor Ω_{m} in reference to the speed of the harmonic current layer Ω_{sh}. If the transition from sub-synchronous to super-synchronous speed is made, for identical stator harmonic order, the induced rotor frequency alters:

$$\Omega_{\mathrm{sh}} - \Omega_{\mathrm{m}} = (1+6k)\frac{\omega_{\mathrm{s}}}{N_{\mathrm{p}}} - (1-s)\frac{\omega_{\mathrm{s}}}{N_{\mathrm{p}}} = (6k+s)\frac{\omega_{\mathrm{s}}}{N_{\mathrm{p}}} \tag{5.5}$$

Table 5.1: Stator and corresponding rotor harmonics for IM and IG

k	Stator Harmonic h	Rotor Harmonic	
		IM	IG
0	1	s	-s
-1	-5	-6+s	-6-s
1	7	6+s	6-s
-2	-11	-12+s	-12-s
2	13	12+s	12-s

According to (5.5) and as illustrated in Table 5.1, the value of $(6k+s)$ changes to $(6k-s)$, consequently, inverse fields due to harmonics of the order $h = 1+6k$ with $k < 0$ should result in higher rotor resistance as a result of a more pronounced skin effect. For a nominal slip of 4% this implies that the frequency induced by the fifth changes from motor to generator operation from 298Hz to 302Hz. The skin effect has been extensively adressed in Chapter 4, and based on the analytical formula the conclusion was presented that the reduced conductor height ξ is function of $\sqrt{f}$. For small deviations of ξ from motor operation ξ_m to generator ξ_g, the variation of the harmonic rotor resistance from motor $\mathrm{R_{h\_r\_motor}}$ to generator $\mathrm{R_{h\_r\_generator}}$ can be calculated as:

$$\frac{R_{h\_r\_generator}}{R_{h\_r\_motor}} = \frac{R_r\xi_g\frac{\sinh(2\xi_g)+\sin(2\xi_g)}{\cosh(2\xi_g)-\cos(2\xi_g)}}{R_r\xi_m\frac{\sinh(2\xi_m)+\sin(2\xi_m)}{\cosh(2\xi_m)-\cos(2\xi_m)}} \approx \frac{\xi_g}{\xi_m} \approx \sqrt{\frac{f_g}{f_m}} \tag{5.6}$$

Due to the reversed slip it is noticed in (5.6) that there is an increase in rotor resistance for harmonics of $h = 1+6k$ with $k < 0$ due to the skin effect when comparing motor and generator operation for identical distortion and slip values. Although the influence of leakage inductance should not be marginalized, if this is neglected, one should expect an increased susceptibility of IG towards supply voltage distortion in reference to motor operation. Subsequently, in contrast to motor operation the harmonic of $k < 0$ generates a small amount of positive torque in generator mode. As a result the balance of increased skin effect in relation to harmonic torques will determine if IGs are more or less susceptible to supply voltage distortion.

5.3.5 Harmonic modeling of IG

Harmonic modeling of IMs is discussed in detail in Chapter 4. This model assumes a non saturated motor operation condition. Consequently, the magnetizing inductance is neglected and superposition of the harmonic losses is allowed. A series harmonic model is composed of stator resistance, total leakage inductance and a resistance which is a measure for rotor Joule losses. Once the harmonic current is calculated, the losses can be derived by using:

$$\begin{aligned} P_{\text{h\_loss}} &= 3.R_s \left(K_{s\_1} I_u^2 + \sum_{h=2}^{\infty} K_{s\_h} I_{s\_h}^2 \right) \\ &+ 3.R_r \left(K_{r\_1} I_u^2 + \sum_{h=2}^{\infty} K_{r\_h} I_{s\_h}^2 \right) \end{aligned} \tag{5.7}$$

Note that the harmonic modeling concept also suggests that all harmonic power is loss. In case of motor operation, this assumption is validated as a fifth harmonic results in an additional breaking torque. Although the seventh harmonic does result in a positive torque, the increased order, generally combined with a decreased magnitude, results in a possible neglect in terms of energy efficiency.

As illustrated in §5.3.2, in case of IG the assumption of linear induction is no longer generally valid. If high efficient motors or specifically designed IGs are used, these are specifically built with low stator resistance and a high amount of lamination steel in the stator to maintain an unsaturated operation. In these cases the assumption of a linear induction may still be valid, however, if standard motors are used as IG, the higher stator resistance combined with the reduced amount of lamination steel can result in saturated operation, and thus prohibiting linearization (Figure 5.2).

A second reason which prohibits straightforward utilization of harmonic IM models for IG is because harmonic orders of $h = 1 + 6k$ with $k < 0$ result in breaking torques in case of motor operation. This implies that all harmonic power for $k < 0$ are additional losses. With $|k|$ increasing, its influence reduces drastically due to both the increase of overall leakage impedance and the fact that for higher values of $|k|$ the magnitude of the voltage distortion generally drops. However, in case of generator operation harmonic orders of $k < 0$ result in additional positive torques. This implies that not all harmonic power are losses Figure 5.6. Although these harmonics do result in additional losses, it is presumed that the torque due to harmonic orders of $k < 0$ influences generator operation less negative in comparison to motor operation.

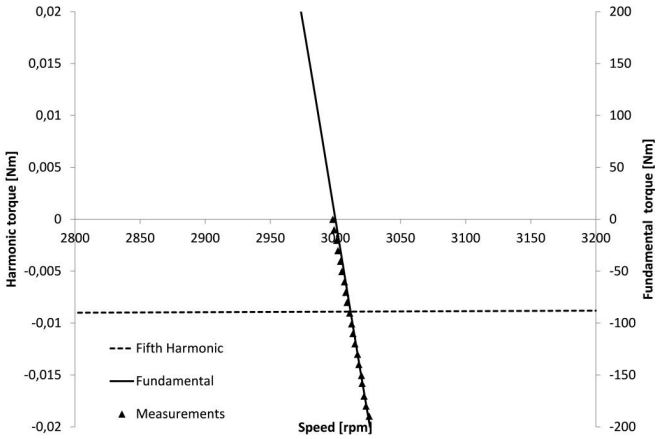

Figure 5.6: Additional torques due to harmonic orders $h = -5$, assuming all rotor harmonic active power is converted to mechanical power

A third cause of estimation error could be straightforward adaptation of skin effect coefficients obtained from motor operation. As already illustrated in §5.3.4 does the induced rotor frequency alters from motor to generator operation, consequently the overall skin effect deviates from motor to generator operation.

5.4 Measuring harmonic losses

5.4.1 Additional fundamental and harmonic power losses in IG

If the influence of supply voltage anomalies are evaluated for IM, identical mechanical output power can be easily achieved by loading the test machine with a machine controlled towards constant output torque or constant output power. The increase in electrical input power is a measure for the additional losses in case of voltage distortion. The previous control is no longer possible when comparing efficiencies of IG under distorted supply conditions. As stated in §5.2.3, the basis to compare IG efficiency is the output electrical power P_{el}. If harmonics are imposed on the voltage, the mechanical power should be increased to obtain identical electrical power in reference to pure sine regime. The evaluation and comparison should be executed at equal P_{RMS} and the increase in mechanical input power $P_{\mathrm{h\_loss}}$ is a measure for the additional harmonic losses:

$$P_{\mathrm{h\_loss}} = P_{\mathrm{mech\_distorted}} - P_{\mathrm{mech\_sinewave}} \tag{5.8}$$

For motor operation the origin of $P_{\mathrm{h\_loss}}$ is relatively straightforward. All additional harmonic power is considered as losses. Subsequently both the fundamental P_{loss} and the harmonic loss $P_{\mathrm{h\_loss}}$ are supplied from the grid. This has been illustrated in Figure 5.7- [A]. However, in case of grid connected IG

systems there is some margin of discussion towards the origin of $P_{\text{h\_loss}}$. As $P_{\text{h\_loss}}$ is induced by higher order harmonics in the supply system the question arises which source supplies $P_{\text{h\_loss}}$. Are the harmonic losses supplied from the grid or are the losses covered by the mechanical input power? Note that this concept of origin of the active harmonic power can affect the overall efficiency for the same amount of $P_{\text{h\_loss}}$:

$$\frac{P_{\text{el}}}{P_{\text{el}} + P_{\text{loss}} + P_{\text{h\_loss}}} \geq \frac{P_{\text{el}} - P_{\text{h\_loss}}}{P_{\text{el}} + P_{\text{loss}}} \tag{5.9}$$

At fundamental operation the magnetizing power in either motor or generator operation is delivered from the grid. A similar concept is suggested in case of this harmonic active power. In motor operation the $P_{\text{h\_el}}$ is supplied by the grid and because the power to distort the voltage originates upstream into the power grid, the assumption has been made that all harmonic power is also delivered by the grid independent of motor or generator operation. Figure 5.7- [B].

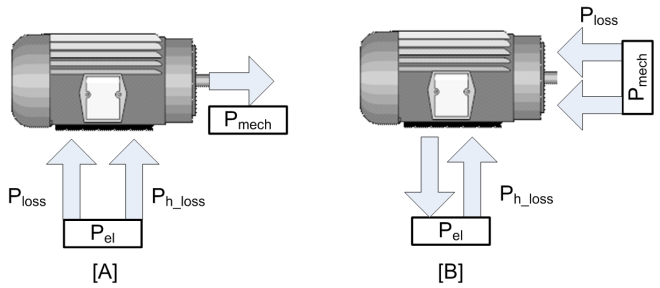

Figure 5.7: Harmonic power concept for both IM and IG systems

Additional to the origin of supply of $P_{\text{h\_loss}}$, the practical evaluation of $P_{\text{h\_loss}}$ according to (5.9) imposes some difficulties. The measurement accuracy is now function of both electrical and mechanical sensors, as are the practical tests more time consuming. In Chapter 4 the parameter $P_{\text{h\_el}}$ has been introduced. In case of sine wave supply voltage P_{RMS} equals $P_{\text{RMS\_1}}$, however, as harmonics are imposed on the supply voltage P_{RMS} no longer equals $P_{\text{RMS\_1}}$. A small amount of active power is delivered at harmonic frequency which corresponds to $P_{\text{h\_el}}$. This parameter proved to be a valuable and accurate tool to evaluate the effects of harmonics in the supply voltage for small IMs up to 110% load. Similar to IM as presented in Chapter 4, is the averaged active power consumed at harmonic frequency easily measured according to:

$$P_{\text{h\_el}} = \sum_{h=5,7\ldots}^{\infty} U_{\text{RMS\_h}}.I_{\text{RMS\_h}} \cos(\varphi_h) \tag{5.10}$$

The presented research should try to validate if evaluation of $P_{\text{h\_el}}$ is representative for the overall losses $P_{\text{h\_loss}}$ inside an IG when supplied with a

distorted supply. In case of motor operation the RMS power is always higher than the fundamental power:

$$P_{\text{h\_RMS}} \geq P_{\text{RMS\_1}} \Rightarrow P_{\text{h\_el}} = P_{\text{h\_RMS}} - P_{\text{RMS\_1}} \geq 0 \tag{5.11}$$

However, all of the measurements in generator mode indicated that $P_{\text{h\_RMS}} \leq P_{\text{RMS\_1}}$. This further strengthens the concept that $P_{\text{h\_loss}}$ is supplied from the grid. The comparison of $P_{\text{h\_el}}$ versus $P_{\text{h\_loss}}$ is illustrated in Figure 5.8. In Figure 5.8 a 4kW EFF2 IM is used as an IG. Additionally 12% fifth distortion is added to the supply voltage and both $P_{\text{h\_loss}}$ and $P_{\text{h\_el}}$ are validated. Because the phase angle is of significant importance, the phase angle is altered from $0°$ to $180°$. As will be noticed is the phase angle of significant importance, but this will be specifically addressed in §5.5.1.

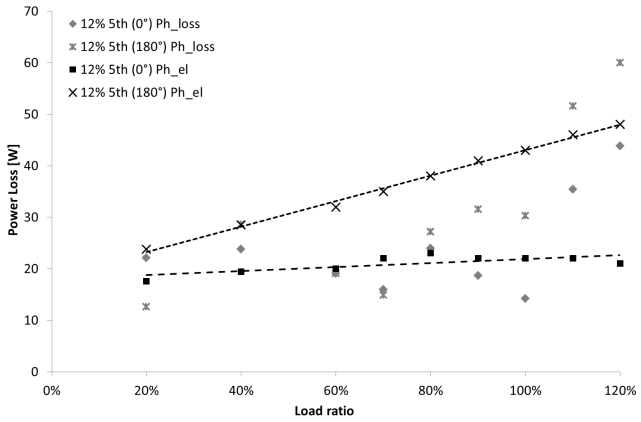

Figure 5.8: Harmonic Active Power $P_{\text{h\_el}}$ and Total Additional Harmonic Losses $P_{\text{h\_loss}}$ of a 4kW 4-pole EFF2 IG caused by 12% fifth voltage distortion

From a theoretical perspective validation of $P_{\text{h\_el}}$ is not 100% accurate in generator mode as the additional harmonic losses $P_{\text{h\_loss}}$ can affect the fundamental current and possible output torque. However, it should also be addressed that, as the test procedure demands an equal P_{RMS} and $P_{\text{h\_loss}}$ is obtained by the increase of mechanical power, this significantly reduces accuracy. Measurement accuracy of the $P_{\text{h\_el}}$ is 0.1%, if equal mechanical power is evaluated the differential measurement accuracy is up to 1,7%. More information concerning measurement accuracy can be found in Appendix 1. Nonetheless Figure 5.8 illustrates that evaluation of the parameter $P_{\text{h\_el}}$ gives a fairly accurate estimation of the total harmonic losses $P_{\text{h\_loss}}$. Although theoretically incorrect, this research will evaluate the $P_{\text{h\_el}}$ to evaluate the influence of harmonic distortion on IG due to the increased measurement accuracy. In Figure 5.9

identical tests have been executed in order to evaluate both $P_{\mathrm{h\_el}}$ and $P_{\mathrm{h\_loss}}$ for an 11kW IG. The reduced accuracy of this test procedure can be noticed in Figure 5.9.

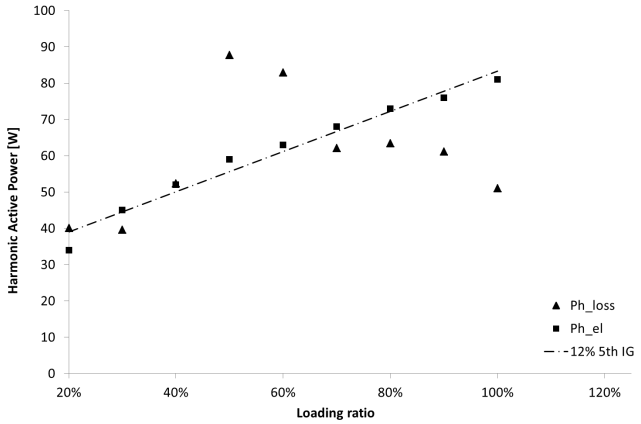

Figure 5.9: Harmonic Active Power $P_{\mathrm{h\_el}}$ and Total Additional Harmonic Losses $P_{\mathrm{h\_loss}}$ of a 4-pole 11kW EFF2 IG caused by 12% fifth voltage distortion

5.4.2 Measurement procedure

IG efficiency is measured according to IEC 60034-2 using the direct method [5]. However, some specific details concerning the test setup need some further elaboration. Generator operation implies that the power supply has to be able to simultaneously control the voltage and dissipate the generated power. The used programmable power source consists of three single phase class A amplifiers of 80kVA per phase. The DC link consists of a DC capacitor link, with a 30 % dissipation possibility. The dissipation is done by dissipation resistors and this enables testing of generator systems to 80kW in a continuous regime. In transient regime higher power ratios can be dissipated within very limited timeframes.

5.5 Effect of varying supply voltage distortion conditions

5.5.1 Influence of the harmonic phase angle

The measurements presented in both Figures 5.5 and 5.8 confirm that the harmonic phase angle has a significant influence on the overall induction, saturation and the corresponding losses. Some important conclusions are:

1. For a harmonic in phase, the machine operates in more saturated condition. This is validated by the increased number of harmonics in the current distortion.(Figure 5.5)

2. Although increased saturation implies a higher induction and corresponding iron losses, the losses are significantly larger if the harmonic phase angle is set to $180°$, implying that the machine operates in less saturated conditions.

3. The higher loss in case of an harmonic phase angle of $180°$ can be designated to the fact that harmonic losses are mainly determined by additional stator and rotor Joule losses. The effect of supply distortion on the iron losses can be neglected in relation to the total harmonic losses. As the machine operates in saturated conditions the mutual induction decreases corresponding to a decrease of rotor Joule losses.

5.5.2 Influence of partial loading and harmonic magnitude

In this paragraph the influence of both the harmonic magnitude and partial loading on the losses is evaluated. The tested machine is a TEFC EFF2 4kW 4-pole IM from Chapter 4, but is now put into supersynchronous operation. Similar to IM operation, Figure 5.10 plots $P_{\mathrm{h\_el}}$. This presents a fairly good estimation when evaluating loading ratios up to 110%, for larger load ratios this method however severely underestimates the additional losses.

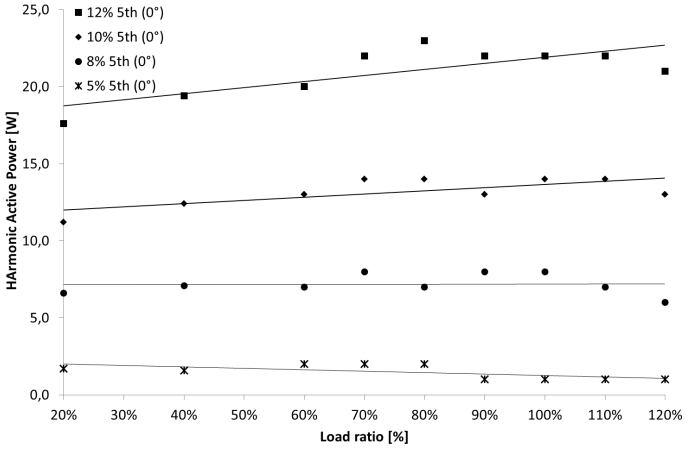

Figure 5.10: Variation of Harmonic Active Power as function of the loading ratio for a 4-pole 4kW IG for 12% fifth harmonic (Y=$0°$)

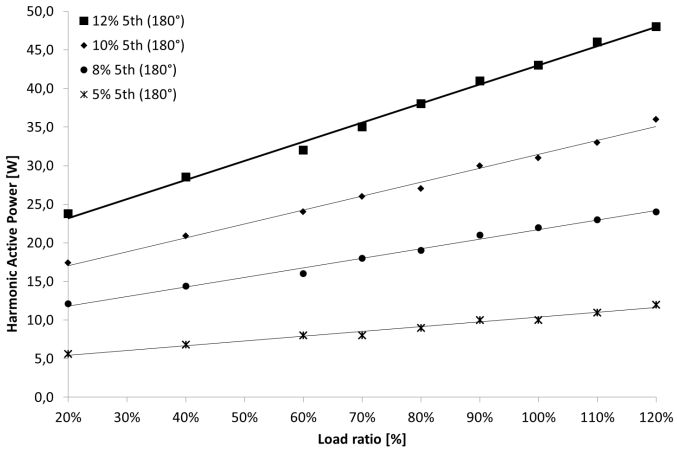

Figure 5.11: Variation of Harmonic Active Power as function of the loading ratio for a 4-pole 4kW IG for 12% fifth harmonic (Y=180°)

5.5.3 Influence of harmonic order and superposition of losses

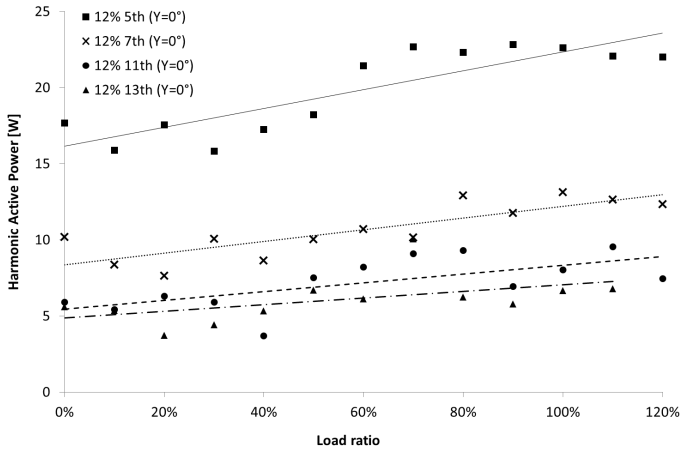

Figure 5.12: $P_{\text{h\_el}}$ for a 4kw EFF2 4kW IM as IG, supplied with 12% distortion of different order and harmonic phase angle =0°

From Figures 5.12 and 5.13 it is noticed that the phase angle of the harmonic distortion has a significant impact on the harmonic losses. Consequently measurements have been performed for 2 distinctive harmonic phase angles. For both harmonic phase angles, the trend is clear that, as the harmonic order increases, the related harmonic losses decrease. As noticeable in Figure 5.14, the effect of varying phase angle is more explicit in case of low frequency distortion. As the frequency increases the effect of varying phase angle reduces drastically.

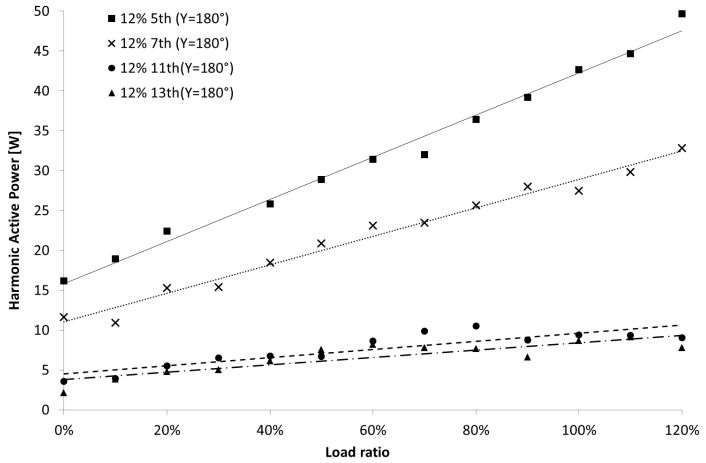

Figure 5.13: $P_{\mathrm{h\_el}}$ for a 4kw EFF2 4kW IM as IG, supplied with 12% distortion of different order and harmonic phase angle =180°

This can be designated that with increasing frequency, the averaged voltage reduces inversely proportional to the order.

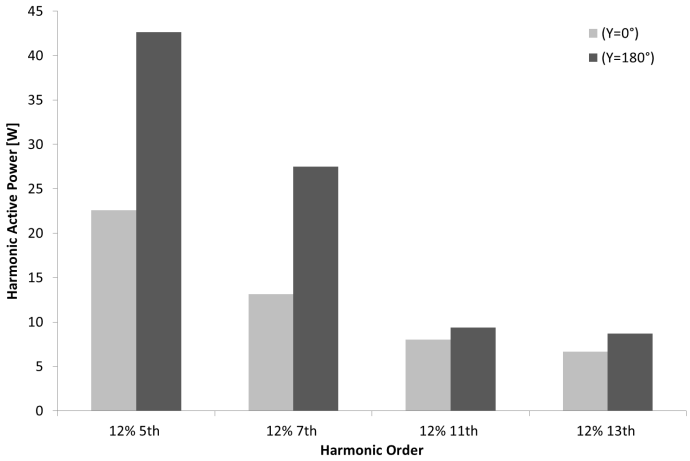

Figure 5.14: Variation of $P_{\mathrm{h\_el}}$ for a 4kW EFF2 IM as IG, as function of both order and phase angle at nominal loading

Similar to Chapter 4 is the superposition principle evaluated in case of IG operation. However, as the phase of the harmonic voltage is dominating the effect of harmonic losses on IG systems, it can already be assumed that the superposition principle is no longer valid.

Table 5.2: Evaluation of the superposition of the harmonic losses

Harmonic content	Superposition	Measured
12% 5^{th} (Y=0°)+ 12% 7^{th} (Y=0°)	35.73	28.41
12% 5^{th} (Y=180°)+ 12% 7^{th} (Y=0°)	55.78	67.76
12% 5^{th} (Y=0°)+ 12% 7^{th} (Y=180°)	50.08	–
12% 5^{th} (Y=180°)+ 12% 7^{th} (Y=180°)	70.13	54.07

Measurements were executed on the 4kW IG at nominal load (nominal electric power) in order to evaluate the validity of the superposition rule. The results listed in Table 5.2 clearly illustrate the inaccuracy of superposition of losses in case of IG operation. It is also noticed that for the situation with "*12% 5^{th} (Y=0°)+ 12% 7^{th} (Y=180°)*" no measurements are listed. This is due to the technical limitations of the power source, which prohibited actual measurement of this wave form.

5.6 Effect of varying IG conditions

5.6.1 Influence of the machine efficiency rating

In Chapter 4 measurements are presented concerning the influence of the efficiency rating of the machine in relation to its susceptibility towards supply voltage distortion. For motor operation the higher efficiency related to a reduced stator and rotor resistance and consequently the conclusion was presented that a higher rating of efficiency also resulted in lower harmonic losses. However, IG operation increases the difficulty due to saturation. With increased efficiency the related rotor and stator resistance are reduced. Consequently higher efficient machines remain in unsaturated operation. Although a reduced rotor resistance results in reduced rotor Joule losses, the absence of saturation does not actively dampen harmonic rotor current. In order to validate the influence of efficiency rating on the susceptibility of IG systems 4 measurements are presented. Two efficiency ratings of 11kW 4-pole induction machines are tested as an IG. The machines are supplied with 10% 5^{th} harmonic distortion but, as the phase angle has a significant influence on the harmonic phase angle 4 different measurements are illustrated in Figure 5.15.

It can generally be stated that harmonics with Y=180° generate higher losses. This relates to the conclusions of §5.5.1 that for Y=180° the machine operates in less saturated conditions and that there is less damping by the mutual inductance. Consequently, it can be explained that for machines of higher efficiency the harmonic losses reduce. The harmonic losses are mainly determined by rotor Joule losses and for higher efficiency ratings machines have a reduced rotor resistance. For an EFF2 the machine operates in increased saturated conditions. In relation to the harmonic losses the saturation actively dampens the harmonic losses and

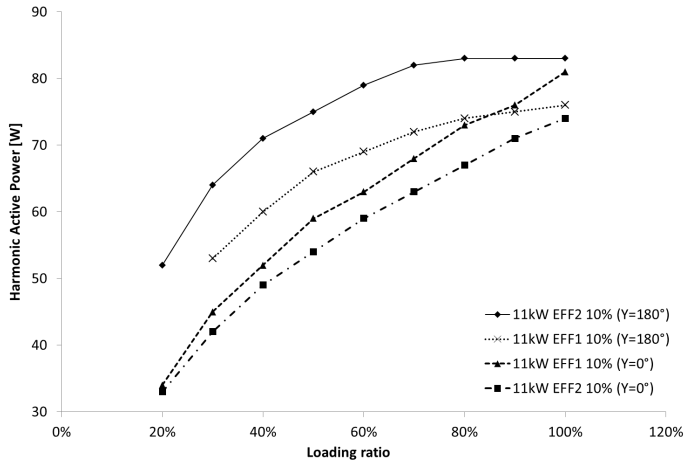

Figure 5.15: Variation of Harmonic Active Power as function of the loading ratio and its efficiency rating for a 4-pole 11kW IG for 12% fifth harmonic.

subsequently this implies that an EFF2 machine is less susceptible to supply voltage distortion if the machine operates in an increased saturated operation. Although the saturation results in a more effective damping of the harmonic losses in case of Y=0°, a general preliminary conclusion could be that -on average- an increased efficiency of machines result in less harmonic power.

5.6.2 Influence of specific generator design

As already stated in the introduction a standard induction machine can operate in both sub-synchronous (motor) or in super-synchronous (generator) mode. However, machines can be specifically designed towards generator operation. Consequently, in this research two 55kW 2-pole machines have been tested. The first machine is a 55kW IM constructed for motor use, but tested as a generator. The second machine is a high efficiency 55kW generator, especially designed for generator use (more magnetic material, lower stator resistance). The IM has a reduced efficiency (92.5% at nominal motor load) according to the nameplate as compared to the IG (96.5% at nominal load in generator mode). Mechanical power is controlled with a four quadrant programmable DC-machine with a rated power of 85kW at 3000 rpm.

From Figures 5.16 and 5.17 it can be observed that the losses related to supply voltage distortion of both the machine designed for motor operation and the machine specifically designed for generator operation are within the same order of magnitude. Because of the use of current clamps, the reduced accuracy does not allow to present an in depth comparison.

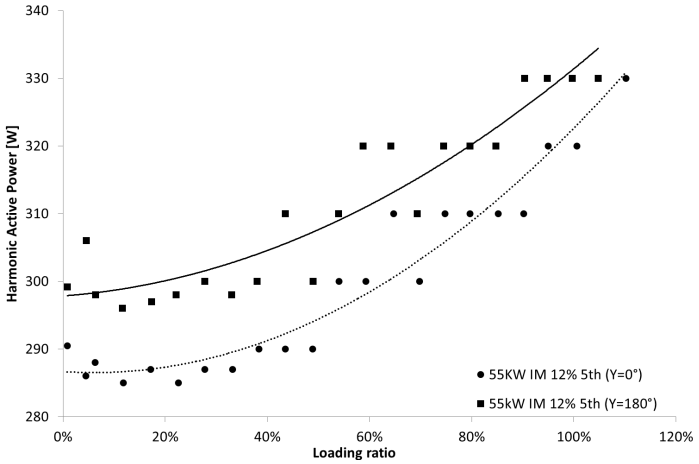

Figure 5.16: Variation of Harmonic Active Power as function of the loading ratio and its efficiency rating for a 2-pole 55kW IM for 12% fifth harmonic.

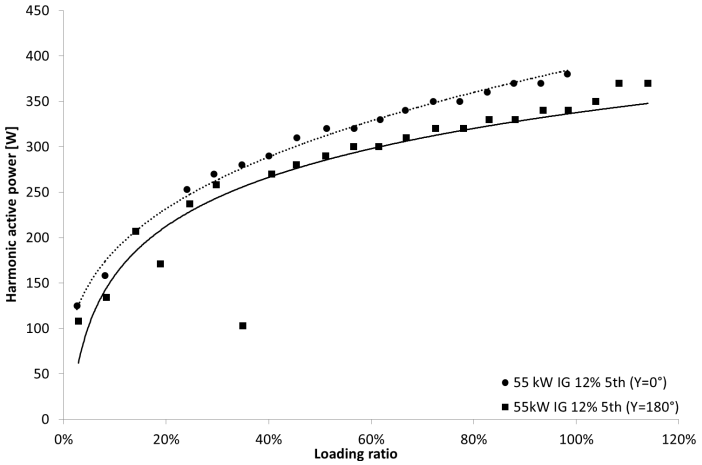

Figure 5.17: Variation of Harmonic Active Power as function of the loading ratio and its efficiency rating for a 2-pole 55kW IG for 12% fifth harmonic.

5.6.3 Influence of the machine output power rating

As already illustrated in Chapter 2 the loss distribution is related to the machine's output power. Consequently, it is can be suggested that the effect of harmonic voltage distortion on IG is function of the power ratio of the machine. As the machines output power increases the harmonic losses in p.u. tend to drop in case of motor operation. This effect is also validated for IG operation as can be derived from Table 5.3. For a 4kW IG the losses linked to a distortion of 12% 5^{th} relate to a maximum loss of 1.2%, and for a 55kW IM used as a IG the pu harmonic losses

reduce to 0.75%.

Table 5.3: Influence of the power ratio of the IG in relation to $P_{\mathrm{h\_el}}$ at nominal load

P_{mech}	4kW (EFF2)		11kW (EFF2)		55kW (EFF1)	
$P_{\mathrm{h\_el}}$	[W]	[pu]	[W]	[pu]	[W]	[pu]
10% 5^{th} (Y=0°)	14	0.39	74	0.75	-	-
10% 5^{th} (Y=180°)	33	0.92	83	0.84	-	-
12% 5^{th} (Y=0°)	22	0.61	-	-	340	0.67
12% 5^{th} (Y=180°)	43	1.19	-	-	380	0.75

5.6.4 Susceptibility of IM to IG operation

Up to this point only the IG operation mode has been evaluated, although one of the main interests is to obtain a comparison of the susceptibility of both IM and IG for a similar supply voltage distortion. The previous already indicated that the drop of the efficiency caused by voltage distortion is not the ideal basis to make a comparison. Consequently, when the comparison is made towards the additional losses caused by voltage distortion, the harmonic active power losses $P_{\mathrm{h\_el}}$ in [W] is used.

If the assumption is made that the machine works in a non saturated condition, the damping due to the bypass via the mutual inductance can be neglected. Consequently, this implies that the harmonic modeling concept as suggested in Chapter 4 can be used to estimate the losses. However, as illustrated in §5.3.4 the transition from motor to generator operation does change the induced rotor frequency. For the 5^{th} harmonic distortion an increase of induced rotor frequency is obtained. Due to the skin effect this results in a reduced impedance and an increased rotor resistance. As also illustrated in Chapter 4 the harmonic current is mainly determined by the leakage inductance. With a reduction of the leakage inductance, the harmonic current will increase. The increase of harmonic current will induce more stator Joule losses and even more rotor Joule losses as not only the rotor current increases, but also the rotor resistance. However, if the machine operates in more saturated conditions, there will be a leakage path via the mutual inductance (I_{m}). Although K_r will rise in reference to motor operation, the saturation will result in less losses in generator operation due to the active damping.

These assumptions have been tested on 2 machines. The first machine is a 4kW IM and the second machine is a 11kW IM, The measurements are plotted in Figures 5.18 and 5.19. It is assumed that for a Y=0° the IG operates in more saturated conditions. This corresponds to the lowest harmonic active power. For a Y=180° the machine operates in less saturated conditions resulting in more

Table 5.4: Effect on the harmonic losses when transitioning from motor to generator operation

IM $\Rightarrow$ IG		
	No sat.	Sat.
K_x	$\searrow$	$\searrow$
X_{σ_h}	$\searrow$	$\searrow$
X_{m}	-	$\searrow$
I_{h}	$\nearrow$	$\nearrow$
$I_{\mathrm{h\_r}}$	$= I_{\mathrm{h}}$	$= I_{\mathrm{h}} - I_m$
K_r	$\nearrow$	$\nearrow$
R_{r_h}	$\nearrow$	$\nearrow$
$P_{\mathrm{h\_el}}$	$\nearrow$	$\searrow$

harmonic losses. In motor operation the phase of the harmonic has no significant influence as illustrated in Chapter 4. It is observed that for both machines, if the machine operates in more saturated conditions, the harmonic losses reduce and consequently the machine is less susceptible to harmonic voltage distortion in generator operation. However, if the machine operates in less saturated conditions, the harmonic losses are higher in generator operation. This validates the assumptions and the generalized conclusions in Table 5.4.

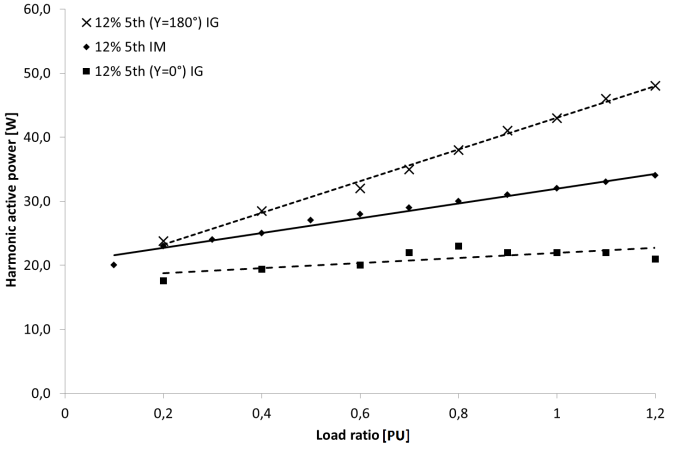

Figure 5.18: Comparison motor versus generator operation of a 4-pole EFF2 4kW induction machine at 12% 5^{th} distortion

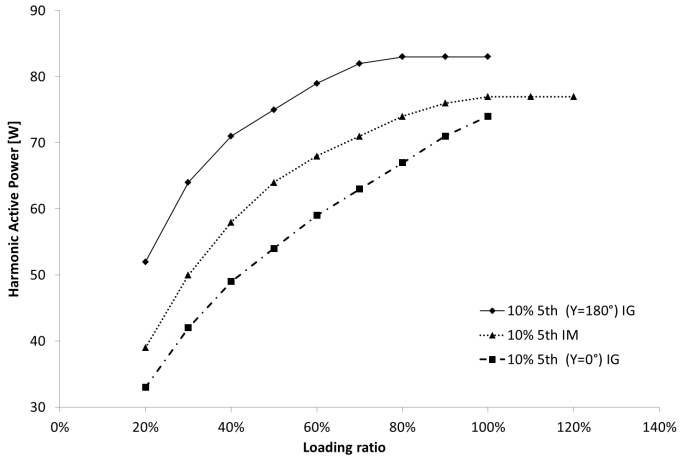

Figure 5.19: Comparison motor versus generator operation of a 4-pole EFF2 11kW induction machine at 10% 5^{th} distortion

5.7 Thermal aspects linked to harmonic losses

Additional losses imply additional heat generation inside the IG. The additional temperature rise caused by supply voltage distortion is presented for IM in Chapter 4. Because the LTM of the machine is also valid for IG operation, this LTM can now be used to estimate the additional temperature rise inside IG. However, some technical aspects should be considered before evaluating the temperature rise. The supersynchronous operation also results in an increased speed of the fan. This will result in a better cooling capacity of the machine. As stated in Chapter 2, this research bypasses the difficult calculations of thermal ambient resistance by monitoring the frame temperature. However, this effect should at least be partially addressed as the thermal resistance from the outer frame to the ambient drops. This has been calculated by using the model of [6] and results are presented according to Table. 5.5.

Table 5.5: Reduction of frame to ambient thermal resistance due to the increased fan speed

	IM		IG
Slip	0.04	0	-0.04
Rotor Speed [rpm]	1440	1500	1560
Airflow rate [m/s]	3.76E-04	3.92E-04	4.08E-04
Radial Thermal Frame Resistance [K/W]	0.032741	0.032564	0.03239

However, as suggested in Chapter 2, this research bypasses the previous problems by directly monitoring the frame temperature. Although simple Thermal Modeling of Chapter 2 suggests that the stator winding to frame resistance remains

constant, the results of [7] show a decrease of resistance of $-3.5e^{-5}K/(W.rpm)$. In [7] a 3kW TEFC IM was supplied with a constant DC power, and the mechanical speed was controlled by the generator system. The conclusion was presented that there is a decrease in total windage temperature as the mechanical speed increases and the losses remained constant. This can probably be designated to the increased heat dissipation in axial direction resulting in a reduced thermal resistance due to the combination of axial and radial heat dissipation.

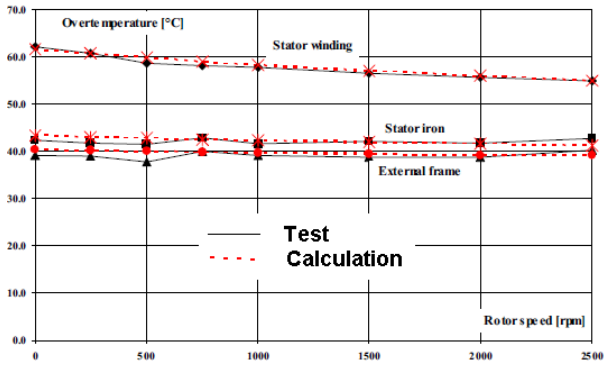

Figure 5.20: 3kW TEFC IM winding-frame temperature for different speeds [7]

The increased fan speed in combination with a higher heat dissipation in axial direction results in a decrease of thermal resistance if machines are operated as an IG. Consequently, the worst case scenario can be obtained by evaluating the harmonic losses for a Y=180° and implementing the LTM of the IM. For a 4kW IM at nominal load and at 12% 5^{th} distortion, the harmonic losses are known from Figure 5.8. The resulting temperature in stator windings can be obtained by implementing the thermal resistance from frame to ambient R_{th} (Chapter 2). The results are listed in Table 5.6.

Table 5.6: Additional temperature rise of a 4-pole 4kW induction machine for both motor and generator operation, caused by 12% 5^{th} supply voltage distortion

	IM	IG @ Y=0°	IG @ Y=180°
$P_{\text{h\_el}}$ [W]	32	22	43
R_{th} [K/W]	0,044	0,044	0,044
ΔT [K]	1,408	0,968	1,892

Note that the simple derivation provided in Table 5.6 does over estimate the temperature increase in generator operation. As the thermal aspects related to harmonic distortion in motor operation are already generally negligible, it can be stated that the effect of harmonic distortion on the operational temperature limits of IG is even of lesser concern.

5.8 Conclusions

If induction generators are used, two specific questions have been addressed. The first question relates to the additional losses caused by supply voltage distortion in generator operation. This can be of significant importance if economical assessments are to be presented. However, in some cases the overall energy efficiency of IG is of lesser concern and the focus is shifted towards robustness and low maintenance. From technical perspective the additional losses could also result in additional heat and consequently premature stator failure.

Literature study indicates that there is a research gap concerning the influence of voltage distortion on IG operation. The presented research takes initial steps towards this issue, which shows the increased difficulty to study these effects. This research has indicated that there is a margin for discussion to the reference of which generator efficiencies are compared. Based on the used reference some conclusions could alter. This research suggests to relate to the output power, and in case of generator systems this is the desired total electrical output power P_{RMS}. In case of pure sine wave supply voltage the P_{RMS} equals $P_{\mathrm{RMS\_1}}$, however, in case of distortion the P_{RMS} differs from $P_{\mathrm{RMS\_1}}$ further increasing possible margins for discussion.

Subsequently, the harmonic modeling concept is evaluated in case of IG operation. Theoretical deduction illustrated the inaccuracy of translating harmonic models built for motor operation to estimate the effect on IG operation. As the rotor frequency shifts this implies a shift of skin effect in reference to motor operation. Additional the neglect of the magnetizing inductance can result in some errors. These reasons resulted in a discard of translating the current harmonic IM models to IG systems.

An extensive amount of measurements have been presented, which evaluate both the influence of voltage distortion parameters such as harmonic magnitude/order or phase angle and constructional parameters such as efficiency class/power rating and load ratio. The generalized conclusion is that, contradictory to motor operation, the susceptibility of IG systems to supply voltage distortion is highly function of saturated operation and consequently the harmonic phase angle. The research presented in Chapter 4 already indicated that the thermal aspects linked to supply voltage distortion in motor operation are only important above nominal load and for excessive distortion ratios ($\mathrm{THD_U} < 12\%$). Although generator systems can indure a small amount of additional harmonic losses, the increased fan speed results in similar thermal susceptibility of IG towards supply voltage distortion.

As illustrated in Chapter 3 the connection mode of the machine (Star or Δ) shifts the harmonic phase angle. Measurements presented in this chapter illustrated that, contrary to IM, the harmonic phase angle has a significant influence on the saturation of the machine. Although a saturated operation results in additional iron losses, the saturation effectively dampens the overall harmonic losses. Consequently, when designing a generator system, a well chosen connection mode can significantly reduce the corresponding harmonic losses.

References

[1] P. Gardner, A. Garrad, P. Jamieson, H. Snodin, and A. Tindal. *Wind Energy - The facts: PartI Technology*. In Wind Energy - The facts. European Wind Energy Association, 2009.

[2] W. Deprez. *Energy efficiency of the induction machines: a critical assessment*. PhD thesis, KU Leuven, 2008.

[3] A. De Almeida, F. Ferreirra, J. Fong, and P. Fonseca. *European Ecodesign Directive on Energy- Using Products (EUP's), Project LOT 11 Motors*.

[4] W. Finley, B. Veerkamp, D. Gehring, and P. Hanna. *Improving motor efficiency levels globally*. IEEE Industry Applications Magazine, 15(1):39–49, 2009.

[5] *IEC 60034-2-1: 2007 (BS EN 60034-2-1) Rotating Electrical Machines-Part 2-1: Standard methods for determining losses and efficiency from tests (excluding machines for traction vehicles).* 2007.

[6] L. Popova, J. Nerg, and J. Pyrhonen. *Combined Electromagnetic and thermal design platform for totally enclosed induction machines*. In Int. Sym. on Diagnostics for Electric Machines, Power Elect. and Drives (SDEMPED), pages 153–158, Bologna, Italy, 2011.

[7] A. Boglietti, A. Cavagnino, D. Staton, M. Popescu, C. Cossar, and M. McGilp. *End Space Heat Transfer Coefficient Determination for Different Induction Motor Enclosure Types*. In IEEE Industry Applications Society Annual Meeting, pages 1–8, Edmonton, Canada, 2008.

6

The effect of harmonic voltage distortion on Line Start Permanent Magnet Machines

6.1 Introduction

Squirrel cage induction motors have a lot of advantages, mainly their robust character and line start capability, with respect to many other electrical machines. The major drawback of a SCIM in terms of efficiency is that the magnetization for both rotor and stator needs to be externally delivered by the external power supply, thus leading to inevitable additional losses. According to [1], three phase LSPMMs are one of the possibilities to achieve IE5 efficiency in the power range below 7.5kW while still complying to the standard frame sizes, as defined in IEC60034-7 [2].

The use of Permanent Magnets (PM) in the rotor is the most common way to bypass the need to externally deliver rotor magnetization. However, adding PM in the rotor results in an additional torque which generally reduces start up capabilities, consequently standard PM machines are unable to start at line frequency. Additional startup methods are required, e.g. VSD PM motor combinations are generally suggested. In specific cases line operation is essential. If the rotor consists of both PM and rotor bars, the motor can start up as an IM and once near synchronism the MagnetoMotive Force (MMF) of the PM can synchronize with the MMF induced in the stator. In this way, the machine

combines the advantages of both asynchronous and synchronous machines. This machine is commonly known as a Line Start Permanent Magnet Machine (LSPMM) [3] [4].

Although the use of PM in electrical machines was already suggested at the end of the 19^{th} century, the poor quality and low energy density of the available PM prohibited the use of PM in high power rotating machines ($>$ 1kW). The popularity of PM motors is increasing due to the availability of magnets with high energy density and cost-effective rare earth PM materials. Consequently, from the mid 80s research resulted in small and fractional horsepower single-phase LSPMM. These machines were specifically developed for small domestic, utility, and special-purpose commercial markets.

The operation of the machine combines asynchronous and synchronous PM operation, however this results in low starting torques and synchronization difficulties. An improvement in steady-state performance (efficiency, power factor, and synchronous torque) by increasing the permanent-magnet strength increases the reluctance torque and leads to a low starting torque. On the other hand, maximizing the induction torque near synchronous speed (in order to increase the synchronization capability) by lowering the cage resistance reduces the starting torque. The poor starting performance of LSPMMs limited its application to loads that require small effort at standstill.

Economical and ecological incentives pushed manufacturers to restudy the LSPMM and its untapped potential. Advances in numerical optimization techniques such as FEM, resulted in LSPMM which have a maximum allowable load inertia up to 30 times the motor inertia, which is enough for most industrial loads. Three phase Line Start Permanent Magnet Machines became off-the-shelf products, available in a power range up to 7.5kW.

6.2 Fundamental loss segregation of an LSPMM

6.2.1 Stator Joule, iron and mechanical loss

Totally Enclosed Fan Cooled (TEFC) LSPMM closely relate to TEFC IM of equal power and speed. They share identical stator winding layout, apart for the PM a fairly similar rotor construction is noticed and both machine frame dimensions are built according to IEC60034-7. Consequently, LSPMM loss mechanisms are often compared to IM. When a loss evaluation at nominal loading and fundamental frequency of an IM is executed, the electrical losses generated in the machine are stator Joule losses, rotor Joule losses and iron losses in both stator and rotor. In order to obtain the overall efficiency mechanical losses caused by friction and

windage should be taken into account. These losses are extensively addressed in Chapter 2. For a LSPMM, the rotor rotates in synchronism with the magnetic field. If spatial and time harmonics are taken out of consideration, no currents are induced inside the rotor. The losses are stator Joule losses, iron losses in the stator and mechanical losses. The Sankey diagram of Figure 6.1 lists the segregated losses obtained from measurement of both a 4kW IM and a 4kW LSPMM. In [5] it has been addressed that the indirect measurement method is favored for small power machines. Consequently, the loss segregation for the IM EFF2 in Figure 6.1 has been executed according to IEC60034-2-1, the indirect measurement method.

However, evaluation of the segregated losses for a LSPMM by using the indirect measurement method is prohibited due to technical limitations. The reduced voltage tests are not applicable because the flux of PM will result in excessive stator currents. A detailed analysis of the indirect measurement method according to IEC60034-2-1 with respect to LSPMM is presented in [6]. Consequently, for the LSPMM the stator Joule losses and mechanical losses were determined by direct measurement, initially assuming the remaining losses are equivalent to the iron losses.

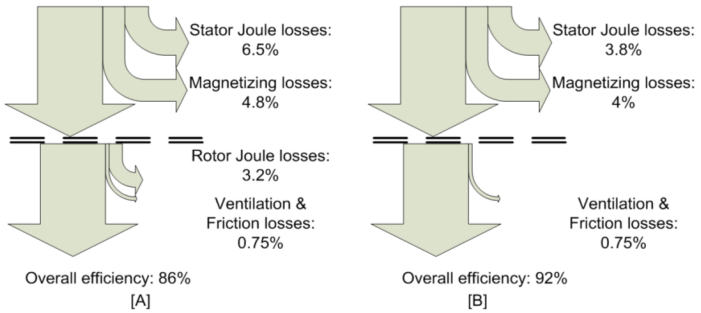

Figure 6.1: Fundamental loss analysis for a 4kW EFF2 IM [A] and a LSPMM [B] at nominal load condition

In Figure 6.1, the additional SLL, caused by imperfect winding layout within the stator and rotor, are excluded. For standard IM the estimation of SLL according to the indirect measurement method is still a topic of discussion [7, 8] and the indirect measurement method, used to determine SLL, is not straightforward applicable for LSPMM. Consequently, FEM has been applied to estimate these SSL.

6.2.2 FEM of stray load losses

The fundamental loss analysis of a LSPMM in Figure 6.1 has indicated that, at fundamental frequency, there are no rotor losses. However, additional rotor losses

do occur due to imperfect winding lay out. These additional losses are generally lumped into the SLL and even for standard IM the measurement procedure and calculation of these SLL have proven to be quite complicated [7]. As already stated in Chapter 2 is there a uniformization by applying standards such as IEC60034-2-1 to present an indication of these losses [8].

In order to correctly estimate the SLL of an LSPMM, FEM modeling of the LSPMM according to the constructional parameters from Table 6.1 has been executed. The mesh and the corresponding induction are plotted in Figure 6.2a and Figure 6.2b. The Finite Element Model (FEM) is a 2D transient FEM, coupled to an electrical circuit. The end winding resistance and inductance are taken into account by an impedance in series with the active part of the winding that is modeled by the 2D FEM. Also for the rotor bars, the electrical circuit adds the resistance and inductance of the rotor end ring, and makes the short circuit between the 28 rotor bars. Based on FEM the SLL are 30W which is 0.6% of nominal electric power, and this relates to similar values as presented in IEC60034-2-1.

Table 6.1: Construction parameters of the 4kW LSPMM

LSPMM	
Rated speed [rpm]	1500
Rated torque [Nm]	25
Output power [kW]	4
Efficiency	92%
Frame size	112M
Insulation class	F
Stator windings	copper wound
Rotor bars	die cast aluminum
Outer frame diameter [mm]	193
Airgap [mm]	0.4
Rotor diameter [mm]	114.2
slots per pole and phase	3
Type of magnets	NeFeB
Remanence of PM [T]	1.25

6.3 Lumped Thermal Modeling

In a loss analysis, knowledge of correct temperatures of the different motor parts is of key value. As an LSPMM contains PM this machine cannot easily be dismantled to insert temperature sensors inside. Monitoring of PM surface temperature would be challenging, because the magnets are inset PM. Because a coupled thermal/electromagnetic FEM with Computational Fluid Dynamics (CFD) is highly time consuming, this is not used for thermal modeling of

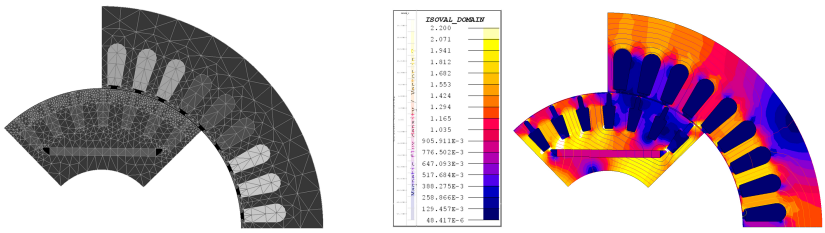

(a) Finite element mesh *(b) Induction distribution*

Figure 6.2: Finite Element Modeling of the 4kW LSPMM

the LSPMM. A lot of effort and computation time is still needed to obtain temperature estimations. LTM has been suggested during the latest decade to reduce the computation time and efforts and still obtain fairly good estimations of temperatures in different parts of the machine [9–11].

Due to the high construction similarity, this research tries to adapt the thermal resistance models of an IM to an LSPMM. The temperature rise $\mathbf{\Delta\Theta}$ for each node is calculated by solving:

$$\mathbf{\Delta\Theta} = (\mathbf{R} + \mathbf{C}) . \mathbf{P} \tag{6.1}$$

with $\mathbf{R}$ the square connection matrix containing the thermal resistances of the motor components, $\mathbf{C}$ the cooling matrix with the thermal resistances of the cooling fluid flow passing the nodes, $\mathbf{P}$ the segregated power loss vector containing the losses at the motor components and $\mathbf{\Delta\Theta}$ the temperature rise of the nodes compared with the initial surface temperature. Because the physical construction of an LSPMM closely relates to an equivalent IM [12], an equivalent thermal conductance matrix $(\mathbf{R} + \mathbf{C})$ is assumed for LSPMM. Modifications were needed to fine tune the model in order to include the PM, the slightly different speed of the fan and the adjusted rotor bars. In contrast to the similar conduction matrix $(\mathbf{R} + \mathbf{C})$ the segregated loss matrix $\mathbf{P}$ alters when comparing IM and LSPMM. This is clearly illustrated in Figure 6.1. In order to validate the similar conduction matrix measurements were executed.

The actual winding temperature can be recalculated from measurement of hot and cold stator resistance and by using:

$$R = R_{20^\circ\mathrm{C}} . (1 + \alpha_r . \Delta\Theta) \tag{6.2}$$

with R the value of the stator coil resistance at temperature Θ, $R_{20^\circ\mathrm{C}}$ the value of the resistance at a reference temperature of 20°C, α_r the temperature dependency of the resistance in [1/K] and $\Delta\Theta$ the temperature rise. At 20°C frame temperature a stator resistance of 2.839Ω was measured for the LSPMM

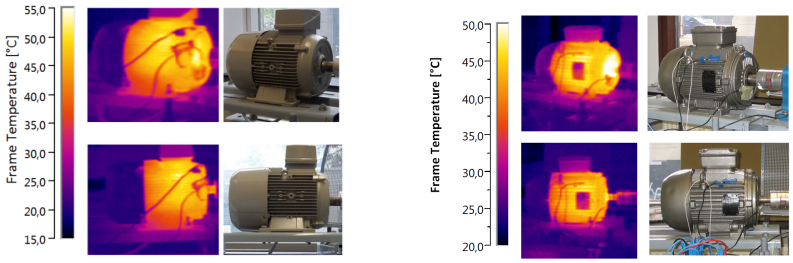

(a) 4kW IM *(b) 4kW LSPMM*

Figure 6.3: Thermal images of a 4kW machines at nominal load

and subsequently 3.264Ω at a stator housing temperature 42°C. The α_r of copper equals $3.910^{-3}\Omega/K$ and consequently a stator coil temperature of 57°C is obtained. Similar calculations have been performed for a standard 4kW IM.

Table 6.2: Validation of LTM

	IM	LSPMM
Efficiency	0.886	0.92
P_{mech} [W]	4000	4000
P_{loss} [W]	514.7	347
$R_s[\Omega]$ at ambient temp	1.35	2.839
$R_s[\Omega]$ at nominal condition	1.64	3.264
Estimated winding temperature at nominal condition $[^\circ C]$	72.7	57
Frame temperature at nominal condition $[^\circ C]$	50.1	42.5
Thermal resistance frame-winding [K/W]	0.043911	0.041688

With the combined knowledge of outer frame temperature, the total amount of power losses and the obtained the winding temperature, the thermal resistance from outer frame to inner winding can be recalculated. A 5% deviation between the IM and LSPMM thermal resistance is observed from Table 6.2. This validates the use of the IM thermal model to estimate LSPMM temperatures. In Figure 6.4 the comparison is presented between a 4kW IM and a 4kW LSPMM. The results were obtained by using the detailed model of [13], including SLL.

The detailed model does not enable fast temperature estimations. According to Figure 6.15, 83% of the heat is generated inside the stator, which will imply that the majority of the losses are dissipated in a radial direction via the stator housing. Consequently the most important thermal resistances are listed in Table 6.3.

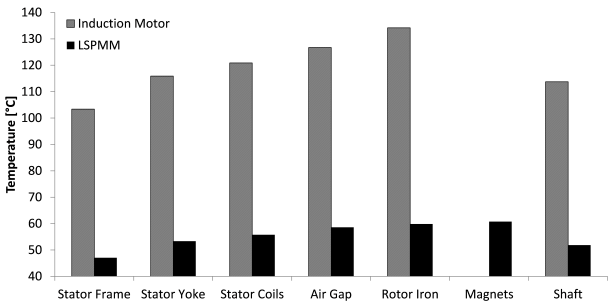

Figure 6.4: Estimated temperatures of rotor iron, stator coil and stator frame of a 4KW IM and a 4kW LSPMM

Table 6.3: Dominant thermal resistances for a 4kW IM and a 4kW LSPMM

	IM	LSPMM
Ambient to Frame [K/W]	0.0322	0.0305
Frame to Stator Yoke [K/W]	0.0072	0.0072
Stator Coil to Stator Yoke [K/W]	0.0141	0.0141
Airgap to Rotor Yoke [K/W]	0.2933	0.2933

As illustrated in Figure 6.5, these values can now be used for fast and straightforward calculation of the nominal operating temperature of the different sections inside the machine. The corresponding temperatures for both IM and LSPMM can be seen in Table 6.4, and the obtained temperatures from this simplified calculation highly relate to the temperatures obtained from the detailed model of [13].

Table 6.4: Temperature of Motor Sections in [°C]

	IM		LSPMM	
	LTM	[14]	LTM	Measured
Stator Yoke	115.9	120	53.3	-
Stator Coil	120.8	120	55.8	57
Rotor Yoke	134.2	150	59.9	-
PM	-	-	60.8	-

Besides a small amount of SLL, no losses are generated inside the rotor. This often results in the approximation that the temperature of the rotor and the PM could be set identical to the temperature of the stator coils [15]. The LTM indicates that there is a 5K difference between stator coil and the PM. Accordingly, the obtained PM temperature of 61°C can be used to estimate the PM temperature. In [6] it has been hinted that the LSPMM is a cool running machine in reference

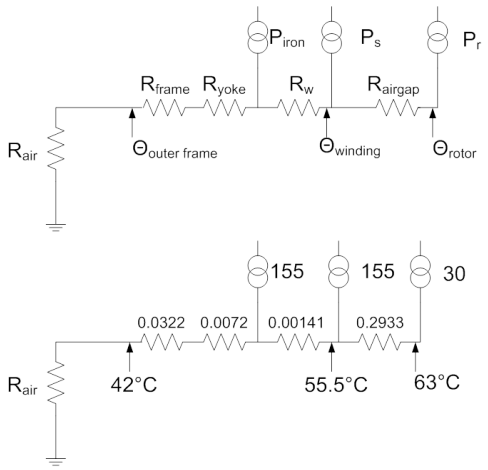

Figure 6.5: Simplified thermal model of a 4kW LSPMM at nominal load

to similar IM and the obtained results confirm these conclusions. Note that the mechanical speed of the fan increases if an IM and an LSPMM are compared. This not only influences the mechanical losses, the absence of slip results in a $\pm 3.3\%$ decrease of thermal frame-to-ambient resistance.

6.4 Loss segregation of an LSPMM as a function of the operating temperature

The goal is to obtain a similar loss evaluation for an LSPMM as a function of the operating temperature as has been presented for an IM in Chapter 2. In the following sections, the different losses of an LSPMM are evaluated as a function of the temperature. In §6.4.1 the stator Joule losses are elucidated. Subsequently, the iron losses are addressed in §6.4.2 and the mechanical losses (P_{w}), are evaluated in §6.4.3. As a result an overall loss analysis as a function of the temperature is obtained in §6.4.5.

6.4.1 Temperature dependent Joule losses

If the temperature rises, the internal resistance of the stator coil will rise. This effect has already been addressed by (6.2). Due to the small conductor sections in the coil, both skin and proximity effects are neglected [16]. If balanced conditions are assumed, the Joule losses in the stator can be calculated by:

$$P_{\mathrm{s}} = 3.R_{\Theta}.I_{RMS}^2 \tag{6.3}$$

with P_{s} the stator Joule losses and I_{RMS} the RMS value of the phase current. Note

that the reactive current demand of an LSPMM is function of the magnet remanent flux. As this remanent flux changes with the temperature, the Joule losses cannot be regarded independently from the iron losses. According to Figure 6.1, the actual P_{s} of an LSPMM has been measured 3.8% of its nominal input power.

6.4.2 Temperature dependent iron losses

IMs are designed to work close to the saturation level conditions. In this way the magnetic material is used at its optimum weight/energy ratio. For commonly used magnetic steel a maximum flux density of typically 1.5T is targeted [17]. For a commercial LSPMM the stator lamination is designed for similar flux density levels. In order to estimate the iron losses, [18] used the Steinmetz equation. However, the Steinmetz equation fails to separate the iron losses into hysteresis, classical and excess losses. In the FEM, the time domain iron loss model [19] is used as it is more accurate than the Steinmetz formula, especially in case of non-sinusoidal waveforms. A similar equation as in the cited paper computes the energy losses per cycle W_{fe} for a given waveform $B(t)$:

$$\begin{aligned} W_{\mathrm{fe}}(B,t,\Theta) &= aB^{\varsigma} + b(\Theta)\int_0^{T_p} \dot{B}(t)^2 \,\mathrm{d}t + \\ &\quad c\int_0^{T_p} |\dot{B}(t)|(\sqrt{1+d(\Theta)|\dot{B}(t)|}-1)\,\mathrm{d}t \end{aligned} \tag{6.4}$$

The three terms represent the hysteresis, classical and excess losses over one electrical period T_p. The coefficients a, ς, c, and d are to be determined by fitting based on Epstein frame measurements. The fitting procedure is explained in [20], and the coefficients are listed in Table 6.6. The coefficient $b = \sigma d^2/12$ is related to the thickness d = 0.50 mm of the material and the electrical conductivity σ = 3.24 MS/m, making it dependent of the temperature Θ. As proven in Equation (15) in the paper [19], the excess losses coefficient $d(\Theta)$ is proportional to σ, but the coefficients a, α and c are not. Because the conductivity depends on the temperature, the coefficients $b(\Theta)$ and $d(\Theta)$ are modified with the temperature by a correction factor (1+$\alpha_{fe}\Delta\Theta$). This factor is similar to (6.2), but with the temperature coefficient $\alpha_{fe} = 0.005/C$ of steel instead of the one for copper α_r. The obtained iron losses have to be corrected according to the construction factor K [13]. The waveforms $B(t)$ are obtained by a transient 2D FEM simulation, with rotating rotor.

The goal of this section is to evaluate the iron losses as a function of the temperature. As illustrated in Figure 6.6, the peak flux density from the magnets is a function of the PM characteristics, the air gap and the MMF in the stator $\mathrm{H}_{\mathrm{stator}}$. Since the current in the stator depends on the load ratio of the machine, the resulting flux density is also coupled to the load ratio. It is the vector sum of both

Table 6.5: Temperature effects of commonly used PM [21]

PM	$\Theta_{\max}$ (°C)	γ (%/°C)	H_{cJ} (%/°C)	Θ_{Curie} (°C)
Ferrite	225	-0.20	+0.2/0.5	460
Composite Ferrite	120-150	-0.2	+0.3	450
NeoFeB	80-230	-0.9≈0.12	-0.45≈0.85	310-380
Composite NeoFeB	160	-0.08≈0.12	-0.5	320
SmCo	250	-0.03≈0.05	-0.3≈0.5	700-800
AlNiCo	450	-0.03	+0.02	850

magneto-motive force from the stator and rotor which determines the saturation of the machine [15]. This effect is often referred to as armature reaction. A constant mechanical output power P_{mech} is assumed, which implies that both the reduction of flux linkage of the magnets and the shift in armature reaction are solely caused by the temperature rise.

If the temperature rises, the PM remanent flux density will reduce as a function of the applied PM according to Table 6.5 [21], with $\Theta_{\max}$ the maximum operating temperature and γ and H_{cJ} the reversible temperature coefficients. At a certain temperature magnets lose all their magnetic characteristics, commonly referred as the Curie temperature. These effects are well known [22] and the influence of the temperature rise is illustrated in Figure 6.6.

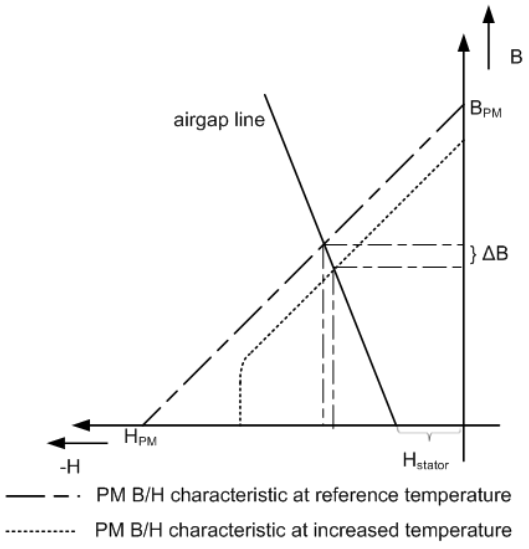

Figure 6.6: Reduction of the peak induction from the PM caused by a temperature rise at identical stator current

6.4.3 Temperature dependent mechanical losses

Friction and windage losses (P_{w}) mainly depend on the size of the fan and mechanical speed of the machine. For IM these losses can be derived by testing the machine at synchronous speed or by using IEC60034-2-1 [12]. LSPMMs rotate at synchronous speed and, because both IM and LSPMM share identical fan size and are constructed according to IEC 60034-7 [2], both friction and windage losses are assumed to be identical. Measurements have been executed on the described LSPMM in Table 6.1 in order to validate this assumption.

This paragraph evaluates the influence of temperature rise on the overall efficiency. According to [14] windage losses are inversely proportional with temperature. Ref. [14] reports that pressure and ventilating power vary with air density which in turn depends on air humidity, pressure and temperature. With a relative humidity of 80% and a normal atmospheric pressure, the windage losses in the considered temperature range decrease approximately 4-5% for each 10K of temperature rise.

As illustrated in Figure 6.1, the mechanical losses for both a 4kW 1500rpm LSPMM and IM are 30W, or 0.75% of the nominal input power. Although temperature rise may have a small influence on the mechanical losses, since the frequency is constant and the mechanical losses are small in relation to the other losses, the mechanical losses can initially be assumed to be constant [12]. This simplification will be justified in §6.4.10.

6.4.4 Temperature dependent SLL

Although some pragmatical and intuitive approaches could be presented in relation to the temperature effect on the SLL, to the author's knowledge no specific study has been performed which presents the temperature effect on the SLL. Consequently, the temperature dependency of the SLL will be evaluated by FEM and will be discussed in §6.4.10.

6.4.5 Variation of the efficiency as a function of the temperature

The mechanical power demand P_{mech} is assumed constant and at nominal loading. As the temperature rises, the Joule losses will increase while the iron losses will decrease. The resulting influence on the losses can be expressed as:

$$\frac{dP_{\mathrm{loss}}}{d\Theta} = \frac{dP_{\mathrm{s}}}{d\Theta} + \frac{dP_{\mathrm{iron}}}{d\Theta} + \frac{dP_{\mathrm{w}}}{d\Theta} + \frac{dP_{\mathrm{SLL}}}{d\Theta} \tag{6.5}$$

with dP_{loss} the variation in losses inside the LSPMM due to the temperature shift $d\Theta$, dP_{s} the shift in Joule losses in the stator, dP_{iron} the shift in iron losses in

the machine, dP_{w} the shift in mechanical losses and dP_{SLL} the variation in SLL. Consequently, the $\frac{dP_{\mathrm{loss}}}{d\Theta}$ can be obtained. If the $\frac{dP_{\mathrm{loss}}}{d\Theta}$ is positive, the resulting efficiency η will decrease, if the result is negative, the efficiency will increase.

6.4.6 Evaluation of the temperature effect by FEM

Three FEM simulations were executed in identical conditions of supply voltage and load. The only difference was the higher temperature, resulting in a reduced magnet remanence by 0.1%/K, and increased rotor bar and stator winding resistances.

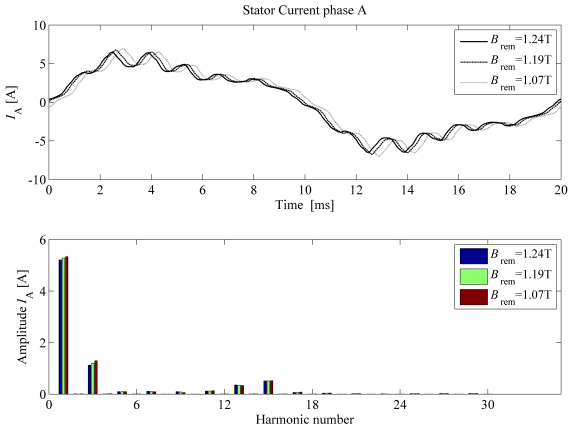

Figure 6.7: Stator current for several temperatures of the machine obtained by FEM

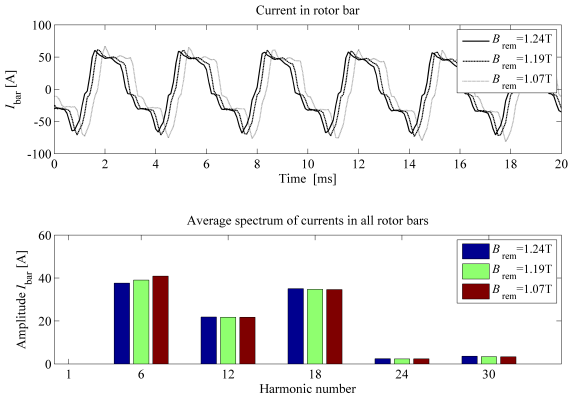

Figure 6.8: Rotor current in a bar obtained by FEM, and spectrum averaged over all rotor bars for several temperatures of the machine

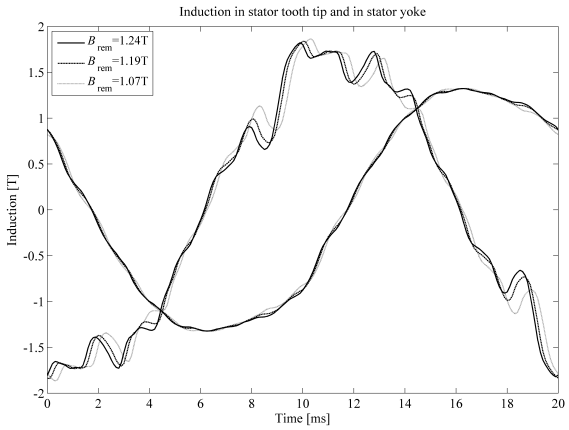

Figure 6.9: Induction waveforms in the yoke (almost sinusoidal waveform) and in the tooth tip (more distorted waveform) for several temperatures of the machine obtained by FEM

In the postprocessing, all losses were computed in the same way. For the iron losses, the coefficients b and d of (6.5) were corrected for a absolute iron temperature of 57 °C.

Table 6.6: Loss coefficients and results obtained by FEM. The last simulation assumes a dramatically decreased magnet remanence (-14% remanence for 74 degrees temperature rise)

Magnet temperature	20°C	61°C	94°C
Property	$B_{\rm rem}$ = 1.24 T	$B_{\rm rem}$ = 1.19 T	$B_{\rm rem}$ = 1.07 T
Iron loss coeff. a	0.0353	0.0353	0.0353
Iron loss coeff. ς	1.789	1.789	1.789
Iron loss coeff. b	1.0979 10^{-5}	9.265 10^{-6}	7.818 10^{-6}
Iron loss coeff. c	1.876 10^{-2}	1.876 10^{-2}	1.876 10^{-2}
Iron loss coeff. d	2.4808 10^{-4}	2.094 10^{-4}	1.767 10^{-4}
Stator current [Arms]	3.786	3.852	3.903
Power factor	0.9488	0.9384	0.9106
Stator Joule loss [W]	139.1	144.0	169.1
Stator iron loss [W]	109.3	102.0	95.3
Rotor Joule loss [W]	34.3	36.5	38.7
Windage loss [W]	30	26	22
Total loss [W]	312.7	308.5	325.0
η	0.9218	0.9229	0.919

The results presented in Table 6.6 indicate a possible increase of efficiency as the induction increases, however, the obtained results from the FEM analysis will be discussed in detail in §6.4.10.

6.4.7 Measurements

The influence of the temperature rise on the efficiency of an LSPMM is evaluated by actual measurements. The LSPMM is used as a motor and is loaded at constant nominal load with a controllable DC generator system in closed loop torque control with speed limitation. The temperature is measured by means of thermocouples on the flanges, the ventilator and the stator housing. The ambient temperature is measured and used as reference. The temperature measurements are checked with a calibrated measurement device to ensure the accuracy of the temperature measurement. The motor is started up at ambient temperature and is loaded at constant nominal load until steady-state temperature is reached, the ambient temperature has been maintained constant.

The output torque and the speed of the machine are measured to determine the mechanical output power. The efficiency at nominal operating conditions is measured according to IEC 60034-2-1 using the direct method [12]. The DC generator is in torque control mode and because LSPMMs are synchronous machines, P_{mech} is also constant. As the temperature increases, both the DC machine and LSPMM are monitored. The mechanical output power remains constant during heating and consequently the temperature dependency of the speed and torque transducer are eliminated. The shift in efficiency is calculated based on a constant P_{mech} and varying P_{el}. Accordingly, the measurement accuracy of the $\frac{dP_{\mathrm{loss}}}{d\Theta}$ is only function of the used power analyzer. During the test, the temperature is monitored and results of stator housing temperature are given in Figure 6.10. As the temperature rise can be modeled by a first order thermal circuit consisting of a thermal capacitance and a thermal resistance, the temperature rise can be formulated by:

$$\Theta = \Theta_0 + (1 - e^{-t/\tau_{\mathrm{temp}}})\Delta\Theta \tag{6.6}$$

with Θ_0 the reference temperature, τ_{temp} the thermal time constant and $\Delta\Theta$ the temperature increase of the frame. From the measurements, the thermal time constant τ_{temp} can be derived. The ambient temperature Θ_0 is equal to 20°C, at steady state the outer housing temperature is 42.5°C. At an initial time interval equal to τ_{temp}, the temperature rise is equal to 63% of the steady state temperature, or thus 14K. Therefore τ_{temp} equals 31 minutes.

In order to confirm the frame's temperature rise, thermal images were taken and plotted in Figure 6.3b. As noticeable in Figure 6.11, the efficiency increases as the LSPMM reaches nominal operating temperature. Similar to (6.6), the time constant of the efficiency variation can be calculated from Figure 6.11. As the same time constant τ_{temp} is obtained as in (6.6), this leads to the conclusion that the measured effect is solely caused by the temperature rise.

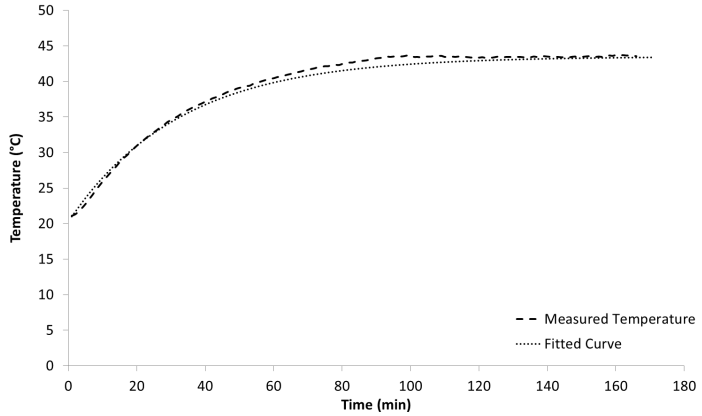

Figure 6.10: Outer frame temperature as a function of the time

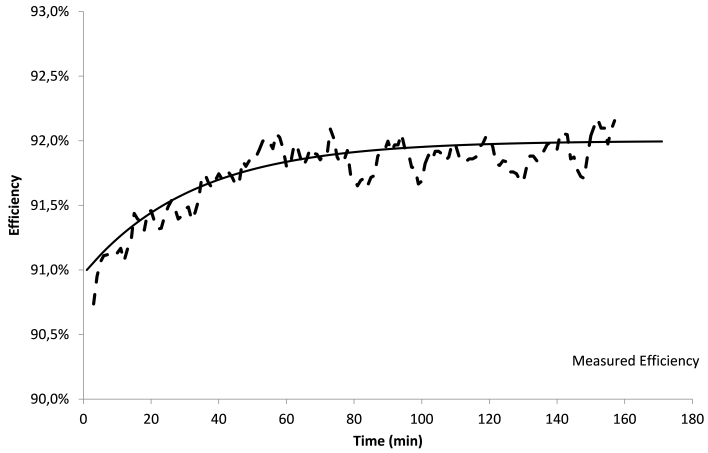

Figure 6.11: Efficiency as a function of the time

The efficiency increases as the temperature increases and this effect is opposite to IM. In order to explain this effect an in-depth loss analysis is presented. A more profound loss analysis is given based on FEM (§6.2.2) and the measurement results (§6.4.8). Additional measurements needed for §6.2.2 and §6.4.8 are plotted in Figure 6.12 to Figure 6.27.

6.4.8 Loss analysis using the measurement results

A segregated loss evaluation based on the practical measurements as a function of the frame temperature is presented in Figure 6.15.

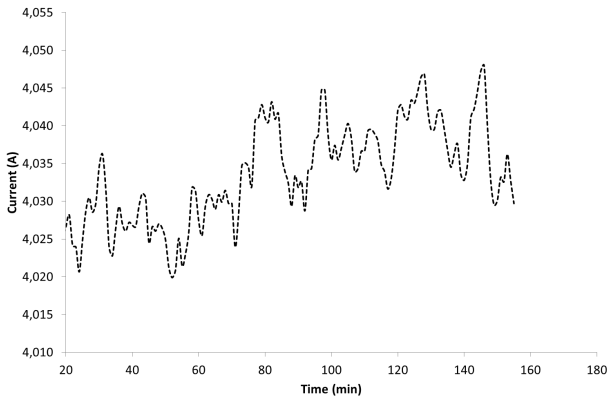

Figure 6.12: I_{RMS} as a function of time

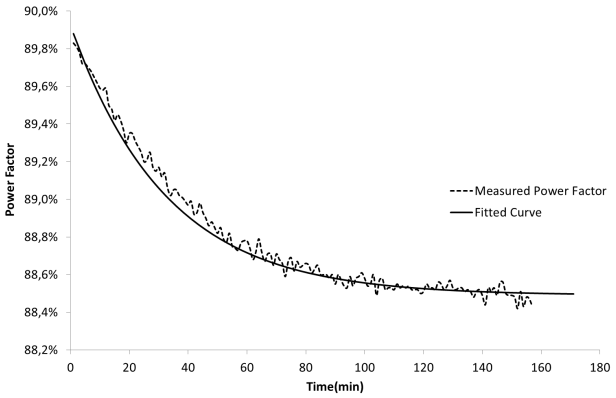

Figure 6.13: PF as a function of time

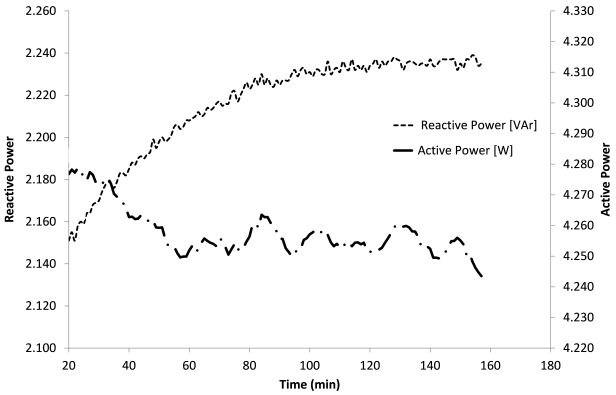

Figure 6.14: Active and Reactive power as a function of time

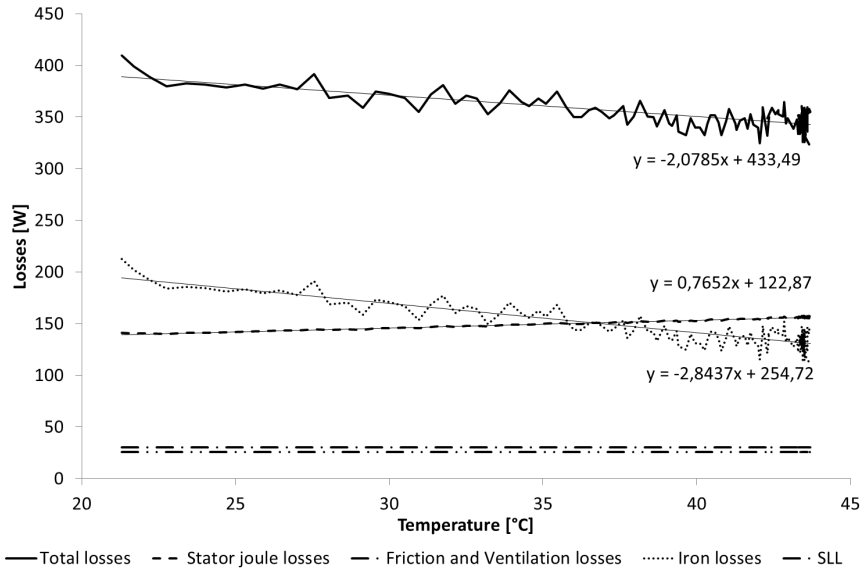

Figure 6.15: Loss evaluation as a function of the frame temperature

All calculations are done with actual measurement results. In this analysis the mechanical losses, with an absolute value of 30W, and SLL were assumed to be independent of the temperature. From the overall measured losses the calculated Joule losses, mechanical losses and SLL obtained by FEM were subtracted, assuming that the resulting losses represent the iron losses. Note that the reference temperature is the temperature measured at the frame and not the real temperature of windings and rotor. In Figure 6.12 the current is plotted as a function of time. The current shifts about 10mA with increasing temperature, which is barely measurable and noticeable. As the Joule losses are function of I^2_{RMS} this minor shift in current does not influence the stator Joule losses significantly. This is explained due to the fact that, although the reactive power increases, the active power decreases (Figure 6.27). According to (6.7), the Joule losses increase as the temperature increases:

$$\begin{aligned} \frac{dP_{\mathrm{joule}}}{d\Theta} &= 3.I^2_{\mathrm{RMS}}.R_{20}.\alpha \\ &= 0.71\frac{\mathrm{W}}{\mathrm{K}} \end{aligned} \tag{6.7}$$

Within Figure 6.13, it is noticed that the power factor PF has the same thermal time constant τ_{temp}. This leads to the obvious conclusion that also the power factor is a function of the temperature. As the supply voltage remains constant, the peak induction in the machine is nearly constant. With the remanence of the PM

reducing for increasing temperatures, an increased magnetizing current from the stator is needed. This explains the increase in reactive power consumption of the LSPMM. Subsequently, the efficiency of the LSPMM does slightly increase. For the same amount of active output power P_{mech}, this implies a decrease of active electric power consumed by the machine.

6.4.9 FEM evaluation of I_{RMS}, PF and efficiency

A comparison between the results obtained by FEM and the measurements is listed in Table 6.7.

Table 6.7: Comparison of FEM and measurements

	FEM		Measured	
Stator coil temperature [°C]	20	57	23	57
Stator current [A_{RMS}]	3.786	3.852	4.021	4.035
Power factor	0.9488	0.9384	0.899	0.885
Stator Joule losses [W]	139.1	144	140.46	155.7
Total losses [W]	312.7	308.5	385	345.7
η	0.9218	0.9229	0.910	0.917

The FEM model results in slightly higher values of PF in reference to the actual PF. The reason may be that the machine has a slightly lower remanent magnet flux than given by the manufacturer specifications. The measurements also indicated that the RMS current remains almost constant because the reactive power increases with temperature and the active electrical power reduces a bit. The latter is because of the decreasing losses and the constant mechanical power. FEM proves this result: the reactive power increases also in FEM, the PF decreases. Evidently, the active power remains constant in FEM (and equal to the mechanical power), because the losses are computed a posteriori in FEM.

Nevertheless, FEM confirms that there is a slight increase in energy efficiency as the temperature rises. FEM also illustrates that this effect is not to be extrapolated. The third column of Table 6.6 indicates that at an excessive reduction of the PM remanent field, the efficiency tends to reduce due to excessive stator losses. Consequently, there is an optimal temperature at which the LSPMM operates at maximum efficiency.

6.4.10 Mechanical and stray load losses

Both the FEM and the measurement analysis confirm that with increasing temperature, the Joule losses increase and the iron losses decrease, resulting in a reduction of the overall losses and an increase of efficiency. In the measurement analysis both mechanical losses as the SLL are excluded. For mechanical losses,

the increased temperature results in a reduced viscosity of both the bearing lubricant and the cooling air flow. For IM it is reported that there is a reduction in windage losses of 5% per 10°C [14]. In terms of loss variation this effect is not negligible. For a 4kW LSPMM the mechanical losses will reduce from 30W to 26W when reaching the nominal operating temperature. However, the SLL are within the same order of magnitude of the mechanical losses. Because SLL are mainly harmonic losses, the SLL will increase with increasing rotor bar resistance and hence with increasing temperature. This is observed from the FEM simulations in Table 6.6. Because the mechanical losses reduce and the SLL increase with increasing temperature these effects compensate each other partially.

6.4.11 Conclusions

The presented research uses FEM to address the individual loss mechanisms. All the losses are function of the temperature, of the implemented permanent magnets and the resulting stator current. As the operating temperature increases, the iron losses reduce and the Joule losses increase. For the vast majority of IM, the sum of stator and rotor Joule losses are dominant, accounting for more than 50% of the total losses in the IM [23]. The stator and rotor Joule losses increase with rising temperature, consequently the overall efficiency changes inversely to the temperature. However, for LSPMM the iron losses is within the same order of magnitude of the Joule losses, if the decrease of the iron losses is dominant, the overall energy efficiency can increase. This effect has been validated by FEM and consequently confirms the measurements.

However, before a thorough evaluation of the temperature effect can be presented, both partial loading and different power ratios of LSPMM should be taken into account. The effect of the temperature rise on the overall efficiency is function of the relative ratio between the segregated losses. Should the Joule losses become dominant it is possible that the overall efficiency will drop and consequently the conclusion of efficiency increase should not yet be generalized.

6.5 Additional losses caused by supply voltage distortion

6.5.1 Introduction

If LSPMMs are to become an actual substitute for standard IMs, the influence of voltage anomalies on their overall energy efficiency should be evaluated. Although initial work has been published which evaluates the effect of voltage unbalance on the energy efficiency of LSPMM [24], to the authors knowledge no third party studies have been executed concerning the influence of voltage

distortion on LSPMM efficiency. Due to the very familiar physical construction straightforward adaptation of the harmonic loss mechanisms for IM to LSPMM seems to be appropriate at first glance.

In order to compare the behavior of LSPMM and IM when supplied with a distorted voltage, the electromechanical design of both machines has to be addressed. Two of the most distinctive differences are [4, 25]:

1. The induction level of an LSPMM is not only a function of the applied voltage as is the case for an IM. The presence of PM in combination with the stator MMF are determining the peak induction. Due to the more difficult construction and the increased unbalanced magnetic pull of the rotor, a larger air gap is obtained in an LSPMM compared to a standard IM.

2. It is commonly assumed that for an LSPMM the flux rotates in synchronism with the rotor. Therefore no currents are induced in the rotor. This sometimes leads to a simplified construction of massive rotors. The massive rotor not only simplifies construction, a massive rotor construction will have an increased skin effect at start-up thus increasing start-up capability.

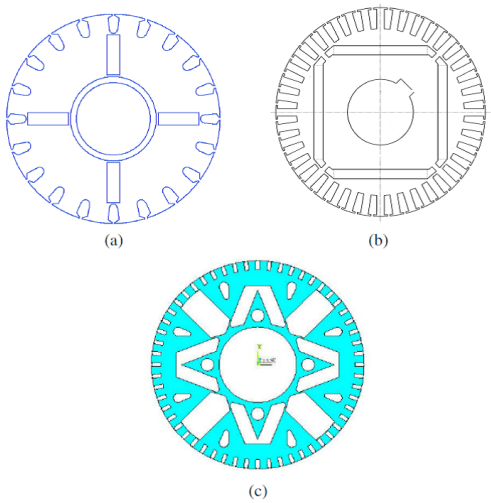

Figure 6.16: common rotor configurations for an LSPMM

Common rotor configurations of LSPMM rotors are presented in Figure 6.16 [4]. When the machine is supplied with a non sine waveform these two design parameters are assumed to have a more pronounced effect on LSPMM with respect to standard IM because:

1. The larger airgap, in combination with the presence of PM, leads to a higher magnetic reluctance. The high reluctance means a decrease of the inductivity. For the same harmonic voltage distortion, the decrease of inductivity results in larger harmonic currents thus leading to an increase of harmonic MMF in the machine and increased stator Joule losses.

2. If the rotor is constructed as a massive structure, there will be an increase of induced harmonic currents and more eddy currents in the rotor. Harmonic losses will result in additional heating of the rotor, and as the rotor temperature increases, the induction of the PM will decrease.

3. As the rotor is rotating at synchronous speed, harmonic content will interact in a very specific manner. Harmonic evaluation cannot be done for each harmonic component. Interaction of different harmonic components will be explained in §6.5.3.

The goal is to evaluate the energy efficiency of DOL operation of LSPMM with respect to the supply voltage distortion. As harmonic voltage distortion affects several loss components of LSPMM an evaluation of the segregated losses should be executed. However, it has already been illustrated that evaluation of the segregated losses for an LSPMM by using the IEC60034-2-1 method is prohibited due to technical limitations. The presented research resolves the lacuna of segregated loss evaluation in case of supply voltage distortion by implementing Finite Element Modeling.

6.5.2 Additional stator Joule, iron and mechanical losses

As illustrated in Chapter 3 an additional harmonic voltage results in additional stator and rotor Joule losses in case of IM. In case of IM the harmonic phase also affects the resulting induction in the machine and the corresponding iron losses, although this effect can be neglected. Similar to IM a supply voltage harmonic also results in additional losses in LSPMM. Concerning the stator Joule losses in case of supply voltage distortion, the presence of harmonic currents in the stator winding causes an increased copper losses. When skin effect is negligible, which generally is the case in copper wound machines, the stator copper losses in case of non-sinusoidal supply is proportional to the square of the total RMS current [16]. In terms of iron losses the same derivation as in Chapter 3 can be presented. However, as the iron losses are more dominant in the total losses, the effect of harmonic phase shift could be more pronounced in case of supply voltage distortion.

The mechanical losses, consisting of both friction and windage losses, are mainly determined by the mechanical speed of the machine. For low distortion ratios the speed of LSPMM is fixed by the fundamental supply frequency. Consequently, the mechanical losses are assumed independent of supply voltage distortion.

6.5.3 Additional rotor Joule losses

Although at fundamental frequency practically no rotor Joule losses are induced, if supply harmonics are present, this will induce a significant amount of additional rotor Joule losses. The frequency of the induced harmonic currents in a single rotor bar is coupled to the relative movement of the rotor bar Ω_{m} in reference to the speed of the harmonic current layer Ω_{sh}:

$$\Omega_{\mathrm{sh}} - \Omega_{\mathrm{m}} = (1+6k)\frac{\omega_{\mathrm{s}}}{N_{\mathrm{p}}} - (1-s)\frac{\omega_{\mathrm{s}}}{N_{\mathrm{p}}} = (6k+s)\frac{\omega_{\mathrm{s}}}{N_{\mathrm{p}}} \tag{6.8}$$

According to (6.8) the relative movement of stator harmonic current layers in reference to the rotor speed can be calculated for each individual stator harmonic, consequently, the instantaneous rotor bar current i_r is equal to:

$$i_{r\_k} = \sum_{k=-\infty}^{k=+\infty} \hat{I}_{\mathrm{r\_k}} \sin\left((6k+s)\,\omega_s t + \varphi_h\right) \tag{6.9}$$

Suppose two different stator harmonics k_1 and k_2 result in rotor bar harmonic currents $i_{\mathrm{r\_k1}}$ and $i_{\mathrm{r\_k2}}$. Calculating the rotor bar current RMS value based on (6.9) results in:

$$\begin{aligned} I^2_{\mathrm{r\_RMS}} &= I^2_{\mathrm{r\_k1\_RMS}} + I^2_{\mathrm{r\_k2\_RMS}} + \frac{2.I_{\mathrm{r\_k1\_RMS}}.I_{\mathrm{r\_k2\_RMS}}}{T}. \\ &\int_0^T \cos\left(6(k_1-k_2)\omega t + (\varphi_{k1}-\varphi_{k2})\right) dt. \\ &\int_0^T \cos\left((6(k_1+k_2)+2s)\,\omega t + (\varphi_{k1}+\varphi_{k2})\right) dt \end{aligned} \tag{6.10}$$

Equations (6.9) to (6.10) were already derived in Chapter 4. However in case of LSPMM, due to the synchronous operation, the fundamental rotor current equals zero, as does the slip value s. As s equals zero and if k_1 equals $-k_2$ the third part of the integral in (6.10) differs from zero. Suppose two individual stator harmonics k_1 and k_2 each result in rotor harmonics. If k_1 equals $-k_2$ the induced harmonic rotor currents will be of equal order. With increasing h the magnitude of the harmonic supply voltage distortion will generally reduce [26, 27]. Additionally, the increased frequency and the resulting stator impedance results in additional damping [28], consequently $\hat{I}_{\mathrm{r\_k_2}} < \hat{I}_{\mathrm{r\_k_1}}$.

Based on (6.10) and it can be observed that:

- the presence of the third term in (6.10) indicates that, in order to obtain the rotor bar current, superposition is no longer valid if Ω_{s1} is equal to Ω_{m}.

- as the phase shifts of $i_{\mathrm{r\_k_1}}$ in reference to $i_{\mathrm{r\_k_2}}$, this can result in either an amplification or compensation of the resulting rotor bar current. If the individual harmonic currents are of equal magnitude this implies a doubling or complete cancellation of the harmonic rotor current $I_{\mathrm{r\_k_1\_RMS}}$ of order $6\,|k|$.

- The corresponding harmonic rotor bar losses are equal to the current squared. If $\hat{I}_{\mathrm{r\_k_2}}$ should equal $\hat{I}_{\mathrm{r\_k_1}}$, the harmonic rotor current can double and the losses within this rotor bar would vary with a factor 4.

The latter can be illustrated by Table 6.8. In case of synchronous operation, certain stator harmonics can result in specific interaction due to the absence of slip. In case of synchronous operation, there is interaction between harmonic $h = -5$ and $h = +7$, for $h = -11$ and $h = +13$ etc.

Table 6.8: Stator and corresponding rotor harmonics for IM and LSPMM

k	Stator Harmonic h	Rotor Harmonic	
		IM	LSPMM
0	1	s	0
-1	-5	-6+s	-6
1	7	6+s	6
-2	-11	-12+s	-12
2	13	12+s	12

The previous deduction however neglected the spatial distribution of the rotor bars over the circumference. If a symmetrical rotor construction is assumed, both geometrically and magnetically, the rotor bars are equally spread over the circumference. The relative harmonic phase shift no longer is fixed, but is now also function of the relative position of the rotor bar to the harmonic current layer:

$$i_{r\_k\_N} = \sum_{k=-\infty}^{k=+\infty} \hat{I}_{\mathrm{r\_k}} \sin\left((6k)\,\omega_s t - j\alpha_r + \varphi_h\right) \tag{6.11}$$

with j the specific rotor bar and $j\alpha_r$ the spatial phase shift of the rotor bar over the circumference. α_r can be calculated taking into account the number of pole pairs N_p and the number of rotor bars N_r according to:

$$\alpha_r = \frac{2\pi N_p}{N_r} \tag{6.12}$$

In order to obtain the overall losses current, there should also be an integration over the complete circumference. A similar derivation as 6.10 can be obtained, but now the spacial distribution has been taken into account:

$$P_{\mathrm{loss\_r}} \propto I^2_{\mathrm{r\_k1\_RMS}} + I^2_{\mathrm{r\_k2\_RMS}} + \frac{2.I_{\mathrm{r\_k1\_RMS}}.I_{\mathrm{r\_k2\_RMS}}}{T}. \tag{6.13}$$
$$\sum_{j=0}^{N_r-1} \int_0^T \cos\left((6(k_1+k_2)+2s)\,\omega t - 2j\alpha_r + (\varphi_{k1}+\varphi_{k2})\right) dt$$

In case of a perfect symmetrical rotor, the integration of the circumference results in a fixed value of the RMS current and consequently the interaction of the different harmonics is eliminated. Consequently, the overall rotor Joule loss $P_{\mathrm{loss\_r}}$ can be obtained by:

$$P_{\mathrm{loss\_r}} = \sum_{k=-\infty}^{k=+\infty} I^2_{\mathrm{r\_k\_RMS}}.R_r.K_{\mathrm{rh}} \tag{6.14}$$

However, if the rotor is not symmetrical, either mechanically or magnetically, the induced currents are not identical and this would imply that the total loss is related to $\cos(\varphi_{k_1} + \varphi_{k_2})$. Both the effect of the interaction of the harmonics in specific rotor bars and the cancellation of the effect in case of a symmetrical rotor are simulated in §6.6.1.

6.6 Modeling the interaction of rotor bar induced currents

6.6.1 Using Electric Equivalent Networks in Matlab Simulink

Although the actual operation of the LSPMM differs in reference to standard IM, the mechanisms resulting in harmonic rotor currents are fairly similar in relation to a standard IM. Consequently, a discrete Matlab Simulink 4kW IM model was used to calculate the RMS current in each rotor phase. The parameters used within the simulation are listed in Table 6.9. To simulate synchronous operation the slip s was simply set to zero.

Table 6.9: 4kW IM parm.

Parameter	Value	Unit
R_{s}	1.43	Ω
R_{r}	1.48	Ω
X_{m}	0.15355	H
$X_{\sigma \mathrm{s}}$	0.008	H
$X_{\sigma \_\mathrm{r}}$	0.008	H

In order to estimate the current in a rotor phase, the fifth $k_1 = -1$ and seventh $k_2 = 1$ harmonic voltage were set to equal magnitude of 10% and its relative phase shift $(\varphi_{k2} + \varphi_{k1})$, denoted as γ, was altered. The corresponding waveforms are presented in Figure 6.17.

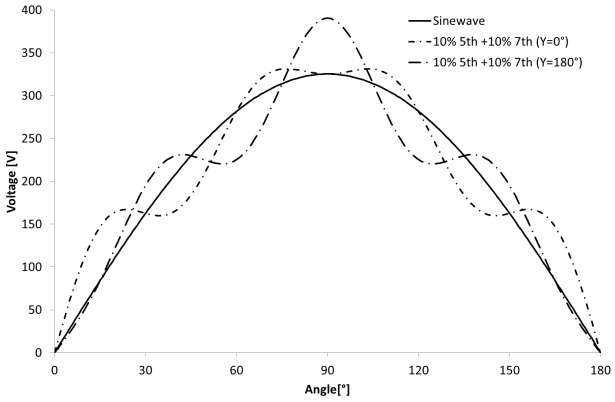

Figure 6.17: Actual waveform supplied to the LSPMM

In Figure 6.18 the slip value was altered from 4% to 0%. A slip of 4% is a common value for nominal operation of a 4kW IM and a slip of 0% indicates synchronous operation, which relates to an LSPMM.

Figure 6.18 validates the assumption that at synchronous operation the fundamental rotor current is equal to zero. Additionally Figure 6.18 confirms (6.10), if the slip value differs from zero, the RMS current in the rotor remains constant, indicating that there is no interaction of the rotor harmonics induced by the stator harmonics h 5 and 7. Consequently, absence of slip results in an interaction of rotor harmonics induced by separate stator harmonics.

In a second simulation, the magnitude of the harmonic components has been altered. The results are plotted in Figure 6.19 and compared to the variation $(1 + \cos(\varphi_{k_2} + \varphi_{k_1}))$ as deduced from (4.41). Although an equal magnitude of harmonic voltage h 5 and 7 has been superimposed on the fundamental voltage,

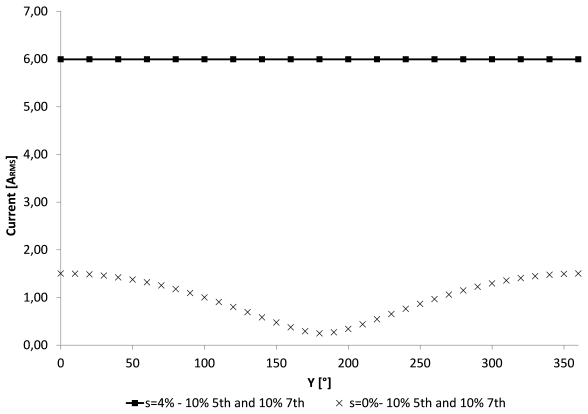

Figure 6.18: The RMS rotor current induced in phase A caused by stator harmonics 5 and 7 and varying γ, for both synchronous and asynchronous operation

the damping caused by the total leakage inductance results in $\hat{I}_{s\_5} > \hat{I}_{s\_7}$. The previous simulations do not result in accurate estimations of rotor bar currents for LSPMM, as will be elucidated in § 6.6.3. Subsequently, only the variation of the rotor current as illustrated in (6.10) is plotted in Figure 6.18. These simulations are merely executed to evaluate the interaction of rotor induced harmonic currents as deduced in § 6.5.3.

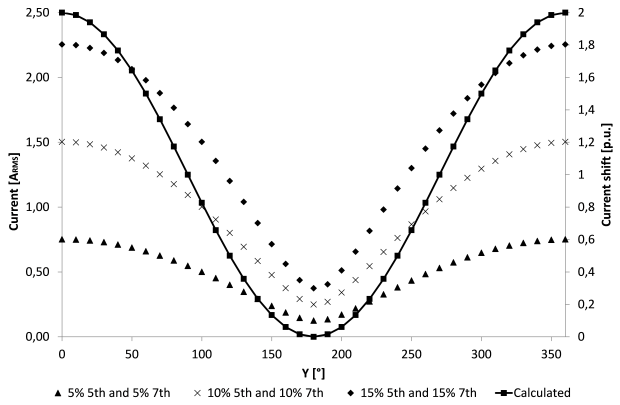

Figure 6.19: Variation of current in phase A of the rotor as a function of the relative phase difference between harmonic 5 and 7 at synchronous operation and for varying harmonic magnitude

As already analytically derived in §6.5.2, if a perfect symmetrical rotor is assumed, the effect of interaction of rotor induced current will cancel out in terms of total loss if the spatial distribution is taken into account. This is clearly illustrated in Figure 6.20. LSPMM are complex machines which have inherent

differences in magnetic reluctance over the rotor circumference, additionally local saturations may arise. Consequently, it can be assumed that the losses vary with $\cos(\varphi_{k_1} + \varphi_{k_2})$. For LSPMMs the linear matlab model will prove to be inadequate to estimate the rotor bar current and the corresponding rotor Joule loss.

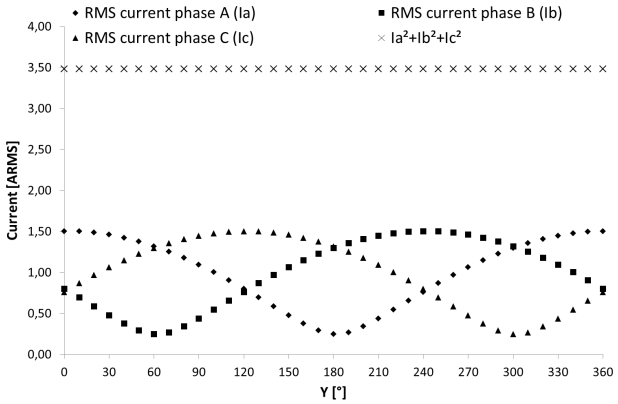

Figure 6.20: Variation of RMS current in rotor phases A, B and C and the squared sum as a function of the relative phase difference between harmonic 5 and 7 at synchronous operation

6.6.2 Using Finite Element Modeling

In Table 6.10 the segregated losses of the LSPMM are listed for both a sine wave and a distorted voltage. The losses are listed for a distortion identical to Figure 6.17 and different values of γ. P_w is measured at 30W and assumed independent of γ.

Table 6.10: Variation of the different losses as a function of γ

		$I_s[A_{RMS}]$	$P_{\mathrm{s}}[W]$	$P_{\mathrm{fe}}[W]$
Sinewave		3.8522	143.9703	67.9879
$\gamma[^\circ]$	30	3.9105	148.3652	71.227
$\gamma[^\circ]$	120	3.9009	147.6368	70.0497
$\gamma[^\circ]$	210	3.9449	150.9836	68.0335
$\gamma[^\circ]$	300	3.9586	152.0352	70.0064
		$P_{\mathrm{r}}[W]$	$P_{\mathrm{loss}}[W]$	η [%]
Sinewave		36.5244	278.4826	0.9304
$\gamma[^\circ]$	30	49.3817	298.9739	0.9253
$\gamma[^\circ]$	120	53.1359	300.8224	0.9248
$\gamma[^\circ]$	210	65.9118	314.9289	0.9213
$\gamma[^\circ]$	300	59.4404	311.4820	0.9221

Based on FEM the simulated segregated losses will be compared to the measurement results presented in § 6.7. The considered LSPMM does not use skewing and consequently this has not been taken in into account. A thorough evaluation of the rotor induced current is presented in § 6.6.3.

6.6.3 Evaluation of the rotor induced current

In §6.6.1 the LSPMM rotor current variation to γ is illustrated using a basic IM model. Although the variation is validated by the measurements in §6.8.3 and confirms the analytical equations from §6.5.3, the IM model is unsuitable to estimate the harmonic LSPMM rotor current and the resulting rotor losses. The errors occur due to two main causes. First and foremost, in case of IM the resulting rotor current is relatively similar between consecutive rotor bars, which simplifies the calculation in case of IM. However, in case of LSPMM the current between consecutive rotor bars differs significantly. This is believed to be caused by local saturations in the rotor resulting in different flux linkages between rotor bars. Local saturation can be noticed at the tips of the PM in Figure 6.2b, and the different rotor bar currents obtained by FEM can be evaluated in Figure 6.21 and Figure 6.22.

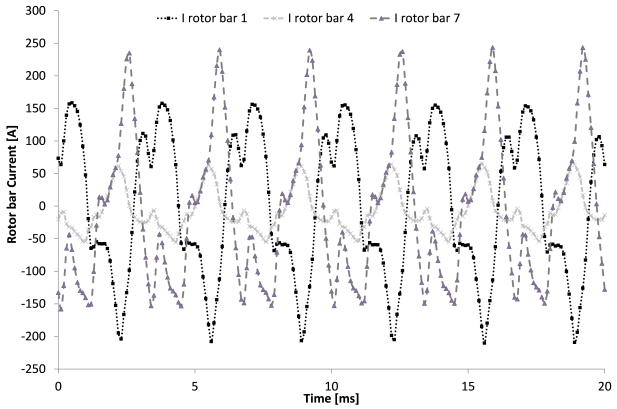

Figure 6.21: LSPMM rotor bar current of bar 1, 4 and 7 obtained by FEM

Consequently, according to (6.14), the resulting rotor losses can be obtained with correct knowledge of the harmonic current, the fundamental rotor resistance and the skin effect. One of the technical drawbacks of LSPMM is the low starting torque. Consequently, LSPMM have an adjusted rotor bar design in respect to IM [29]. As the skin effect is highly affected by the rotor bar geometry [30], straightforward adaptation of skin effect coefficients K_{rh} from IM to estimate the actual rotor losses of LSPMM is invalid. In addition, the induced rotor frequencies are different for an equal h of IM compared to LSPMM.

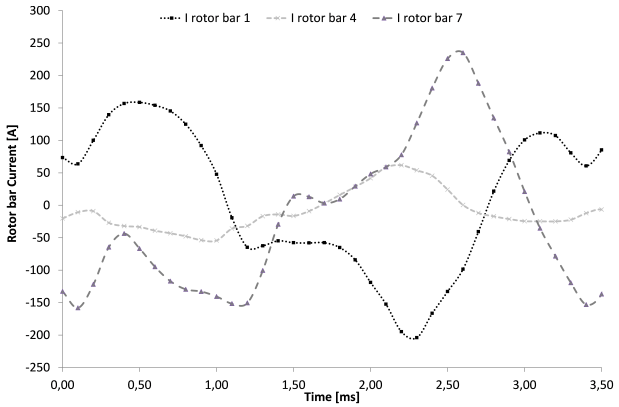

Figure 6.22: LSPMM rotor bar current of bar 1,4 and 7, detail of Figure 6.21

Although Figure 6.18 and Figure 6.19 do not give accurate current values, these graphs are valuable. Figure 6.18 indicates the essence of the parameter s in order to allow superposition of the harmonic rotor bar losses for each stator harmonic h. Figure 6.19 additionally confirms the importance of the leakage induction which results in increased damping for increased h.

6.7 Measuring harmonic losses

6.7.1 The combined temperature and voltage distortion effect

Harmonics in the supply voltage will result in additional losses, however, because the LSPMM uses PM, this machine is also more sensitive to temperature deviations. It has been reported that with increasing temperature, although the stator Joule losses increase, the reduction of the iron losses results in a slight increase of total efficiency. This effect is opposite to the reduction of efficiency due to the harmonic voltage distortion and could have serious consequences if the interaction of harmonic distortion towards the overall energy efficiency is to be evaluated. In a first measurement the combined effect of voltage distortion / thermal effect is evaluated based on measurements. The LSPMM is loaded at nominal load and once thermal equilibrium is achieved, 12% 5^{th} (Y=0°) is added. Several parameters are evaluated, such as the active power and the overall efficiency, the total RMS and fundamental current and finally the PF and the $\cos(\phi)$.

Measurements indicate that initial temperature increase result in a reduction of consumed power. It has proven to be tricky to evaluate the combined

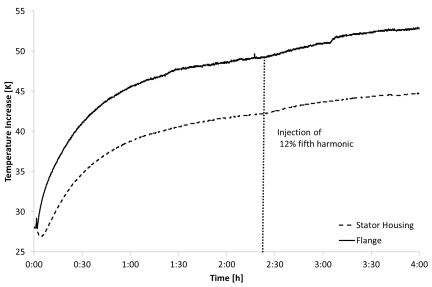

(a) Temperature increase of a 4kW 4-pole LSPMM

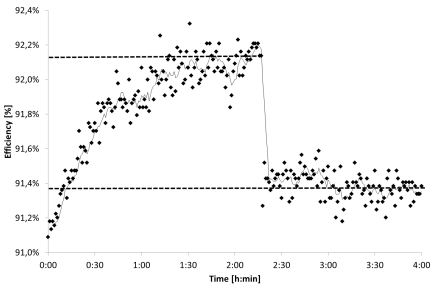

(b) Efficiency in relation to both temperature and supply distortion

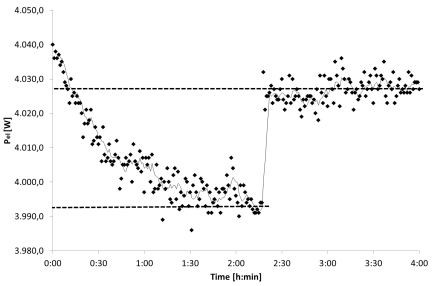

(c) Increase of consumed active power due to supply voltage distortion of a 4kW 4-pole LSPMM

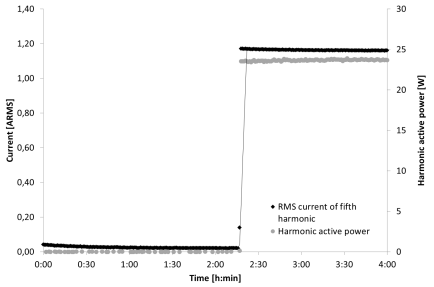

(d) Evaluation of I_{RMS_5} in star equivalent and $P_{\mathrm{h\_el}}$

Figure 6.23: The combined thermal harmonic effect

temperature-voltage distortion. As the measurements span over more than 4 hours, the ambient temperature heated up with approx 10K. For a more thorough evaluation measurements could be repeated in a climate controlled room. However, measurements indicate that the effect of supply voltage distortion can be regarded relatively independent of the temperature effect.

6.7.2 Additional fundamental and harmonic power losses

Measurements also indicated that the evaluation of the harmonic active power $P_{\mathrm{h\_el}}$ is insufficient to evaluate the effect of supply voltage distortion on the overall losses. A $P_{\mathrm{h\_el}}$ of 23W was measured, and the total additional losses $P_{\mathrm{h\_loss}}$ are 33W. As illustrated in Figure 6.24 the addition of harmonic voltage results in a shift of fundamental current. Validation of the parameter $P_{\mathrm{h\_el}}$ would underestimate the total losses linked to supply voltage distortion by approximately 33%. Consequently, the losses evaluation of $P_{\mathrm{h\_el}}$ as set out in Chapter 4 is insufficient for the analysis and the total reduction of power $P_{\mathrm{h\_loss}}$ is to be used. Throughout Chapter 6 only the parameter $P_{\mathrm{h\_loss}}$ is used.

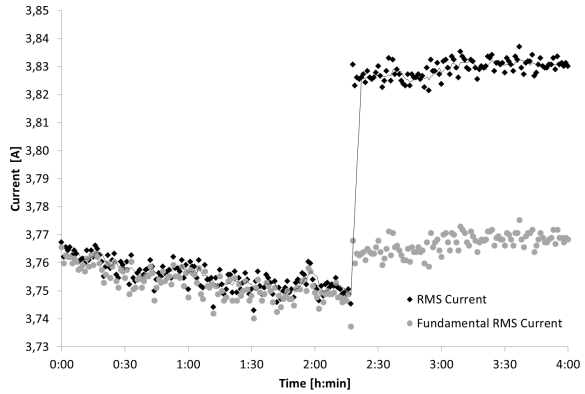

Figure 6.24: Fundamental and RMS stator coil current

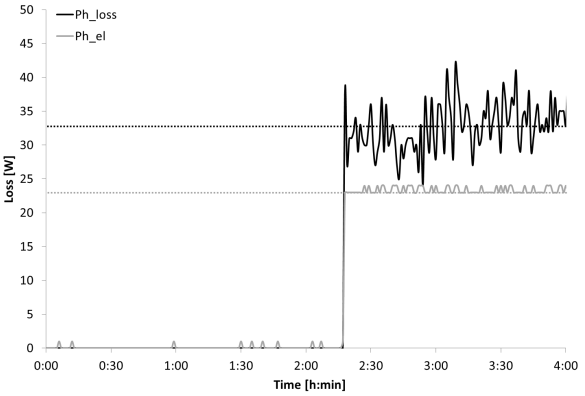

Figure 6.25: The variation of $P_{\mathrm{h\_loss}}$ and $P_{\mathrm{h\_el}}$

In Chapter 2 both the minimal limits as stated in [12] as the accuracy levels of the used equipment in the actual test setup have been listed. Consequently, the measurement error of the different methods to obtain the additional power losses related to harmonic supply voltage distortion can be recalculated. This has been listed in Table. 6.11.

Some harmonic effects are taken out of consideration when evaluating P_{h_el}, however, the measurement accuracy increases with a factor 5 in reference to the evaluation of the parameter P_{h_loss}. Although this parameter proved to be very appealing when evaluating IM, the evaluation of the parameter P_{h_el} is no longer valid for LSPMM. Consequently only the parameter P_{h_loss} should be used.

Table 6.11: Accuracy comparison

Reference	Evaluated parameter	Accuracy
Change of efficiency	$\Delta\eta$	20.8 [W]
Direct Input Power	P_{h_loss}	8 [W]
Harmonic Active Power	P_{h_el}	4 [W]

The reduced measurement accuracy will have consequences in terms of the general evaluation of LSPMM in relation to supply voltage distortion.

6.8 Effect of varying supply voltage conditions

6.8.1 Influence of the harmonic phase angle

If the harmonic phase angle is equal to $0°$, this implies that the averaged voltage is higher. If the averaged voltage is higher, this should result in an increase of iron losses. However, if saturation is taken into account, the reduced flux linkage between stator and rotor could dampen certain harmonic effects. Additionally, the harmonic distortion can also affect the fundamental stator Joule losses. Consequently, the overall effect of the phase angle is determined by the ratio of iron to stator Joule losses and the saturation condition of the machine. As has already been theoretically deduced in Chapter 4, the largest influence related to a harmonic phase shift is linked the lowest order of harmonic distortion with the highest magnitude. Similar to the results presented for an IM, the test results are plotted for 15% fifth harmonic distortion with a shifting phase angle of $0°$ to $180°$.

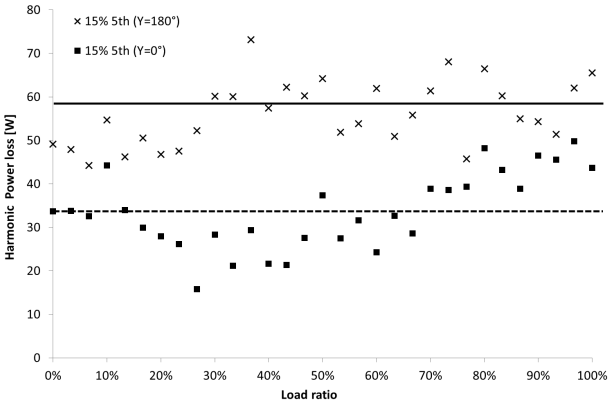

Figure 6.26: Efficiency of LSPMM when supplied with a distorted voltage

As noticeable in Figure 6.26 there is a significant influence on the harmonic phase angle. In this specific case it is noticed that the losses related to harmonics

are higher if the phase angle is 180°, which would indicate that the machine is working in less saturated conditions. Although the iron losses would reduce, the increased flux linkage between stator and rotor would imply higher losses in the rotor.

Initial FEM modeling confirmed that the rotor Joule losses are related to the relative phase angle. In the FEM modeling 10% 5^{th} distortion has been added, and the phase angle has been shifted. In sinewave condition the rotor Joule losses are approximately 26W and these losses are linked to the fundamental SLL. If the distortion is added, for Y=0° the rotor Joule losses are 35.5W and for Y=180° the rotor Joule losses are 38.6W. However, FEM modeling should be extensively expanded before clear and concise conclusions can be presented.

6.8.2 Influence of partial loading and harmonic order and magnitude

In §6.8.1 measurements have been presented in Figure 6.26. In these measurements it is noticed that the losses are not constant in relation to the loading ratio. Although the measurements are executed with the highest level of precision and accuracy, the reduced measurement accuracy makes it incorrect to present any clear conclusion related to the influence of the loading ratio. Therefore the additional harmonic loss have been assumed constant over the load range, and consequently the averaged loss is presented in Table 6.12. Both fifth and seventh distortion is added, the magnitude is raised from 8%, 10% ,12% up to 15% and measurements were executed for a harmonic phase angle of $0°$ and $180°$. During consecutive measurements, the mechanical output power remained unaltered. Consequently, the loss variation can be evaluated based solely on the variation of electrical loss.

Table 6.12: Influence of the harmonic magnitude and order in relation to the averaged $P_{\text{h\_loss}}$

	5^{th}	7^{th}
6% (Y=0°)	19.8	5.4
6% (Y=180°)	12.5	-8.7
8% (Y=0°)	7.2	-0.8
8% (Y=180°)	5.7	1.9
10% (Y=0°)	15.3	-3.2
10% (Y=180°)	26.1	-0.4
12% (Y=0°)	18.9	14.4
12% (Y=180°)	34.1	19.3
15% (Y=0°)	36.1	32.6
15% (Y=180°)	58.3	37.1

In case of a seventh harmonic superimposed on the fundamental, it is observed that for a small amount of supply voltage distortion the harmonic losses become negative. Theoretically this makes no sense, however, the variation is within the measurement accuracy of 16W. It can be assumed that small amounts of seventh distortion ($> 8\%$) generate a small amount of additional losses, but this effect can be neglected. Subsequently measurements of the 11^{th} and the 13^{th} harmonic are not executed as it is assumed that this effect is even less pronounced. Although the variation of efficiency is solely determined by the variation of input power, the absolute efficiency when supplied with a pure sine wave voltage is being presented in Figure 6.27. Efficiency is measured using the direct input-output method and the obtained efficiency is 93,8% which corresponds to manufacturer data [31].

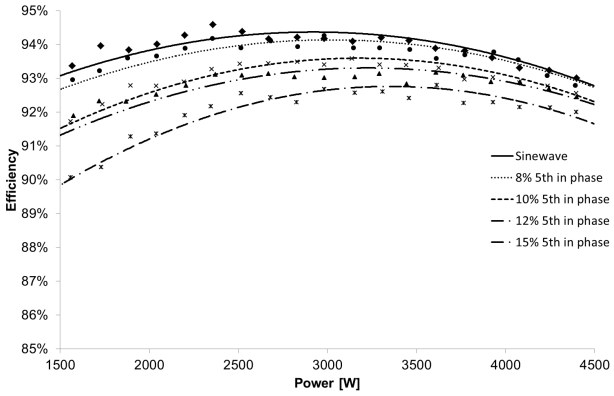

Figure 6.27: Efficiency of LSPMM when supplied with a distorted voltage

Similar trends between fifth and seventh harmonic distortion are noticeable but as already stated, the seventh harmonic content has a reduced influence in reference to the fifth. This is probably related to the additional damping caused by the higher frequencies stator leakage inductance.

6.8.3 Superposition of harmonics: interaction of rotor induced harmonic currents

In order to illustrate the effect of the interaction of harmonic induced rotor bar currents, 4 identical measurements were executed. After the 4kW LSPMM machine reached steady state temperature, the specific losses $P_{\mathrm{loss\_N}}$ occurring at a specific phase shift $(\varphi_{k2} + \varphi_{k1})$ of 10% fifth and seventh harmonic was measured. A total of $N = 12$ measurements were executed in which $(\varphi_{k2} + \varphi_{k1})$ shifted from 0° to 360°. The measurements have been executed at fixed mechanical output power, consequently the loss variation can be evaluated based solely

on the variation of electrical losses. Subsequently, this also indicates that the measurement accuracy is only a function of the used power analyzer. Because the transition to overall efficiency prohibits accurate evaluation of the losses, the variation of the losses are presented in [W] according to:

$$\begin{aligned} P_{\text{loss\_avg}} &= \frac{1}{N} \sum_{(\varphi_{k2}+\varphi_{k1})=0^\circ}^{(\varphi_{k2}+\varphi_{k1})=360^\circ} P_{\text{loss\_N}} \\ \Delta P_{\text{loss}} &= P_{\text{loss\_N}} - P_{\text{loss\_avg}} \end{aligned} \tag{6.15}$$

All the losses $P_{\text{loss\_N}}$ were averaged to $P_{\text{loss\_avg}}$ in order to obtain the averaged losses due to harmonic voltage distortion. The shift in actual losses in reference to the total averaged loss ΔP_{loss} as a function of the relative phase shift (6.15) is presented in Figure 6.28.

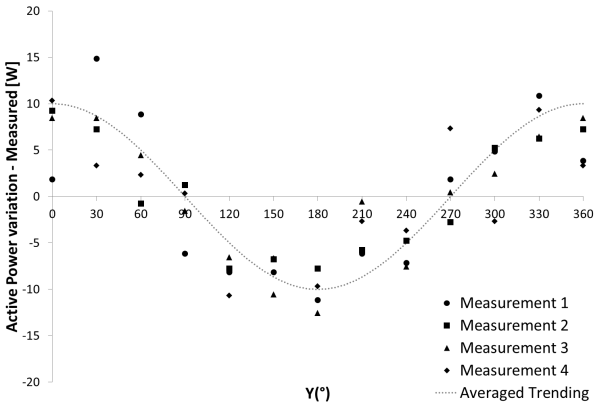

Figure 6.28: Shifting the relative phase shift between harmonic h 5 and 7 and its influence on the overall losses

The variation of the losses caused by the interaction of rotor induced harmonic voltages has been presented in Figure 6.28. The measurements do follow a variation equal to $(1 + \cos(\varphi_{k_2} + \varphi_{k_1}))$. As already stated in §6.8.3, the measurements have been executed at fixed mechanical output power. This implies that the measurement accuracy of the loss variation is only a function of the used power analyzer. The measurement accuracy is 0.1% or 4W, and the losses shift on average a 20W. A shift of 20W relates to approximately 0.5% points of the total efficiency Figure 6.29.

6.8.4 Comparison of FEM vs measurements

All measurements and equations are recalculated towards the star equivalent, however the actual machine was connected and modeled in Δ. This explains the

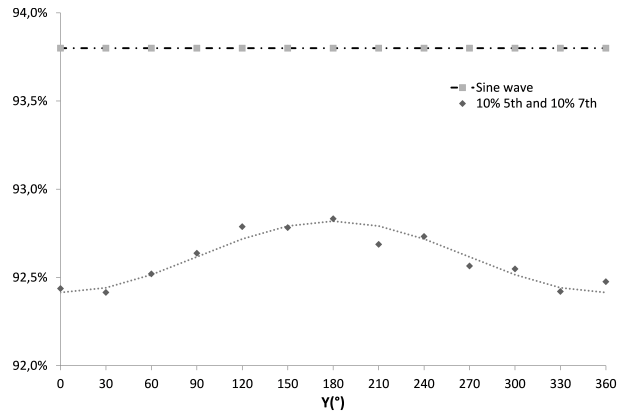

Figure 6.29: Shifting the relative phase shift between harmonic h 5 and 7 and its influence on the overall efficiency

drop of the iron losses obtained in FEM in reference to the fundamental. As the γ shifts, the averaged voltage of shifts 3%. This implies that the peak flux reduces 3%. The FEM simulation does confirm that the iron losses are 4.5% lower. In order to evaluate the iron losses, they were calculated in post FEM using the time domain iron loss model of [19].

Although the values of overall efficiency differ slightly between measurements and simulations, the excess electrical losses can be evaluated decoupled from the mechanical output power. Similar to (6.15), the rotor losses obtained by FEM has been post processed according to (6.16) and plotted against the measurement results.

$$\begin{aligned} P_{\mathrm{r\_avg}} &= \frac{1}{N} \sum_{(\varphi_{k2}+\varphi_{k1})=0^\circ}^{(\varphi_{k2}+\varphi_{k1})=360^\circ} P_{\mathrm{r\_N}} \\ \Delta P_{\mathrm{r}} &= P_{\mathrm{r\_N}} - P_{\mathrm{r\_avg}} \end{aligned} \tag{6.16}$$

A striking coincidence between FEM and measurements is noticeable in Figure 6.30. When evaluating the FEM results, the variation in total losses of 16.0 W is almost entirely caused by the variation in rotor bar losses of 16.5W. The variation in stator Joule losses is limited to about 4.4W and the variation in iron losses to 3.2W. Moreover, the two last loss terms compensate each other to a certain degree, for 0° the iron losses is maximal but the stator Joule losses is minimal.

At pure sine wave conditions, FEM listed in Table 6.10 indicates some rotor losses. FEM confirms that, at sine wave supply conditions, there is no fundamental current induced in the rotor, consequently the obtained rotor losses are equivalent

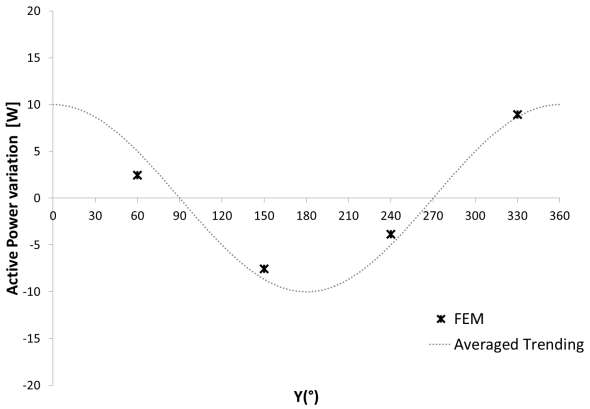

Figure 6.30: Shifting the relative phase shift between harmonic h 5 and 7 and its influence on the overall losses

to the SLL. FEM supports the conclusions from §6.5.2, that:

- the majority of the losses linked to supply voltage distortion are generated within the rotor.
- a small rise of stator Joule losses is noticeable, this is mainly caused by the increase of the stator RMS current.

FEM indicates at 10% fifth and 10% seventh, a maximum reduction of the efficiency with approximately 0.9% points, the measurements indicate a drop of 1.5% points. Comparing efficiencies obtained by the direct measurement method is still delicate, generally due to the inaccuracies in torque transducers and the error in the overall efficiency [5]. Additionally, the spread between measured and simulated efficiency drop can be explained by a number of side effects which take place inside the machine and are not taken into account in FEM, such as the additional temperature effect, the spread in PM remanent magnet flux as given by the manufacturer specifications etc.

6.9 Conclusions

Because segregated loss evaluation of a three phase LSPMM according to IEC60034-2-1 -the indirect method- is prohibited due to technical limitations, FEM has been implemented to address the individual loss mechanisms. All the losses are a function of the temperature, of the implemented permanent magnets and the resulting stator current. As the operating temperature increases, the iron losses reduce and the Joule losses increase. If the decrease of the iron losses is dominant, the overall energy efficiency can increase. This effect has been validated by FEM and is confirmed by measurements. However, before a thorough

evaluation of the temperature effect can be presented, both partial loading and different power ratios of LSPMM should be taken into account. The effect of the temperature rise on the overall efficiency is a function of the relative ratio between the segregated losses. Should the Joule losses become dominant it is possible that the overall efficiency will drop and consequently the conclusion of efficiency increase should not be generalized. The latter is subject of future research.

The main goal of this chapter is to evaluate the effect of supply voltage distortion for an LSPMM. Measurements indicated that this effect can be regarded independently from the temperature effect. Additionally, both measurements and FEM indicate that there is a complex interconnection between separate harmonic components. If the effect of supply voltage distortion is to be evaluated, correct knowledge of both magnitude and phase angle of the present distortion should be taken into consideration. For standard IM, the presence of slip enables simple superposition of the additional rotor losses induced by harmonic supply voltage distortion. However, due to the synchronous operation in combination with the none symmetrical magnetic properties of the rotor superposition is no longer justified for LSPMM.

References

[1] A. De Almeida, F. Ferreira, and J. Fong. *Standards for Efficiency of Electric Motors*. IEEE Ind. App. Magazine, 17(1):12–19, 2011.

[2] *IEC 60034-7 ed2.1 Consol. with am1 : Rotating electrical machines - Part 7: Classification of types of construction, mounting arrangements and terminal box position (IM Code)*, 2001.

[3] R. Krishan. *Permanent Magnet Synchonous and Brushless DC Motor Drives*. CRC Press, 2010.

[4] X. Feng, L. Liu, and Zhang Y. *Super Premium Efficient Line Start-up Permanent Magnet Synchronous Motor*. In 19th Int. Conf. on Electrical Machines (ICEM), pages 1–6, Rome, Italy, 2010.

[5] E. Agamloh. *Induction Motor Efficiency*. IEEE Ind. App. Magazine, 17(6):20–28, 2011.

[6] F. Ferreira and A. De Almeida. *Technical and Economical Considerations on Line-Start PM Motors including the Applicability of the IEC60034-2-1 Standard,*. In 7th Energy Efficiency in Motor Driven Systems (EEMODS'11), Alexandria, USA, 2011.

[7] K. Yamazaki and Y. Haruishi. *Stray Load Loss Analysis of Induction MotorComparison of Measurement Due to IEEE Standard 112 and Direct Calculation by Finite-Element Method*. IEEE Trans. on Ind. App., 40(2):543–549, 2004.

[8] A. De Almeida, F. Ferreira, J. Busch, and P. Angers. *Comparative analysis of IEEE 112-B and IEC 34-2 efficiency testing standards using stray load losses in low-voltage three-phase, cage induction motors*. IEEE Trans. on Ind. App., 38(2):608–614, 2002.

[9] F. Incropera, D. Dewitt, T. Bergman, and A. Lavine. *Fundamentals of Heat and Mass Transfer*. John Wiley&Sons, 6 edition, 2007.

[10] A Gerlando and I. Vistoli. *Improved thermal modeling of induction motors for design purposes*. IEEE Trans. on Energy Con., 15(2):135–142, 2000.

[11] J. Nerg, M. Rilla, and J. Pyrhonen. *Thermal Analysis of Radial-Flux Electrical Machines With a High Power Density*. IEEE Trans. on Ind. Elect., 55(10):3543–3554, 2008.

[12] *IEC 60034-2-1: 2007 (BS EN 60034-2-1) Rotating Electrical Machines-Part 2-1: Standard methods for determining losses and efficiency from tests (excluding machines for traction vehicles).* 2007.

[13] L. Popova, J. Nerg, and J. Pyrhonen. *Combined Electromagnetic and thermal design platform for totally enclosed induction machines*. In Int. Sym. on Diagnostics for Electric Machines, Power Elect. and Drives (SDEMPED), pages 153–158, 2011.

[14] H. Auinger. *Determination and designation of the efficiency of electrical machines*. Power Engineering Journal, 13(1):15–23, 1999.

[15] T. Sebastian. *Temperature effects on torque production and efficiency of PM motors using NdFeB magnets*. IEEE Trans. on Ind. App., 31(2):353–357, 1995.

[16] G. Singh. *A research survey of induction motor operation with non-sinusoidal supply wave forms*. Electric Power Systems Research, 75(23):200–213, 2005.

[17] F. D'Hulster. *Optimisation platform for torque control of 8/6 SRM*. PhD thesis, KU Leuven, 2005.

[18] C. Debruyne, S. Derammelaere, J. Desmet, and L. Vandevelde. *Temperature dependency of the efficiency of Line Start Permanent Magnet Machines*. In 20th Int. Conf. on Electrical Machines (ICEM), 2012, pages 1846–1853, Marseille, France, 2012.

[19] E. Barbisio, F. Fiorillo, and C. Ragusa. *Predicting loss in magnetic steels under arbitrary induction waveform and with minor hysteresis loops*. IEEE Trans. on Magnetics, 40(4):1810–1819, 2004.

[20] P. Sergeant and A. Van den Bossche. *Reducing the permanent magnet content in fractional-slot concentrated-windings permanent magnet synchronous machines*. In 20th Int. Conf. on Electrical Machines (ICEM), 2012, pages 1405–1411, Marseille, France, 2012.

[21] Goudsmit Magnetics. *Permanent Magnets*.

[22] N. Bianchi, D. Durello, and A. Fasolo. *Relationship between rotor losses and size of permanent magnet machines*. In Int. Sym. on Diagnostics for Electric Machines, Power Elect. and Drives (SDEMPED), pages 251–257, 2011.

[23] A. Emadi and J. Andreas. *Energy-efficient electric motors*. Marcel Dekker, New York, 2005.

[24] F. Ferreira, A. De Almeida, and M. Cistelecan. *Voltage Unbalance Impact on the Performance of Line Start Permanent Magnet Synchronous Motors*. In Proceedings 6th Int. Conf. Energy Efficiency in Motor Driven Systems (EEMODS '09), pages 123–137, Nantes, 2009.

[25] I. Boldea. *The Electric Generators Handbook ' Synchrounous Generators'*. Taylor & Francis Group, 2006.

[26] *EN50160: Voltage Characteristics of electricity supplied by public electricity networks*, 2010.

[27] S. Bhattacharyya, S. Cobben, P. Ribeiro, and W. Kling. *Harmonic emission limits and responsibilities at a point of connection*. IET: Generation, Transmission Distribution, 6(3):256–264, 2012.

[28] P. Cummings. *Estimating Effect of System Harmonics on Losses and Temperature Rise of Squirrel-Cage Motors*. IEEE Trans. on Ind. App., 22(6):1121–1126, 1986.

[29] A. Aliabad, M. Mirsalim, and N. Ershad. *Line-Start Permanent-Magnet Motors: Significant Improvements in Starting Torque, Synchronization, and Steady-State Performance*. IEEE Trans. on Magnetics, 46(12):4066–4072.

[30] F. Ferreira, A. De Almeida, W. Deprez, R. Belmans, and G. Baoming. *Impact of steady-state voltage supply anomalies on three-phase squirrel-cage induction motors*. In Int. Aegean Conf. on Electrical Machines and Power Electronics, ACEMP '07., pages 607–615, 2007.

[31] *WQuatro motordata -0.55-7.5 kW*.

7 Conclusions

7.1 End-user voltage distortion

Chapter 3 ends with some essential conclusions. First of all a maximal limit has been obtained of the supply voltage distortion at end-user. To the author's knowledge no such limit has yet been presented. This upper limit is subsequently used throughout Chapters 4, 5 and 6. Additionally, the research suggested summation rules of background distortion and internally generated distortion. This would also imply that, based on two measurements, one at POC and one at end-user, the internally generated distortion can roughly be estimated. Chapter 3 also illustrates the positive influence of Shunt Harmonic Active Filters on the end-user voltage quality. If the internally generated distortion can be segregated from the background distortion, this could also result in on-site estimations concerning the effect of integrating active filters on end-user voltage quality.

The phase angle of the supply voltage distortion is often neglected, and simplified Power Quality parameters such as the THD, HD, HVF, Form Factor or Crest Factor do not take the effect of both the order and phase angle into account. Although Chapter 4 validates that the harmonic phase angle has no significant influence in IM motor operation, the results in Chapters 5 and Chapter 6 indicate that the harmonic phase angle is essential in evaluating the effect of supply voltage distortion on IG or LSPMM. Consequently, Chapter 3 presents detailed information concerning the harmonic phase angle at end-user.

A large amount of the results of Chapter 3 have been simulated using a simple

resistive model of a low voltage cable. However, at increased frequency the inductance and capacitance of the cable could affect the overall supply voltage distortion. The combination of inductance and capacitance could result in either amplification, damping or even resonance effects due to harmonic supply voltage distortion. More detailed PI- or T-models of cables can be used. However, this has not been executed in this research because of 2 reasons. First of all, the effect of distortion on machines is inversely proportional to the frequency. So low frequent distortions are more interesting. Secondly, the parameters inductance and capacitance of LV cables are hard to estimate because practical lay-out of these cables highly affect the values.

Although this chapter presents the effects of active filters, the effect of filtering current harmonics in relation to the resulting voltage distortion is largely depending on the physical location of the filer inside the installation. Future research could evaluate the effect of the location of integrating a filter on the resulting end-user voltage quality. A second suggested topic of interest is filtering to achieve maximum voltage quality at end-user. The current filter designs generally are controlled to minimize current harmonics. However, active filters are technically perfectly capable to inject more harmonics to increase end-user voltage quality. This control strategy is not without any consequence for the upstream network, as harmonics are now injected by the filter.

If Shunt Harmonic Active Filters are implemented, the reduction of the supply voltage distortion to DOL machines could also positively affect machine efficiency and consequently reduce the overall energy consumption. However, this straightforward assumption should be evaluated more delicately. The shift in $\mathrm{THD_U}$ in compensated and non-compensated situation can originate from both a reduction of the harmonic content and from an increase of fundamental RMS voltage. The voltage rise could also result in an increased total power consumption, even at an increased efficiency. The previous shows that the impact of SHAF on the energy efficiency of DOL machines is function of the reduced harmonic losses in relation to the increased fundamental power consumption. The latter is in turn function of the increase in fundamental voltage and the speed-torque characteristic of the load. The influence of the harmonic voltage distortion on DOL IM efficiency is evaluated in Chapter 4.

7.2 The effect of harmonic voltage distortion on IM

Literature review indicated that there is still a research gap concerning how to accurately measure the effect of supply voltage on IM. One of the major contributions of this research is introducing the parameter "harmonic active power" $P_{\mathrm{h\_el}}$. Although this parameter does not fully cover the additional losses

due to supply voltage harmonics, this parameter can be easily measured and calculated according to:

$$P_{\mathrm{h\_el}} = \sum_{h=3,5,7\ldots}^{\infty} U_{\mathrm{RMS\_h}}.I_{\mathrm{RMS\_h}} \cos(\varphi_h) \tag{7.1}$$

The use of this parameter has been validated by measurements and consequently this parameter has been used to evaluate the effect of the supply voltage quality on IM. Several parameters specifically related to the supply voltage distortion such as the harmonic phase angle, harmonic order and harmonic magnitude have been addressed. As is the influence of more machine related parameters tested such as loading ratio, building size and efficiency rating.

Some parameters have not yet been taken into account. For example the fundamental supply frequency is assumed 50Hz, because this research is focused towards European DOL machines. However, similar effects occur at a fundamental supply frequency of 60Hz, which is typical for North-American power grids. The number of pole pairs has also been excluded form the research, although it can be assumed that the number of pole pairs has some minor influence on the overall susceptibility towards harmonics.

The harmonic modeling concept has been elucidated and one of the major constraints of this modeling is that saturation is neglected. This constraint has been validated by measurements. Directly linked to the harmonic modeling are the derating methods of IM towards supply voltage distortion. A generalized conclusion is that for high efficient machines, the harmonic losses are generally limited. The additional losses also increase the machine's operating temperature. This temperature rise has been validated for a 4kW IM by Lumped Thermal Modeling and this validated that, due to supply voltage distortion, the temperature can increase approximately 2 degrees. For small IMs the overall effect of supply voltage distortion can be important, however, from an industrial point of view both the harmonic losses and the additional thermal stress are generally within acceptable margins. These acceptable margins are: the additional power losses are limited to less than 1.5% -which lays within efficiency measurement accuracy- and the additional thermal stress does not exceed the maximal thermal limits as suggested in IEC 60085.

This chapter mainly focuses on theoretical deductions and validation by measurement. Although measurements are very valuable, a segregated loss evaluation of both $P_{\mathrm{h\_el}}$ and $P_{\mathrm{h\_loss}}$ could be presented based on FEM. Literature study failed to find any study concerning the interaction of voltage distortion with IMs which implements FEM to accurately address the additional losses. The

presented research assumed balanced harmonic conditions, although unbalance is also possible at higher frequencies. This has not been evaluated and should be of interest. A lot of research has already been presented concerning voltage unbalance [1] and its impact on operation of IM. The interaction of both distortion and unbalance on the overall energy efficiency of IM has been addressed in [2].

The goal of Chapter 4 has been to evaluate the effect of the supply voltage distortion on the overall energy efficiency and the related additional thermal stress. This has been executed from the concept that approximately 16% of al IM faillure is linked to stator insulation faillure and thus generally linked to excessive stator temperatures. This research presents the additional temperature rise caused by supply voltage distortion. Initially the study could have integrated Computational Fluid Dynamics or other numerical heat flow techniques, however, simple LTM already illustrated that the temperature rise effect is marginal. However, if an accurate thermal evaluation is to be presented hot spot temperatures should be taken into account. The simplified LTM is in this case no longer valid and a combination of FEM/CFD could result in hot spot estimations.

This study indicates that there is a torque ripple due to harmonic interaction. In terms of efficiency this ripple is irrelevant. However these additional torque ripples could result in additional bearing stress. It could be interesting to try to relate premature bearing failure to supply voltage distortion. Again, FEM could prove to be an accurate analysis tool.

7.3 The effect of harmonic voltage distortion on IG

Similar to induction motor operation are IGs susceptible to supply voltage distortion. However, generator operation has highly increased the difficulty as:

- measurements of efficiency in generator mode are more complex because the power source has to able to simultaneously deliver harmonic power and dissipate fundamental power.

- measurements of efficiency in generator mode are less accurate as a variation in both electrical and mechanical power has to be evaluated.

- the basis on which parameter the comparison of efficiency is to be established. Nearly every parameter can be argued, but finally it is concluded to evaluate generator susceptibility based on the electric output power. As harmonics are introduced P_{RMS} no longer equals $P_{\mathrm{RMS\_1}}$, additionally increasing difficulty.

- in order to avoid discussion the use of the parameter $P_{\mathrm{h\_el}}$ is also suggested and evaluated for IG evaluation. However, before this parameter can be used, both the concept and origin of this power is to be clarified.

Because IGs are the same machine and operate by the same fundamental principles, the harmonic modeling concept of IM is evaluated in reference to generator operation. From a first simple point of view, the increased rotor frequency for harmonics with inverse rotation would result in an increased harmonic current and increased skin effect, resulting in an increase of harmonic losses. However, the harmonic modeling concept eliminates the saturation effect and measurements presented in Chapter 5 illustrated that this simplification is no longer valid. By shifting the harmonic phase angle the machine can operate in different saturated conditions. Increased saturated operation results in a decrease of the consumed harmonic power and is beneficial in terms of excess harmonic losses. As the concept of harmonic phase angles is of significant importance, the basic modeling as suggested in Chapter 4 is no longer valid.

The harmonic phase angle has a dominant effect in generator. Consequently both effect of the supply voltage quality and the influence of IG machine parameters is evaluated. Additionally motor and generator mode are compared for the same machine, and machines are tested which are specifically designed towards IG mode. Similar to motor operation is the additional temperature rise validated in case of generator operation. Similar conclusions can be presented as is Chapter 4.

Although the presented research takes initial steps concerning the energy efficiency of induction generators linked to supply voltage distortion, the presented research does fail to address several points of interest. First of all, it would be interesting to obtain an analytical model to estimate the influence of harmonic distortion on IG systems. Measurements indicate that a simple linear model as suggested for motor operation is insufficient to estimate the effect of harmonics on the supply voltage distortion. One of the future topics of interest should be to try to obtain a non linear model which is capable to estimate the harmonic active power losses with relatively high accuracy in case of IG.

However, before any accurate harmonic model of an induction generators can be integrated, a detailed segregated loss evaluation in case of supply voltage distortion is needed. Especially the segregation between stator and rotor Joule losses and possible additional iron losses should be obtained. Although the stator Joule losses can be segregated, this still fails to accurately obtain both iron and rotor Joule losses. Additionally the skin effect at generator mode should be addressed more accurately. FEM modeling could answer a large amount of the questions. However, in FEM one of the constraints is the mechanical output

power. If the equal electrical criteria from this study is used, this would largely increase FEM difficulty. Iterative solvers could partially solve this problem, but this would largely increase computational efforts.

Besides the absence of a more detailed segregated loss analysis and the failure to present harmonic modeling, the presented research focuses solely towards grid connected IG. However, if the magnetization is delivered from capacitors, IGs can also deliver power in island operation. This is often done in gensets for emergency or backup purposes, supplying electricity in remote regions or for example in large ocean liners. Local electricity generators are often preferred for small isolated grids for remote regions as it is still economically beneficial in some cases to deliver oil derivatives instead of the huge investment costs linked to grid connected electrical distribution. A similar situation can occur with the emergence of local smart grids, which link renewable and classic back up power. Due the anticipated rise of IG systems in island operation, it would be highly interesting to evaluate the behavior of IG systems which are directly connected to non-linear loads specifically in island situation.

7.4 The effect of harmonic voltage distortion on LSPMM

The Line Start Permanent Magnet machine is often pushed as the high efficiency competitor in reference to IM. Chapter 6 not only presents a rigorous fundamental loss segregation of an LSPMM, it evaluates the effect of supply voltage distortion on LSPMM. In Chapters 4 and 5 the parameter $P_{\mathrm{h\_el}}$ proved to be very efficient in terms of evaluating the total harmonic losses. However, research presented in Chapter 6 illustrated that the use of parameter $P_{\mathrm{h\_el}}$ is no longer valid in terms of the overall losses induced by supply voltage harmonics. Consequently, the additional losses are obtained fairly similar to IEC600034-2-3:

$$P_h = P_0 - P_{0,1} \tag{7.2}$$

The reason to discard $P_{\mathrm{h\_el}}$ is related to the interaction of supply voltage distortion onto the fundamental current. As the fundamental current is altered significantly, the parameter $P_{\mathrm{RMS\_1}}$ no longer stays constant if harmonics are superimposed. Additional to the pitfalls in extrapolating the measurement procedures of Chapter 4 and 5, there are some additional technical limitations which prohibit translation of the harmonic modeling concepts of IM towards LSPMM.

- The temperature increase can result in an slight increase of efficiency. This is effect has been validated by measurements and FEM simulations, which

indicated that although the stator Joule losses increase, there is a significant decrease of iron losses which results in a general decrease of the losses. Although other sources already confirmed this effect [3], this effect should not yet be extrapolated to every PM machine as this effect is highly function of the loss ratio of the individual losses.

- The synchronous operation does present a very specific interaction of the rotor induced harmonic currents. This effect is caused by the absence of slip and asymmetrical non linearities, which results in discard of the superposition principle as suggested in Chapter 4.

Although the concepts of rotor induced currents and the effect of harmonic phase angles is generally valid for nearly any type of synchronous machine, there is a wide variety of rotor designs available. One of the major technical drawbacks of an LSPMM is the relatively low starting torque due to the combination of a synchronous and an asynchronous torque. This is often compensated by specific rotor bar design. As illustrated in Chapter 4 is the specific rotor and rotor bar design of the utmost importance in relation to its susceptibility towards the skin effect and the overall rotor Joule losses. In this research only one machine from one power rating has been evaluated. In order to accurately validate the effects of supply voltage distortion, a large amount of extra testing should be performed in order to present generalized conclusions.

As linear harmonic modeling already seems impossible for IG, this is specifically the case for LSPMM. The interaction of rotor induced harmonic currents, combined with the high effect of the harmonic phase angle on the resulting RMS current, prohibit simple superposition methods to recalculate the energy efficiency of LSPMM in case of supply voltage distortion. The LSPMM is also a perfect candidate for generator use, as this machine is self exciting, no additional start up methods are required. Although the effect of rotor induced harmonic currents will remain, the reversed stator voltage drop can additionally affect the machine's sensitivity towards supply voltage distortion. No measurements have been executed yet concerning this topic.

7.5 Future research

The author would like to end this dissertation on a more personal note. A lot of research has been executed on increasing the energy efficiency of machines. Consequently, there is now a new regulation which imposes certain efficiency levels for certain machines. The regulation 640/2009/EC requires machines on the market to be of IE3 for 7.5 to 375kW IM or IE2 for converter fed machines from 1/1/2015. However, if the energy efficiency is to be evaluated one should evaluate the complete power train from input to desired output. The desired output is a

certain airflow for fans or a mechanical displacement of products. Although the efficiency of electromechanical energy conversion is performed with relatively high accuracy, a lot of energy saving is achievable downstream. Gearboxes and fan efficiency could be increased. Although VSDs inversely affect the energy efficiency of the IM, the implementation of VSDs does largely increase the overall energy efficiency. Focus should be placed on the overall energy efficiency of processes, rather than focusing on quick patching of individual components.

To the authors delight this trend is now noticed by the industry and legislations. This new type of energy saving is introduced as "'The Extended Product Approach"', which is a way of capturing the motor-system energy savings by regulating the entire motor driven product, for example the pump, motor, transmission and controls of a pumpset. Initial steps are placed by introducing the EN 50598. *The EN 50598 provides the general requirements to energy efficiency standardization for any extended product by using the guidance of the extended product approach (EPA). It enables product committees for driven equipment with embedded motor systems (so called extended products) to interface with the relative power losses of the embedded motor system in order to calculate the system energy efficiency for the whole application.*

References

[1] W Deprez. *Energy efficiency of the induction machines: a critical assessment*. PhD thesis, KU Leuven, 2008.

[2] F. Ferreira, A. de Almeida, W. Deprez, R. Belmans, and G. Baoming. *Impact of steady-state voltage supply anomalies on three-phase squirrel-cage induction motors*. In International Aegean Conference on Electrical Machines and Power Electronics, 2007. ACEMP '07., pages 607–615, Bodrum, Turkey, 2007.

[3] J. Schutzhold and W. Hofmann. *Analysis of the temperature dependence of losses in electrical machines*. In 2013 IEEE Energy Conversion Congress and Exposition (ECCE), pages 3159–3165, Denver, U.S.A., 2013.

A

Measurement error calculations

A.1 Measurement of electrical power

Electrical power is measured by a calibrated[1] Voltech PM3000A Power Analyzer. Calculation of measurement accuracy of the electric input power is done as set out by the specifications of the manufacturer of the Power Analyser [2].

$$
\begin{aligned}
V_{\mathrm{err}} &= \pm 0.1\%\mathrm{read} \pm 0.05\%\mathrm{range} \pm 0.5\mathrm{mV} \\
A_{\mathrm{err}} &= \pm 0.1\%\mathrm{read} \pm 0.05\%\mathrm{range} \pm 100\mu A \\
P_{\mathrm{err}} &= \pm(A_{\mathrm{read}}.V_{\mathrm{err}}.PF) \pm (V_{\mathrm{read}}.A_{\mathrm{err}}.PF) \pm (0.04/PF)\%_{\mathrm{reading}} \pm 100\mu W
\end{aligned}
\tag{A.1}
$$

For the measurements of the 4kW IM, the accuracy of the measured electrical power is 0.1%. In case of the 55kW IM, the line current was $\pm$ 94.5 $\mathrm{A_{RMS}}$, this implies that additional current transformers (CT) are needed. These CT's have a reduced accuracy, in comparison with the internal shunts, of 0.5% full scale [3]. In case of measurement of the 55kW machines, the power analyser accuracy is calculated by A.1,and is 0.1%.

[1] Stork Intermes N.V. Kalibratiecertificaat 0802-05957
[2] Manual Voltech PM3000ACE , VPN98-051/10, version 10: pg 11-1 & 11-2
[3] Chauvin Arnoux, certificate of verification 103 319 UAS

A.2 Measurement of mechanical power

A.2.1 Measurement of torque

In order to evaluate the total amount of mechanical power both the mechanical torque and speed should be measured. The calculations presented in this appendix will point out that the main cause of error in relation to the mechanical power is measuring the torque accurately. Measuring the speed is often far less critical. In this dissertation torque measurements have been executed with a Lorenz Messtechnik DR2212R. However, in order to obtain an actual value of torque, the signal should be converted to a display [4]. The overall error is composed of these two errors. Based on Table A.1, the absolute error of the torque sensor is 0.2Nm, the error of the process meter is 0.005V. As a signal of 5V relates to a signal of 200Nm, the process meter additionally adds an error of 0.2Nm. The reading accuracy on the digital display is limited to one digit, and this corresponds to 0.01Nm. This corresponds to an absolute measurement accuracy of 0.4Nm.

Table A.1: Measurement of mechanical power

Equipment	Full Scale	Accuracy	Absolute error
Torque measurement	$\pm$200Nm	$\leq$0,1% FS	$\leq$0,2Nm
Analog to digital conversion	$\pm$5.000V	$\pm$0,1% FS $\pm$ 1 digit	0,005V $\pm$ 1dgt

Although the measurement accuracy is only 1.6% for a 4kW 4-pole IM, a lot of the presented research does not evaluate the actual output torque, but rather evaluated the variation of mechanical power. If the variation of torque is evaluated, one should take the factor repeatability into account which is 0.02% [Figure A.2].

Additional to the actual measurement accuracy is the temperature of the equipment is of extreme importance. As can be evaluated from [Figure A.2] does the variation of operation temperature results in 2 effects which influence the output of the torque meter. An offset is generated which can result in a shift of measured output torque, and additionally the sensitivity of the measurement device is altered. In order to try to compensate for these effects, the temperature of the torque measurement was monitored and served as an input for a simple spreadsheet which compensated for the additional temperature.

Note that the accuracy can be drastically increased by applying a smaller torque sensor. For the same error Full Scale, does the smaller range imply more accurate torque measurements. However, torque meters are very sensitive to excessive torques. For an IM the maximum torque is approximatly 2.5 times

[4] Omron-K3MA-J

TECHNISCHE DATEN - *SPECIFICATIONS*

Typ - *Type*		**DR-2212 (DR-2212-R)**	**DR-2512 (DR-2512-R)**
Genauigkeitsklasse - *Accuracy class*	% v. E. - *f. s.*	0,1 (0,2)	
Reproduzierbarkeit - *Repeatability* (DIN 1319)	%	±0,02 (±0,04)	
Versorgung - *Excitation voltage*	V DC	12 ... 28	
Stromaufnahme - *Current consumption*	mA	<60	
Ausgangssignal - *Output signal*		0 ... ±5 V	±25000 digits
Belastbarkeit - *Output current max.*	mA	5 kurzschlussfest *Short circuit resist.*	
Eingang Kontrollaufschaltung - *Calibration control*	V	L <2,0; H >3,5	per Software
Messrate - *Sample rate*	kSample	10	5
Referenztemperatur - *Reference temperature*	°C	+23	
Nenntemperaturbereich - *Nominal temperature range*	°C	+5 ... +45	
Gebrauchstemperaturbereich - *Service temperature range*	°C	0 ... +60	
Lagerungstemperaturbereich - *Storage temperature range*	°C	-10 ... +70	
Temp. koeff. des Kennwertes - *Temp. coeff. of sensitivity*	% v. E./K - *f. s./K*	±0,01 (±0,015)	
Temp. koeff. des Nullsignals - *Temp. coeff. of zero signal*	% v. E./K - *f. s./K*	±0,02 (±0,03)	
Gebrauchsdrehmoment (statisch) - *Service torque (static)*	% v. E. - *f. s.*	150	
Grenzdrehmoment (statisch) - *Limit torque (static)*	% v. E. - *f. s.*	200	
Bruchdrehmoment (statisch) - *Ultimate torque (static)*	% v. E. - *f. s.*	>300	
Schwingbreite - *Bandwidth* (DIN 50100)	%	70 (Spitze - Spitze) - *(peak - peak)*	
Schutzart - *Level of protection* (DIN EN 60529)		IP50	
Elektrischer Anschluss - *Electrical connection*		12-polig Serie 581 - *12-pin series 581*	

Figure A.1: Technical data of the torque measurement equipement

the nominal torque[5]. As also an 11kW 4-pole machine has been evaluated, this implies a maximum torque of 175Nm. This explains why a torque sensor of 200Nm has been chosen for the setup.

In case of the 55kW machines the torque has been measured by an internally calibrated torque sensor[6]. The calibration was executed by applying calibrated weights to a fixed leveler length. After calibration the error is less than 0.1%.

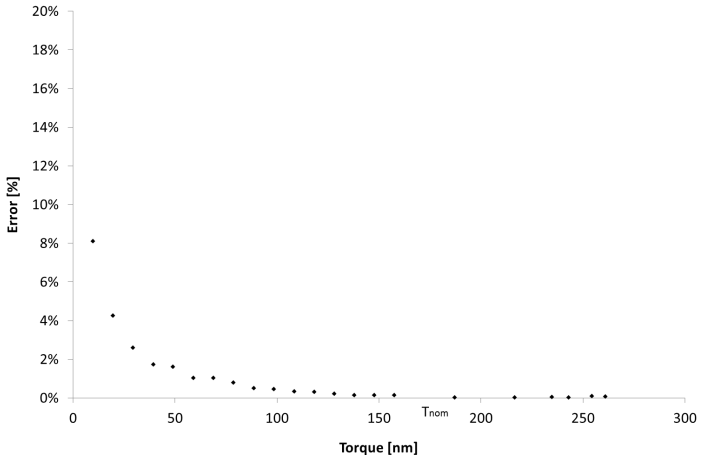

Figure A.2: Torque measurement error of the 55kW IM after internal calibration

[5]Jan A Melkebeek. Electrische Aandrijftechniek: Course presented at the Ghent University, Faculty of Applied Sciences(in Dutch), 2010.

[6]Torque transmitter TE110.2 SN 428

A.2.2 Measurement of speed

Speed can be measured by applying an speed measurement equipment (such as a tacho generator, a resolver or encoder), however in the small test setup the torque meter had the possibility to additionally obtain the speed. The measurement device uses a encoder with according data: Speed/angle D-W, =1000 Nm, 360 imp/rev, TTL-level 2 traces 90 °. The measurement scale is 7000RPM, with an accuracy of 0.1% A frequency counter is used to obtain the speed in RPM which limits the accuracy to 1 digit. For the 55kW 2-pole machines, the speed has been measured using a tacho generator[7]. The readout has been calibrated by means of an external calibrated speed measurement[8]. The obtained error within the full range of 0 to 3100 rpm is is within 1 rpm. Consequently the error on the speed is less than 0.03%.

A.3 Measurement of efficiency

As already stated a simple spreadsheet has been developed. Accordingly the overall measurement accuracy of the efficiency can be plotted for different types of speed and power ratio's. As both a 4-pole 4kW and a 4-pole 11kW IM have been used, the efficiency accuracy obtained by the direct measurement is plotted in Figure A.3.

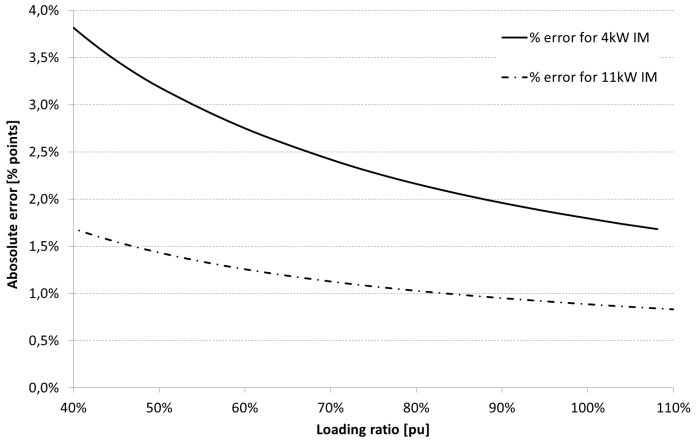

Figure A.3: Measurement error for a 4-pole 4kW IM and a 4-pole 11kW IM

However, the presented research is trying to evaluate the additional loss caused by supply voltage distortion. Although the measurement accuracy is 1.6% according to TableA.2 the differential accuracy of the torque is 0.02% or in terms

[7]Radio-energy:dynamo tachymetrique REo 444R1 sn 3003395
[8]Monarch RPM-603883-3390 NIST traceable

of overall mechanical power: 0.16%. By evaluating the differential torque and consequently output power, the measurement accuracy is largely increased. In Table.A.2 the absolute measurement error for the additional loss is presented for the different measurement procedures.

Table A.2: Accuracy comparison for different measurement methods for a 4-pole 4kW machine

Reference	Evaluated parameter	Accuracy
Differential Active Power	P_{h_loss}	20.8 [W]
IEC 60034-2-3	P_{h_loss}	8 [W]
Harmonic Active Power	P_{h_el}	4 [W]

As noticeable in Table.A.2 is the obtained measurement accuracy still very low in relation to the effects which are to be evaluated. In Chapter 4 a new measurement procedure has been suggested which roughly related to the IEC60034-2-3. Although some harmonic effects are taken out of consideration, the measurement accuracy increases with a factor 5. The increased measurement accuracy highly outweighs the abstraction of minor harmonic effects

A.4 Comparison of power source output distortion

As already stated in the main introduction, two different power sources have been used. Because the two sources operate on different operating principles, the output spectrum of these two sources is compared. At a pure 50Hz output voltage, the switching frequency of the 15kW PWM inverter should either be high enough ($\geq$ 2kHz) or the low pass band filter should adequately filter all the switching harmonics. As is confirmed by both Figure A.4 and Figure A.5, the distortion presented in the supply voltage due to its operating principle is negligible in the range up to 4kHz.

Figure A.4: Output spectrum of the used power sources [0-h=99] [DC-4kHz]

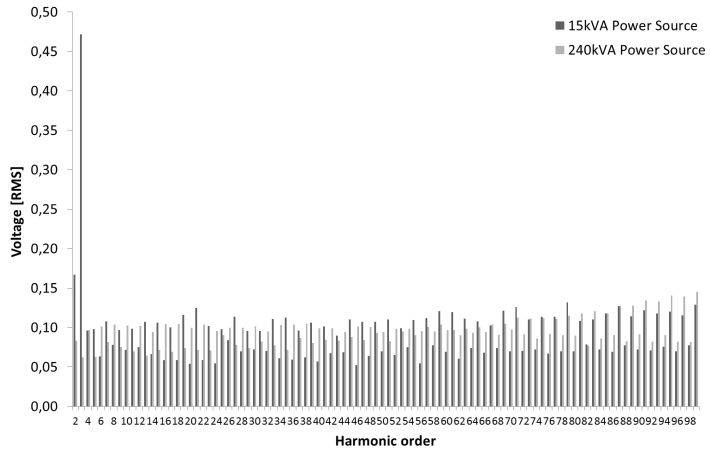

Figure A.5: Output spectrum of the used power sources, excluding the fundamental [h=2-99][100Hz-4kHz]

B

Publication list Colin Debruyne

[1] C. Debruyne, M. Polikarpova, S. Derammelaere, P. Sergeant, J. Pyrhonen, J. Desmet, and L. Vandevelde. *Evaluation of the efficiency of Line Start Permanent Magnet Machines as function of the operating temperature*. IEEE Transactions on Industrial Electronics, 2013.

[2] C. Debruyne, P. Sergeant, S. Derammelaere, J. Desmet, and L. Vandevelde. *Influence of Supply Voltage Distortion on the Energy Efficiency of Line Start Permanent Magnet Motors*. IEEE Transactions on Industry Applications, 2013.

[3] C. Debruyne, L. Vandevelde, and J. Desmet. *Harmonic effects on induction and line start permanent magnet machines*. In Proceedings 8th International Conference on Energy Efficiency in Motor Driven Systems. (EEMODS'13), 28-30 Oct. 2013,Rio de Janeiro, Brasil.

[4] C. Debruyne, S. Derammelaere, J. Desmet, and L. Vandevelde. *Rotor induced harmonic voltages caused by supply voltage distortion, the interaction and its influence on the overall energy efficiency of line start permanent magnet machines*. In Proceedings of the 2013 International Electric Machines & Drives Conference, pages 1097–1012. IEEE Ind. Electron. Soc., 2013. (IEMDC 2013), 12-15 May 2013, Chicago, IL, USA.

[5] J. Desmet, B. Verhelst, L. Vandevelde, and C. Debruyne. *Test field for LV distribution systems*. In 22nd International Conference and Exhibition on

Electricity Distribution, page 1015 (4 pp.), 2013. (CIRED 2013), 10-13 June 2013, Stockholm, Sweden.

[6] B. Verhelst, C. Debruyne, K. Stockman, and J. Desmet. *Dip behaviour of grid connected invertors*. In 22nd International Conference and Exhibition on Electricity Distribution, page 1009 (4 pp.), 2013. (CIRED 2013), 10-13 June 2013, Stockholm, Sweden.

[7] C. Debruyne, S. Derammelaere, J. Desmet, and L. Vandevelde. *Comparative study of the influence of harmonic voltage distortion on the efficiency of induction machines versus line start permanent magnet machines*. In Proceedings of 2012 IEEE 15th International Conference on Harmonics and Quality of Power, pages 342–9, 2012. (ICHQP), 17-20 June 2012, Hong Kong, China.

[8] C. Debruyne, J. Desmet, and L. Vandevelde. *Estimation of end user voltage quality including background distortion*. In 2012 IEEE Power & Energy Society General Meeting. New Energy Horizons - Opportunities and Challenges, page 7 pp., 2012. (PESGM), 22-26 July 2012, San Diego, CA, USA.

[9] C. Debruyne, B. Verhelst, J. Desmet, and L. Vandevelde. *Technical SWOT analysis of decentralised production for low voltage grids in Flanders*. In Innovation for Sustainable Production, 2012. (i-SUP 2012), 07-09 May 2012, Brugges, Belgium.

[10] C. Debruyne, S. Derammelaere, J. Desmet, and L. Vandevelde. *Temperature dependency of the efficiency of line start permanent magnet machines*. In Proceedings of the 20th International Conference on Electrical Machines, pages 1846–1853. IEEE, 2012. (ICEM), 2-5 Sept. 2012, Marseille, France.

[11] C. Debruyne, S. Derammelaere, J. Desmet, and L. Vandevelde. *Using general synchronous machine theory to integrate PLL controller dynamics into a static power electronic converter model*. In 2012 IEEE Industry Applications Society Annual Meeting, page (7 pp.). Ind. Appl. Soc., 2012. , 7-11 Oct. 2012, Las Vegas, NV, USA.

[12] C. Debruyne. *Decentrale productie, een uitdaging voor het huidige net*, 2012.

[13] B. Verhelst, C. Debruyne, J. Desmet, and L. Vandevelde. *Tripping of circuit breakers in PV installations due to zero sequence field impedance*. In IEEE Power and Energy Society General Meeting PESGM. IEEE, 2011. (PESGM), 24-28 July 2011, Detroit , MI, USA.

[14] J. Cappelle, J. Vanalme, S. Vispoel, T. Van Maerhem, B. Verhelst, C. Debruyne, and J. Desmet. *Introducing small storage capacity at*

residential PV installations to prevent overvoltages. In 2011 IEEE Second International Conference on Smart Grid Communications , pages 534–539, 2011. (SmartGridComm 2011), 17-20 Oct. 2011, Brussels, Belgium.

[15] C. Debruyne, J. Desmet, S. Derammelaere, and L. Vandevelde. *Derating factors for direct online induction machines when supplied with voltage harmonics: A critical view*. In 2011 IEEE International Electric Machines & Drives Conference (IEMDC), pages 1048–1052, 2011. (IEMDC),15-18 May 2011, Niagara Falls, ON, Canada.

[16] C. Debruyne, B. Verhelst, J. Desmet, and L. Vandevelde. *Influence of grid configuration on current conducting behaviour in PV installations*. In 2011 10th International Conference on Environment and Electrical Engineering , page 4 pp. IEEE, 2011. (EEEIC), 8-11 May 2011, Rome, Italy.

[17] C. Debruyne, J. Desmet, B. Vervish, S. Derammelaere, and L. Vandevelde. *Influence of harmonic voltage distortion on asynchronous generators*. In Proceedings of the 8th IEEE International Symposium on Diagnostics for Electric Machines, Power Electronics and Drives, pages 159–164, 2011. (SDEMPED 2011), 5-8 Sept. 2011, Bologna, Italy.

[18] C. Debruyne, J. Vanalme, B. Verhelst, J. Desmet, J. Capelle, and L. Vandevelde. *Preventing overvoltages in PV grids by integration of small storage capacity*. In 2011 Proceedings of the 2nd IEEE PES International Conference and Exhibition on Innovative Smart Grid Technologies, page 7 pp. IEEE Power Energy. Soc., 2011. (ISGT Europe), 5-7 Dec. 2011, Manchester, UK.

[19] S. Derammelaere, H. Grimonprez, S. Dereyne, B. Vervisch, C. Debruyne, K. Stockman, G. Van den Abeele, P. Cox, and L. Vandevelde. *Efficiency of two-phase hybrid stepping motor drive algorithms*. In Proceedings 7th International Conference on Energy Efficiency in Motor Driven Systems, 2011. (EEMODS'11), 12-14 Sept. 2011,Alexandria V.A, USA.

[20] W. Kling, A. Orths, V. Cuk, J. Cobben, R. Timens, B. Verhelst, C. Debruyne, J. Desmet, L. Vandevelde, and P. Bibeiro. *Power quality issues related to new means of distributed generation and loads*. In IEEE Power and Energy Society General Meeting PESGM. IEEE, 2011. (PESGM), 24-28 July 2011, Detroit , MI, USA.

[21] B. Verhelst, C. Debruyne, J. Vanalme, J. Desmet, J. Capelle, and L. Vandevelde. *Economic evaluation of the influence of overvoltages and the integration of small storage capacity in residential PV-installations*. In 2011Proceedings of the 2nd IEEE PES International Conference and Exhibition on Innovative Smart Grid Technologies, page 6 pp. IEEE Power Energy. Soc., 2011. ((ISGT Europe), 5-7 Dec. 2011, Manchester, UK.

[22] C. Debruyne. *Netstructuren*, 2012.

[23] J. Desmet, C. Debruyne, L. Hespel, J. Vanalme, D. Vanhove, B. Verhelst, J. Capelle, and S. Vispoels. *Impact van hernieuwbare decentrale productie op de spanningskwaliteit en zijn invloed op de energie efficientie van lineaire en niet lineaire verbruikers*. HoWest-Lemcko, 2012.

[24] J. Desmet, C. Debruyne, J. Vanalme, and L. Vandevelde. *Power injection by distributed generation and the influence of harmonic load conditions*. In 2010 IEEE Power & Energy Society General Meeting, page 6 pp., 2010. (PESGM), 25-29 July 2010, Minneapolis, MN, USA.

[25] C. Debruyne, S. Dereyne, J. Desmet, L. Hespel, and B. Verhelst. *Laagspanningsinstallaties : technologie en ontwerp*. Lemcko, 2011.

[26] S. Derammelaere, L. Carlier, B. Vervisch, C. Debruyne, K. Stockman, L. Vandevelde, P.r Cox, and G. Van den Abeele. *The opportunities of two-phase hybrid stepping motor back EMF sampling*. In 2011 IEEE energy conversion congress and exposition (ECCE), pages 83–87. IEEE, 2011.

[27] D. Vanhove, L. Hespel, C. Debruyne, and J. Desmet. *Verhoogde netwerkverliezen door harmonische stromen*. Electrotechnisch Ingenieur, Belgotronic, (135):6–9, 2011.

[28] C. Debruyne, J. Desmet, J. Vanalme, B. Verhelst, G. Vanalme, and L. Vandevelde. *Maximum power injection acceptance in a residential area*. In Proceedings of the International Conference on Renewable Energies and Power Quality. European Association for the Development of Renewable Energies, Environment and Power Quality. (ICREPQ'10), 23-25 Mar. 2010, Granada, Spain.

[29] J. Desmet, C. Debruyne, J. Vanalme, and B. Verhelst. *Implementatie van innovatieve duurzame energiebronnen en hun interactie op het distributienet*. Howest. Lemcko, 2010.

[30] J. Desmet, G. Vanalme, C. Debruyne, and L. Vandevelde. *Influence of harmonic currents on cable losses for different grid configurations*. In 2010 Proceedings of the 14th International Conference on Harmonics and Quality of Power, page 6 pp., 2010. (ICHQP 2010), 26-29 Sept. 2010, Bergamo, Italy.

[31] L. Hespel, C. Debruyne, J. Desmet, C. Van Laere, and Y. Thomas. *Dimensioneren elektrische installaties*. Electrotechnisch Ingenieur, Belgotronic, (juni):6–8, 2010.

[32] B. Verhelst, J. Desmet, C. Debruyne, G. Vanalme, and J. Vanalme. *Is zonne-energie economisch interessant?* Electrotechnisch Ingenieur, Belgotronic, (125):6–8, 2010.

[33] B. Verhelst, J. Desmet, C. Debruyne, H. Van Landeghem, and L. Vandevelde. *Technical and business economic study of photovoltaic systems*. In Proceedings of the International conference on Renewable Energies and Power Quality. (ICREPQ'10), 23-25 Mar. 2010, Granada, Spain.

[34] C. Debruyne, J. Desmet, L. Hespel, B. Verhelst, G. Vanalme, and J. Vanalme. *Gevolgen van de sterke groei van PV-panelen*. Electrotechnisch Ingenieur, Belgotronic, (124):15–17, 2009.

[35] J. Desmet, G. Vanalme, C. Debruyne, and B. Verhelst. *Profoto : proefveld voor fotovoltaïsche toepassingen*. Electrotechnisch Ingenieur, Belgotronic, (123):9, 2009.

[36] J. Desmet, G. Vanalme, D. Putman, C. Debruyne, and B. Verhelst. *9.2% van het electriciteitsverbruik gaat verloren in netwerkverliezen*. Technology Upgrade, (mei), 2007.